KAUNAS UNIVERSITY OF TECHNOLOGY

NAVEEN MASIMUKKU

DERIVATIVES CONTAINING ACRIDAN, DIPHENYL SULFONE OR 1,8-NAPHTHALIMIDE MOIETIES FOR ORGANIC LIGHT EMITTING DIODES

Doctoral dissertation
Technological Sciences, Materials Engineering (T 008)

2023, Kaunas

This doctoral dissertation was prepared at Kaunas University of Technology, Faculty of Chemical Technology, Department of Polymer Chemistry and Technology during the period of 2018–2022.

Scientific Supervisor:
Dr. Asta DABULIENĖ (Kaunas University of Technology, Technological Sciences, Materials Engineering, T 008) (2021–2022)
Dr. Dalius GUDEIKA (Kaunas University of Technology, Technological Sciences, Materials Engineering, T 008) (2018–2021)

Scientific Advisor:
Prof. Dr. Habil. Juozas Vidas GRAŽULEVIČIUS (Kaunas University of Technology, Technological Sciences, Materials Engineering, T 008)

The dissertation was edited by: English language editor Dovilė Blaudžiūnienė (Publishing House *Technologija*), Lithuanian language editor Aurelija Gražina Rukšaitė (Publishing House *Technologija*)

Dissertation Defence Board of Materials Engineering Science Field:
Prof. Dr. Habil. Arvaidas GALDIKAS (Kaunas University of Technology, Technological Sciences, Materials Engineering, T 008) – **chairperson**;
Prof. Dr. Narine DURGARYAN (Yerevan State University, Armenia, Natural Sciences, Chemistry, N 003);
Prof. Dr. Saulius GRIGALEVIČIUS (Kaunas University of Technology, Technological Sciences, Materials Engineering, T 008);
Prof. Dr. Jolita OSTRAUSKAITĖ (Kaunas University of Technology, Technological Sciences, Materials Engineering, T 008);
Prof. Dr. Irina SAVCHENKO (Taras Shevchenko National University of Kyiv, Ukraine, Technological Sciences, Materials Engineering, T 008).

The official defence of the dissertation will be held at 1 p.m. on 19 January, 2023 at the public meeting of the Dissertation Defence Board of Materials Engineering Science Field in Santaka Valley Hall A228 at Kaunas University of Technology.

Address: K. Baršausko g. 59, Kaunas LT-51423, Lithuania
Phone (+370) 37 30 00 42; email doktorantura@ktu.lt

The doctoral dissertation was sent out on 19 December, 2022.
The doctoral dissertation is available on the internet at http://ktu.edu and at the library of Kaunas University of Technology (Donelaičio 20, Kaunas, LT-44239, Lithuania).

KAUNO TECHNOLOGIJOS UNIVERSITETAS

NAVEEN MASIMUKKU

AKRIDANO, DIFENILSULFONO AR 1,8-NAFTALIMIDO FRAGMENTUS TURINTYS DARINIAI ORGANINIAMS ŠVIESTUKAMS

Daktaro disertacija
Technologijos mokslai, medžiagų inžinerija (T 008)

2023, Kaunas

Disertacija rengta 2018–2022 metais Kauno technologijos universiteto cheminės technologijos fakultete, Polimerų chemijos ir technologijos katedroje.

Mokslinis vadovas:
Dr. Asta DABULIENĖ (Kauno technologijos universitetas, technologijos mokslai, medžiagų inžinerija T 008) (2021–2022 m.)
Dr. Dalius GUDEIKA (Kauno technologijos universitetas, technologijos mokslai, medžiagų inžinerija T 008) (2018–2021 m.)

Mokslinis konsultantas:
Prof. habil. Dr. Juozas Vidas GRAŽULEVIČIUS (Kauno technologijos universitetas, technologijos mokslai, medžiagų inžinerija T 008).

Disertaciją redagavo: anglų kalbos redaktorė Dovilė Blaudžiūnienė (leidykla „Technologija“), lietuvių kalbos redaktorė Aurelija Gražina Rukšaitė (leidykla „Technologija“).

Medžiagų inžinerijos mokslo krypties disertacijos gynimo taryba:
prof. habil. dr. Arvaidas GALDIKAS (Kauno technologijos universitetas, technologijos mokslai, medžiagų inžinerija, T 008) – **pirmininkas**;
prof. dr. Narine DURGARYAN (Jerevano valstybinis universitetas, Armėnija, gamtos mokslai, chemija, N 003);
prof. dr. Saulius GRIGALEVIČIUS (Kauno technologijos universitetas, technologijos mokslai, medžiagų inžinerija, T 008);
prof. dr. Jolita OSTRAUSKAITĖ (Kauno technologijos universitetas, technologijos mokslai, medžiagų inžinerija, T 008);
prof. dr. Irina SAVCHENKO (Taraso Ševčenkos nacionalinis Kijevo universitetas, Ukraina, technologijos mokslai, medžiagų inžinerija, T 008).

Disertacija bus ginama viešame Medžiagų inžinerija mokslo krypties disertacijos gynimo tarybos posėdyje 2023 m. sausio 19 d. 13 val. Kauno technologijos universiteto Santakos slėnyje, Posėdžių kambaryje A228.

Adresas: K. Baršausko g. 59, Kaunas, LT-51423, Lietuva.
Tel. (+370) 37 300 042; el. paštas doktorantura@ktu.lt

Disertacija išsiųsta 2022 m. gruodžio 19 d.
Su disertacija galima susipažinti interneto svetainėje http://ktu.edu ir Kauno technologijos universiteto bibliotekoje (K. Donelaičio g. 20, Kaunas LT-44239).

CONTENTS

LIST OF ABBREVIATIONS

AIEE	Aggregation-induced emission enhancement
CCT	Correlated color temperature
CE/PE	Current and power efficiencies
CRI	Color rendering index
CELIV	Charge extraction by linearly increasing voltage technique
CIE	Commission Internationale de l'Eclairage
CT	Charge transfer
CV	Cyclic voltammetry
DCM	Dichloromethane
DSC	Differential scanning calorimetry
D-A	Donor-acceptor
D-π-A	Donor-π-acceptor
DFT	Density functional theory
$EA_{acceptor}$	Electron affinity of acceptor
EA_{donor}	Electron affinity of donor
Eelcg,	Electrical energy band gap
Eopt	Optical energy band gap
E_{ox}	Oxidation potential
E_{red}	Reduction potential
ESIPT	Excited-state intramolecular proton transfer
$Etheor_g$	Theoretical energy band gap
EA_{CV}	Electron affinity measured by CV
EA_{PE}	Electron affinity measured by photoelectron spectroscopy
EL	Electroluminescence
EML	Emitting layer
EQE	External quantum efficiency
$\hbar$	Planck constant
HOMO	Highest occupied molecular orbital
HTL	Hole-transporting layer
IC	Internal conversion
ICT	Intramolecular charge transfer
ISC	Intersystem crossing
IQE	Internal quantum efficiency
IP_{CV}	Ionization potential measured by CV
IP_{PE}	Ionization potential measured by photoelectron spectroscopy
ITO	Indium-tin oxide
J	Exchange energy

JAF	J-aggregate formation
K	Electron repulsion energy
k_B	Boltzmann constant
LE	Locally excited state
LCD	Liquid-crystal display
LED	Light-emitting diodes
LiF	Lithium fluoride
LEAB	Low energy absorption band
LUMO	Lowest unoccupied molecular orbital
mCBP	3,3′-Di(9*H*-carbazol-9-yl)-1,1′-biphenyl
mCP	1,3-Bis(*N*-carbazolyl)benzene
NIR	Near-infrared
NBPhen	2,9-bis(naphthalen-2-yl)-4,7-diphenyl-1,10-phenanthroline
NPB	*N*,*N*'-Di(1-naphthyl)-*N*,*N*'-diphenyl-(1,1'-biphenyl)-4,4'-diamine
o-DiCbzBz	9,9'-(2-(1-phenyl-1*H*-benzo[d]imidazol-2-yl)-1,3-phenylene)bis(9*H*-carbazole)
OLED	Organic light emitting diode
PE	Power efficiency
PL/PH	Photoluminescence/phosphorescence
PLQY	Photoluminescent quantum yield
RISC	Reverse intersystem crossing
S, T	Singlet, triplet state
TADF	Thermally activated delayed fluorescence
TCTA	Tris(4-carbazoyl-9-ylphenyl)amine
TGA	Thermogravimetric analysis
T_g	The temperatures of glass transition
T_m	The temperatures of melting point
T_d	The temperature of the onset of weight loss
T_{ID}	The temperatures of the onset of the thermal decomposition
$T_{ID-5\%}$	The 5% weight loss temperatures
$_T$HF	Tetrahydrofuran
TOF	Time-of-flight
t_{tr}	Transit times
TREL	Transient electroluminescence
TPBi	2,2',2''-(1,3,5-Benzinetriyl)-tris(1-phenyl-1*H*-benzimidazole)
TSPO1	Diphenyl-4-triphenylsilylphenylphosphine oxide
UPS	Ultraviolet photoelectron spectroscopy
UV-vis	Ultraviolet-visible
λ	Wavelength

μ	Drift mobility of charge carriers
τ	Emission lifetime
Φ	Photoluminescence quantum yield
XRD	X-ray diffraction
γ	Charge balance factor
ΔES-T	Singlet-triplet energy splitting
-ΔG	Gibbs energy
ηfr	Singlet ratio
ηL	Current efficiency in cd A^{-1}
ηout	Optical out coupling efficiency
ηP	Luminous efficiency
λEL	Electroluminescence peak
λPL	Photoluminescence peak
τ	Excited-state lifetime

1. INTRODUCTION

Light has been one of the fundamental sources or needs of living beings since primitive times. Humanity's evolution over the decades is primarily attributed to the existence of light, which directly or indirectly gave life from microorganisms to plants to animals to humans[1-4]. The only known source of light on earth was the Sun, later humans invented various sources, like fire from sun, kerosene, etc[5,6]. Afterwards there have been immense efforts put forward by humanity to explore the mysteries regarding light, including sir Isaac Newton's idea of obtaining seven different colors when the Sun's light passes through a prism, and light being made up of tiny corpuscles[7], a concept reflected in the division of light into photons today[8]. Thereafter, Albert Einstein fully developed this concept of photons in his theory of relativity[10]. Electromagnetic radiation consists of seven different types of waves, from longest wavelength to shortest: radio waves, microwaves, infrared, optical, ultraviolet, X-rays, and gamma-rays[11] (Fig.1). Humans can only see visible light or waves from 380 nm to 700 nm in the electromagnetic spectrum[11]. There are two primary sources of light. Luminescence (cold light) is a natural or spontaneous emission of light without obtaining or generating heat caused by chemical or biochemical reactions, the activity of subatomic particles, radiation, or stress on a crystal. Incandescence (hot light) is defined as light emission that is produced when the substances are hot enough to glow. All emissions caused by electromagnetic radiation can be considered as incandescence emissions.

The further progress of human beings towards the modern era of life heavily depends on artificial light sources, which depend on electricity[5]. Scientists from all over the world put tremendous efforts in order to develop various arterial light sources. The rapid increase in population increases the consumption of artificial light sources of the world, and it has become challenging for scientists and governments to find new alternative arterial light sources based on efficient, eco-friendly, reliable, cost-effective, and sustainable solid-state lighting technologies[14]. These challenges and demands push the boundaries of the research and development sector which subsequently leads to advancement and breakthroughs in achieving the outstanding device efficiencies in various fields including artificial light sources including organic light emitting diodes (OLEDs)[15]. The OLEDs technology grabs the attention of researchers due to lower consumption of energy. They were developed in the late 1980s and became a revolutionary concept in the display and lighting technologies[16]. The evolution of OLEDs can be classified into three generations based on fluorescence, phosphorescence, and thermally activated delayed fluorescence (TADF)[17]. The first generation of OLEDs containing fluorescent molecular emitters exhibited limited maximum internal quantum efficiency (IQE) of 25% because of electrical excitation that results in 25% singlet excitons (S_1) and 75% triplet excitons (T_1) due to forbidden radiative transition triplet to singlet (or reverse) because of conservation of spin angular momentum[17-18]. The second generation of OLEDs containing phosphorescent emitters are not completely organic, and their devices depend on an inorganic emitter complex containing a heavy metal like iridium or

platinum[19]. The advantages of heavy metal complex-based OLEDs is that the presence of the metal ion accelerates the transition of the singlet to triplet excited states through increased intersystem crossing. This boosts phosphorescence and the IQE of the OLED can be achieved or increased up to 100%. However, these heavy metal complexes are rare, toxic, expensive, and unstable. They increase costs from OLED manufacturing to recycling and disposal[19]. The third generation of OLEDs utilizes highly luminescent organic materials exhibiting TADF[20]. This mechanism involves triplet excitons (T_1) which undergo thermally assisted reverse intersystem crossing (RISC) to S_1 state where they radiatively transit to S_0 state which results in delayed fluorescence. IQEs of OLEDs of 100% can be achieved due to this delayed fluorescence emission without any type of heavy metals[21]. However, OLEDs are still disadvantaged by short lifetimes and low stability of blue devices, relatively high cost, vulnerability to exposure to water[22]. OLEDs that overcome the above-mentioned drawbacks need to be developed. Meanwhile, to achieve this, careful design and accurate modification of organic material that involves donor (D) and acceptor (A) moieties for OLEDs can enhance the stability and efficiency of OLEDs[23].

The most frequent method for modifying photophysical, electrical properties, lowest unoccupied molecular orbital (LUMO), and the highest occupied molecular orbital (HOMO) of organic electroactive compounds is to link an electron-rich donor (D) and an electron-deficient acceptor (A) group directly or via π-spacer[23,24]. A pull−push structure utilizes an intramolecular charge transfer (ICT) from the donor to the acceptor which is vital for light harvesting via TADF. The D and A units can be connected through a π-spacer that results in a D–π–A, or D–A–π–A, or D–D–π–A type of conjugated molecular system, in which the photophysical, electronic properties of D–π–A or D–A–π–A designs can be adjusted by modifying the strength of the donor or the acceptor units and also by altering the π -linker between the donor and the acceptor units, depending on its linkage type, electron density, co-planarity. An aromatic π-conjugation linkage also plays a crucial role in balancing electronic communication and the extent of charge transfer between the donor and acceptor[23-25]. So far, there has been a wide variety of D-A aromatic conjugated organic derivatives reported across multidisciplinary fields[23]. The organic electroluminescent (EL) material should meet the following requirements in order to employ them in the OLEDs: (1) to have an appropriate ionization potential and electron affinity for energy level matching for charge carrier injection at the electrode/organic material and organic material/organic material interfaces; (2) allow the formation of an even film without pinholes; (3) ensure the morphological stability of the layers; (4) ensure thermal and electrochemical stability; (5) ensure highly efficient luminescence and bipolar charge transport[27]. Therefore, there is a need to develop novel organic materials with appropriate donor-acceptor architecture to overcome the drawbacks of earlier obtained OLED materials and improve the efficiency of OLEDs.

Over several years, various orange/red emitters, including fluorescence, phosphorescence, and TADF have been used in various ways in developing OLEDs[28]. Among these three generations of materials, TADF materials have an advantage over traditional fluorescent emitters due to the possibility to achieve 100% internal quantum efficiency of OLEDs[29]. The development of orange/red TADF emitters is

considerably slower when compared to blue and green TADF emitters[30]. Blue and green TADF compounds-based OLEDs shown high external quantum efficiencies (EQE). EQE of nearly 37% was reported for sky blue and over 30% EQE for green TADF OLEDs. However, in the case of orange-to-red OLEDs only very few of them achieved EQE of ca. 30% EQE[31]. The reason for slower development of orange/red TADF emitters could be attributed to their complicated molecular design and various other difficulties including difficulties in reaching smaller energy gap (ΔE_{ST}) to generate efficient TADF emission and increased non-radiative transition affected by energy-gap law for orange-to-red emitters[32]. By making some structural modifications and incorporation of efficient donor and acceptor moieties to orange/red TADF emitters, OLEDs based on them could potentially reach efficient numbers of EQE[31-32]. In order to overcome these difficulties, the variation and better design of architecture of new donor-acceptor systems are very much required for further development of orange/red TADF OLEDs. The most efficient orange/red TADF OLEDs still fall behind the blue and green TADF OLEDs due to the above-mentioned reasons. The demand and development of more efficient orange/red TADF OLEDs are very much required by display industries, research and development sector. The high rigidity of molecules and efficient charge transfer (CT) in donor-acceptor (D-A) systems are required for developing efficient and high-quality orange-to-red emitters[33]. Owing to strong electron withdrawing nature and high electron affinities of 1,8-naphthalimide (NI) acceptor moiety it could potentially fill the research gap of downsides of characteristics of orange/red TADF emitters. We selected the NI moiety as an acceptor unit since its potential, in our opinion, is not yet fully exploited. The expected exploitation of NI acceptor moiety could be achieved when a combination of NI acceptor moiety together with various donor moieties under various structural variations such as D-A, D-A-D, D-π-A are used.

The aim of this work is the synthesis and investigation of the properties of new electroactive donor-acceptor derivatives containing acridan, diphenyl sulfone or 1,8-naphthalimide moieties to obtain perspective materials for the third generation of OLEDs.

To achieve the aim of the work the following tasks were raised:

- Design, synthesis, and comparative investigation of the thermal, photophysical and photoelectrical properties of new aryl-substituted acridan derivatives for the TADF-based OLEDs.
- Design, synthesis, and study of the properties of tetraphenyl-substituted carbazolyl disubstituted diphenyl sulfone with donor-acceptor-donor architecture for the highly efficient OLEDs with low efficiency roll-offs.
- Design, synthesis, and investigation of thermal, photophysical, photoelectrical, and electroluminescent properties of new derivatives of donor-acceptor structure having phenoxazine, phenothiazine, or acridan as donor moieties

and 1,8-naphthalimide as the acceptor unit for the high-electron-mobility and red AIE-active TADF materials for OLED applications.

- Design, synthesis and investigation of thermal, photophysical, photoelectrical, and electroluminescent properties of new derivatives of donor-acceptor and donor-acceptor-donor architecture containing 1,8-naphthalimide, diphenylamino phenyl, and vinyl diphenylamino phenyl moieties for the red fluorescent OLED emitters.

Novelty of the work:

- A series of new aryl-substituted derivatives of acridan were synthesized and their applicability for TADF based OLEDs was demonstrated.
- New tetraphenyl-substituted carbazolyl disubstituted diphenyl sulphone was synthesized and its applicability as TADF host for highly efficient OLEDs with low-efficiency roll-offs was demonstrated which showed maximum EQE of 23.3% with low efficiency roll-off, which only decrease by 4% (EQE = 22.3%) at 1000 cd/m^2.
- New derivatives of 1,8-naphthalimide containing phenoxazine, phenothiazine and acridan donor moieties exhibiting high electron mobility and red aggregation induced emission (AIE)-active TADF were synthesized and their applicability in OLEDs was demonstrated; the compounds were used as emitters in red electroluminescent devices, which showed maximum EQEs up to 8.2%, maximum current efficiency of 13.21 cd A^{-1}, power efficiency of 6.75 lm W^{-1}.
- New derivatives of 1,8-naphthalimide containing diphenylamino phenyl, and vinyl diphenylamino phenyl donor moieties were synthesized and their applicability in OLEDs was demonstrated; the compounds were used as red fluorescent emitters in two different matrices. The device demonstrated maximum EQE, maximum current efficiency and maximum power efficiency of 4.7%, 11.8 cdA^{-1} and 6.7 ImW^{-1}, respectively.

The contribution of the author:

The author has designed, synthesized, purified, and characterized four new series of compounds. The author has performed cyclic voltammetry measurements. The author has analyzed thermogravimetric analysis and differential scanning colorimetry, single crystal XRD. The mass spectrometry, TGA and DSC measurements was performed by dr. Eigirdas Skuodis. Single crystal XRD measurement was performed in collarboration with the dr. Audrius Bucinskas (Kaunas University of Technology). The ionization potential of solid samples and charge-transporting was done by dr. Dmytro Volyniuk (Kaunas university of technology). The photophysical measurements and fabrication of OLEDs was performed in collaboration with dr. Oleksandr Bezvikonnyi (Kaunas University of technology) and Malek Mahmoudi (Kaunas University of Technology).

2. LITERATURE REVIEW

2.1 OLEDs and their importance

Organic light-emitting diodes (OLEDs or organic LEDs) are energy converting devices (electricity-to-light) which are based on electroluminescence (EL) of organic compounds[34]. OLED field of study comes under optoelectronics. The first electroluminescence phenomenon of organic materials was observed for acridine orange at high voltage[35]. OLED consists of organic layers that are made of organic compounds or polymers[34]. An OLED is a solid-state device that has a thickness of ca. 100 to 500 nanometres[36]. The field of OLEDs gained immense popularity in 1987 after ground-breaking discoveries by Tang and VanSlyke, who presented a unique OLED working at low voltage[34]. OLEDs are used for next-generation full-color flat panel displays[36]. They have been considered as outstanding competitive candidates due to their steadily increased efficiency and unique features such as solid-state self-emission, great flexibility, no-turn on delay, lightweight, wide viewing angle, facile color tunability, and processability[34-35]. However, OLEDs still lag in some areas, such as shorter lifetimes, sensitivity to water, relatively lower stability, and the degradation of organic molecules over time[34-35]. Chemists, physicists, engineers from all over the world continue to work trying to solve the drawbacks of OLEDs that consequently leads towards achievement of efficient OLEDs.

OLEDs consist of organic thin films that are sandwiched between two conductive electrodes[37].

Holes and electrons from the cathode and anode are injected into the emissive layer when the voltage is applied to the device. Consequently, holes and electrons migrate through hole-transporting (HTL) and electron-transporting (ETL) layers, which are generally used to help in carrier injection. Finally, the recombination of the hole and electron pairs in the emission layer produces light[37].

The basic OLED (**Fig. 1**) consists of the following layers[38]:

1. Substrate (plastic, glass, or metal foil).
2. Anode, i.e., pure transparent electrode to inject holes (Indium tin oxide (IT0))
3. Hole injection layer (HIL). This layer is responsible for receiving holes and injecting them into further layers.
4. Hole transporting layer (HTL). This layer is responsible for the transportation of holes and blocking electrons.
5. Light emitting or emission layer (EML). This is the key layer of a device where generation of light takes place.
6. Electron transporting layer (ETL). This layer is responsible for the transportation of electrons and blocking holes.
7. Cathode is the negatively charged electrode that injects electrons into organic layers (Ag, Li, Al, Ca, LiF, MgOx, and thin insulator).

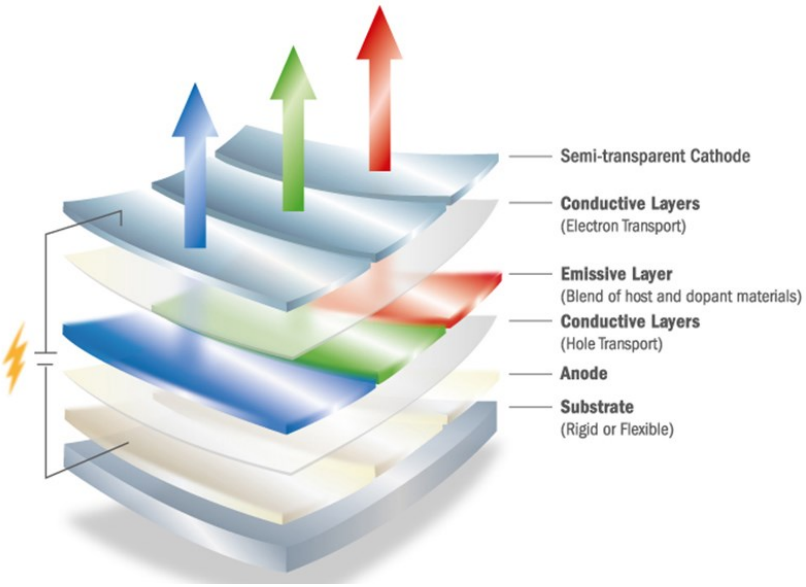

Fig.1 The schematic representation of components of OLED structure[196]

The desired color or wavelength or some other parameters of light emission depend on the structure of the organic molecule that is the core factor which determines efficiency, longevity, and various factors of OLEDs.

The efficiency of an OLED is characterized by the following parameters: external quantum efficiency (EQE), internal quantum efficiency (IQE), and luminescence efficiency (η_P) in lmW^{-1} etc[39]. The fabrication process of OLEDs can be completed via two important methods, i.e. (1) vacuum deposition or vacuum thermal evaporation (VTE) method and (2) solution-processing (inkjet printing, spin coating, casting etc.). Both methods possess their own pros and cons depending on the conditions they are operating[40]. The advantages and disadvantages of vacuum deposition technique include easy control of mixing or doping ratio, high performance, good reliability, and expensive, inefficient, organic material should have sufficient volatility and thermal stability, respectively. The advantages and disadvantages of solution processed technique include inexpensive OLED manufacturing, can be printed onto very large films, are environmentally friendly and speed, maintenance, durability, smudges, respectively[40]. The quality of light emission from OLED can be estimated by using three parameters including the commission Internationale de l'Éclairage (CIE) coordinates, the color rendering index (CRI), and the corelated color temperature (CCT).

By the efforts of scientists, researchers, engineers, and technologists over the world the evolution of OLEDs over the years has gone through immense changes and reached tremendous achievements. The timeline of development of OLEDs is summarized in **Table 1**.

Table 1. The evolution of OLEDs over the years[41]

Year	Progress or achievement in OLEDs
1987	Ching W. Tang and Steven Van Slyke presented the world's first working OLED at Eastman Kodak[75].
1990	Cambridge university fabricated world's first polymer OLED[76].
1994	Yamagata university announced first white OLED[76].
1996	The first commercial PMOLED produced by the Pioneer and the first public demonstration of OLED given by CDT (Cambridge display technology)[76]
1997	Pioneer Electronic produced EL display with 260,000 colors and flexible flat panel display technology was demonstrated by UDC (Universal display corporation)[76].
1998	Kodak, Sanyo announced full-color active-matrix organic display[76].
2000	Organic El displays for mobile gadgets developed by LG electronics and Motorola demonstrated the first 1.8-inch colorful PMOLED phone[76].
2001	Sony announced 13-inch full color OLED[76].
2003	Sony launched a 24.2-inch OLED panel and Kodak demonstrated the first AMOLED digital camera (the kodak EasyShare LS63)[76].
2005	CDT printed 14-inch PLED display and Samsung Electronics introduced 21-inch OLED for TVs.
2007	Novaled reached 100,000h lifetime for a highly efficient white OLED and Sony introduced the first ever OLED TV (11") (the XEL-1)[76].
2011	OSRAM demonstrated the world's most efficient white OLED and LG Display showed their 55-inch OLED TV prototype[76].
2015	Samsung demonstrated the Galaxy S6 and the S6 edge and LG Chem started to commercialize their 320×320 nm OLED lighting panels[76].
2019	LGD announced an 88-inch 8K OLED TV and LGD demonstrated the world's first rollable OLED TV. Wisechip introduced the world's first hyperfluorescence OLED display[76].
2020	Intel announced a foldable concept device with 17.3-inch OLED display and Cynora demonstrated the world's most efficient fluorescent blue OLED emitter[76].

2.2 1,8-naphthalimide (NI) core moiety and its donor-based derivatives

1,8-naphthalimide (NI) or naphthalene-1,8-dicarboximide or naphthalimide is a colorless, crystalline compound[42] (Scheme 1).

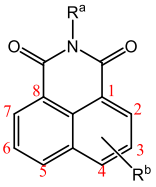

Ra, **Rb** – alkyl, aryl

Scheme 1. Chemical structure of 1,8-naphthalimide core structure system

The synthesis of NI (Scheme 2) occurs in two steps including the oxidation of acenaphthene to naphthalic anhydride, subsequently conversion to imide[43].

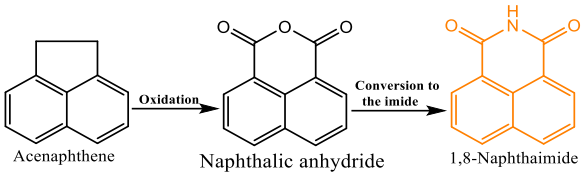

Scheme 2. Synthesis1,8-naphthalimide

1,8-Naphthalimide moiety is well-known, versatile, and attractive to researchers as a fluorophore unit due to its outstanding and diverse applications in dyes, fluorescent probes, OLEDs and other optoelectronic devices, solar energy collectors, for biological/cellular imaging, as DNA targeting agents, anion sensors, and antitumor agents[43-54]. In the case of OLEDs, 1,8-naphthalimides are desirable to researchers since they can potentially produce strong intermolecular charge transfer (ICT) that consequently gives rise to both absorption band and emission band in the visible region (a broad range between 350 nm-450 nm, in some cases, can extend up to 650 nm)[44]. In addition, the derivatives of 1,8-naphthalimide have high electron affinity, outstanding thermal stability[52]. Moreover, 1,8-naphthalimide derivatives exhibit excellent photostability, high fluorescent quantum yields (an extensive range between 20% and 80%), and broader range of Stokes shifts (a vast range between 3500 and 6500 cm^{-1})[45]. Furthermore, NI based derivatives exhibit good hole-blocking or electron-transporting properties because of the availability of an electron-deficient aromatic center with good thermal and chemical stability. NI shows hole-blocking ability because of high electron affinity, which is useful for the balanced carrier injection in OLEDs[44-46].

Owing to several standout advantages of NI derivatives such as easy and cost-effective synthetic procedure, conjugated electron system (i.e., π electron system), and rigid planar structure, NI could be easily modified via different synthetic strategies yielding attractive NI derivatives[47]. The 1,8-naphthalimide structure contains eight positions and one imide group (Scheme 1). There are six active positions (C-2, C-3, C-4, C-5, C-6, C-7) out of eight positions in the NI core structure[48]. The substitution of halo, nitro, or sulfonic acid groups at these readily exchangeable or substitutable active positions by alkoxy, aryloxy, amino, and mercapto substituents of NI compound, has a potential impact on their electronic behavior that affects photophysical properties. The C-4 position of NI core structure has been the most explored position out of the six active positions as reported in literature[43]. NI core system acts as a very good electron acceptor. The interaction of a NI compound as an electron acceptor with the electron donor moieties results in the formation of donor-acceptor (D-A) type compounds. The interaction happens between the carbonyl groups of the imide structures and the selective donor substituent at the selective position C-2, C-3, C-4, C-5, C-6, C-7 of the NI core system[43]. The supposed or expected interaction of NI compound with the solvent molecules is reduced due to the very strongly fused aromatic conjugated naphthalene ring structure. Consequently, there is a less external transfer of energy during NI compound interacting with solvent molecules which is advantageous for the emission of strong fluorescence[50]. NI derivatives are divided into two groups based on the various colors of fluorescence

which appears in the visible region[49]. Derivatives of the first group exhibit fluorescence with a maximum of intensity in the range of 380–460 nm (violet, blue, or blue-green), while the compounds of the second group emit fluorescence in the wavelength range exceeding 460 nm (yellow-green to orange-red)[51]. The synthesis of 1,8-naphthalimide derivatives with desirable emission color characteristics and fluorescence intensity can be modelled by altering the electron donor capability of the selective substituent at the selective C-2, C-3, C-4, C-5, C-6 or C-7 position. The presence of selective electron-donating groups, such as amino and alkoxy groups in the aromatic rings of the NI core system has advantages including the enhancement of the fluorescence QY[49]. They trigger a polar charge-transfer excited state (a non-polar excited state is in unsubstituted NIs) and they can also shift the absorption to the visible region[54]. The above-mentioned substituted NI with polar charge-transfer excited state character has potential oxidizing or reducing capabilities, which are intensely exploited in optoelectronic applications[52].

The derivatives of substituted NI can be developed in different ways such as the substitution at the N-imide with a suitable donor or acceptor unit and the substitution at the C-2, C-3, C-4, C-5, C-6, C-7 positions of the aromatic conjugated core of NI moiety. The photophysical properties (wavelength maxima of absorption and emission spectra, fluorescence quantum yields, and fluorescence lifetimes) of the various D-A NI derivatives are all affected by the properties of solvents[49]. There were a considerable number of studies reported on donor-substituted NI derivatives[47]. There is still a great scope to explore the relationship between the structures of NI-based D-A conjugated systems and their thermal, photophysical, and electrochemical properties. The results of such investigations are consequently helpful in enhancing the efficiency of OLEDs. The following review has addressed recent advances in the design and development of NI-based D–A conjugated systems.

2.2.1 Phenoxazine substituted 1,8-naphthalimides

Five D-A type compounds **N1**, **N2**, **N3**, **N4**, **N5** consisting of NI acceptor moiety and phenoxazine moiety as a donor were reported in four references[55,56,57,58]. They were applied as red-TADF emitters in OLEDs (Scheme 3).

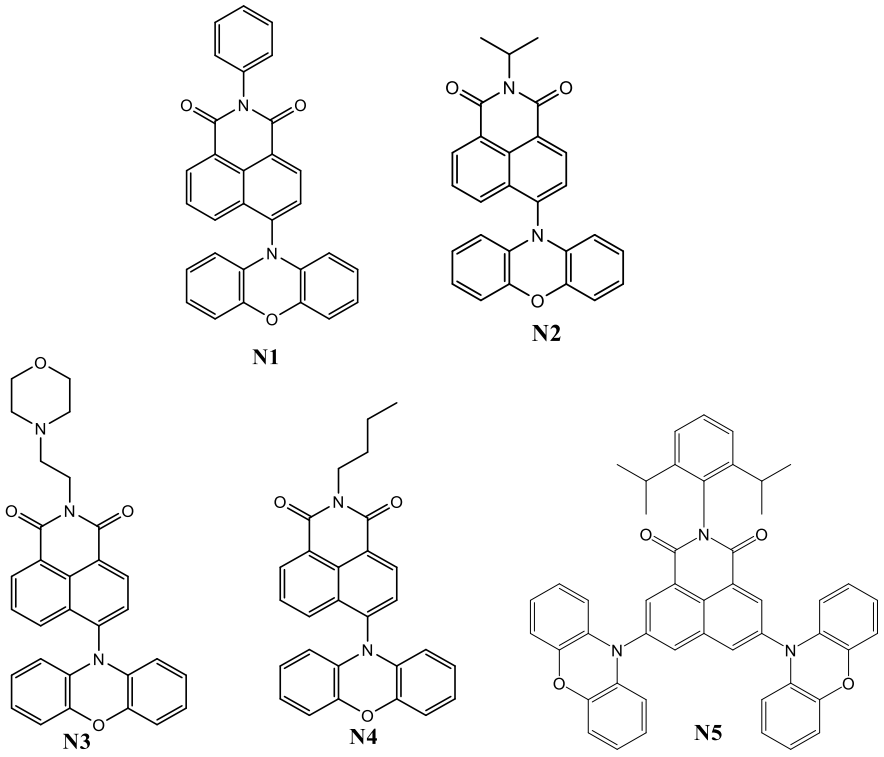

Scheme 3. NI-Phenoxazine containing derivatives

The NI-phenoxazine derivatives were synthesized by Buchwald-Hartwig coupling reactions[55-58]. Compounds **N1** and **N5** can form molecular glasses. Their glass transition temperatures (T_g) were found to be 387°C (**N5**) and 123°C (**N1**). Compounds **N1** and **N5** were found to be highly thermally stable. The temperatures of the onset of the thermal decomposition (T_{ID}) of **N1** and **N5** were 310°C, and 389°C, respectively. The OLED based on compound **N1** exhibited EQE of 13%. Compound **N5** exhibited lower EQE. Materials **N1** and **N5** showed remarkably small ΔE_{ST} values of 0.10 and 0.01, respectively. Consequently, this leads to reverse intersystem crossing (RISC) and TADF. The photoluminescence quantum yields (PLQY, Φ^{PL}) of toluene solutions of compounds **N1** and **N5** were found to be of 15.5% and 3.1%, respectively.

Table 2. Characteristics of derivatives of **N1**–**N5** and of OLEDs based on them

Materials	T_g, (°C)	T_{ID}, (°C)	λ_{abs}[a], (nm)	λ_{em}[a], (nm)	ΔE_{ST}, (eV)	EQE_{max}, (%)	λ_{EL}	Ref
N1	123	310	334	588	0.10	13	624	55
N2	-	-	330/495	578	-	-	-	56
N3	-	-	330/500	584	-	-	-	
N4	-	-	334	697	-	-	-	57
N5	387	382	327/525	755	0.01	0.13	671	58

[a] λ_{abs} and λ_{em} (nm) in toluene solution

PLQY of hexane solutions of compounds **N2** and **N3** were found to be of 4.8 and 3.7 %, respectively. The relatively low PLQY values reported for compounds **N1**, **N2, N3,** and **N5** could be attributed to the PL quenching of oxygen[55-58]. The characteristics of OLED based on compound **N1** were one among the best for red TADF OLED with EL peaks beyond 620 nm. Compound **N1** has HUMO/LUMO values of -5.21/-3.21 eV. The OLED based on it showed maximum luminescence efficiency of 3197 cdm^{-2}, and turn-on voltage of 3.2 V. In addition, OLED based on **N1** showed maximum EQE and maximum power efficiency of 13% and 14.8 lm/W, respectively. At the brightness of 1000 cd/m2, the EQE values dropped to 9.4%, indicating that the OLED device had relatively small efficiency roll-offs. The absorption maxima of the solutions of compounds **N1**, **N2, N3, N4,** and **N5** were in the range of 327–334 nm. Compounds **N2, N3,** and **N5** also exhibited second absorption peaks due to the ICT in the range of 495–525 nm. The fluorescence emission spectra of toluene solutions of compounds **N1**–**N5** showed the emission maxima (λ_{em}) in the range of 588 nm to 755 nm. OLED prepared by vacuum deposition with emitting layer compound **N5** molecularly dispersed bis(N-carbazolyl)benzene (mCP) host at 5% doping ratio exhibited EQE of 0.13% with electroluminescence intensity peak at 671 nm[55-58]. However, the solution-processed device exhibited a lower EQE of 0.05% with electroluminescence intensity peak at 631 nm. The D-A-D architecture and wedge-shape configuration of compound **N5** lead to a reduction of ΔE_{ST} value to 0.01 eV. It also exhibited TADF in deep red to near infra-red (DR-NIR) region. Compounds **N1** and **N6** as emitters were employed as dopant in the host material 9'-(2'-(1H-benzo[d]imidazol-1-yl)-[1,1′-biphenyl]-3,5-diyl)bis(9H-carbazole) (*o*-mCPBI) which is a universal host material for both phosphorescent and TADF OLEDs[55].

2.2.2 Phenothiazine containing 1,8-naphthalimides

Phenothiazine contains electron-rich sulfur and nitrogen heteroatoms. Its derivatives can be used as an electron donor in the second order nonlinear optical chromophores[55,57]. The phenothiazine units act as electron-donating groups in organic electroactive compounds commonly used in OLEDs, dye-sensitized solar cells (DSSCs)[61]. This section discusses seven compounds consisting of NI moiety as an acceptor and phenothiazine moiety as a donor which were reported as materials for OLEDs[55,56,57,59,60] (Scheme 4).

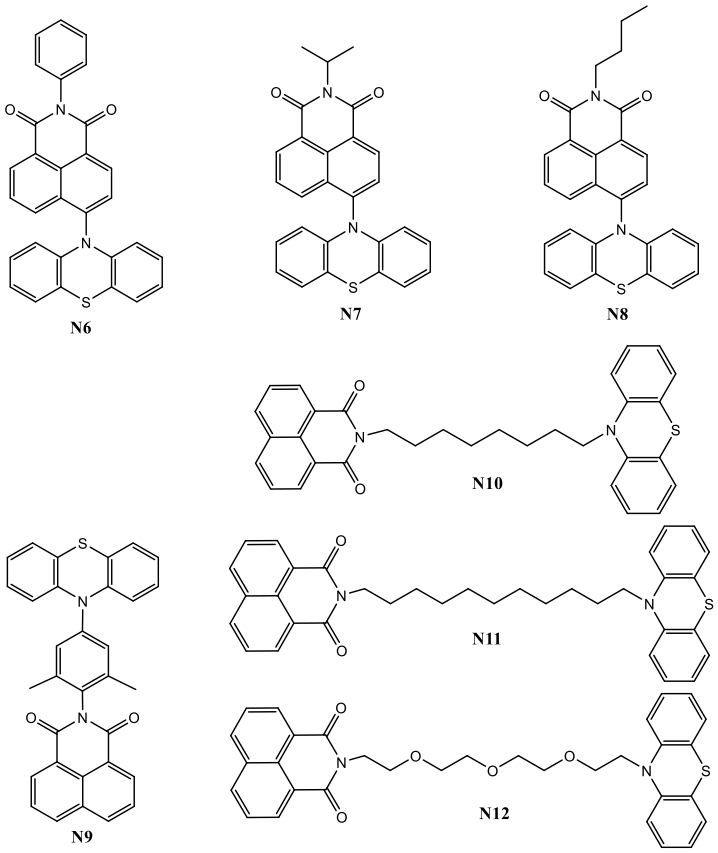

Scheme 4. NI-Phenothiazine containing derivatives

The absorption maxima of the solutions of compounds **N6**–**N12** range from 330 to 335 nm. Such absorption can be attributed to the π- π* transition. The larger additional absorption bands of N**8** are around 400 nm due to the ICT from the donor moiety to Ni acceptor moiety. The solutions of compounds **N6**–**N12** exhibited emission intensity maxima in the wide range from 388 to 601 nm[55-60]. OLED based on compound **N9** exhibited EQE of 9.3% with red electroluminescence peaking at around 635 nm. Compound **N9** showed AIE due to the presence of the steric hindrance of the π-bridge (2,6-dimethyl phenyl) between phenothiazine donor and NI acceptor with red emission around 624 nm and high PLQY in the solid sate of 55%. The fluorescence quantum yield of the solutions of materials **N11**, **N12**, **N13** were in the order 0.26 (**N12**)> 0.19 (**N11**)> 0.080 (**N13**). Compound **N12** with a long alkyl chain exhibited higher fluorescence quantum yield than **N11** with relatively smaller alkyl chain whereas **N13** exhibited considerably lower fluorescence quantum yield. Compounds **N6, N7,** and **N9** showed remarkably small ΔE_{ST} values of 0.11, 0.01, and 0.05, respectively. The device characteristics of OLED based on compound **N6** were among the best devices for red TADF OLEDs. The device showed an EL peak beyond 620 nm. OLED based on compound **N6** showed maximum luminescence efficiency of 2325 cdm^{-2}, the turn-on voltage of 3.4 V, the maximum EQE and maximum power

efficiency of 11.4% and 9.8 lm/W, respectively[55]. The device based on **N6** exhibited relatively small efficiency roll-offs, with the EQE values reducing to 6.0% at a luminance of 1000 cd/m2. The CIE coordinates were 0.630 and 0.368.

Table 3. Characteristics of derivatives of **N6**–**N9** and OLEDs based on them

Materials	T_g, (°C)	T_{ID}, (°C)	λ_{abs}[a], (nm)	λ_{em}[a], (nm)	ΔE_{ST}, (eV)	EQE_{max}, (%)	λ_{EL}	Ref
N6	138	327	335	600	0.11	11.4	632	55
N7	-	-	332	431	0.01	-	-	56
N8	-	-	330	58	-	-	-	57
N9	-	417	335	601	0.05	9.3	635	59

[a] λ_{abs} and λ_{em} (nm) in toluene solution

Compounds **N13**, **N14**, **N15**, **N16, N17**, **N18**, **N19**, and **N20** consisting of NI moiety as an acceptor and phenothiazine as a donor chromophore along with various other donors, such as carbazole, ferrocene and triphenylamine, were reported by *Poddar et al* (Scheme 5)[61]. The phenothiazine donor moiety was substituted with 4-ethynyl-1,8-naphthalimide on one side and different donors such as phenothiazine, carbazole, ferrocene and triphenylamine on the opposite side.

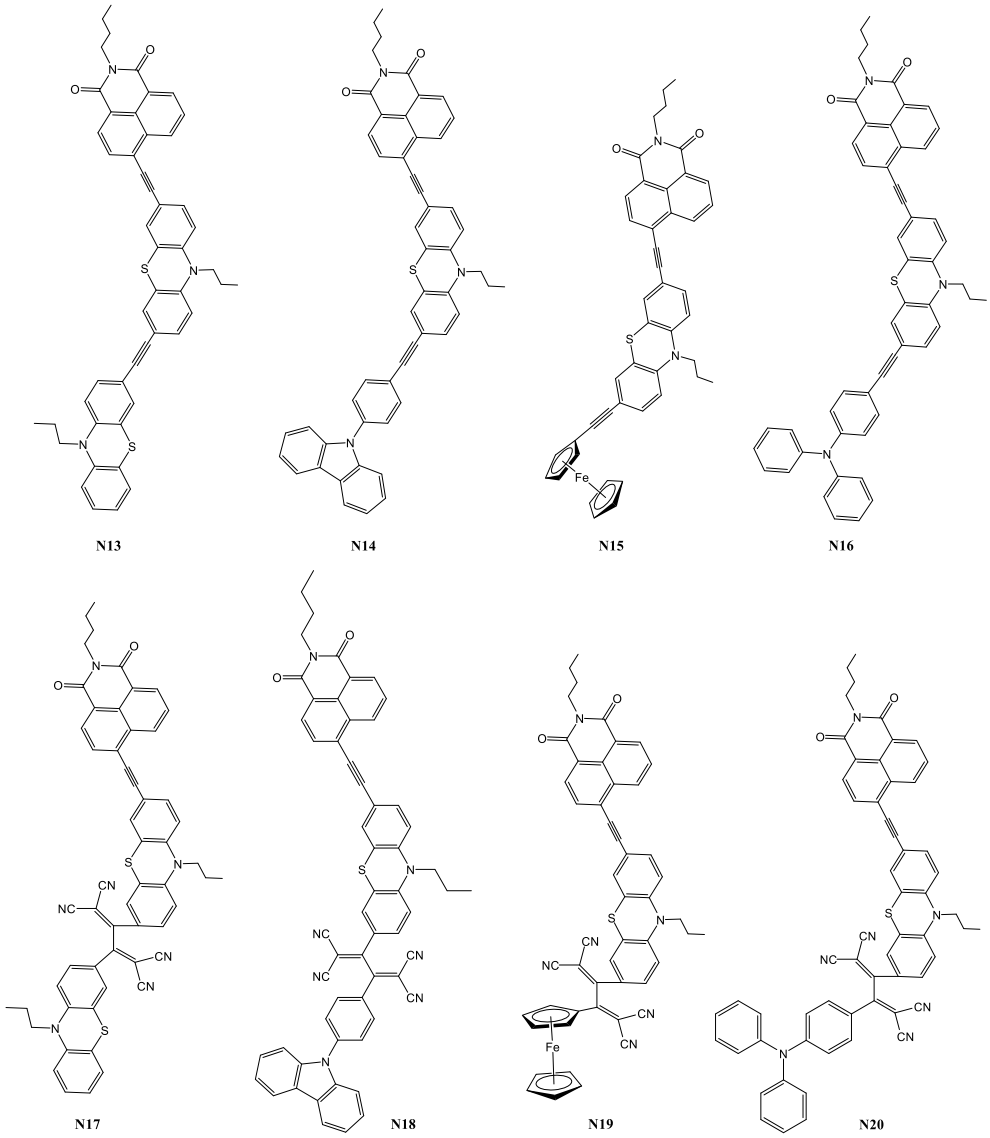

Scheme 5. Phenothiazine containing derivatives of NI

The NI acceptor moiety and phenothiazine-based chromophores were arranged in D-π-D-π-A, D'-π-D-π-A, D-A'- D-π-A and D'-A'-D-π-A manner. Compounds **N13**, **N14**, **N15**, and **N16** were synthesized via Pd-catalyzed Sonogoshira cross-coupling reaction. Compounds **N17**, **N18**, **N19**, and **N20** were obtained using [2+2] cycloaddition-electrocyclic ring opening reaction of **N13**, **N14**, **N15**, **N16** and tetracyanoethylene (TCNE). The absorption spectra of dichloromethane (DCM) solutions of compounds **N13**–**N16** and **N17**–**N20** are discussed[61] further. The absorption spectra of compounds **N13**–**N16** exhibited maxima in the range of 325–600 nm. The additional lower intensity absorption peaks were also observed for compounds **N13**, **N14**, **N15**, and **N16** at 445 nm, 445 nm, 448 nm, and 446 nm,

respectively, due to ICT which happened due to donor-acceptor interactions. The absorption maxima of compounds **N17**–**N20** were red-shifted when compared to the emission maxima of compounds **N13**–**N16.** Compounds **N17**, **N18**, **N19**, and **N20** also showed additional absorption peak due to ICT at 554 nm, 548 nm, 539 nm, 495 nm, respectively. A comparative study of variation of different donors of compounds **N13**, **N14**, **N15**, and **N16** revealed that a change in the donors' strength does not have influence on the optical properties. On the other hand, the introduction of 1,1,4,4-tetracyanobuta-1,3-diene (TCBD) in compounds **N17**, **N18**, **N19**, and **N20** leads to stronger donor-acceptor interactions, consequently, red shift in absorption spectra bands compared, low HOMO/LUMO levels and stabilized LUMO energy levels compared to those of **N13**, **N14**, **N15**, and **N16.** The experimental results were proved by theoretical calculations via density functional theory (DFT) and time-dependent functional theory (TD-DFT) methods.

2.2.3 Dihydroacridine substituted 1,8-naphthalimides

9,9-Dimethyl-9,10-dihydroacridine (further dihydroacridine) is a 9-membered aromatic ring that contains two phenyl rings and has a nitrogen heteroatom in its central ring. Photophysics and electronic behavior of dihydroacridine and its derivatives have recently been well studied theoretically and experimentally[62]. Dihydroacridine derivatives have been widely applied to emissive layers and hole-transport layers in the fabrication of OLEDs[64]. Redox behavior, optical properties, and electronic properties can be finely tuned by structural modification in the dihydroacridine moiety, particularly by extension of p-conjugation and incorporation of electron push-pull action together with various acceptors[63]. Dihydroacridine derivatives have been widely reported as blue and green TADF emitters[62]. Dihydroacridine-based donors are predominantly employed in blue and green TADF emitters for their favorable steric effects in constructing the twisted donor-acceptor structures for TADF emitters with small ΔE_{ST} values. In addition, due to the rigidness of diphenyl groups of dihydroacridine moiety, TADF emitters with dihydroacridine as a donor are usually little affected by concentration quenching[62-64]. The incorporation of dihydroacridine donor moiety(s) into the various positions of NI acceptor can potentially influence the absorption and emission properties toward red shift (above 600 nm). Compounds **N21** and **N22** containing rigid dihydroacridine donor moiety and its derivative at C-4 position of NI moiety were reported by *Zeng et al.* as orange-red emitters (Scheme 6)[62]. Compounds **N21** and **N22** exhibited small ΔE_{ST} values of 0.09 eV and 0.17 eV, respectively. Such small ΔE_S values are highly favorable for efficient RISC process. Consequently, the compounds exhibited very good orange/red TADF characteristics. Compounds **N21** and **N22** exhibited high thermal stabilities with 5% weight loss temperatures of 374°C and 412°C, respectively. The glass temperatures of compounds **N21** and **N22** were 155°C and 188°C, respectively. The absorption maxima of the solutions of compounds **N21** and **N22** appeared at around 370 nm. Another very weak absorption peak was observed at 460 nm. It could be attributed to ICT from the dihydroacridine donor moiety to the NI acceptor moiety.

Compounds **N21** and **N22** were doped into the mCPCN host with different doping concentrations to act as the emitting layers in the OLED based on these materials. OLEDs based on **N21** and **N22** exhibited EQE values of 23.4% and 29.2%, respectively. Characteristics of OLED based on compound **N22** with EQE of 29.2% were among the best for orange/red TADF OLEDs[62]. The spectra of electroluminescence of OLEDs based on **N21** and **N22** exhibited the maxima at 597 nm, and 584 nm, respectively. The turn-on voltage values of devices based on compounds **N21** and **N22** are the same, i.e., 3.0 V. The maximum power efficiency values of the devices based on compounds **N21** and **N22** are 53.1 lm W^{-1}, 79.7 lm W^{-1}, respectively. Compounds **N23**, **N24**, and **N25** containing phenyl or *tert*-butyl groups attached to acridine moiety were used as red TADF emitters for solution-processable OLEDs (**Scheme 6**)[63]. Compounds **N23**, **N24**, and **N25** exhibited good solubility in a wide range of solvents, outstanding thermal stability, and good capability of film forming. The 5% weight loss temperatures of compounds **N23**, **N24**, and **N25** ranged from 399–439°C. The glass temperatures of the compounds were observed in the range of 173–223°C. The host that was found suitable for materials **N23**, **N24**, and **N25** in making solution processable OLEDs was 1,3-bis(N-carbazolyl)benzene (mCP). The suitable selection of a host can help in the exploitation of favorable electronic states for making efficient OLEDs. The application of compound **N25** in OLED resulted in record-high EQE of 22.5% for solution processed red TADF OLEDs. It was reported that such systems could open new opportunities for developing new kind of solution processable TADF systems to achieve high-efficiency OLEDs[63]. Materials **N23**, **N24** and **N25** were doped into the mCP or mCPCN host and served as emitting layers in the OLED. The devices based on compounds **N23**, **N24**, and **N25** as emitters with mCP as host exhibited maximum EQE values of 9.0%, 11.5%, 22.5%, respectively. The turn-on voltage values of the devices based on compounds **N23**, **N24**, and **N25** as emitters with mCP as host are 5.0 V, 4.0 V, 7.0 V, respectively. The power efficiency values of the devices based on compounds **N23**, **N24**, and **N25** as emitters with mCP as host are 5.3 lm W^{-1}, 10.3 lm W^{-1}, 9.4 lm W^{-1}, respectively. The devices based on compounds **N23**, **N24**, and **N25** as emitters with mCP as host exhibited CIE values of (0.58, 0.41), (0.57, 0.42), (0.60, 0.40), respectively. The devices based on compounds **N23**, **N24**, and **N25** as emitters with mCPCN as host exhibited maximum EQE values of 9.4%, 15.1%, 7.6%, respectively. The turn-on voltage values of the devices based on compounds **N23**, **N24**, and **N25** as emitters with mCPCN as host are 8.0 V, 7.5 V, 7.5 V, respectively. The power efficiency values of the devices based on compounds **N23**, **N24**, and **N25** as emitters with mCPCN as host are 4.5 lm W^{-1}, 8.2 lm W^{-1}, 3.8 lm W^{-1}, respectively. The devices based on compounds **N23**, **N24**, and **N25** as emitters with mCPCN as host exhibited CIE values of (0.58, 0.41), (0.52, 0.42), (0.59, 0.41), respectively.

Compounds **N26** and **N27** with NI as an acceptor moiety and dihydroacridine as donor moiety were reported[58,59] (**Scheme 6**). OLED based on compound **N26** with mCP host at 5% doping ratio showed electroluminescence peak at 629 nm, exhibited EQE of 0.89% and EQE of 0.89% when it was prepared by using the vacuum deposition technique. Meanwhile, in solution-processed mode OLED with compound **N26** exhibited EQE of 0.80% and electroluminescence peak at 631 nm. The D-A-D

architecture variation and wedge-shape configuration of compound **N26** lead to the reduction of ΔE_{ST} value to 0.07 eV. It exhibited TADF emission in deep red to near infra-red (DR-NIR) region. Compound **N26** exhibited good thermal stability, with 5% weight loss temperatures at 392°C. It showed glass transition temperatures of 385°C. Compound **N27** also exhibited good thermal stability with 5% weight loss temperatures at 349°C. Compound **N27** exhibited no glass temperature. There were no morphological changes in the long range of temperature region before its high melting temperature (T_m) of 329°C. The absorption maxima of compounds **N26** (toluene solution) and **N27** (THF solution) were found in the range of 283–380 nm. This absorption could be attributed to π- π^* transition of local excited (LE) states. There were additional absorption bands observed for both **N26** and **N27** in the range of 450–471 nm which were due to ICT between NI acceptor moiety and dihydroacridine donor moiety. The emission maxima of the solutions of compounds **N26** and **N27** appeared in the range of 600–654 nm. The EQE based on compound N27 obtained through vacuum deposition technique was found to be of 5.38% at electroluminescence peak of 595 nm.

There are several factors impacting the efficiency of OLEDs. One of the important factors is dipole orientation of organic emitters[64]. It has significant impact on the optical outcoupling efficiency, hence it also affects the performance of the OLED device. Controlling the dipole orientation of organic emitters remains a challenge in the field of OLEDs. *Zeng et al* reported on compounds **N28** and **N29** and demonstrated an efficient method of controlling the dipole orientation of organic emitters (Scheme 6)[64].

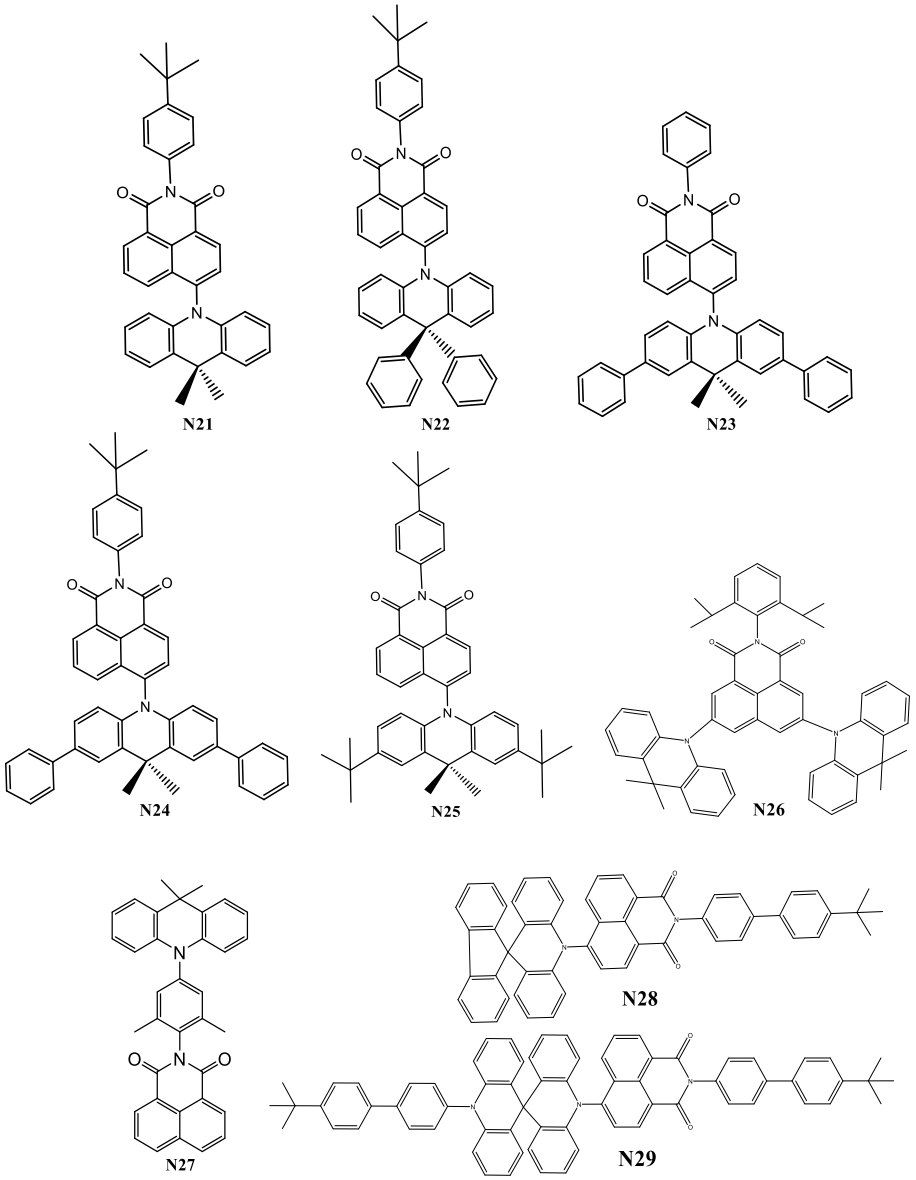

Scheme 6. NI derivatives containing dihydroacridine units

Compound **N29** was designed in a linear strain line-axis manner through NI-dihydroacridine (A-D) framework that controls the dipole orientation. It reached 95% of horizontal ratio of emitting dipole which is higher than that of isotropic emitters with 75%. Moreover, OLED based on the **N29** compound reached outstanding optical outcoupling efficiency of 43.2% which is one of the highest for red electroluminescent devices.

Table 4. Characteristics of derivatives **N21**–**N29** and of OLEDs based on them

Materials	T_g, (°C)	T_{ID}, (°C)	λ_{abs}[a], (nm)	λ_{em}[a], (nm)	ΔE_{ST}, (eV)	EQE_{max}, (%)	λ_{EL}	Ref
N21	155	374	370/460	582	0.09	23.4	597	61
N22	188	412	370/450	570	0.17	29.2	584	
N23	-	-	330	58	-	-	-	62
N24	-	417	335	601	0.05	9.3	635	
N25	-	-	335	388	-	-	-	
N26	385	392	283/471	654	0.07	0.89	629	58
N27	-	349	350/450	600	0.13	5.38	595	59
N28	-	-	<380	625	0.06	-	610	64
N29	-	-	<380	628	0.05	22.3	615	

Compounds **N28** and **N29** were synthesized by Pd-catalyzed C-N coupling reaction. The HOMO/LUMO levels of compounds **N28** and **N29** measured by cyclic voltammetry were -5.31/-3.21 eV and -5.34/-3.30 eV, respectively. The compounds **N28** and **N29** with 1.5 wt% was doped into the mCPCN host as emitting layer in the OLED based on these materials. Compounds **N28** and **N29** showed ΔE_{ST} values of 0.06 eV and 0.05 eV, respectively, and exhibited optical out-coupling efficiency of 40.3% and 43.2%, respectively. Compounds **N28**, **N29** exhibited red EL peak at 610 nm and 615 nm, respectively. **N28** showed EQE of 22.5% and the CIE values of (0.59, 0.41). **N29** showed EQE of 22.3% and the CIE value of (0.60, 0.40). Both compounds exhibited identical turn on voltage of 3.1 V.

2.2.4 Triphenylamino-substituted 1,8-naphthalimides

Much attention has been paid to triarylamines and especially triphenylamines during the recent years[66]. Triphenylamine (TPA) is employed as a molecular core to build various branched and complex molecules due to its unique star-shaped structure. It possesses outstanding electron donating abilities. Its derivatives are favorable for device fabrication[66]. Owing to their redox activity, fluorescence, and hole-transporting capabilities via radical-cation species, triphenylamine-based compounds are frequently employed as both molecular electronic materials and luminous probes[65]. Triphenylamines show an extended π-conjugation compared to other donors such as phenothiazine, phenoxazine, acridine, etc., which allows TPA derivatives to exhibit a red-shifted absorption and emission[66]. Compounds containing NI moiety as an electron acceptor (A) and TPA moiety as an electron donor (D) are suitable for the fabrication of highly efficient TADF OLEDS[65], NI acceptor moiety and TPA donor unit can be combined in various ways depending on the requirement. For example, such combinations of the moieties are possible: NI-TPA (D-A) through direct linkage, NI- π-TPA (D- π-A) through π-linkage and NI-π-TPA-π-NI (A- π-D- π-A) through two π -linkages etc[65-72]. By carefully selecting the donor, acceptor unit(s) and π -linker between them, the material properties can be tuned easily, along with the HOMO and LUMO levels of the materials. Compounds **N30**, **N31**, **N32**, and **N33** as ambipolar organic semiconductors with NI moiety as an acceptor and TPA as donor were reported[65] (**Scheme 7**)[65]. These compounds were synthesized by using Suzuki

cross-coupling reaction. All four compounds exhibit considerably high thermal stability. The temperatures of onset thermal decomposition of compounds **N30**, **N31**, **N32**, and **N33** ranged from 429°C to 483°C. All four compounds exhibited the ability of glass formation. Their glass transition temperatures were in the range from 45°C to 84°C. The fluorescence spectra of the solutions in non-polar solvent cyclohexane and of neat films of these compounds were recorded. The emission maxima (λ_{em}) observed for the solutions were in the range from 465 nm to 506 nm whereas for the neat films, they were found to be in the range from 493 nm to 541 nm. The absorption maxima (λ_{abs}) of the solutions of the compounds in non-polar solvent ranged from 407 nm–434 nm whereas those of the neat films were found to be in the range from 425 nm to 448 nm. The low energy and high wavelength absorption bands of the films are broader and slightly red-shifted when compared to the absorption bands recorded for the solutions in non-polar solvent. This observation is attributed to the smaller dihedral angles in neat film which gives rise to more pi-conjugation (stronger intermolecular interactions) and decreased HOMO-LUMO gap and consequently to 20 nm red shift[66]. Three derivatives of triphenylamine and NI **N34**, **N35**, and **N36** were reported as hole-transporting materials for OLEDs[66] (Scheme 7).

Compounds **N34**, **N35**, and **N36** were synthesized by using Suzuki cross-coupling reaction between 4-bromo-N-phenyl-1,8-naphthalimide and triphenylamine moieties. The compounds exhibited outstanding high thermal stabilities. The 10% weight loss temperatures of these compounds were in the range from 398°C to 527°C. The melting points of these compounds were in the range from 264°C to 477°C. Two compounds (**N34** and **N35)** showed the ability to form glasses. They both show identical glass transition temperatures of 254°C. Such high thermal stability and high glass transition temperatures of the compounds are very much in demand for the optoelectronic materials especially for those applied in OLEDs. The absorption spectra and the fluorescence spectra of the solutions in polar solvent chloroform and of spin-casted thin films of compounds **N34**, **N35**, and **N36** were recorded. For chloroform solutions, the absorption maxima (λ_{abs}) of these compounds were observed at around 312 nm to 326 nm due to characteristic π- π^* transition; the ICT observed for these compounds was around 430–433 nm due to charge transfer between NI acceptor moiety and TPA donor moiety. The absorption maxima (λ_{abs}) of solid-state samples were observed in the similar range (316–336 nm, 435–437 nm), however a slight shift in peak wavelength could be due to a stronger π-conjugation caused by the restricted molecular vibration and rotation[66].

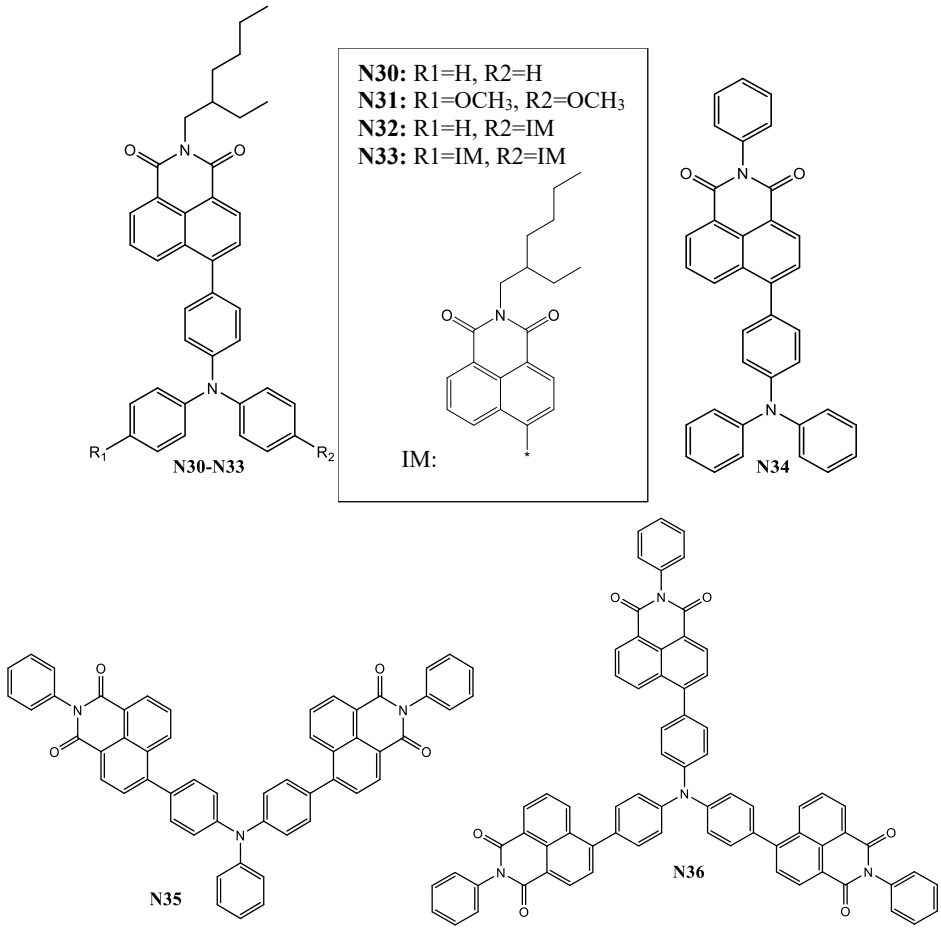

Scheme 7. TPA containing NI derivatives

The emission maxima of the solutions of compounds **N34**, **N35**, and **N36** were observed at 599 nm, 580 nm, and 564 nm, respectively. It was shown that with the increase in number of naphthalimide groups, the emission maxima blue-shifted because of the electron delocalization between NI acceptor and TPA donor. The fluorescence maxima of these compounds in solid state exhibited at shorter wavelengths in the range of 550–555 nm when compared to the fluorescence maxima of the solutions. The photoluminescence quantum yields of the solutions followed the same trend as absorption maxima of the solutions. They both increase as the number of naphthalimide moieties increase. The photoluminescence quantum yields of the solutions of compounds **N34**, **N35**, and **N36** were found to be of 0.34, 0.49, 0.55, respectively. Compound **N34** doped in BCP (dimethyl-4,7-diphenyl1,10-phenanthroline) was employed as hole-blocking material OLED device with the following structure: ITO/PEDOT: PSS/**N34**:CBP/BCP/LiF/Al. Yellowish green electroluminescence with a maximum brightness of 10 404 cd m-2 at an applied voltage of 19 V was observed. D-A type compounds **N37** and **N38** with NI moiety as

an acceptor and TPA as a donor with ethynyl linkages between electrophores were reported[67] (Scheme 8)[67]. Compounds **N37** and **N38** were synthesized by using Heck-coupling reactions of 4-bromo-naphtahlimide with alkyl group at N-centre and TPA with olefin linkages. Compounds **N37** and **N38** formed molecular glasses and exhibited glass transition temperatures of 56°C and 75°C, respectively. Both compounds possessed excellent thermal stabilities with 5% weight loss temperatures of 350°C and 363°C. Fluorescence quantum yields of the dilute solutions of the compounds **N37** and **N38** were found to be 0.065 to 0.72 whereas those of the solid films were 0.028 and 0.034, respectively. It was observed that as the number of naphthalimide groups increased the fluorescence quantum yield also increased. The absorption maxima of solid films of compounds **N37** and **N38** exhibited red shifts by 68 nm and 89 nm, respectively, when compared to those of absorption maxima of toluene solutions. Similarly, the emission maxima of the solid films of compounds **N37** and **N38** exhibited red shifts of 46 nm, 61 nm, respectively due to strong intermolecular interactions of donor and acceptor moieties of compounds **N37** and **N38**. It was observed that the Stokes shifts of the solutions of compounds **N37** and **N38** increased with the increase of the solvent polarity. The ionization potential values of compounds **N37** and **N38** measured by the cyclic voltammetry were found to be 5.22 and 5.27 eV, and the ionization potentials measured by using electron photoemission technique were found to be 5.47 and 5.49 eV.

Li et al. reported a D-pi-A type compound **N39** consisting of NI moiety as an acceptor and TPA as a donor moiety coupled by -NH-N= bridge with N-alkyl chain extension[68] (Scheme 8). Compound **N39** was synthesized via simple condensation reaction between N-alkyl-1,8-naphthalimide with -NHN= bridge donor moiety and TPA donor moiety. The development of highly emissive compounds with shifted red wavelengths of emission maxima is essential for advancing optoelectronics and materials science. The absorption and emission spectra of the solutions of compound **N39** in the different solvents (from the most polar solvents to the least polar ones) were recorded. **N39** was highly emissive in nonpolar media. The most intensive peak was observed for the solution of **N39** in dioxane with the emission maximum at 540 nm. **N39** was also highly emissive with the similar emission peak at 550 nm when it was molecularly dispersed in polycarbonate film. As a result of tightly molecular packing and extensive pi-conjugation, the emission maxima of compound **N39** exhibited at the red region 633 nm in the solid powder state.

Compound **N40** containing a TPA moiety attached at C-1, C-2, C-6, and C-7 positions of NI acceptor moiety was reported[69] (Scheme 8). Optical, electronic, and charge-transporting properties to explore compound **N40** as luminescent material were explored. The architecture of compound **N40** is designed in D- π-A manner. Compounds **N41**, **N42**, and **N43** consisting of NI moiety as an acceptor, TPA as a donor and acetylene unit as π-conjugation bridge with D- π-A, A-π-D-A, A-π-D- π-A, architecture, respectively, were reported as highly fluorescent materials for OLEDs[70] (Scheme 8). Compounds **N41**, **N42**, and **N43** were synthesized by using the Sonogashira reaction of N-butyl-4-bromo-1,8-naphthalimide and mono-, di-, and tri-ethylated TPA. The absorption spectra and emission spectra of toluene and dichloromethane (DCM) solutions of compounds **N41**, **N42**, and **N43** were measured.

The absorption maxima of toluene and DCM solutions of the compounds appeared in the similar ranges of 445–448 nm and 448–454 nm, respectively. The emission maxima of the compounds of DCM solutions of **N41**, **N42**, and **N43** showed red shifts (617–639 nm) when compared to the emission maxima of the toluene solutions (502–530 nm) due to the difference in polarity of the solvents. Compounds **N44**, **N45**, and **N46** consisting of TPA moiety as a donor unit and NI as an acceptor moiety designed in D-pi-D architecture manner (Scheme 9) were reported[71].

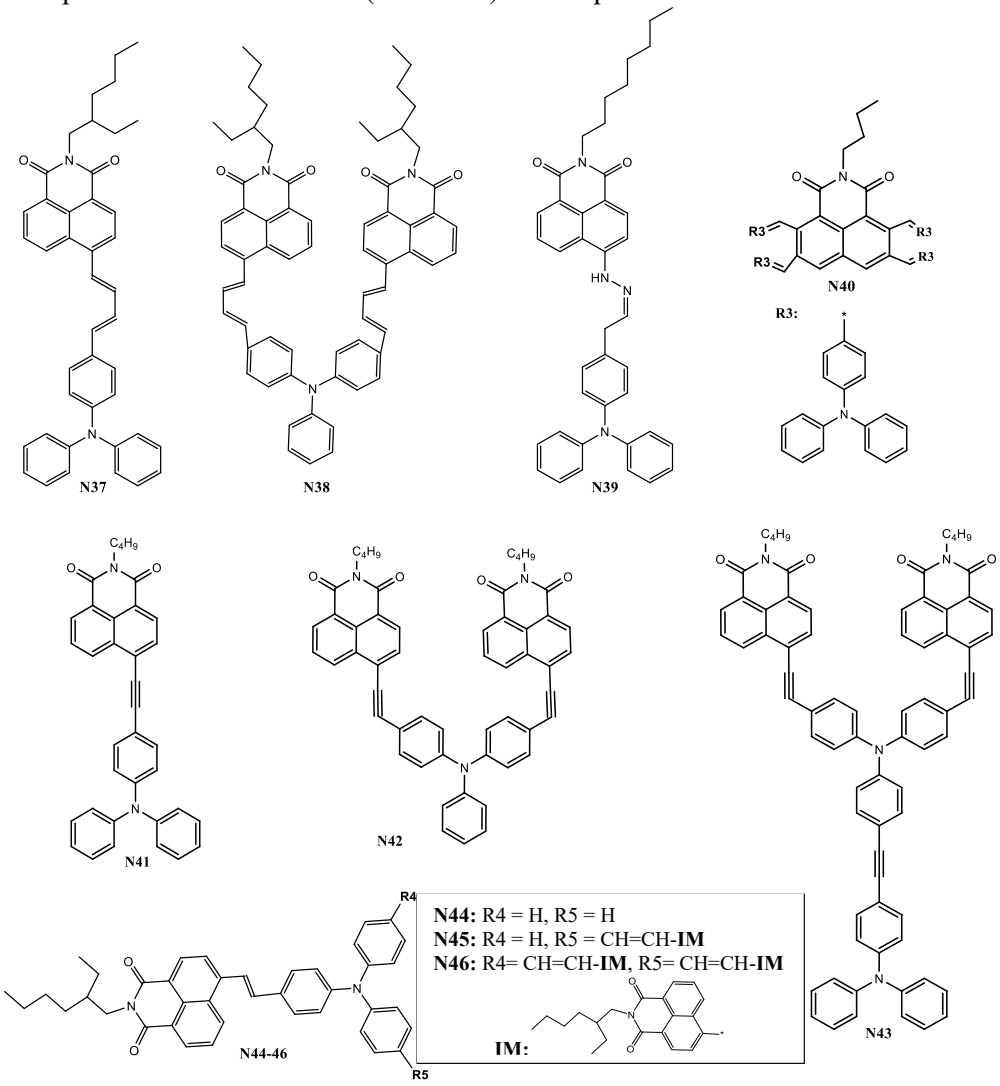

Scheme 8. TPA containing derivatives of NI

Compounds **N44**, **N45**, and **N46** were synthesized by using palladium-catalyzed Heck reaction between N-ethylhexyl-4-bromo-1,8-naphthalimide and vinyl-TPA moiety. These compounds showed outstanding thermal stabilities with 5% weight loss temperatures ranging from 431°C to 448°C. They formed molecular glass with glass-

transition temperatures from 55°C to 107°C. The 5% weight loss temperature, melting point, and glass transition temperature values showed an increasing trend in the order **N44**<**N45**<**N46**. The HOMO/LUMO energy values of compounds **N44**, **N45**, and **N46** are -5.18/-3.06 eV, -5.24/-3.07 eV, -5.25/-3.08 eV, respectively. The slight variation of HOMO/LUMO energy values can be attributed to the variation of electron withdrawing nature towards NI moiety or arm. The absorption maxima of neat films of compounds of **N44**, **N45**, and **N46** showed red shifts compared to those of THF solutions. The emission maxima of neat film of compound **N46** also showed red shift compared to those of THF solution. The solution and the film of compound **N45** showed the same wavelengths of emission intensity maxima at 643 nm, while PL spectrum of the film of compound **N44** showed blue shift compared to that of THF solution.

Compounds **N47**, **N48**, and **N49** in the structures of which the acceptor NI moiety and donor TPA moiety both are connected by ethynyl linkages were synthesized to study the correlation between the thermal properties, electrochemical properties, charge transporting properties, and their structures (**Scheme 9**)[72]. These compounds were synthesized by using the Sonogashira cross-coupling reaction between N-ethylhexyl-4-bromo-1,8-naphthalimide and acetylene-TPA moiety. Compounds **N47**, **N48**, and **N49** showed outstanding thermal stabilities. The temperatures of the onsets of their thermal degradation ranged from 421°C to 462°C. The presence of ethynyl linkages in the chemical structures of compounds **N47, N48,** and **N49** influenced the high hole mobility and high TADF efficiency which were due to the extended planarity and conjugation. These observations revealed that compounds **N47**, **N48**, and **N49** were great candidates as hole-transporting and emitting materials for OLEDs. In electrophores previously reported compounds **N44**, **N45**, and **N46,** the chromophores are connected through ethenyl, while in compounds in **N47**, **N48**, and **N49** the donor and acceptor units are linked through ethynyl linkages. The ethenyl linkages in compounds **N44**, **N45**, and **N46** and ethynyl linkages in compounds **N47**, **N48**, and **N49** prevent their fragments from free rotation which directly impact the optical, thermal and electronic properties of the compounds and consequently affect the efficiency of OLEDs. Rotation around the double bond or triple bond exhibit a unique type of isomerism that requires more energy for free rotation, thus the rotation around these compounds is restricted (electron overlap at both above and below the plane), which effects the properties (optical, thermal, electronic) of compounds **N44**, **N45**, and **N46** and **N47**, **N48**, and **N49**. Star-shaped NI derivatives **N50**, **N51**, and **N52** containing TPA donor moiety were synthesized (**Scheme 9**)[73]. The study of photophysical properties of compounds **N50**, **N51**, and **N52** revealed the occurrence of considerable fluorescence quenching due to N-ethyl4-piperidin-1-yl-1,8-naphthalimide parent chromophore. The excitation of N-ethyl4-piperidin-1-yl-1,8-naphthalimide chromophore into TPA or 1,8-naphthalimide moieties during the absorption process which leads to the formation of effective single energy transfer and photoinduced electron transfer (PIET). Consequently, the fluorescence lifetimes of compounds **N50**, **N51**, and **N52** are considerably reduced due to the intermolecular PIET process between the NI acceptor moiety and TPA donor moiety. The solutions of compounds **N50**, **N51**, and **N52** exhibited absorption

maxima in the range of 396–420 nm. The solutions of compounds **N50**, **N51**, and **N52** exhibited emission maxima in the range of 508–518 nm. The HOMO levels of compounds **N50**, **N51**, and **N52** are 5.47 eV, 5.43 eV, 5.36 eV, respectively. The HOMO levels of these compounds were obtained using cyclic voltammetry.

Compounds **N53**, **N54**, and **N55** consisting of NI moiety as an acceptor and TPA as a donor moiety were reported (**Scheme 9**)[74].

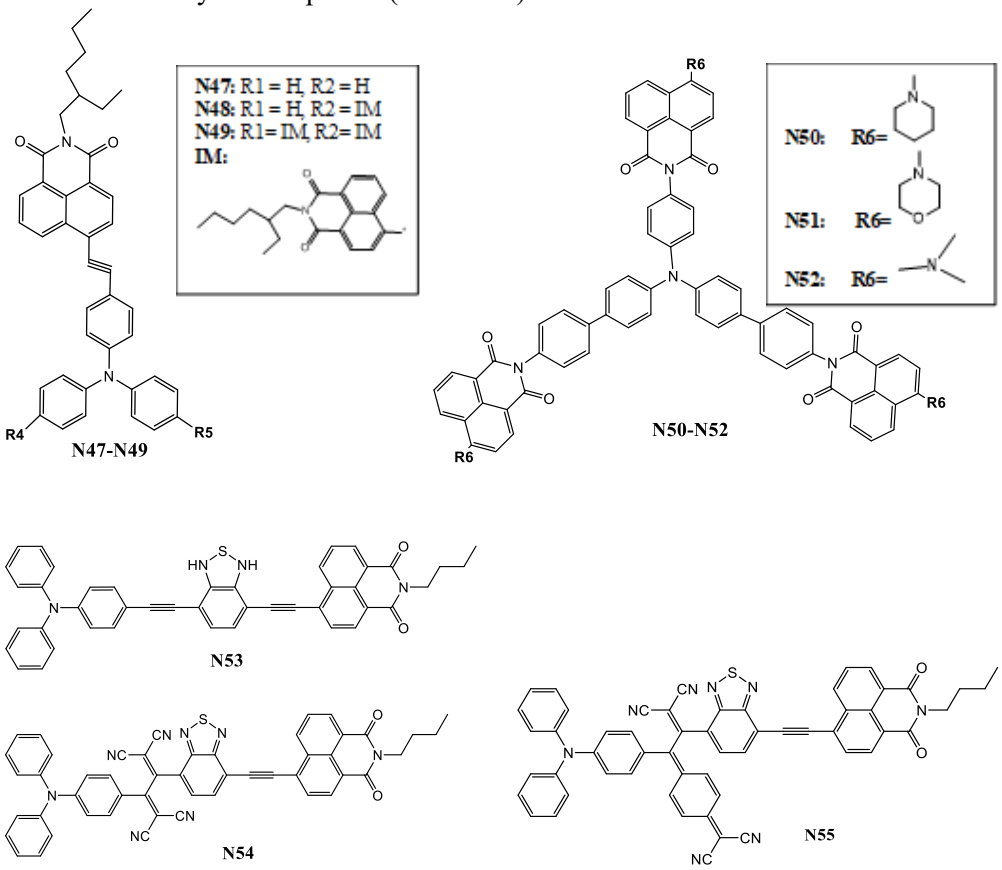

Scheme 9. NI-TPA containing derivatives

Compounds **N53**, **N54**, and **N55** were synthesized via Pd-catalyzed Sonogoshira cross-coupling reaction between benzothiadiazole, as the central core unit together with TPA and 1,8-naphthalimidemoiety serves as acceptor units, and TPA as donor units followed by [2+2] cycloaddition-electrocyclic ring opening reaction with Tetracyanoethylene (TCNE) and 7,7,8,8-tetracyanoquinodimethane (TCNQ). Along with NI moiety acceptor, benzothiadiazole (BTD) used in compound **N53**, Tetracyanoethylene (TCNE) used in compound **N54**, 7,7,8,8-tetracyanoquinodimethane (TCNQ) used in compound **N55** are used as additional electron withdrawing groups. The absorption spectra of DCM solutions of compounds **N53**, **N54**, and **N55** were recorded. The solutions of the compounds exhibited absorption maxima around 408–455 nm, which could be attributed to π-π^* transition.

Compounds **N54** and **N55** showed ICT at 455 nm and 690 nm, respectively. The optical band gaps of the compounds **N53**, **N54**, and **N55** are 2.0 eV, 1.7 eV, 1.4 eV, respectively. The HOMO and LUMO values of these compounds are -5.29 eV, -5.39 eV, -5.14 eV and -3.48, -3.68 eV, -3.72 eV, respectively. The HOMO and LUMO levels of these compounds were obtained with cyclic voltammetry.

2.2.5 Carbazole-substituted 1,8-naphthalimides

Nine compounds (**N56**–**N64**) containing NI moiety as an electron acceptor and carbazole as an electron donating group were reported (**scheme 10**)[197]. Compounds **N56**–**N64** were synthesized by using palladium-catalyzed C-N and C-C coupling reactions between 4-bromo-*N*-ethylhexyl-1,8-naphthalimide and various carbazole derivatives. Compounds **N56**–**N64** showed high thermal stabilities with the 5% weight loss temperatures ranging from 351°C to 476°C. Compounds **N56**–**N64** were able to form glass with glass transition temperatures ranging from 30°C to 87°C. The CV measurements of the compounds exhibited solid state ionization potentials and their values ranged from 5.46 eV to 5.76 eV, while the electron affinity values of these compounds ranged from -3.04 eV to -2.92 eV. The ionization potentials of the compounds which were measured by photoemission spectroscopy appeared in the range of 5.76–6.09 eV. The onset oxidation potential values of compounds **N56**–**N64** obtained by using CV ranged from 0.66–0.96 eV. The PLQY values of solutions of compounds **N56**–**N64** were showed in the range of 0.66 to 0.83, whereas the PLQY values of solid films of the compounds **N56**–**N64** were recorded in the range of 0.01 to 0.45. The absorption maxima of solution of the compounds **N56**–**N64** were in the range of 336–433 nm. The emission maxima of solution and solid films of compounds **N56**–**N64** ranged from 520–579 nm and 501–563 nm, respectively.

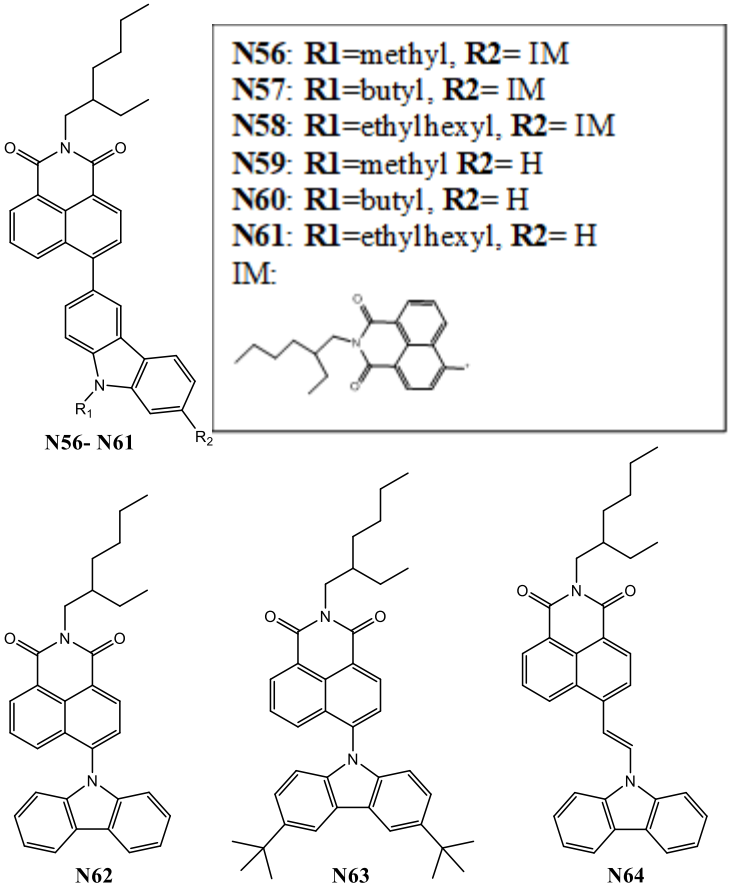

Scheme 10. NI-carbazole containing derivatives

Three compounds (**N65**–**N67**) having NI moiety as an electron acceptor and carbazole as an electron donating group were reported (Scheme 11)[198]. Compounds **N65**–**N67** were synthesized by using palladium catalyzed reactions between 4-bromo-1,8-naphthalimide with three different N-centres methyl, cyclohexyl, phenyl, and carbazole moiety. The absorption and emission properties of these compounds were recorded from low-polarity solvents to high-polarity solvents. The obtained absorption and emission properties revealed that as the solvent polarity increases exhibited red shifts, this effect attributed to the absorption and emission properties influenced by polarity of solvents. The stokes shifts of compounds **N65**–**N67** were in the range of 6169–6629 cm^{-1}. The stokes shift of these compounds indicated that stokes shifts are more significant in polar solvents compared to non-polar solvents because of polar solvents possessing efficient excited state. Two compounds, **N68** and **N69,** containing the NI moiety as an acceptor and carbazole as a donor are connected through hydrazone bond were reported (Scheme 11)[199].

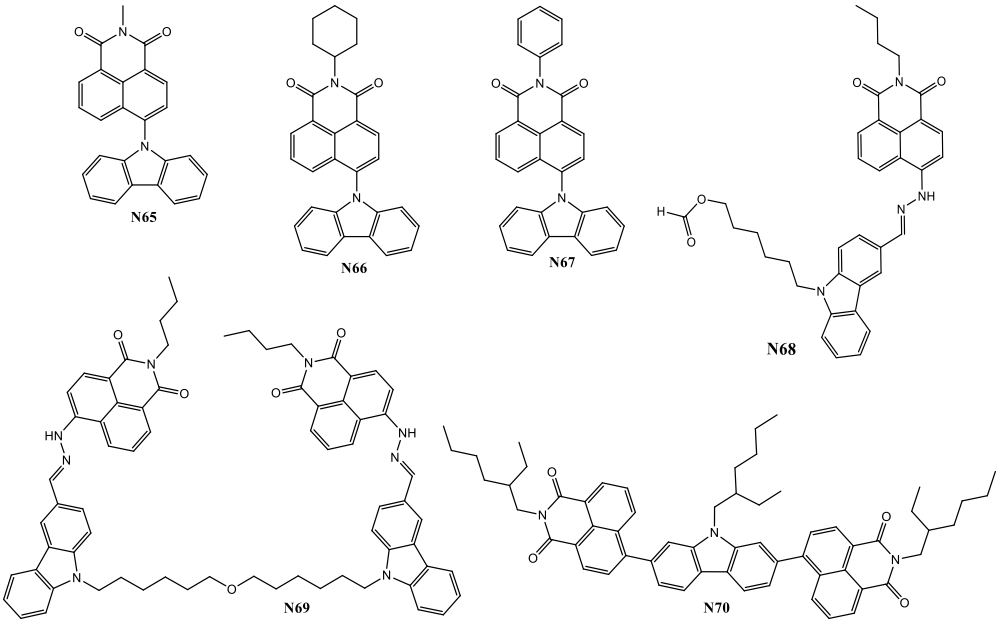

Scheme 11. NI-TPA containing derivatives

Compounds **N68** and **N69** are reported as efficient alternatives to traditional semiconductors based on inorganic materials in memory devices. Compounds **N68** and **N69** exhibited 5% weight loss temperatures are 266.3°C and 301.6°C, respectively. The HUMO and LUMO energy levels of compounds **N68** and **N69** are **-**5.73 eV and -3.35 eV. The absorption maxima of the solution and film of compound **N69** are 466nm and 494 nm, respectively, there was 28 nm red-shift from its solution state to thin film state due to the molecular stacking of compound **N69**. The emission maxima of compound **N69** exhibited at 610 nm. Compound **N70** containing A-D-A architecture having the NI moiety as an acceptor and carbazole moiety as a donor was reported (Scheme 11)[200].

Compound **N70** was synthesized by using Suzuki-Miyaura coupling reaction between 4-bromo-*N*-(2-ethylhexyl)-1,8-naphthalimide and carbazole derivative. Compound **N70** exhibited high thermal stability with 5% weight loss temperature of 438°C and glass transition temperature of 45°C. The ionization potential of the compound **N70** obtained by CV was found to be at 5.70 eV, while the ionization potential obtained by photoemission method was found to be at 5.90 eV. The electron affinity values were found to be at -3.42 eV.

2.2.6. Summary of the literature review

Even though the progress of OLEDs has been gradually continuing with advantages such as offering flat, thin, flexible and bright displays, there are still some areas OLEDs are lagging due to short lifetimes and insufficient color purity. Solution processable OLEDs are more promising than those fabricated by vacuum deposition technique for further development due to the simpler and more environmentally friendly technology. Most of the TADF-based materials could potentially help to

overcome some of the difficulties posed by OLEDs. To obtain TADF materials, there is a need to activate the RISC process which is usually possible for the compounds with donor-acceptor architecture having twisted structural variation with sufficient steric hindrance. Such compounds can achieve negligible singlet-triplet splitting. Most of the previously reported orange-to-red TADF emitters have poor PLQY despite having small singlet-triplet energy splitting due to aggregation quenching effects. Thereafter, many studies were reported to fulfil the requirements of orange-to-red TADF emitters based on just donor-acceptor combination without any structural variation which leads with little to no success. In addition, the development of orange/red TADF emitters is considerably slower when compared to that of blue and green TADF emitters. The development of orange-to-red TADF emitters has started to progress after beginning to use the rigid acceptors. However, the EQE values are relatively low due to poor PLQY values. This became the essential reason behind the lack of application of red emitters in the commercial market. By employing such rigid acceptors orange-to-red emitters with efficient TADF can be obtained. The later studies reported that non-radiative transition was relatively reduced by using a highly twisted and conjugated rigid acceptor with suitable incorporations of donors which consequently rises the EQE of OLEDs. Finding the appropriate rigid acceptors with suitable donor substitution and dipole orientation for orange-to-red TADF emitters was recently a challenge for researchers working on further development OLEDs emitting in orange-to-red region. 1,8-naphthalimide acceptor moiety can provide and fulfil the requirement posed by orange-to-red TADF emitters due to its rigidity and great electron withdrawing nature. In this review, the development of reported orange-to-red TADF emitters consisting of various donors, such as phenoxazine, phenothiazine, acridine and triphenyl amine being incorporated into the various positions (C-2, C-3, C-4, C-5, C-6, C-7) of 1,8-naphthalimide acceptor moiety, were briefly described and a comparative study of selected 1,8-naphthalimide -based derivatives is presented. The thermal, photophysical, and electrochemical properties of donor–acceptor conjugated systems containing 1,8-naphthalimide moiety are discussed. The influence of structural changes of donor moieties linked with 1,8-naphthalimide acceptor on thermal, photophysical, electrochemical properties, and on OLED performance are discussed. This review considers 70 derivatives of 1,8-naphthalimide. Most of the materials exhibited orange-to-red emission with emission wavelengths exceeding 600 nm. There were very few 1,8-naphthalimide derivatives which allowed to reach EQE of OLEDs in the range of 20 to 30%. By making appropriate modifications in the architectures of 1,8-naphthalimide derivatives combined with various donors, and proper substitution at N-imide center (for dipole orientation), efficient orange-to-red TADF emitters for of OLEDs can be developed.

3. EXPERIMENTAL SECTION

3.1 Instrumentation

The Nuclear magnetic resonance spectra (NMR) (^{1}H, ^{13}C and ^{19}F NMR) were recorded in deuterated chloroform ($CDCl_3$) by using a *Bruker Avance III 400* spectrometer at 400 MHz (^{1}H), 100 MHz (^{13}C) and 375 MHz (^{19}F)) frequency at room temperature. Chemical shifts (δ) are reported in ppm referenced to tetramethylsilane or the internal solvent signal.

The Infrared spectra (IR) in the range of 400–4000 inverse centimeters (cm^{-1}) were recorded on a *Perkin Elmer Spectrum BX II FT-IR* System. The spectra of solid compounds were performed for KBr 1pellets. The FT-IR spectra were analyzed as a function of transparency (T) expressed in percent against the wavenumber (ν) expressed in cm^{-1}.

The mass spectra were recorded by employing the electrospray ionization mass spectrometry (ESI-MS) method on an *Esquire-LC 00084* mass spectrometer.

Elemental analysis was done with an *Exeter Analytical CE-440 Elemental Analyzer*.

Differential scanning calorimetry (DSC) measurements were recorded by using *PerkinElmer DSC 8500* equipment at heating and cooling rates of 10°C/min in a nitrogen atmosphere.

Thermogravimetric experiments (TGA) were conducted by using a *PerkinElmer TGA 4000* apparatus at a heating rate of 20°C/min in a nitrogen atmosphere. The melting points were measured with a *MEL-TEMP* (Electrothermal) melting point apparatus.

The Ultraviolet-visible absorption spectra of dilute solutions and solid samples were recorded on a *PerkinElmer Lambda 35* spectrometer. The fluorescence spectra, fluorescence quantum yields (PLQY), and fluorescence decay curves of both solutions and solid films were recorded with a *FLS980* fluorescence spectrometer. An *Edinburgh Instruments FLS980* spectrometer and a *PicoQuant LDH-DC-375* laser (wavelength 374 nm) as the excitation source were used for recording photoluminescence (PL) decay curves and PL intensity dependencies on the laser flux of the samples at room temperature. The instrument response function (IR) for time-resolved fluorescence measurements was obtained by recording the temporal profile of the excitation light. For the measurements of scattered light, a dilute solution of colloidal silica (*Ludox, Aldrich, Inc.*) was used. An integrated sphere (inner diameter of 120 mm) spherical cavity calibrated with two analytical standards: quinine sulfate in 0.1 M H_2SO_4 and rhodamine 6G in ethanol was used for the measurements of fluorescence quantum yields.

Cyclic voltammetry (CV) measurements were performed by using a micro*Autolab III* (*Metrohm Autolab*) potentiostat-galvanostat equipped with the standard three-electrode configuration. A three-electrode cell equipped with a glassy carbon working electrode, an Ag/Ag (0.01 M in anhydrous DMF or DCM or THF) reference electrode, and a Pt wire counter electrode was employed. The measurements were conducted in anhydrous DMF/DCM/THF with 0.1 M tetrabutylammonium hexafluorophosphate ($Bu_4N(PF)_6$) as the supporting

electrolyte under the nitrogen atmosphere at a scan rate of 0.1 V/s. The measurements were calibrated by using a ferrocene/ferrocenium (Fc) system as an internal standard.

The photoelectron emission spectra for previously vacuum-deposited layers were recorded as reported previously[75]. The samples for photoelectron emission measurements were vacuum-deposited by using fluorine-doped tin oxide-coated glass slides as substrates. The photoelectron emission spectra were recorded in an air exploiting setup which included an *ASBN-D130-CM* deep-UV deuterium light source, a *CM110* 1/8m monochromator, and a *6517B Keithley* electrometer.

The charge-transporting properties of vacuum deposited films were estimated by employing the time-of-flight (TOF) technique while using an *EKSPLA NL300* laser (excitation wavelength of 355 nm), *6517B* electrometer (*Keithley*), and a *TDS 3032C* oscilloscope (*Tektronix*). By taking transit times (ttr) from the photocurrent transients at the applied voltage (U) and the thicknesses of the layers (d) measured by the charge extraction by the linearly increasing voltage (CELIV), the technique assuming the dielectric constant ε = 3 for the studied compounds, $\mu = d^2/(U \times ttr)$ were utilized to calculate charge mobilities.

The theoretical calculations were performed by using the *Gaussian 09* quantum chemical package[76]. The geometry optimization of the ground state of the compounds was done with the density functional (DFT) method with *B3LYP* functional along with the *6-31G* (d, p) basis set in vacuum. The absorption spectra of the molecules were calculated by means of the time dependent density functional theory technique (TDDFT) for 20 excited states.

The Lippert-Mataga model describes the Stokes shift in terms of the changes in the dipole moment which occurs upon excitation in the solvents of various dielectric constant (ε) or refractive index (n)[77]:

$$\Delta\nu = \frac{2\Delta f}{4\pi\varepsilon_o \hbar c a_3}(\mu_e - \mu_g)^2 + b \quad (1)$$

where the orientation polarizability of the solvent is defined as follows:

$$\Delta f = \frac{\varepsilon - 1}{2\varepsilon + 1} - \frac{n2 - 1}{2n^2 + 1} \quad (2)$$

$\hbar$ stands for the Planck constant, c is the light velocity in a vacuum, a stands for the Onsager radius,ε_o is the permittivity of vacuum. Each solvent has its own

values of ε, the dielectric constant, and *n*, the refractive index. The linear fit of the dependence of the Stokes shift value on Δf has slopes at 14 and 14.6 thousand cm^{-1} for pCzPPQ and mCzPPQ, respectively. These values correlate with the dipole moments of the emissive excited μ_e and ground μ_g states of the compounds. The slope value is proportional to $(\mu_e-\mu_g)^2$.

The fabrication of OLEDs

Indium tin oxide substrates were patterned and cleaned for the fabrication of OLEDs by using layer-by-layer thermal deposition. Current density-voltage and brightness-voltage characteristics were simultaneously recorded by using a source meter *Keithley 2400* and a certified photodiode *PH100-Si-HA-D0* together with *PCBased Power* and *Energy Monitor 11S-LINK* (developed by *STANDA*). An *Aventes AvaSpec-2048XL* spectrometer was employed to take the electroluminescence (EL) spectra of the devices at different voltages. By using brightness, current density, and the EL spectra, the current, power, and external quantum efficiencies were calculated. *Commission Internationale de l'Eclairage* (CIE 1931) chromaticity coordinates (x, y) and the color rendering index (CRI) were obtained by using the EL spectra and the software of an *FLS980* spectrometer.

3.2 Materials

9,9-Dimethyl-9,10-dihydroacridine, bromoethane, tetrabutylammonium bromide, phenylboronic acid, napthalen-1-ylboronic acid, 4-vinylphenylboronic acid, and 4-fluorophenylboronic acid, Bis(4-fluorophenyl) sulfone, 9*H*-carbazole, phenylboronic acid, *N*-bromosuccinimide(NBS), tetrakis(triphenylphosphine)palladium(0) ($Pd(PPh_3)_4$), sodium hydride (NaH), 10*H*-Phenoxazine, tri-*tert*-butylphosphine solution (1.0 M in toluene), palladium(II) acetate, sodium *tert*-butoxide, 10*H*-Phenoxazine, tri-*tert*-butylphosphine solution (1.0 M in toluene), palladium(II) acetate, sodium *tert*-butoxide, 1,4,5,8-naphthalenetetracarboxylic dianhydride, bromine, 2,6-dimethyl aniline, 4-bromo-2,6-dimethyl aniline, diphenylamine, 4-bromostyrene, diphenylaminophenyl boronic acid, palladium (II) acetate, tri-o-tolylphosphine, triethylamine, potassium hydroxide, propionic acid, and hydrochloric acid were purchased from Sigma Aldrich and used as received.

3.3 Synthesis

2,7-Dibromo-9,9-dimethyl-9,10-dihydroacridine (M1) was synthesized according to the reported procedure[78].

3,3′,5,5′-Tetrabromo-4,4′- difluorodiphenyl sulfone (M2) was synthesized according to the reported procedure[79].

3,3′,5,5′-tetraphenyl-4,4′-difluorodiphenyl sulfone (M3) was synthesized according to the reported procedure[79].

4-Bromo-*N*-(2-ethylhexyl)-1,8-naphthalimide (M4) was synthesized according to the reported procedure[80].

3,7-di-*tert*-butyl-10*H*-phenothiazine (M5) was synthesized according to the reported procedure[81].

2,7-di-*tert*-butyl-9,9-dimethyl-9,10-dihydroacridine (M6) was synthesized according to the reported procedure[82].

4,5-Dibromo-1,8-naphthalenedicarboxylic anhydride (M7) was synthesized according to the reported procedure[83].

4-vinyltriphenylamine (M8) was synthesized according to the reported procedure[84].

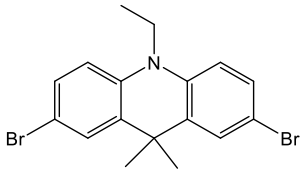

2,7-Dibromo-10-ethyl-9,9-dimethyl-9,10-dihydroacridine (A1):

2,7-Dibromo-9,9-dimethyl-9,10-dihydroacridine (0.7 g, 1.9 mmol) was dissolved in acetone (25 mL), tetrabutylammonium bromide (0.06 g, 0.1 mmol) and potassium hydroxide (0.31 g, 5.7 mmol) were added, and the mixture stirred for 30 min. Then, bromoethane (0.31 g, 2.85 mmol) was added dropwise to the reaction mixture with constant stirring and the mixture refluxed for 1 h. The reaction mixture was then poured into ice water (250 mL) with vigorous stirring. After filtration and crystallization from methanol compound **A1** was obtained as white crystals. Yield (0.60 g, 80%); mp 83–84°C; ^{1}H NMR (400 MHz, $CDCl_3$) δ 7.46 (d, J = 2.3 Hz, 2H), 7.30 (dd, J = 8.7, 2.3 Hz, 2H), 6.84 (d, J = 8.7 Hz, 2H), 3.98 (q, J = 7.0 Hz, 2H), 1.48 (s, 6H), 1.38 (t, J = 7.0 Hz, 3H); ^{13}C NMR (101 MHz, $CDCl_3$) δ 206.9, 139.1, 133.8, 129.4, 127.4, 114.0, 113.1, 40.4, 36.4, 30.9, 28.6, 11.4; MS (APCI$^+$, 20 V) m/z: 396 ([M + H]$^+$).

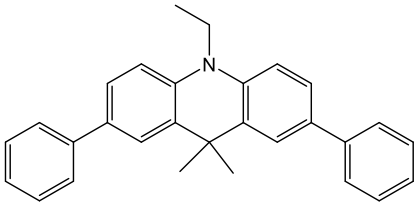

10-Ethyl-9,9-dimethyl-2,7-diphenyl-9,10-dihydroacridine (A2):

2,7-Dibromo-10-ethyl-9,9-dimethyl-9,10-dihydroacridine (0.3 g, 0.75 mmol), phenylboronic acid (0.2 g, 1.57 mmol), K_2CO_3 (0.3 g, 2.5 mmol), and $PdCl_2(PPh_3)_2$ (0.021 g, 0.03 mmol) were dissolved in a mixture of THF and water under argon. The resulting solution was heated at 80°C for 24 h. After cooling to room temperature, the solution was mixed with 150 mL of water and the product extracted with dichloromethane. The obtained crude product was purified by column chromatography using ethyl acetate/*n*-hexane 1:20 as the eluent, recrystallized from the mixture of eluent to afford the target compound **A2** as white crystals (0.15 g, 50%). Mp 170–171°C; ^{1}H NMR (400 MHz, $CDCl_3$) δ 7.67 (s, 2H), 7.63–7.56 (m, 4H), 7.48–7.39 (m, 6H), 7.36–7.25 (m, 2H), 7.13–7.02 (m, 2H), 4.18–4.00 (m, 2H), 1.65 (s, 2H),

1.48 (t, J = 7.0 Hz, 3H); ^{13}C NMR (101 MHz, $CDCl_3$) δ 141.3, 139.4, 128.7, 126.5, 126.4, 125.2, 123.23, 112.7, 40.7, 36.1, 29.4, 29.0, 11.4; MS (APCI$^+$, 20 V) m/z: 390 ([M + H]$^+$); anal. calcd for $C_{29}H_{27}N$: C, 89.42; H, 6.99; N, 3.60; found: C, 89.46; H, 7.03; N, 3.62%

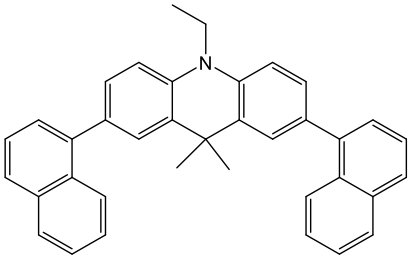

10-Ethyl-9,9-dimethyl-2,7-di(naphthalen-1-yl)-9,10-dihydroacridine (A3):

Compound **A3** was obtained as white crystals following an analogous procedure as described for compound **A2**, only using napthalen-1-ylboronic acid (0.28 g, 1.6 mmol) instead of phenylboronic acid. The crude product was purified by silica gel column chromatography with THF/*n*-hexane 1:20 as the eluent and recrystallized from the mixture of eluent to get the target compound **A3** as white crystals (0.14 g, 41%). Mp 195–196°C; ^{1}H NMR (400 MHz, $CDCl_3$) δ 8.01 (d, J = 8.4 Hz, 2H), 7.90 (d, J = 7.6 Hz, 2H), 7.84 (d, J = 8.3 Hz, 2H), 7.58 (d, J = 1.9 Hz, 2H), 7.54–7.37 (m, 10H), 7.16 (d, J = 8.4 Hz, 2H), 4.20 (q, J = 6.9 Hz, 2H), 1.62 (s, 6H), 1.56 (t, J = 6.9 Hz, 3H); ^{13}C NMR (101 MHz, $CDCl_3$) δ 140.5, 139.4, 133.9, 132.7, 131.9, 131. 7 128.3, 128.2 127.1, 126.7, 126.4 126.2, 125.9, 125.6, 124.4 112.2, 40.6, 36.4, 29.7, 29.4, 11.9; MS (APCI$^+$, 20 V) m/z: 490 ([M + H]$^+$); anal. calcd for $C_{37}H_{31}N$: C, 90.76; H, 6.38; N, 2.86; found: C, 90.81; H, 6.42; N, 2.91%.

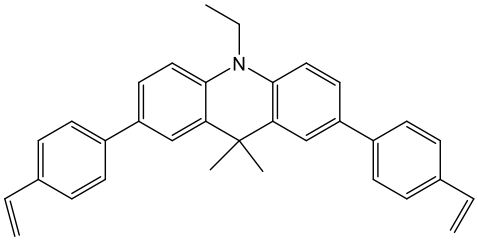

10-Ethyl-9,9-dimethyl-2,7-bis(4-vinylphenyl)-9,10-dihydroacridine (A4):

Compound **A4** was synthesized as white crystals following an analogous procedure as described for compound **A2**, only using 4-vinylphenylboronic acid (0.28 g, 1.6 mmol) instead of phenylboronic acid. The crude product was purified by silica gel column chromatography with THF/*n*-hexane 1:4 as the eluent and recrystallized from the mixture of eluent to get the target derivative **A4** as white crystals (0.09 g, 27%). Mp 177–178°C; ^{1}H NMR (400 MHz, $CDCl_3$) δ 7.67 (d, J = 3.7 Hz, 2H), 7.57 (d, J = 8.2 Hz, 3H), 7.49–7.45 (m, 5H), 7.28–7.22 (m, 1H), 7.19–7.13 (m, 1H), 7.07 (d, J = 8.2 Hz, 2H), 6.79–6.70 (m, 2H), 5.78 (d, J = 10.9 Hz, 2H), 5.25 (d, J = 10.9 Hz, 2H), 4.11 (q, J = 7.0 Hz, 2H), 1.65 (s, 6H), 1.47 (t, J = 7.0 Hz, 3H); ^{13}C NMR (101 MHz, $CDCl_3$) δ 140.7, 139.4, 136.5, 135.8, 132.7, 132.3, 129.0, 128.2, 126.6, 126.5 125.2, 123.3, 113.4, 112.7, 40.4, 36.4, 29.5, 21.4, 11.7; MS (APCI$^+$, 20 V) m/z:

442 ([M + H]$^+$); anal. calcd for $C_{33}H_{31}N$: C, 89.75; H, 7.08; N, 3.17; found: C, 89.79; H, 7.12; N, 3.22%.

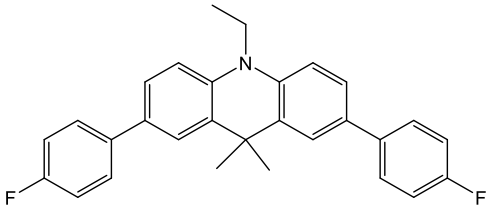

10-Ethyl-2,7-bis(4-fluorophenyl)-9,9-dimethyl-9,10-dihydroacridine (A5):

Derivative **A5** was synthesized as white crystals following the analogous procedure as described for compound **A2**, only using 4-fluorophenylboronic acid (0. 28 g, 1.6 mmol) instead of phenylboronic acid. The crude product was purified by using silica gel column chromatography with ethyl acetate/*n*-hexane 1:10 as the eluent and recrystallized from the mixture of eluent to afford the target compound **A5** as white crystals (0.1 g, 34%). Mp 180–181°C; ^{1}H NMR (400 MHz, $CDCl_3$) δ 7.60 (d, *J* = 2.1 Hz, 2H), 7.55–7.51 (m, 4H), 7.40 (dd, *J* = 8.4, 2.1 Hz, 2H), 7.14–7.03 (m, 6H), 4.11 (q, *J* = 7.0 Hz, 2H), 1.63 (s, 6H), 1.47 (t, *J* = 7.0 Hz, 3H); ^{13}C NMR (101 MHz, $CDCl_3$) δ 160.8, 139.4, 137.2, 132.3, 132.1, 128.6, 128.5, 128.0, 127.9, 127.2, 127.0, 125.3, 123.3, 115.5, 115.4, 114.2, 113.7, 112.7, 40.4, 36.4, 29.3, 11.7; MS (APCI$^+$, 20 V) *m*/*z*: 426 ([M + H]$^+$); anal. calcd for $C_{29}H_{25}F_2N$: C, 81.86; H, 5.92; F, 8.93; N, 3.29; found: C, 81.91; H, 5.99; N, 3.31%.

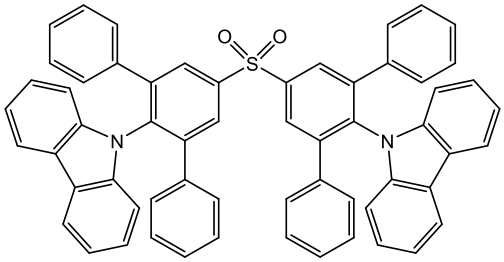

9,9'-(Sulfonylbis([1,1':3',1''-terphenyl]-5',2'-diyl))bis(9H-carbazole) (B1):

9*H*-Carbazole (0.63 g, 3.76 mmol), *N,N*-dimethylformamide (DMF, 12 mL), Sodium hydride (0.17 g, 7.16 mmol) and 3,3',5,5'-tetraphenyl-4,4'-difluorodiphenyl sulfone (1 g, 1.79 mmol) were added into the mixture, and stirred at 85°C for 8 h. The product was extracted using ethyl acetate. The organic layer was collected, filtered and the solvent was evaporated. The residue was purified by column chromatography (eluent – *n*-hexane/ethyl acetate, 8:1), crystallized from the mixture of *n*-hexane and ethyl acetate to obtain **B1** as white powder. FW = 853.05 g/mol, yield: 1.08 g, 71%. ^{1}H NMR (400 MHz, $CDCl_3$, δ, ppm): 8.23 (d, *J* = 11.6 Hz, 4H), 7.82 (d, *J* = 7.3 Hz, 4H), 7.20–7.14 (m, 2H), 7.09 (t, *J* = 7.3 Hz, 4H), 7.01 (t, *J* = 7.3 Hz, 5H), 6.94–6.83 (m, 21H). ^{13}C NMR (101 MHz, $CDCl_3$, δ, ppm): 144.3, 141.4, 140.2, 137.3, 137.2, 129.8, 128.2, 128.1, 127.6, 125.6, 123.1, 120.1, 119.8, 109.9. MS (APCI$^+$, 20 V), m/z: 854 ([M+H]$^+$). Elemental analysis calcd (%) for $C_{60}H_{40}N_2O_2S$: C, 84.48; H, 4.73; N, 3.28; O, 3.75; S, 3.76 Found: C, 84.52; H, 4.77; N, 3.25.

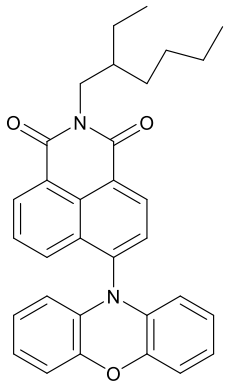

2-(2-Ethylhexyl)-6-(10*H*-phenoxazin-10-yl)-1*H*-benzo[*de*]isoquinoline-1,3(2*H*)-dione(C1):

4-Bromo-*N*-(2-ethylhexyl)-1,8-naphthalimide (0.5 g, 1.3 mmol), 10*H*-phenoxazine (0.29 g, 1.6 mmol), palladium(II) acetate (0.006 g, 0.027 mmol), tri-*tert*-butylphosphine solution (1.0 M in toluene) (0.032 g, 0.158 mmol), sodium *tert*-butoxide (0.31 g, 3.23 mmol) were dissolved in 15 ml of toluene and heated at 120°C for 24 h under nitrogen atmosphere. When the reaction was completed, the reaction mixture was diluted with ethylacetate. The product was purified by column chromatography (eluent – *n*-hexane/ethyl acetate, 10:1), crystallized from the mixture of *n*-hexane and ethylacetate to get **C1** as red crystals. FW = 490.60 g/mol; (yield 0.35 g, 57%); m. p. 176–177°C. ^{1}H NMR (400 MHz, $CDCl_3$) δ = 8.71 (d, *J* = 7.7 Hz, 1H), 8.58 (d, *J* = 7.7 Hz, 1H), 8.35 (d, *J* = 8.4 Hz, 1H), 7.77 (d, *J* = 7.7 Hz, 1H), 7.66 (t, *J* = 7.9 Hz, 1H), 6.71 (d, *J* = 7.9 Hz, 2H), 6.62 (t, *J* = 7.7 Hz, 2H), 6.44 (t, *J* = 7.7 Hz, 2H), 5.62 (d, *J* = 8.4 Hz, 2H), 4.17 – 4.00 (m, 2H), 1.96–1.83 (m, 1H), 1.42–1.20 (m, 8H), 0.94–0.76 (m, 6H). ^{13}C NMR (101 MHz, $CDCl_3$) δ = 164.2, 163.8, 143.8, 141.5, 133.7, 132.5, 132.1, 130.4, 130.2, 129.6, 128.1, 123.8, 123.5, 123.2, 122.2, 115.9, 113.4, 44.3, 38.0, 30.7, 28.7, 24.0, 23.1, 14.1, 10.6. IR, (KBr), cm^{-1}: 3067 ($CH_{Aromatic}$), 2957, 2926, 2867 ($CH_{Aliphatic}$), 1698 ($C{=}O_{imide}$), 1660, 1618, 1584, 1486 ($C{=}C_{Aromatic}$), 1353, 1334, 1291, 1268 (C-N), 1092, 1065, 1025 (C-O-C), 784, 758, 729, 673 ($CH_{Aromatic}$). MS (APCI$^+$, 20 V), m/z: 491 ([M+H]$^+$). Elemental analysis calcd (%) for $C_{32}H_{30}H_2O_3$: C, 78.34; H, 6.16; N, 5.71; O, 9.78. Found: C, 78.31; H, 6.14; N, 5.72.

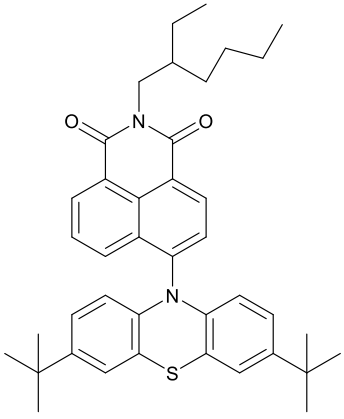

6-(3,7-Di-*tert*-butyl-10*H*-phenothiazin-10-yl)-2-(2-ethylhexyl)-1*H*-benzo[*de*]isoquinoline-1,3(2*H*)-dione (C2):

Following the synthetic procedure used for the synthesis of derivative **C1**, compound **C2** was obtained using 3,7-di-*tert*-butyl-10*H*-phenothiazine (0.29 g, 0.92 mmol) instead of 10*H*-phenoxazine. The product was purified by column chromatography (eluent- *n*-hexane/ethylacetate, 10:1), crystallized from the mixture of *n*-hexane and ethylacetate to get **C2** as orange crystals. FW = 618.88 g/mol; Yield: 0.24 g, 56%; m. p. 170–171°C. ^{1}H NMR (400 MHz, $CDCl_3$) δ = 8.72 (d, *J* = 7.7 Hz, 1H), 8.56 (d, *J* = 7.7 Hz, 1H), 8.45 (d, *J* = 8.6 Hz, 1H), 7.84 (d, *J* = 7.7 Hz, 1H), 7.64 (t, *J* = 7.7 Hz, 1H), 7.03 (d, *J* = 2.0 Hz, 2H), 6.68 (dd, J_1 = 8.6 Hz, J_2 = 2.0 Hz, 2H), 5.90 (d, *J* = 8.6 Hz, 2H), 4.19–3.99 (m, 2H), 1.99–1.85 (m, 1H), 1.43–1.20 (m, 8H), 1.14 (s, 18H), 0.94–0.75 (m, 6H). ^{13}C NMR (101 MHz, $CDCl_3$) δ = 164.3, 163.9, 146.1, 143.6, 141.1, 132.1, 131.9, 131.1, 130.5, 130.2, 128.0, 124.0, 123.8, 122.9, 119.8, 115.2, 44.3, 38.0, 34.0, 31.1, 30.7, 28.7, 24.0, 23.1, 14.1, 10.6. IR, (KBr), cm^{-1}: 3067 ($CH_{Aromatic}$), 2958, 2926, 2860 ($CH_{Aliphatic}$), 1703 ($C{=}O_{imide}$), 1656, 1619, 1589, 1478 ($C{=}C_{Aromatic}$), 1387, 1357, 1269, 1180 (C-N), 809, 788, 773, 751 ($CH_{Aromatic}$), 709, 673, 614 (C-S-C). MS (APCI$^+$, 20 V), m/z: 620 ([M+H]$^+$). Elemental analysis calcd (%) for $C_{40}H_{46}N_2O_2S$: C, 77.63; H, 7.49; N, 4.53; O, 5.17, S, 5.18. Found: C, 77.67; H, 7.53; N, 4.56.

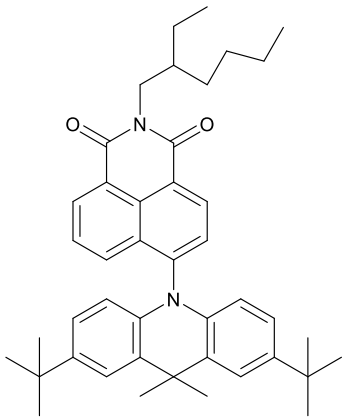

6-(2,7-Di-*tert*-butyl-9,9-dimethylacridin-10(9*H*)-yl)-2-(2-ethylhexyl)-1*H*-benzo[*de*]isoquinoline-1,3(2*H*)-dione (C3):

Following the synthetic procedure used for the synthesis of derivative **C1**, compound **C3** was obtained using 2,7-di-*tert*-butyl-9,9-dimethyl-9,10-dihydroacridine (0.4 g, 0.12 mmol) instead of 10*H*-phenoxazine. The product was purified using column chromatography (eluent – *n*-hexane/ethylacetate, 10:1), crystallized from the mixture of *n*-hexane and ethylacetate to get **C3** as orange crystals. FW = 628.90 g/mol; Yield: 0.32 g, 50%; m. p. 176–177°C. ^{1}H NMR (400 MHz, $CDCl_3$) δ = 8.71 (d, *J* = 7.7 Hz, 1H), 8.56 (d, *J* = 7.7 Hz, 1H), 8.02 (d, *J* = 8.6 Hz, 1H), 7.69 (d, *J* = 7.7 Hz, 1H), 7.56 (t, *J* = 7.7 Hz, 1H), 7.46 (d, *J* = 2.0 Hz, 2H), 6.78 (dd, J_1 = 8.6 Hz, J_2 = 2.0 Hz, 2H), 5.79 (d, *J* = 8.6 Hz, 2H), 4.18–4.03 (m, 2H), 2.01–1.87 (m, 1H), 1.75 (d, *J* = 18.5 Hz, 6H), 1.42–1.24 (m, 8H), 1.21 (s, 18H), 0.97–0.77 (m, 6H). ^{13}C NMR (101 MHz, $CDCl_3$) δ = 164.4, 164.1, 144.7, 143.4, 138.0,

132.6, 131.9, 130.7, 129.3, 127.8, 123.7, 123.4, 122.7, 113.4, 44.3, 38.0, 36.4, 34.2, 32.5, 31.4, 30.7, 28.7, 24.0, 23.1, 14.1, 10.6. IR, (KBr), cm^{-1}: 3067 ($CH_{Aromatic}$), 2957, 2926, 2859 ($CH_{Aliphatic}$), 1699 ($C=O_{imide}$), 1656, 1587, 1491, 1409 ($C=C_{Aromatic}$), 1387, 1363, 1236, 1186 (C-N), 806, 786, 745, 717 ($CH_{Aromatic}$). MS ($APCI^+$, 20 V), m/z: 630 ($[M+H]^+$). Elemental analysis calcd (%) for $C_{43}H_{52}N_2O_2$: C, 82.12; H, 8.33; N, 4.45; O, 5.09. Found: C, 82.17; H, 8.38; N, 4.47.

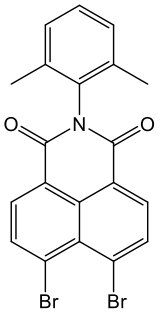

N-(2,6-Dimethylphenyl)-4,5-dibromo-1,8-naphthalimide (**D1**):

The compound **D1** was synthesized using the following procedure: the two-neck round bottom flask was charged with 4,5-dibromo-1,8-naphthalenedicarboxylic anhydride (5.00 g, 14.10 mmol) in 30 ml of propionic acid and 30 ml of N-methyl-2-pyrrolidone (NMP). 2,6-Dimethyl aniline (6.80 g, 56.52 mmol) was added, and the reaction was stirred at 160°C overnight. After being cooled to room temperature, the reaction mixture was poured into water, filtered and recrystallized from toluene, the final product **D1** obtained as yellowish orange crystals (m.p. 216–217°C). Yield: 4.00 g (62%). ^{1}H NMR (400 MHz, $CDCl_3$) δ 8.49 (d, J = 7.9 Hz, 2H), 8.29 (d, J = 7.9 Hz, 2H), 7.34–7.23 (m, 3H), 2.14 (s, 6H). ^{13}C NMR (101 MHz, $CDCl_3$) δ 162.51, 136.29, 135.39, 133.22, 131.93, 129.11, 128.76, 128.61, 128.13, 123.10, 17.85. MS ($APCI^+$) m/z: 457 ($[M + H]^+$). Elemental analysis calculated for $C_{20}H_{13}Br_2NO_2$ (%): C, 52.32; H, 2.85; N, 3.05; O, 6.97. Found: C, 52.29; H, 2.83; N, 3.06.

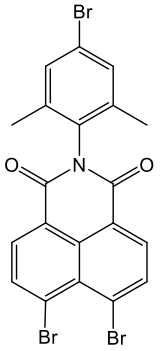

N-(4-Bromo-2,6-dimethylphenyl)-4,5-dibromo-1,8-naphthalimide (**D2**):

The compound **D2** was synthesized using the following procedure: the two-neck round bottom flask was charged with 4,5-dibromo-1,8-naphthalenedicarboxylic anhydride (5.00 g, 14.10 mmol) in 30 ml of propionic acid and 30 ml of NMP. 4-

Bromo-2,6-dimethyl aniline (11.30 g, 56.52 mmol) was added and the reaction was stirred at 160°C overnight. After cooling to room temperature, the reaction mixture was poured into water, filtered, and recrystallized from toluene, the final product **D2** was obtained as yellowish orange crystals (m.p. 244–245°C). Yield: 4.20 g (55%). ^{1}H NMR (400 MHz, $CDCl_3$) δ 8.47 (d, J = 6.4 Hz, 2H), 8.28 (d, J = 6.1 Hz, 2H), 7.38 (s, 2H), 2.10 (s, 6H). ^{13}C NMR (101 MHz, $CDCl_3$) δ 162.53, 136.31, 135.40, 133.23, 131.94, 131.92, 129.13, 128.78, 128.63, 128.15, 123.12, 77.25, 17.86. MS (APCI$^+$) m/z: 538 ([M + H] $^+$). Elemental analysis calcd (%) for $C_{20}H_{12}Br_3NO_2$: C, 44.65; H, 2.25; N, 2.60; O, 5.95. Found: C, 44.62; H, 2.26; N, 2.54.

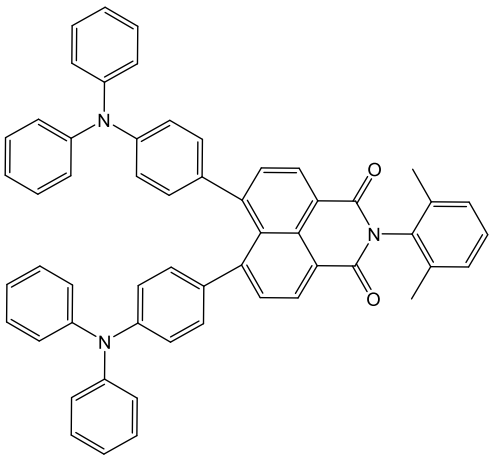

2-(2,6-dimethylphenyl)-6,7-bis(4-(diphenylamino)phenyl)-1H-benzo[de]isoquinoline-1,3(2H)-dione (D3):

D1 (0.50g, 1.09 mmol), diphenylaminophenyl boronic acid (0.75 g, 2.62 mmol), sodium tert-butoxide (0.48 g, 5.01 mmol) and palladium (II) acetate (0.0098 g, 0.04 mmol) was added in 20 ml of dry toluene and 2 ml of water under argon gas atmosphere. The reaction mixture was evacuated and purged with argon gas three times. The resultant solution was heated at 80°C for 24 hours. After cooling to room temperature, the solution was mixed with 150 mL of water and the reaction mixture was extracted with ethyl acetate. The obtained crude product was purified using column chromatography using tetrahydrofuran/n-hexane 1:10 as an eluent and recrystallized from the mixture of dichloromethane and methanol in equal proportions to afford the target compound **D3** as deep orange crystals (m.p. 317–318°C). Yield: 0.60 g (70%). ^{1}H NMR (400 MHz, $CDCl_3$) δ 8.65 (d, J = 7.6 Hz, 2H), 7.67 (d, J = 7.6 Hz, 2H), 7.24–7.07 (m, 19H), 7.02–6.96 (t, 4H), 6.88–6.75 (dd, 8H), 2.11 (s, 6H). ^{13}C NMR (101 MHz, $CDCl_3$) δ 163.68, 148.03, 147.29, 147.03, 135.61, 134.81, 134.04, 131.39, 131.10, 130.82, 130.56, 129.45, 128.79, 128.51, 128.20, 125.42, 123.62, 121.36, 120.59, 17.99. MS (APCI$^+$) m/z: 787 ([M + Na]$^+$). Elemental analysis calculated for $C_{56}H_{41}N_3O_2$ (%): C, 85.36; H, 5.24; N, 5.33; O, 4.06. Found: C, 85.32; H, 5.7; N, 5.35.

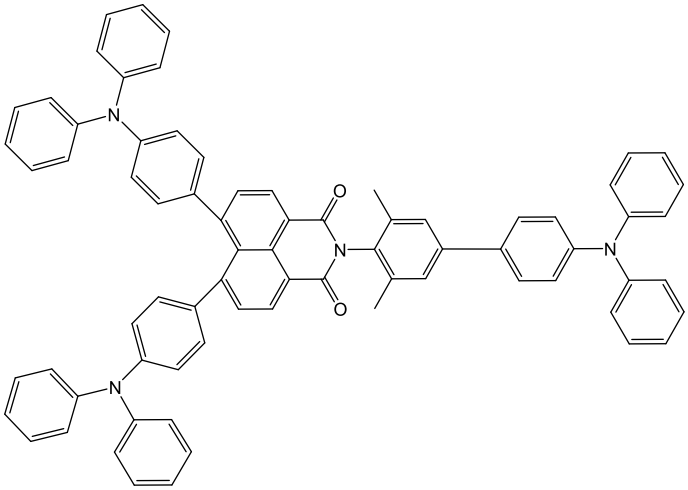

2-(4'-(diphenylamino)-3,5-dimethyl-[1,1'-biphenyl]-4-yl)-6,7-bis(4-(diphenylamino)phenyl)-1H-benzo[de]isoquinoline-1,3(2H)-dione (D4):

D2 (0.50 g, 0.93 mmol), diphenylaminophenyl boronic acid (0.97 g, 3.25 mmol), sodium tert-butoxide (0.62 g, 6.41 mmol) and palladium (II) acetate (0.0125 g, 0.05 mmol) was added in 20 ml of dry toluene and 2 ml of water under argon gas atmosphere. The reaction mixture was evacuated and purged with argon gas three times. The resultant solution was heated at 110°C for 24 hours. After cooling to room temperature, the solution was mixed with 150 mL of water and the reaction mixture was extracted with ethyl acetate. The obtained crude product was purified by using column chromatography using tetrahydrofuran/n-hexane 1:10 as an eluent and recrystallized from the mixture of dichloromethane and methanol in equal proportions to afford the target compound **D4** as deep orange crystals (m.p. 341–342°C). Yield: 0.75g (76 %). ^{1}H NMR (400 MHz, $CDCl_3$) δ 8.67 (d, J = 7.6 Hz, 2H), 7.68 (d, J = 7.6 Hz, 2H), 7.44 (d, J = 8.4 Hz, 2H), 7.34 (s, 2H), 7.22–7.16 (m, 12H), 7.12–7.06 (m, 14H), 7.01–6.94 (m, 6H), 6.86–6.80 (dd, J_1 = 25 Hz, J_2 = 8.5 Hz, 8H), 2.17 (s, 6H). ^{13}C NMR (101 MHz, $CDCl_3$) δ 163.80, 148.09, 147.76, 147.29, 147.17, 147.05, 141.18, 135.83, 135.03, 134.80, 132.88, 131.42, 131.17, 130.84, 130.58, 129.46, 129.33, 129.29, 129.21, 129.06, 128.22, 128.06, 127.07, 125.43, 124.55, 124.45, 124.18, 123.83, 123.63, 122.89, 121.35, 120.60, 18.21. MS (APCI$^+$) m/z: 1030 ([M + H]$^+$). Elemental analysis calcd (%) for $C_{74}H_{54}N_4O_2$: C, 86.19; H, 5.28; N, 5.43; O, 3.10. Found: C, 86.18; H, 5.30; N, 5.06.

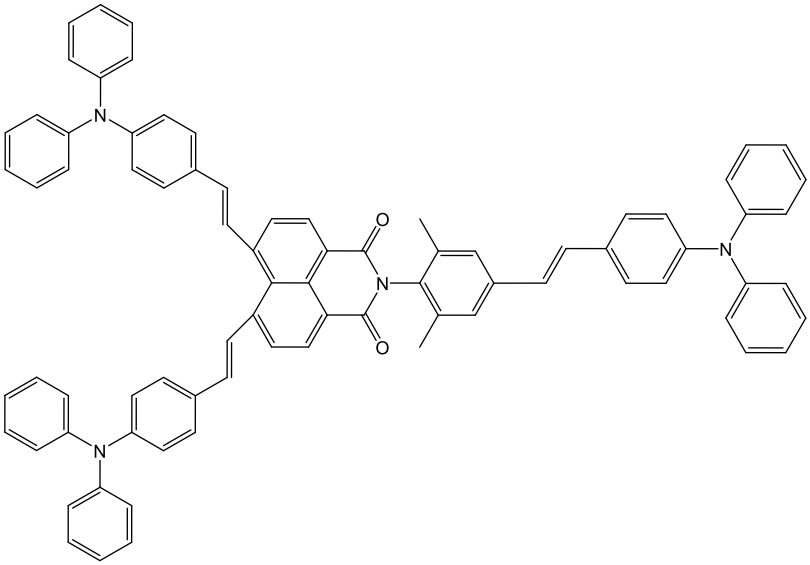

6,7-bis((E)-4-(diphenylamino)styryl)-2-(4-((E)-4-(diphenylamino)styryl)-2,6-dimethylphenyl)-1H-benzo[de]isoquinoline-1,3(2H)-dione (D5):

D2 (0.50 g, 0.93 mmol), vinyl triphenylamine (0.83 g, 3.35 mmol), tri-o-tolylphosphine (0.065 g, 0.21 mmol), palladium (II) acetate (0.10 g, 0.40 mmol) and 4 ml of triethylamine were added in 10 ml of dry dimethyl formamide. The reaction mixture was evacuated and purged with argon gas three times. The resultant solution was heated at 110°C for 24 hours. After cooling to room temperature, the solution was mixed with 150 ml of water and the reaction mixture was extracted with ethyl acetate. The obtained crude product was purified using column chromatography with pure toluene as an eluent and the obtained material was washed with methanol to afford the target compound **D5** as light red powder. Yield: 0.65 g (63%). ^{1}H NMR (400 MHz, $CDCl_3$) δ 8.68 (d, J = 7.7 Hz, 2H), 7.93–7.89 (m, 4H), 7.45–7.38 (m, 8H), 7.32–7.24 (m, 14H), 7.16–6.98 (m, 26H), 2.20 (s, 6H). ^{13}C NMR (101 MHz, $CDCl_3$) δ 163.57, 148.38, 147.60, 147.22, 144.74, 135.78, 131.68, 131.59, 130.61, 130.30, 129.42, 129.29, 128.66, 127.99, 127.43, 126.63, 126.52, 124.82, 124.48, 123.68, 123.49, 122.99, 122.92, 121.38, 18.04. MS (APCI$^+$) m/z: 1108 ([M + H]$^+$). Elemental analysis calcd (%) for $C_{80}H_{60}N_4O_2$: C, 86.61; H, 5.45; N, 5.05; O, 2.88 Found: C, 86.58; H, 5.42; N, 5.03.

4. RESULTS AND DISCUSSION

4.1. Acridan-based derivatives

Organic compounds exhibiting thermally activated delayed fluorescence (TADF) are widely used as emitters for OLEDs[142]. The great interest in TADF emitters is mainly explained by their heavy-atoms-free molecular structure and 100% theoretical limit of internal quantum efficiency (IQE) of electroluminescent (EL) devices based on the TADF phenomenon[143]. To successfully exploit TADF emitters in OLED structures, appropriate hosts are required [144]. Since the selection of suitable hosts is very important for achieving high OLED efficiencies, there was considerable interest in host compounds for TADF emitters in recent years[145,146]. The host compounds for TADF-based OLEDs must match a number of censorious requests. For example, high singlet and triplet energies (higher than those of the guest) are required for host compounds for qualifying host–guest energy transfer, thus implying restrict of the emissive excitons on the TADF emitters[147]. High glass transition temperatures are also required for increasing the morphological stability of light-emitting layers and consequently for elongating the device lifetimes[147]. Proper energy levels and bipolar charge-transporting properties of host materials may endow good charge-injection properties and charge balance in the guest–host light-emitting layers of TADF OLEDs[148-150]. Therefore, the synthesis of host materials with the combination of all required properties especially of those intended for blue TADF OLEDs is a great challenge[147,150]. Up to now, most of the compounds used as hosts in TADF-based devices demonstrate a deep HOMO energy level and shallow LUMO energy level. This poses difficulties to the injection of electrons and/or holes into the light-emitting layer [151]. These weaknesses of hosts result in low power efficiencies and high turn-on voltages of TADF-based OLEDs [152]. To overcome these challenges, several molecular design strategies were proposed including the incorporation of electron-accepting and electron-donating moieties into the same molecule[153,154]. Conventional hosts, such as 1,3-bis(*N*-carbazolyl)benzene (*m*CP) and bis[2-(diphenylphosphino)phenyl] ether oxide (DPEPO), are generally used as hosts in blue phosphorescent OLEDs, are also widely applied in TADF-based OLEDs so far[155,156]. Although these hosts demonstrate relatively good results, it can be presumed that the further improvement of the performance of TADF-based OLEDs is possible, if some drawbacks of widely used hosts such as unipolar charge transport or uncomplimentary energy levels are overcome[163]. The only hole or electron-transporting property of hosts leads to charge recombination near the interface between the charge-transporting layer and the emissive layer, thus decreasing the device's efficiency[163]. Four acridan derivatives were prepared using simple synthetic procedures and characterized as hosts for TADF-based OLEDs.

4.1.1. Synthetic routes

The synthesis procedure and structures of the acridan derivatives are shown in scheme 12. The target acridan-based derivatives **A2–A5** were obtained by employing the Suzuki cross-coupling reactions between brominated acridan **2** and the various

phenylboronic acids in the presence of a palladium catalyst with yields ranging from 27 to 50%. The structures of the synthesized final compounds **A2–A5** was confirmed by ^{1}H and ^{13}C NMR spectroscopy, elemental analysis, and mass spectrometry.

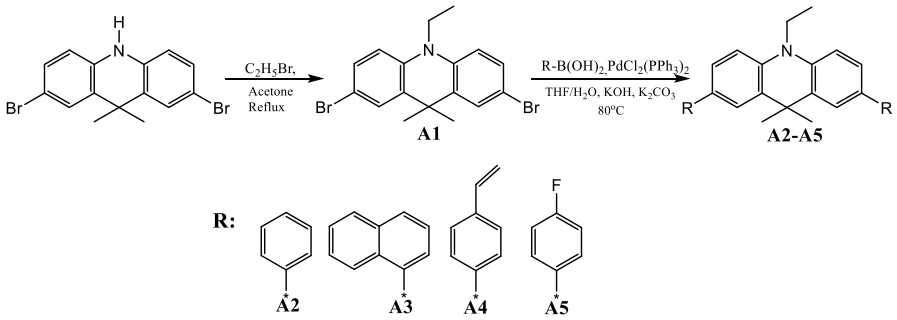

Scheme 12. Synthesis of acridan-based derivatives **A2–A5**

4.1.2. Theoretical calculations

The optimized structures of **A2–A5** were obtained by density functional theory (DFT) calculations at the B3LYP/6-31G(d,p) level of theory (Fig. 2). The dihedral angles between the acridanyl and phenyl moieties in compound **A2** (37.0° and 36.3°) are comparable with the dihedral angles between the acridanyl and vinylphenyl or 4-fluorophenyl moieties in compounds **A4** and **A5** (34.8° and 36.7°, respectively). Thus, the nature of the phenyl moiety attached to the central acridan unit does not affect the dihedral angle significantly. The naphthyl-substituted acridan **A3** is characterized by slightly higher dihedral angles of 52.3° as compared to compounds **A2**, **A4**, and **A5**. The highest occupied molecular orbitals (HOMOs) and the lowest unoccupied molecular orbitals (LUMOs) of **A2–A5** are distributed over the entire molecules.

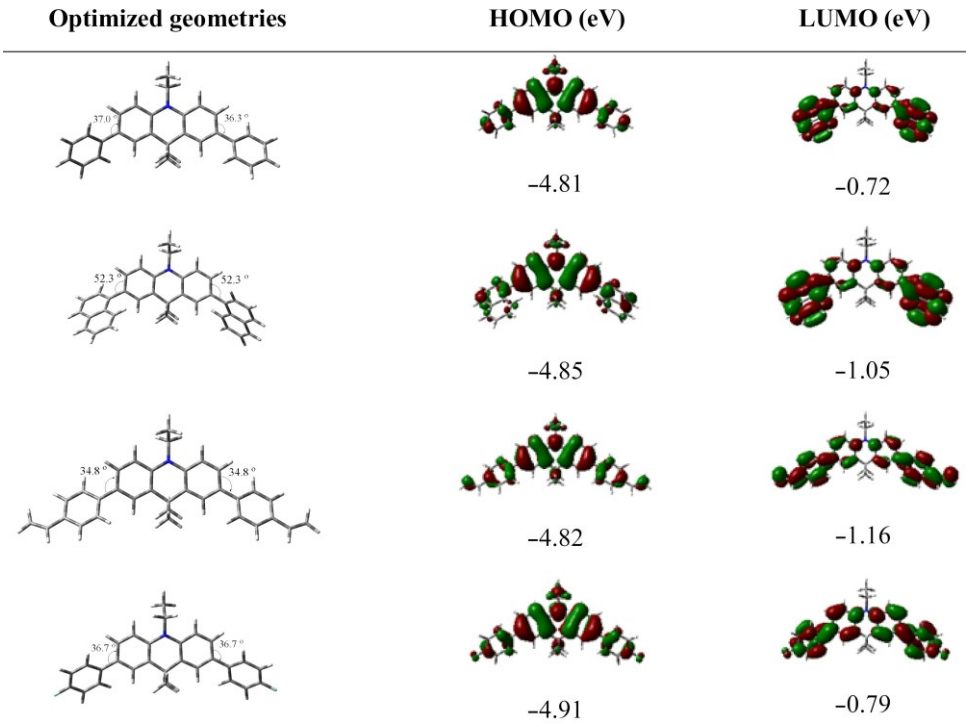

Fig. 2. Theoretically calculated HOMO and LUMO level distributions and optimized geometries of **A2–A5** DFT calculations were performed at the B3LYP/6-31G(d,p) level[85]

4.1.3. Thermal properties

The thermal behavior of derivatives **A2–A5** under heating was examined by DSC and TGA under a nitrogen atmosphere. The 5% weight-loss temperatures of compounds **A2–A5** were observed in the range of 271–395°C (Table 5). Compounds **A2** and **A5** underwent sublimation during the TGA experiments and exhibited complete weight losses. It was therefore impossible to compare their thermal stabilities with those of compounds **A3** and **A4**. Derivatives **A3** and A**4** exhibited relatively high thermal stabilities with 5% mass loss temperatures of 344°C and 395°C, respectively. Compounds **A2–A5** were obtained as crystalline substances after the synthesis and purification. However, derivatives **A2–A5** could also form molecular glasses. The DSC thermograms of compound **A3** and **A4** are shown in Fig. 3 (a, b). The crystalline sample of **A3** melted at 201°C on the first heating. The melt transformed into a solid amorphous material upon cooling.

Table 5. Thermal characteristics of **A2–A5**

Compound	T_m, °C	T_g, °C	T_{cr}, °C	$T_{ID-5\%}$, °C
A2	174	79[a]	102[a]	285
A3	201	86[a]	183[a]	344
A4	180	97[a]	242	395
A5	186	-	118	271

[a] –2nd heating; - – not observed.

When the amorphous sample was heated on the second scan, the glass transition (T_g) was noticed at 86°C, followed by an exothermic crystallization (T_{cr}) signal observed at 183°C to obtain crystals, which melted at 201°C.

The crystalline sample of derivative **A2** demonstrated a similar behavior. It melted upon the first heating at 174°C and exhibited a glass transition at T_g of 79°C in the second heating, followed by an exothermic T_{cr} at 102°C. Derivative **A5** demonstrated different behavior in the DSC experiments. The crystalline sample of **A5** melted at 186°C on the first heating and on cooling, the melted sample crystallized at 118°C. When the sample was heated again, only a melting peak was observed at 186°C. The T_g values observed for compounds **A2–A4** ranged from 79°C to 97°C, with the phenyl-substituted acridan **A2** exhibiting the lowest glass-transition temperature. The higher T_g values can be explained by the higher molecular weights resulting in a stronger intermolecular interaction and by larger volumes restricting molecular motion. These observations confirm that compounds **A2–A4** can be used for the preparation of thin amorphous layers on substrates.

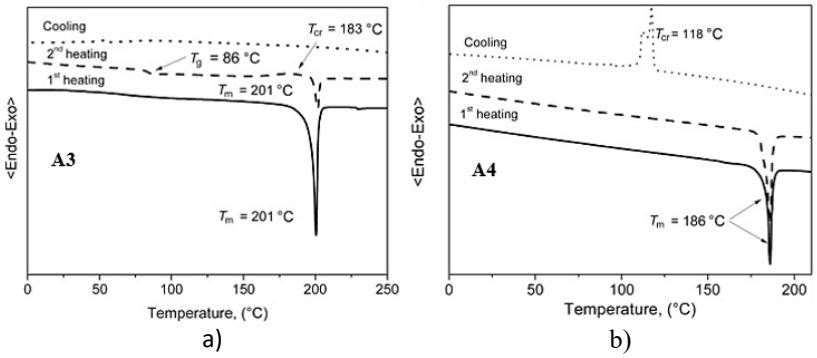

Fig. 3. DSC curves of compounds **A3** and **A4**

4.1.4. Electrochemical and photoelectrical properties

The electrochemical properties of the acridan derivatives **A2–A5** were investigated by cyclic voltammetry (CV). The cyclic voltammograms of compounds **A2–A5** are shown in Fig. 4a, and the data are summarized in Table 6.

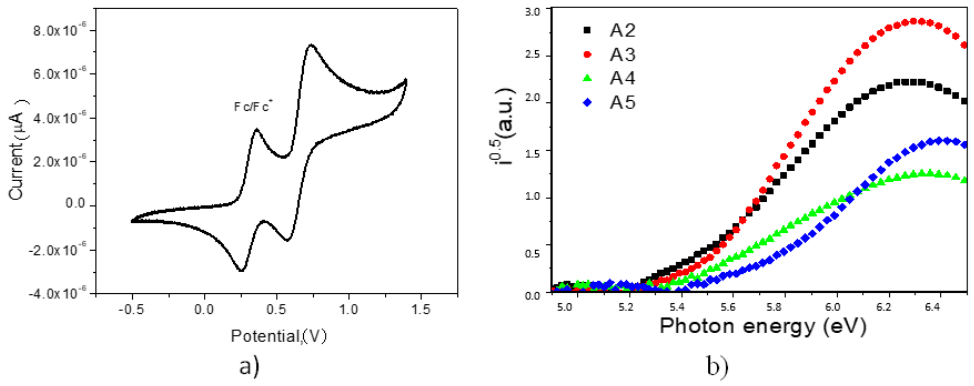

Fig. 4. (a) Cyclic voltammogram of derivative **A2** in dichloromethane (a three-electrode cell consisting of a platinum coil as a counter electrode, a glassy carbon working electrode, and a silver wire as a reference electrode was used; sweep rate – 100 mV/s, 0.1 M solution of tetrabutylammonium hexafluorophosphate (*n*-Bu_4NPF_6)) and (b) photoelectron emission spectra of the layers of derivatives **A2–A5**.

Close values for the potentials of reversible oxidation of ca. 0.3–0.4 V were observed for the compounds. During the anodic oxidation sweeps, compounds **A2–A5** showed single reversible oxidation peaks, which could be tributed to the oxidation of the acridanyl moiety. Also, close values of ionization potentials (IP_{cv}) of compounds **A2–A5** obtained from the onset potentials of their oxidation signals were found in the range of 5.11–5.18 eV. The electron affinity values were deduced from the IP_{cv} and energy gap (E_g^{opt}) obtained from the onsets of the UV–vis absorption spectra. The ionization potentials IP_{PES} of the solid films of derivatives **A2–A5** were estimated by photoelectron emission spectrometry (Fig. 4b, and Table 6). The IP_{PES} values were further used for constructing OLED structures. The highest IP_{PES} of 5.62 eV was obtained for compound **A5** which contains electron accepting fluorine atoms. The other compounds (**A2–A4**) demonstrated similar IP_{PES} values mainly attributed to removing an electron from the acridan unit. Slightly higher IP_{PES} values were obtained by PES measurements for compounds **A2–A5** in comparison to those estimated by CV and can apparently be explained by a more difficult removal of electrons from materials in the solid state than in solution due to the strong intermolecular interaction.

Table 6. Electrochemical characteristics of compounds **A2–A5**

Compound	[a]E_{ox}, eV	[b]IP_{CV}, eV	[c]E_g^{opt}, eV	[c]EA_{CV}, eV	[d]IP_{PE}, eV	[e]E_g^{opt}, eV	[f]EA_{PE}, eV
A2	0.35	5.15	3.29	1.86	5.4	3.19	2.21
A3	0.36	5.16	3.25	1.91	5.46	3.1	2.36
A4	0.31	5.11	3.25	1.86	5.39	2.8	2.59
A5	0.38	5.18	3.41	1.77	5.62	3.25	2.37

[a]Onset oxidation potential versus Ag/Ag^+; [b]calculated using formula $IP_{CV} = (E_{ox} - E_{Fc/Fc^+}) + 4.8$ (eV); [c]estimated from an onset wavelength (λ_{edge}) of absorption spectra for toluene solutions using an empirical formula $E_g^{opt} = 1240/\lambda edge$; [d]calculated using the formula EA_{CV}

= $IP_{CV} - E_g^{opt}$; [e]obtained from PES spectra; [f]estimated for solid films (Fig. 3a); [g]calculated using the formula $EA_{PES} = IP_{PES} - E_g^{opt}$.

4.1.5. Photophysical properties

The absorption and photoluminescence (PL) spectra of neat films, and dilute THF and toluene solutions of the studied derivatives are presented in Fig. 5a. Derivatives **A2**, **A3,** and **A5** exhibited intense acridan-related lowest energy bands (LEB) of absorption at ≈340 nm, affected by the type of substituents. The LEB of the solutions and films of **A4** were decreased by ca. 0.23 eV with respect to that of the other studied compounds due to the π-electronic coupling between the acridan and vinylphenyl moieties. The absorption spectra were not affected by the polarity of the solvent. Relatively structured PL spectra were obtained for solutions and solid films of **A2–A5** suggesting their fluorescence resulted from emissive recombination of local excited states in nature (Fig. 5a). Slight red-shifts of PL spectra were observed in higher-polar THF solutions and films of derivatives **A2–A5** in comparison to PL spectra measured in low-polar toluene due to polarity and aggregation effects. Despite these observations, emission of compounds **A2–A5** can mainly be assigned to π–π* transitions of local excited states. However, a slight contribution of charge transfer (CT) can be also recognized in the emission of the studied compounds **A2–A5** (Fig. 5a). The observed spectral behavior is typical for the twisted intramolecular CT phenomenon[86]. Even though the HOMOs and LUMOs are distributed over the entire molecule for all compounds, the strong electron-donating nature of acridan is manifested by a partial spatial separation of the frontier orbitals. As it can be seen from Figure 2, the LUMOs are mostly located on phenyl, naphthalenyl, vinylphenyl, and fluorophenyl moieties of the molecules. These moieties accept electrons causing a change of the dipole moments in the excited states. As a result, separate radiative processes can be accompanied by intermolecular CT state relaxation. Such emission is evidenced by solvatochromic effects, i.e., a bathochromic shift of the emission peak due to the change of the environment to a more polar one.

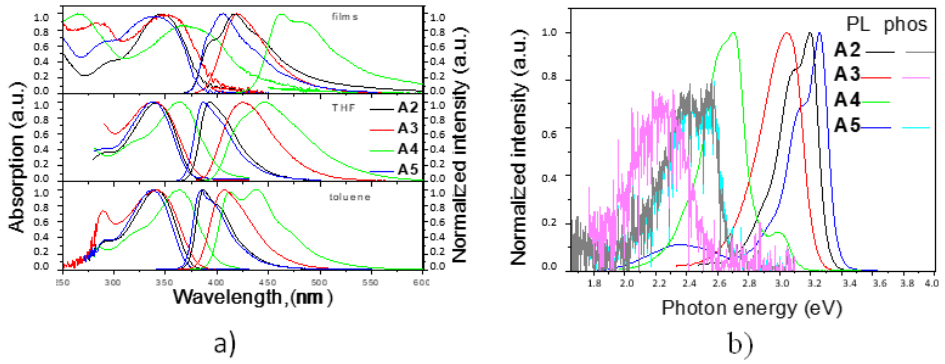

Fig. 5. (a) Absorption spectra of neat films, dilute THF and toluene solutions of **A2–A5**. (b) Photoluminescence and phosphorescence spectra in dilute THF solutions at 77 K of **A2–A5**

By replacing the solvent toluene with THF, the solution of **A3** exhibited a bathochromic shift of the PL peak from 407 to 425 nm. Thus, compound **A3** clearly exhibited an intermolecular CT emission. In contrast, the PL peaks related to π–π* states of the solutions of the other studied compounds were only slightly affected by the solvent replacement. The different behavior of compound **A3** may be explained by the dihedral angle between the acridanyl and naphthyl moieties, that is the largest one among all the studied compounds, leading to a reduction of π-conjugation. This observation explains the distinct ICT character of the luminescence of compound **A3**. The dihedral angles in molecules of **A2** and **A5** are relatively small, and their LE emissions are mainly ultraviolet. There was practically no positive solvatochromism observed for the dilute solutions of compounds **A2**, **A4**, and **A5**. Only tails related to CT can be observed in the PL spectra of these compounds. Quenching of internal molecular motion stabilizes the twist conformers stimulating the formation of intermolecular CT states. Consequently, in the PL spectra of neat films of the derivatives the emission band assigned to CT is more prominent. The PL quantum yields of neat films of compound **A2**, **A3**, **A4**, and **A5** were found to be 0.03, 0.08, 0.32 and 0.08, respectively. The relatively high PL efficiency of the film of **A3** originates from the more efficient CT contribution to the emission. The PL and phosphorescence spectra of dilute THF solutions of the studied derivatives recorded at 77 K are shown in Fig. 5b. The PL spectra recorded at liquid nitrogen temperature were found to be highly similar to those recorded at room temperature (Fig. 5a). The energy values of singlet (E_{S1}) and triplet (E_{T1}) excited states were estimated from the onsets of the spectra. The E_{S1} were found to be 3.31, 3.24, 3.12 and 3.37 eV for compounds **A2–A5**, respectively. The E_{T1} values were estimated as 2.54 eV for **A3**, and 2.67 eV for **A2** and **A5**. The triplet energy could not be estimated for derivative **A4**, since the phosphorescence at 77 K was practically undetectable for this compound.

4.1.6. Charge transporting properties

To unclose the potential of acridan-based derivatives containing phenyl or naphthyl substituents as hosts for blue TADF OLEDs, charge-transport properties of the vacuum deposited layers of the acridanes were tested by the methods of time-of flight (TOF) and charge extraction by linearly increasing voltage (CELIV)[87,88]. TOF photocurrent transients with well-visible transit times were recorded for holes in layers of compound **A3** (Fig. 6a). Using the values of transit times, hole drift mobilities at different electric fields were calculated and plotted in Fig. 6 according to the Poole–Frenkel model $\mu = \mu_0 \exp(\beta \cdot E^{0.5})$, where μ and μ_0 are, respectively, hole and field-free mobilities, β is the Poole–Frenkel constant, and E is the electric field[87]. The values of hole mobility in the layers of **A3** exceeded 10^{-3} cm^2/V·s at electric fields higher than ca. 2.5×10^5 V/cm. Electron transport was not detected for the tested samples by TOF experiments. TOF photocurrent transients with well-visible transit times for samples **A2**, **A4**, and **A5** were not observed apparently due to either strong crystallinity of thick films or strongly dispersive transport of charges. Therefore, the CELIV method, which is less sensitive to charge-transport dispersity than the TOF method, was additionally exploited for charge-transport characterization of the

compounds. Indeed, well discernible maxima were observed not only for the layers of compound **A3** but also for the layers of **A4** and **A5** (Fig. 7a, b). Close values of hole mobilities in the layers of compound **A3** were obtained with both methods (Fig. 6b). Similar hole mobilities were also obtained for compounds **A4** and **A5** with the CELIV measurements (Fig. 6b). Thus, a negligible effect of the nature of substituents of acridan in compounds **A2–A5** on the hole-transporting properties was detected.

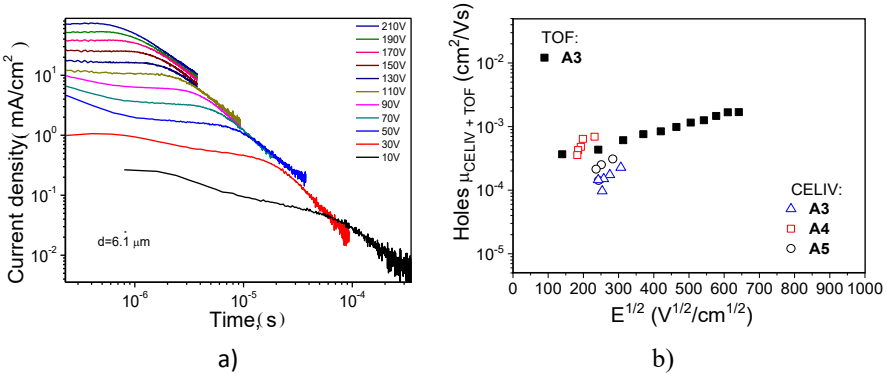

Fig. 6. TOF photocurrent transients for holes in vacuum-deposited layers of compound **A3** (a); hole mobility versus electric field for layers of compounds **A3–A5** (b)

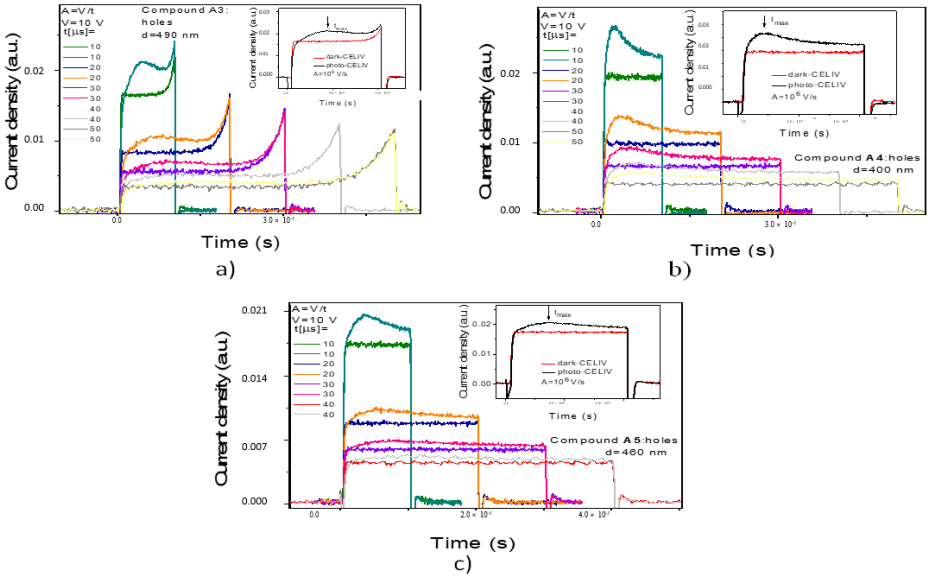

Fig. 7. Dark-CELIV and photo-CELIV signals for compounds **A3** (a), **A4** (b), and **A5** (c)

4.1.7 OLED fabrications

To test the studied compounds as host compounds in OLEDs, devices based on the well-known TADF emitter 9-[4-(4,6diphenyl-1,3,5-triazin-2-yl)phenyl]-*N*^{3},*N*^{3},*N*^{6},*N*^{6}-tetraphenyl9*H*-carbazole-3,6-diamine (DACT-II) were fabricated and

characterized[89]. The DACT-II-based OLEDs are expected to reach an internal quantum efficiency (IQE) of 100%. The low energy absorption bands at ≈410 nm of the film of the emitter DACT-II and the emission bands of the films of the studied compounds overlapped to a greater extent in derivatives **A2**, **A3**, and **A5** than in compound **A4** that showed an unsuitably red-shifted emission. Taking this observation into account, DACT-II (10 wt %) was used as the emitter doped into hosts **A2**, **A3**, and **A5** in OLEDs **A**, **B** and **C**, respectively. The structures and equilibrium energy diagrams of the devices are presented in Fig. 8a. The values of ionization potentials and electron affinities of solid samples of compounds **A2**, **A3**, and **A5** were taken as HOMO and LUMO levels as the first approximation (Fig. 4b, Table 6). In the devices, MoO_3 and LiF were employed as materials for injection layers for holes and electrons, respectively. *N*,*N*'-Di(1-naphthyl)-*N,N*'-diphenyl-(1,1'biphenyl)-4,4'-diamine (NPB) was used for the preparation of the hole-transporting layer. 1,3-Bis(*N*-carbazolyl)benzene (*m*CP) was selected as exciton blocking material. Diphenyl-4triphenylsilylphenylphosphine oxide (TSPO1) was used as hole blocking material, while the layer of 2,2',2"-(1,3,5benzenetriyl)-tris(1-phenyl-1*H*-benzimidazole) (TPBi) was employed as the electron-transporting layer. Electroluminescence (EL) spectra of devices **A–C** and their external quantum efficiencies (EQE) are presented in Fig. 8b, c.

Table 7. Electroluminescence characteristics of OLEDs

Device	Turn-on voltage, V	Maximum brightness, 10^3 cd/m^2	External quantum efficiency (EQE) maximum, %	Maximum power efficiency (PE), lm/W	EQE and (PE) efficiencies at 100 cd/m^2	CIE 1931 UCS coordinates at 9v
A	3.2	16.2	3.2	9.5	3.1% (8.8 lm/W)	(0.29, 0.5)
B	3.6	22.9	3.2	5.6	1.8% (4.4 lm/W)	(0.24, 0.47)
C	3.2	18.6	3	7.2	2% (5.9 lm/W)	(0.28, 0.51)

The characteristics of the fabricated OLEDs are summarized in Table 7. The intensity maxima of the EL spectra recorded at 5V for devices **A–C** were found in the narrow range from 520 to 530 nm due to the slight differences in the dipole moments of the hosts used (Fig. 8b). Additionally, low-intensity peaks in the violet/blue region of the EL spectra of devices **A** and **B** appeared illustrating an incomplete energy transfer from hosts **A2**, **A3**, and **A5** to DACT-II in the emitting layers of devices **A–C**. However, the changes in EL colors of the fabricated devices were not significant meaning that the EL spectra represent DACT-II emission according to the corresponding CIE coordinates (Table 7).Low turn-on voltages of 3.2–3.6 V recorded for devices **A–C** indicate good charge-injecting and charge-transporting properties of the hosts used due to their lower HOMO in comparison to that of *m*CP (turn-on voltage of 3.7 V was observed for device **M**, Fig. 8d, and Table 7). Close values of maximum EQEs were obtained for devices **A–C** displaying similar host performances of compounds **A2**, **A3**, and **A5** (Fig. 8c, Table 7). Maximum EQE values of 3–3.2%

were observed for devices **A–C**. The rather low EQE values of devices **A–C** can be explained by the following reasons: 1) incomplete energy transfer from hosts to the guest; 2) formation of a recombination zone near to the light-emitting layer/hole-blocking layer interface due to the unipolar hole mobility of the synthesized hosts; 3) poor balance of holes and electrons in the light-emitting layer, etc. The results obtained suggest that the developed compounds could be more appropriate for an application as hole-transporting materials in organic optoelectronic devices.

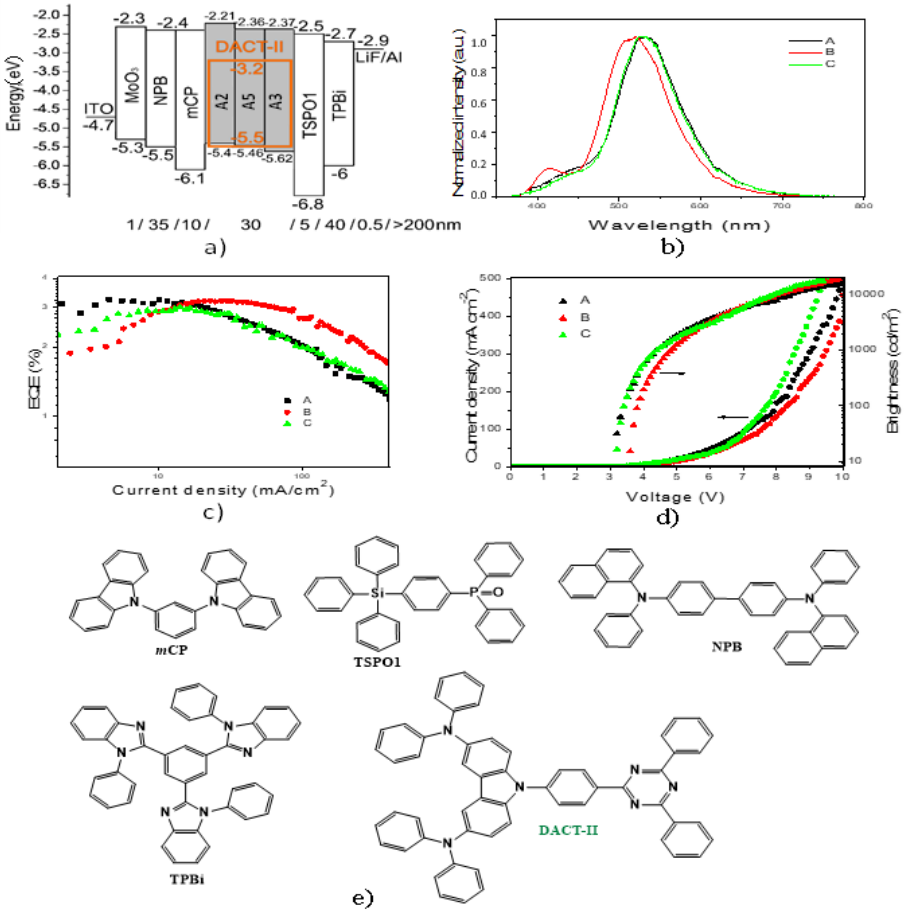

Fig. 8. Energy diagrams of the fabricated OLEDs (a); normalized electroluminescence spectra of devices **A–C** recorded at 5 V (b); EQE versus current density plots (c), brightness and current density versus applied voltages plots (d) of the tested OLEDs; molecular structures of the organic derivatives used in the devices (e)

4.2. Carbazolyl disubstituted diphenyl sulfone derivative

The OLED-based TADF emitters allow to convert all excitons formed under electrical excitation into light. To utilize the full potential of OLED emitters, the device structure has been well designed and optimized involving additional functional

materials such as hole/electron injecting/transporting materials, charge/exciton blocking materials or hosts[165]. In properly designed and optimized OLEDs, hole-electron recombination within the light-emitting layer with efficiency close to unity can be achieved[166]. Host-guest emitting layers are common for phosphorescent and TADF-based OLEDs because phosphorescent and TADF compounds usually suffer from severe concentration quenching, especially in pristine films[167]. To achieve high efficiency of exciton utilization for TADF emitters, their host materials should possess high triplet energy (E_T) to reduce the possibility of triplet energy transfer back to a host[168]. Also, their triplet emission lifetime has to be long enough with suppressed triplet non-radiative channel. TADF compounds can also be employed as host materials with two following strategies. According to the first strategy, triplet energy of TADF host can be harvested *via* reverse intersystem crossing (RISC) as singlet exciton. Then the following Forster resonance energy transfer from host singlet state to dopant singlet state occurs[169,170]. However, this requires highly efficient RISC to extract most triplet excitons from host which may be accompanied by high energy loss during the transfer processes.

Another strategy is to consider the possibility of RISC of TADF hosts, which can allow their singlet energy transfer to the triplet state[171]. If the singlet-triplet energy gap is not small enough, low RISC efficiency with long triplet lifetime is observed and the energy is stored in its triplet state as energy tank. Then the triplet energy of a host can be depleted by TADF or phosphorescent emitter with the sufficient Dexter energy transfer time. Recently, many TADF emitters and hosts for OLEDs were discovered mainly exploiting donor-acceptor (D-A) and donor-acceptor-donor (D-A-D) molecular structures[172]. When HOMO and LUMO are well separated in D-A or D-A-D molecules, small singlet-triplet energy splitting (ΔE_{ST}) can be achieved which is commonly required for intramolecular TADF[173]. HOMO-LUMO separation is very sensitive to dihedral angle between donor and an acceptor unit[174]. When flexible linkage between D and A moieties is used, the dihedral angle is sensitive to media in which TADF molecules are dispersed. It is in not constant even in the same medium due to the molecular vibrations which take place at high temperatures[175]. Such variation of dihedral angles between a donor and an acceptor of the same TADF molecule may lead to the change of its TADF efficiency. In addition, flexible D-A linkages may also lead to either different conformer/aggregate/polymorph formations, through-space or intermolecular D-A interactions which strongly affect the emission of D-A and D-A-D type molecules[176,177]. Since the behavior of D-A-D type molecules with the flexibly linked donor and acceptor units depends on many factors[178-180], it is often difficult to predict their behavior in OLEDs in combination with the different emitters or hosts. Aiming to restrict the variations of D-A dihedral angles and D-A interactions, in this work we propose the approach of ornamenting the TADF molecules by phenyl groups. We synthesized tetraphenyl-substituted derivative of diphenylsulfone and carbazole.

4.2.1. Synthetic procedure

The synthesis procedure of the target compound **B1** was shown in scheme 13. The first step was bromination followed by the Suzuki coupling reaction and the final

step of the synthesis of compound **B1** was the substitution of the fluorine atoms of intermediate compound **M3** with 9*H*-carbazole using sodium hydride in dimethylformamide. The chemical structures of the compounds were fully characterized by ^{1}H and ^{13}C NMR, IR spectroscopies, mass spectrometry, as well as by elemental analysis. Derivative **B1** exhibited good solubility in most common organic solvents.

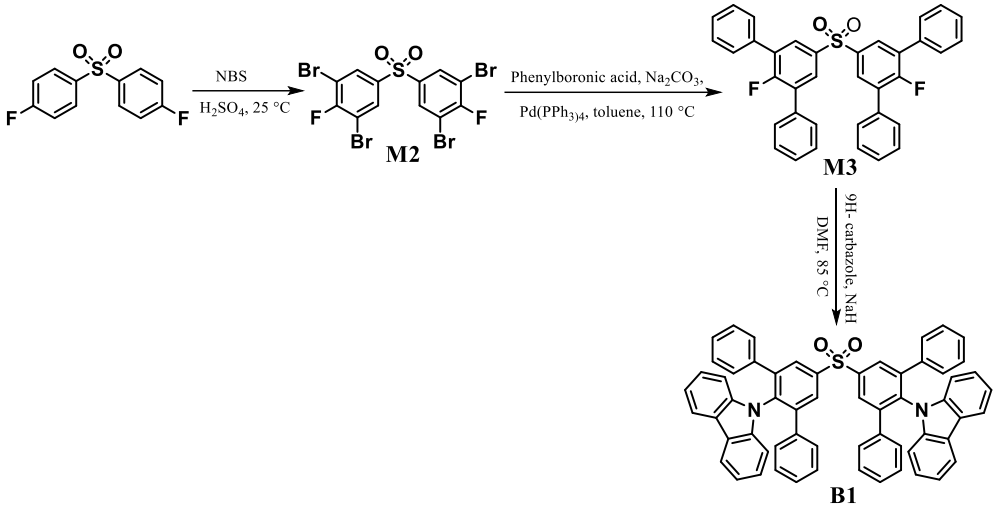

Scheme 13. Synthetic procedure of compound **B1**

4.2.2 Theoretical calculations

Density functional theory (DFT) simulations with the B3LYP functional at the basis set level of 6-31G(d,p) were conducted to investigate the electronic structure of compound **B1**. The data obtained are presented in Fig. 9. The theoretical HOMO and LUMO energies of the new molecule were found to be -5.41 eV and -1.81 eV, respectively. As shown in Fig. 9, the geometry of **B1** is highly twisted, which alleviates the separation of HOMO and LUMO. HOMO is mainly located on the carbazolyl group with a slight extent on the adjacent benzene rings, while LUMO of **B1** is distributed on the tetraphenyl substituted diphenyl sulfone unit. Energies of S_1 of 3.13 eV, a T_1 of 2.93 eV, and a ΔE_{ST} of 0.2 eV were obtained for **B1**.

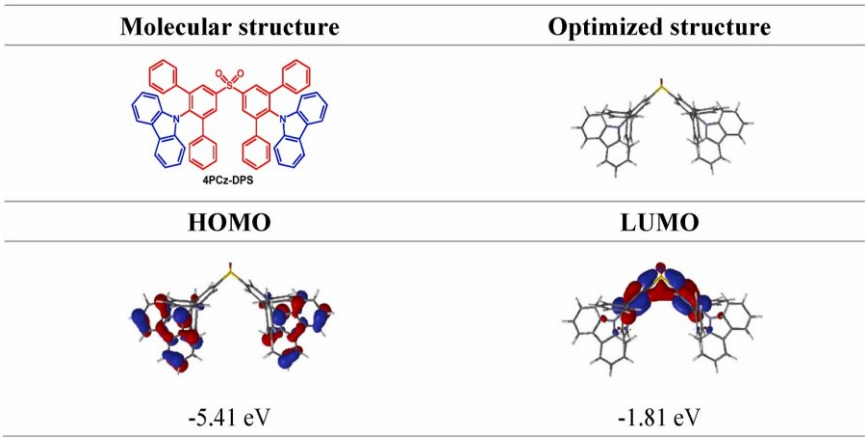

Fig. 9. Optimized, molecular structure and spatial distribution of HOMO and LUMO of **B1**, calculated by the B3LYP functional at the basis set level of 6-31G (d,p)

4.2.3 Thermal and electrochemical properties

Differential scanning calorimetry (DSC) measurements confirmed that **B1** was obtained as an amorphous compound. When the sample of **B1** was heated during the first scan, no peaks due to melting and crystallization appeared. During the DSC heating second scan it exhibited only glass transition at 153°C (Fig. 10a). The temperature of the onset of weight loss was found to be 467°C. The full weight loss in the TGA experiment implies that sublimation started at this temperature.

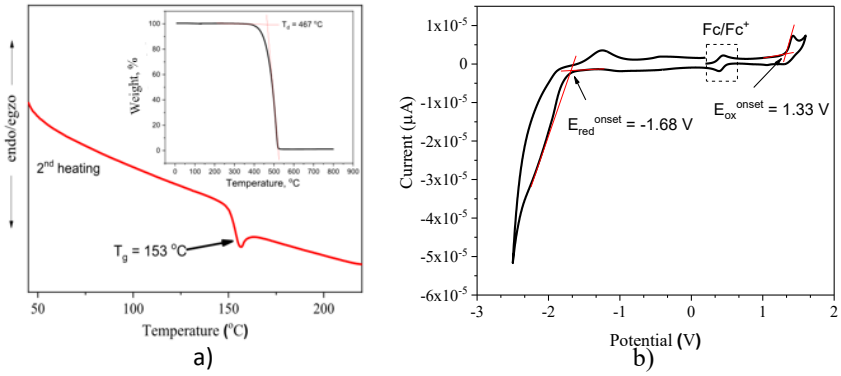

Fig. 10. DSC thermogram of **B1**. The onset weight loss value of TGA curve of **B1**(a); CV curve of the solution of **B1** in dichloromethane (100 mV/s) (b)

Electrochemical properties of **B1** were studied by cyclic voltammetry (CV). The cyclic voltammogram is depicted in Fig. 10b. The oxidation peak observed at 1.33 V can be attributed to the single electron oxidation process of carbazolyl moiety resulting in the formation of radical cation. Ionization potential (IP_{CV}) was estimated by the formula $|-(1.4 \times 1e^{-} . E^{ox}$ *vs* Fc/V) − 4.6| eV[90]. The IP_{CV} of B**1** was revealed to be 5.88 eV. The value of electron affinity (EA_{CV}) was assessed to be 2.78 eV from IP_{CV} and optical band gap value measured for the neat film (E_g = 3.1 eV). Compound

B1 exhibited polymerisation during the repeated cycles (Fig. 10b), the polymerisation happened through position 3 and 6 of the carbazole moietiees of compound **B1**. The polymerization of compound **B1** impacts the morphology of the films, layers of the device, photophysical and charge-transporting properties of the device. Consequently, such polymerization provides stability, durability, flexibility, and efficiency to the OLED device. On the other hand, such polymerization of a compound could possess vulnerability to damage caused by contact with water or moisture.

4.2.4. Photophysical properties

The major data of photophysical investigation are summarized in Fig. 11. The absorption spectra of neat film and the solutions of **B1** were found to be similar. More specifically, peaks at ca. 289, 323 and 334 nm can be attributed to the π-π* transitions of carbazole moiety[91]. The shoulder at ca. 350 nm can be assigned to the state of intramolecular charge transfer (ICT) between donor and acceptor units. Slight blue shift and decrease of absorbance upon increase of polarity of solvent evident in Fig. 11a points to the ICT character of the lowest energy absorption band. Enhanced intermolecular interactions in the solid state causes the broad spectral tail of absorption of the neat film at wavelengths longer than 385 nm. Emission spectra of the solutions contain a single narrow peak which is red-shifted by 25 nm when a non-polar toluene is replaced with a THF. Further red-shifts of 32 and 54 nm were observed for PL spectra of the solutions of **B1** after replacing the low-polarity solvent toluene with highly polar DCM and MeCN, respectively. The emission was found to be sensitive to the presence of oxygen which intercepts electronic excitation energy enhancing non-radiative deactivation of excited states. Increase of intensity of emission of the toluene solution of **B1** by the factor of 1.4

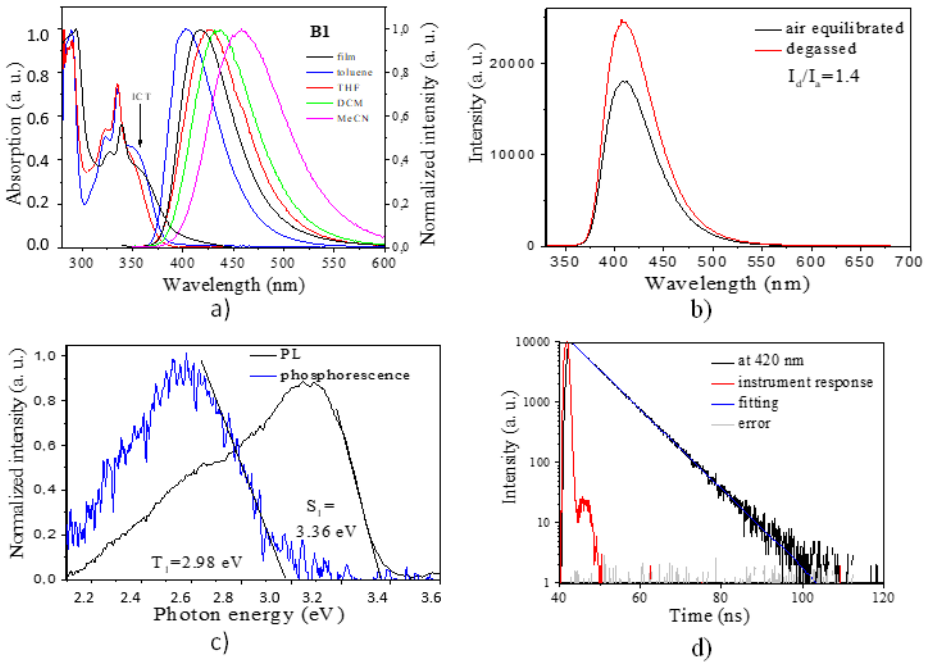

Fig. 11. Absorption and PL spectra of deoxygenated dilute toluene, THF solutions and neat film (a), PL spectra of air equilibrated and degassed dilute toluene solutions (b) PL and phosphorescence spectra (c) of dilute THF solution; PL decay curve of deoxygenated dilute toluene solution (d) of **B1** Cut-offs of toluene and THF

was observed upon removing air (Fig. 11b). The phosphorescence spectrum of the THF solution of **B1** measured at 77 K corresponds to the carbazole emission[94]. The energy levels of the first excited singlet and triplet states estimated from the onsets of PL and phosphorescence spectra recorded at liquid nitrogen temperature were found to be 3.36 and 2.98 eV, respectively (Fig. 11c). High triplet levels allow to use this material as the host matrix for the emissive dopant. The energy splitting of 0.38 eV between the first excited states excludes the efficient reverse intersystem crossing. As a result, the evidence of the presence of only prompt fluorescence was observed in PL decay curve of the toluene solution of **B1** (Fig. 11d).

The lifetime values of emission estimated from the double exponential fit were found to be 1.69 and 6.6 ns (weighted sum of square deviations of calculated values χ^2 is 1.002) pointing to the mixture of optical centers of ICT and local excited states. It should be additionally mentioned that long-lived fluorescence of **B1** under optical and electrical excitation was detected when an appropriate host was used. Photophysical and electroluminescent investigations of **B1**-based guest:host systems are discussed in section 4.2.6. Emission spectra of **B1** in different solid states (aggregates formed in THF/water mixtures, non-doped or doped films) are practically the same which are apparently caused by the restricted by phenyl substituents changes of dihedral angles between donor and acceptor moieties and by reduced possibilities of the formation of the different conformers and aggregates in solid state.

4.2.5. Charge injecting and charge transporting properties

To properly design the structure of **B1**-based OLEDs with good charge-injecting properties, ionization potential (IP_{PESA}) of 5.9 eV was estimated for the solid sample of **B1** by electron photoemission spectroscopy in air (Fig. 12a). The value of electron affinity was assessed to be 2.8 eV from IP_{PESA} and optical band gap value measured for the neat film (E_g = 3.1 eV). These values are in good agreement with the corresponding ones taken by CV measurements for the solution of **B1** (Fig. 10b)**.** Charge-transporting properties of compound **B1** were investigated by using the time-of-flight (TOF) method. The samples we pulsed laser excited at 355 nm through optically transparent ITO electrode. Both hole and electron transport were detected. The corresponding carrier transit times (t_{tr}) were seen as the crossing of the asymptotes to the current plateau and the current tails of TOF current transients plotted in log-log scales. The current transients display a high degree of dispersion of hole and electron transport. Room-temperature TOF hole (μ_h) and electron (μ_e) mobilities of 4.15 μm thick vacuum-deposited film **B1** placed between ITO and Al electrodes as a function of electric field are plotted in Fig. 12b. Higher hole mobility (μ_h) of 1.48×10^{-5} $cm^2V^{-1}s^{-1}$ at electric field of 3.6×10^5 Vcm^{-1} were obtained relative to electron mobility (μ_e) of 1.37×10^{-6} $cm^2V^{-1}s^{-1}$ observed at the same electric field. The higher μ_h by ca. one order of magnitude than μ_e can be attributed to the higher number of electron-donating units in **B1.**

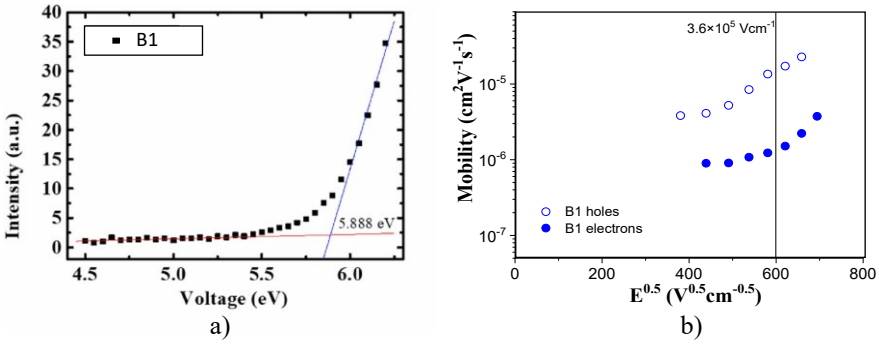

Fig. 12. Photoelectron emission spectrum (a) and TOF hole and electron mobilities as a function of electric field for vacuum-deposited film (b) of **B1**

4.2.6. Performance in OLEDs

Table 8. EL characteristics of OLEDs with emitting layers of **B1**, DPEPO:**B1** and **B1**:4CzIPN

EML	Voltage (V) @ 1 (cd/m^2)	CE (cd/ A)[a]	PE (lm/ W)[a]	EQE (%)[a]	CIEx,y[b]
B1	3.46	0.78/-	0.70/-	0.69/-	(0.15, 0.09)
DPEPO:**B1**	5.43	0.81/-	0.51/-	0.71/-	(0.15,0.08)
B1:4CzIPN	3.16	67.74/ 64.51	60.94/ 39.58	23.38/ 22.34	(0.25,0.55)

[a] Recorded at maximum and 1,000 cd/m^2; [b] CIE 1931 coordinate at 6 V; - – not observed.

Fig. 13 shows the chemical structures of the compounds used and energy levels of the layers. The device structure of TADF-OLED employing **B1** as host and 4CzIPN as dopant was ITO/50 nm 1,1-bis[*N*,*N*-di(4-tolyl)aminophenyl]cyclohexane (TAPC)/10 nm *meta*- bis(*N*-carbazolyl)phenylene (*m*CP)/30 nm, 10% **B1**:4CzIPN/70 nm diphenylbis[4-(3-pyridyl)phenyl]silane (DPPS)/0.8 nm LiF/120 nm Al, where TAPC, *m*CP, and DPPS are materials used for the preparation of hole-transporting layer (HTL), hole-injection layer (HIL), and electron-transporting layer (ETL), respectively. The layer of LiF was the electron injection layer and Al was the cathode. The device structure of TADF-OLED employing DPEPO as host and **B1** as dopant was ITO/50 nm TAPC/10 nm *m*CP/30 nm, 10% DPEPO:4CzIPN/50 nm DPPS/0.8 nm LiF/120 nm Al. DPEPO is commonly used as a wide bandgap host material for deep blue emitters with ultra-high triplet energy of 3.30 eV[95,96]. Non-doped device with 30 nm layer of neat **B1** as emitting layer was also prepared to compare the performances and exciton dynamics with those of the doped OLEDs. Three OLEDs with emitting layers (EML) of **B1**, DPEPO: **B1** and **B1**:4CzIPN were fabricated to investigate the device performances and exciton dynamics. Only small turn-on voltage differences at 1 cd/m^2 in J-L-V characteristic were observed between OLED based on **B1**:4CzIPN (V = 3.16 V) and device with a neat layer of **B1** (V = 3.46 V), which indicated that electrons and holes were efficiently transported and recombined on the host material instead of being trapped by 4CzIPN emitter (Fig. 14a). For the OLED with the emitting layer of DPEPO: **B1** high turn-on voltage of 5.43 V was observed which originated from the large electron barrier from ETL to DPEPO. The CE, PE and EQE characteristics of three devices are shown in Fig. 13(b) and (c) and summarized in Table 8. OLEDs with the emitting layers of DPEPO: **B1** and **B1** showed poor device performances with EQE less than 1% despite its delayed fluorescence with life-time of 186.2 μs in DPEPO host (Fig. 15b). However, TADF-OLED with the emitting layer of **B1**:4CzIPN showed good performance with the maximum current efficiency (CE_{max}) of 67.7 cd/A, the maximum power efficiency (PE_{max}) of 60.9 lm/W, and the maximum external quantum efficiency (EQE_{max}) of 23.3% with low efficiency roll-off, which only decrease by 4% (EQE = 22.3%) at 1,000 cd/m^2. This observation indicates that triplet energy of **B1** can be effectively extracted by dopant with high PL quantum yield without being wasted. Electroluminescence spectra of OLEDs with emitting layers of DPEPO: **B1** and **B1** ranged from 380 to 700 nm with the peak wavelengths of 426 nm and 430 nm and FWHM of 74 nm and 80 nm, respectively (Fig. 14d). They were similar to the PL spectrum of thin film of **B1**. The CIE 1931 coordinate was (0.15, 0.09) and (0.15, 0.08) at 6 V which corresponds to deep blue color. For **B1**:4CzIPN TADF-OLED, all the emission originated from 4CzIPN with no leakage from **B1**, which indicated efficient energy transfer from **B1** to 4CzIPN.

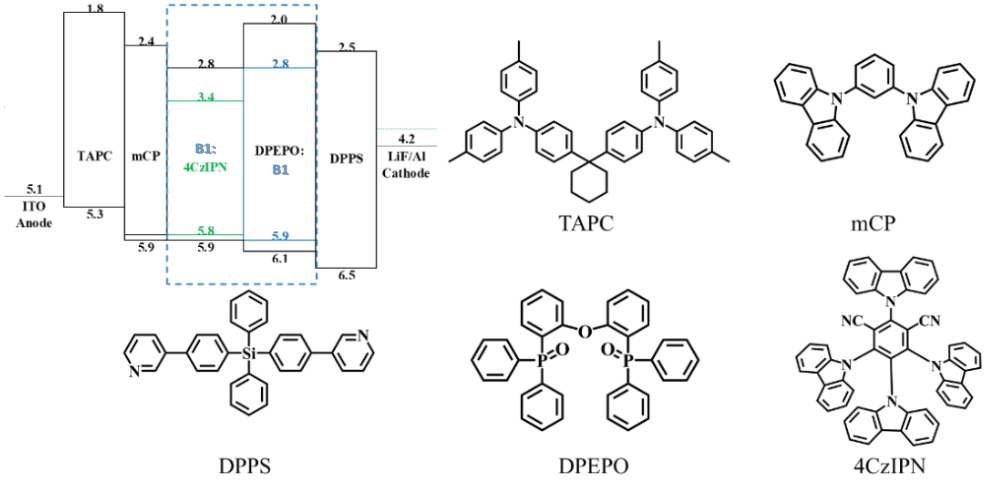

Fig. 13. The chemical structures of materials and energy levels of the layers of OLED containing **B1** as host material with 4CzIPN as emitter, and as dopant with DPEPO as host

In order to investigate the exciton dynamics of **B1**-based OLEDs, transient photoluminescence (TRPL) and transient electroluminescence (TREL) experiments were conducted. Fig. 15a shows the steady state PL spectra and fluorescence decay curves in 2 μs window of the films of **B1** in **B1**:4CzIPN. No leakage of emission from **B1** in thin film of **B1**:4CzIPN can be observed from the PL spectra, indicating excellent Forster resonance energy transfer with good wave function overlap between the host and dopant. Photoluminescence quantum yields of 34% and 90% were observed for thins films of for **B1** and **B1**:4CzIPN, respectively. These results confirm efficient triplet energy extraction from **B1** by the 4CzIPN dopant. In TrPL signal, no delayed fluorescence from pristine film of **B1** was observed, which might be due to more severe triplet-polaron quench (TPQ) with high density of long-living triplet exciton and poor RISC[97].

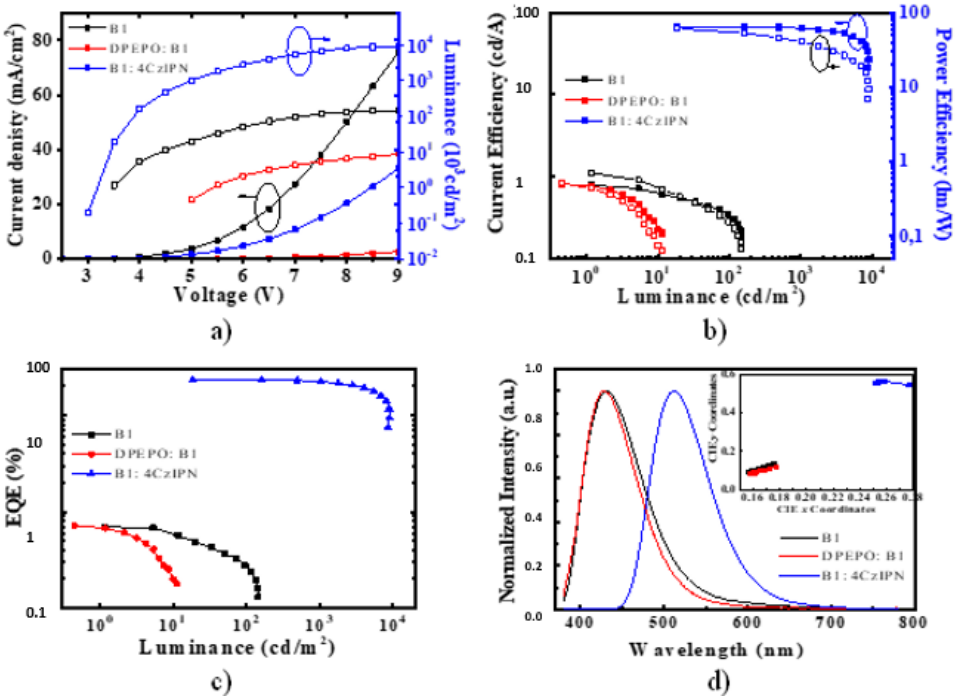

Fig. 14. Current density (J) and luminance (L) versus voltage (V) (a); current efficiency (CE), power efficiency (PE) as a function of current density(b); external quantum efficiency (EQE) as a function of current density and (c); normalized EL spectra at 6 V. The inset of shows the color coordinates (d)

Once 4CzIPN was doped in **B1**, delayed fluorescence from 4CzIPN emitter with the lifetime of 1.88 μs was observed. The lifetime is close to the intrinsic lifetime of delayed fluorescence of 4CzIPN[97]. Fig. 15 b, c show the TREL signals of OLEDs with emitting layers of DPEPO: **B1**, **B1**:4CzIPN and **B1** recorded under different driving voltages. For OLED with the emitting layer of DPEPO: **B1** with the weak intermolecular interaction of the dopant molecules, a clear delayed fluorescence was observed with the lifetime of 97.2 μs under 7.5 V driving. Delayed fluorescence ratio and lifetime decreased as the driving voltage (current) increased. This observation can be attributed to stronger triplet-polaron quench[99]. TREL signal of OLED based on **B1**:4CzIPN showed single exponential decay with the lifetime of 3 μs under all driving conditions[98]. The high efficiency of energy transfer from host to dopant with negligible triplet-polaron quenching can explain the high efficiency and low efficiency roll-off of **B1**:4CzIPN-based TADF-OLED. It should be noted that previously published either carbazolyl or phenothiazinyl-substituted diphenyl sulfones were characterized by mechanochromism as well as by different emission colors including white with TADF properties partly due to the different dihedral angles between the donor and diphenyl sulfone moieties[100]. Such emission variations of TADF compounds based on flexibly-linked carbazole/phenothiazine and diphenyl sulfone moieties in solid-state lead to the formation of different energy states which may act

as additional energy loss pathways if the compounds are used as OLED hosts. Since the above-mentioned compounds[100] were not used as OLED hosts, our presumption concerning additional energy loss pathways in OLEDs containing TADF hosts with flexible molecular structure cannot be verified. Nevertheless, we should note that no emission variations were detected for the developed derivative of tetraphenyl-substituted diphenyl sulfone and carbazole (**B1**). TADF may be dramatically enhanced or suppressed in guest:host emitting systems. Consequently, TADF appears when **B1** is doped in DPEPO exhibiting long-lived component of the PL decay curve with a lifetime of 186.2 μs (Fig. 15b). Practically the same EL spectra were obtained for devices with the emitting layers of **B1** and **B1**:DPEPO (Fig. 14d). Such doping insensitive electroluminescence of OLEDs based on the TADF compound **B1** is very unusual in comparison to the previously reported OLEDs with doped and non-doped emitting layers based on TADF compounds which can be very sensitive to polarity and rigidity of hosting media[101]. Such electroluminescent properties of **B1**-based OLEDs are apparently due to tetraphenyl ornamenting of diphenyl sulfone moiety of **B1**. The restricted variations of dihedral angles between donor and acceptor moieties and restriction of formation of the different conformers and aggregates for **B1**, prevent the formation of additional energy loss pathways in OLEDs resulting in their very low roll-off efficiency (Fig. 14c).

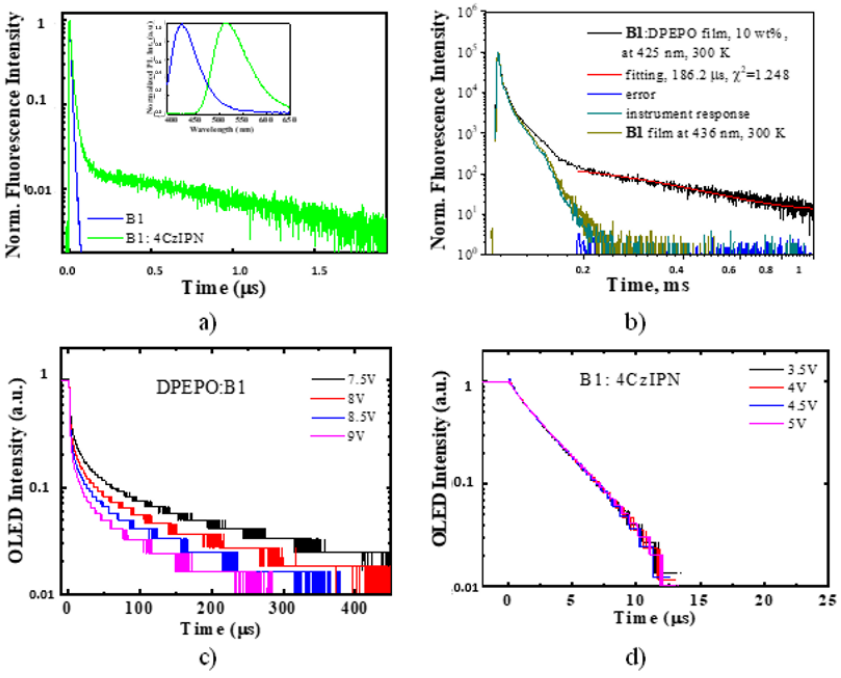

Fig. 15. (a, b) TRPL of thin films of **B1** (60 nm), **B1**:4CzIPN (60 nm, 10%) and **B1**:DPEPO (60 nm, 10%) in 2 μs or 1 ms windows and TREL signal of (c) DPEPO:**B1** and (c) **B1**:4CzIPN based OLEDs. The inset of (d) showed the normalized PL spectra

Therefore, enhancement of TADF for **B1**:DPEPO film is attributed to the high polar DPEPO host adjusting position of energy levels of triplet excited states in the manner that stimulate efficient RISC while the spectral distribution of up-converted excitons deactivated from the first singlet excited state is not altered. Although compound **B1** did not show good performance in OLEDs as emitter due to an inefficient TADF when being non-doped or an efficiency quench when doped in a host, the proposed design strategy of TADF compounds with "frozen" emission color (host-independent emission color) has predictably practical significance for the further development of efficient TADF OLED emitters. Additionally, while no TADF was observed for the neat film of **B1** (Fig. 11d), it can occur for the compound in **B1**:4CzIPN layer as 4CzIPN can alter the TADF kinetics of **B1** similarly to DPEPO which hypothetically can open a path to harvest triplet energy in both **B1** host and 4CzIPN guest resulting in high EQE.

4.3. 1,8-naphthalimide based derivatives

The appropriate design of donor–acceptor type compounds may lead to small singlet–triplet energy splitting (DE_{ST}) assisting efficient harvesting of triplet excitons via thermally boosted reverse intersystem crossing (RISC)[181]. The OLEDs exhibiting electroluminescence (EL) of different energy with 20% or higher external quantum efficiencies (EQEs) were developed without utilizing phosphorescent emitters based on rare-earth metals suffering from complicated synthesis, high cost, or environmental problems[182-184]. Typically, light-emitting layers of state-of-the-art TADF based OLEDs are based on host–guest systems allowing the aggregation-caused quenching and charge-transporting issues of the materials with twisted donor–acceptor molecular structures to be solved[185,186]. However, such OLEDs still suffer from high efficiency roll-offs apparently caused by predominating hole-transport of both the host and guest materials within the light-emitting layers. In this work, we aimed to develop TADF emitters with high electron mobilities. It is shown that roll-off OLED efficiency issues can be fixed by utilizing host–guest systems based on a host with preferable hole-transport and a TADF guest with preferable electron-transport. With this purpose, three new compounds C1–C3 (Scheme 10) were synthesized substituting the 1,8-naphthalimide acceptor moiety with different donors, such as 10H-phenoxazine, 3,7-ditert-butyl-10H-phenothiazine, or 2,7-di-tert-butyl-9,9-dimethyl-9,10dihydroacridine.

4.3.1 Synthetic procedure

The synthetic procedure of compounds **C1**, **C2**, and **C3** is shown in scheme 14. Compounds **C1**–**C3** were synthesized by using Buchwald-Hartwig cross coupling reactions of 4-bromo-*N*-(2-ethylhexyl)-1,8-naphthalimide (**M4**) with 10*H*-phenoxazine, 3,7-di-*tert*-butyl-10*H*-phenothiazine and 2,7-di-*tert*-butyl-9,9-dimethyl-9,10-dihydroacridine, respectively. All compounds were fully characterized by ^{1}H and ^{13}C NMR, IR spectroscopies, mass spectrometry, as well as by elemental analysis.

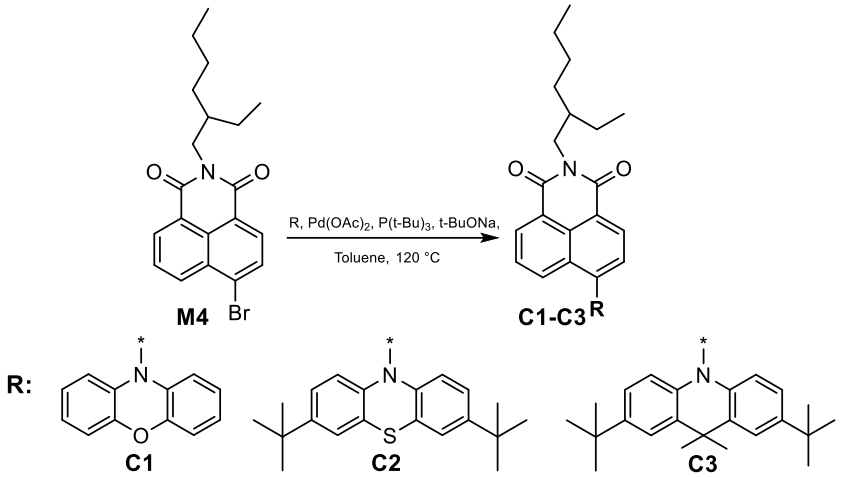

Scheme 14. Synthetic procedure of compounds **C1–C3**

4.3.2. Theoretical calculations

In order to understand the electronic structures of compounds **C1**–**C3** in ground and excited states, DFT calculations were performed at wB97XD/6-31+G(d) level of theory[102]. The calculations were carried out in solutions of toluene and THF. Solvation effects were considered using the SMD model[103] in terms of Linear Response scheme[104]. Previously, we have shown that the mentioned level of theory allows to accurately reproduce the electronic structure of BODIPY dyes in ground and excited states[105]. In the case of calculations of the absorption spectra, the geometry of the ground states S_0 of compounds **C1**–**C3** was fully optimized in solution within DFT approach with subsequent calculation of the spectra within TD-DFT. For the calculations of photoluminescence spectra, the geometry of the first singlet S1 or first triplet T1 excited state was fully optimized in solution within TD-DFT. The values of singlet-triplet splitting (ΔE_{ST}) were estimated as a difference between $E(S_1 \rightarrow S_0)$ and $E(T_1 \rightarrow S_0)$ in the calculated photoluminescence spectra. All calculations were carried out using Gaussian16 program[106]. The analysis of electron density was performed using the Multiwfn software[107]. The wavelengths calculated for compounds **C1**– **C3** corresponding to the first (λ_{ABS}^{ICT}) and the second (λ_{ABS}^{LE}) absorption maxima, wavelengths corresponding to the transitions $S_1 \rightarrow S_0$ in photoluminescence spectra (λ_{PL}^{ICT}), oscillator strengths (f), values of singlet-triplet splitting (ΔE_{ST}), dipole moments variation caused by electron excitation ($\Delta\mu$), separation degree of positive (ρ_+) and negative (ρ_-) parts of electron density (τ-indexes) and overlaps between functions C_+ and C_-[105] (S_{+-}-indexes) are given in Table 9.

Table 9. wB97XD/6-31+G(d) calculated wavelengths corresponding to the first (λ_{ABS}^{ICT}) and second (λ_{ABS}^{LE}) absorption maxima, wavelengths corresponding to maxima in photoluminescence spectrum (λ_{PL}^{ICT},), oscillator strengths (f), values of singlet-triplet splitting (ΔE_{ST}), dipole moments variation caused by electron excitation ($\Delta\mu$), τ- and S_{+-}-indexes of compounds **C1–C3**

Compound / Parameter	C1	C2	C3
λ_{ABS}^{ICT}, nm	420/412[a] (499/491)[b]	399/392 (476/469)	420/417 (499/496)
f	$<1\cdot10^{-4}/<1\cdot10^{-4}$	$<1\cdot10^{-4}/<1\cdot10^{-4}$	0.0002/0.0002
Δμ, Debye	17.4/18.8	17.9/19.2	18.0/19.3
τ-index	0.266/0.646	0.116/0.519	-0.019/0.355
S_{+-}-index	0.744/0.703	0.790/0.750	0.791/0.757
λ_{ABS}^{LE}, nm	314/320 (386/393)	316/321 (388/394)	316/322 (388/395)
f	0.4876/0.5622	0.5271/0.5944	0.5082/0.5755
Δμ, Debye	1.87/2.19	2.23/2.48	2.05/2.33
τ-index	-0.926/-0.748	-0.990/-0.786	-1.028/-0.829
S_{+-}-index	0.959/0.947	0.946/0.938	0.956/0.946
λ_{PL}^{ICT}, nm	520/511	535/523	495/492
τ-index	0.275/0.661	0.150/0.569	-0.017/0.343
S_{+-}-index	0.740/0.699	0.773/0.733	0.792/0.759
ΔE_{ST}[c], eV	0.011/0.011	0.007/0.004	0.011/0.011

[a] The values calculated for toluene/THF as solvent are given through slash. [b] Scaled using correlation equation from our previous paper[105] values of λ_{ABS} are given in brackets: λ_{ABS}(scaled) = 1.062·λ_{ABS}(calc.) + 52.96. [c] Estimated as $E(T_1\rightarrow S_0) - E(S_1\rightarrow S_0)$ in the calculated emission spectra

The electron density difference (Δρ) between the S_1 and S_0 states and $S_0 \rightarrow S_1$ charge transfer (CT) calculated for compounds **C1–C3** electron density difference ($\Delta\rho$) between S_1 and S_0 states and $S_0\rightarrow S_1$ charge transfer (CT) are visualized in Fig. 16, whereas $\Delta\rho$ between S_2 and S_0 states and $S_0\rightarrow S_2$ CT are visualized in Fig. 17. The plots of the molecular orbitals and values of largest coefficients in the CI expansion for $S_0 \rightarrow S_1$ and $S_0 \rightarrow S_2$ excitation calculated for compounds **C1–C3** plots of molecular orbitals and values of largest coefficients in the CI expansion for $S_0\rightarrow S_1$ and $S_0\rightarrow S_2$ excitation are given in Fig. 18.

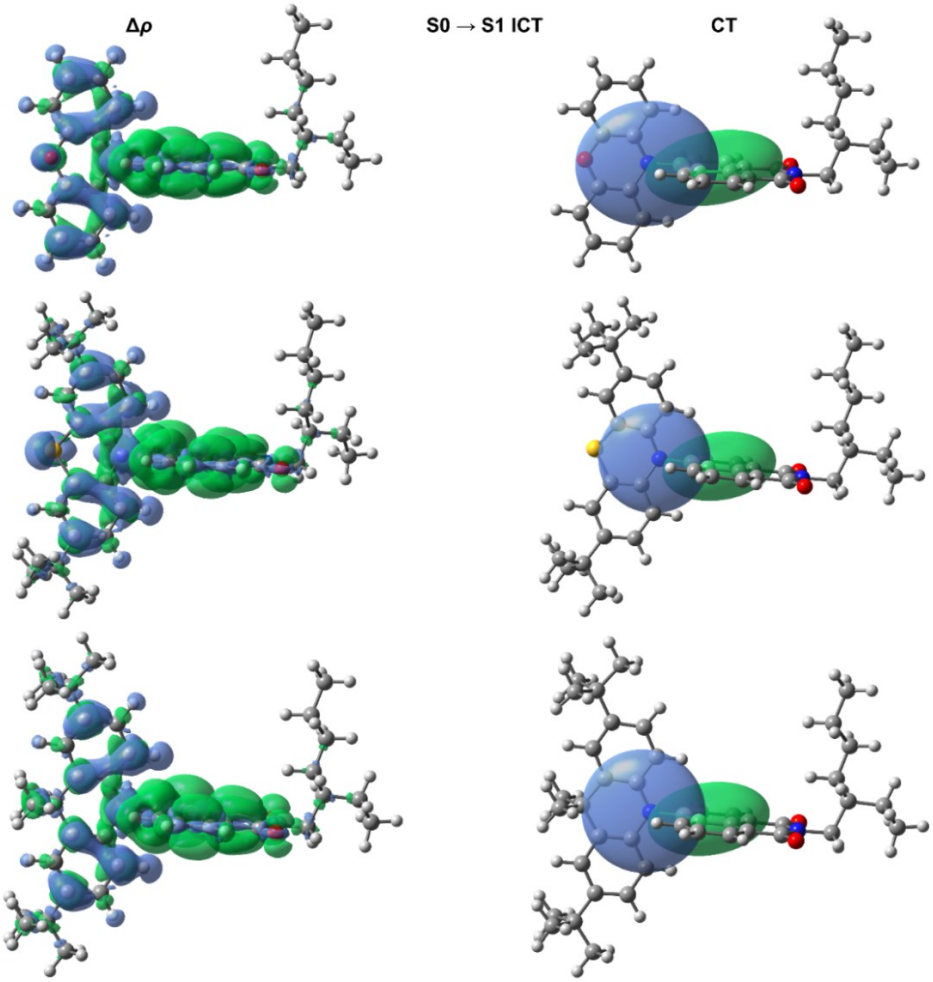

Fig. 16. wB97XD/6-31+G(d) calculated for compounds **C1–C3** in toluene plots of $\Delta\rho$ $S_1 \rightarrow S_0$ and $S_0 \rightarrow S_1$ CT. Green (blue) regions indicate an increase (decrease) in ρ upon electronic transition

Despite wB97XD functional providing accurate reproduction of the absorption spectra by both intensity and the relative peak position[108,109], this functional significantly underestimates the wavelengths of absorption maxima[105,108,109]. Therefore, for comparison of our calculated positions of the first and second absorption maxima with the experimental ones, we scaled the calculated results using correlation equation from our previous paper[105]: $\lambda_{ABS}(\text{scaled}) = 1.062 \cdot \lambda_{ABS}(\text{calc.}) + 52.96$, nm. The scaled values of wavelengths corresponding to the first maxima in absorption spectra of compounds **C1–C3** (Table 9) are in very good agreement with the experimental data (see Table 9). As it can be seen from Fig. 16, the first maxima in absorption spectra ($S_0 \rightarrow S_1$ transitions) of compounds **C1–C3** can be attributed to the intramolecular charge transfer (ICT) states formed between the electron-donating moieties and electron-accepting 1,8-naphthalimide. It is also confirmed by the data of

Table 9. Thus, the $S_0 \rightarrow S_1$ excitation for all considered compounds is accompanied by a very large variation of the dipole moment (more than 17 Debye) and it corresponds to a positive value of the τ-index (with the exception of compound **C3** in toluene solution). It should be noted that a larger positive τ-index value means a lager separation degree of ρ_+ and ρ_- and therefore a larger CT. If the value of τ-index is much less than zero, it implies that ρ_+ and ρ_- are not substantially separated due to excitation. According to the data in Table 9 the largest separation of electronic density corresponds to $S_0 \rightarrow S_1$ excitation of compound **C1** and the smallest separation corresponds to compound **C3**. It is in agreement with the calculated and the experimentally observed values of hypsochromic shifts in the row of compounds **C1**–**C3** with increasing of solvent polarity (compare the λ_{ABS}^{ICT} values in toluene (ε=2.3741) and THF (ε=7.4257) given in Tables 8 and 9). Thus, the lowest value of hypsochromic shift corresponds to compound **C3** and the largest one – to compound **C1**. The calculated overlaps between functions C_+ and C_- (S_{+-}-indexes) are significantly less than **C1**, meaning that these functions are substantially separated. Therefore, $S_0 \rightarrow S_1$ excitation is characterized by very low values of the oscillator strength *f* (Table 9). In the case of compound **C3**, the slightly larger value of S_{+-}-index corresponds to slightly larger f. The largest coefficients in the CI expansion for $S_0 \rightarrow S_1$ excitation correspond to HOMO→LUMO transitions for all compounds (see Fig. 18). That is S_1 state mainly results from the HOMO→LUMO excitation that implies an electron transfer from phenoxazine, 3,7-di-*tert*-butylphenothiazine, or 2,7-di-*tert*-butyldimethyl-9,10-dihydroacridine as donors, where the HOMO is localized, to the 1,8-naphthalimide as acceptor, where the LUMO resides (Fig. 18).

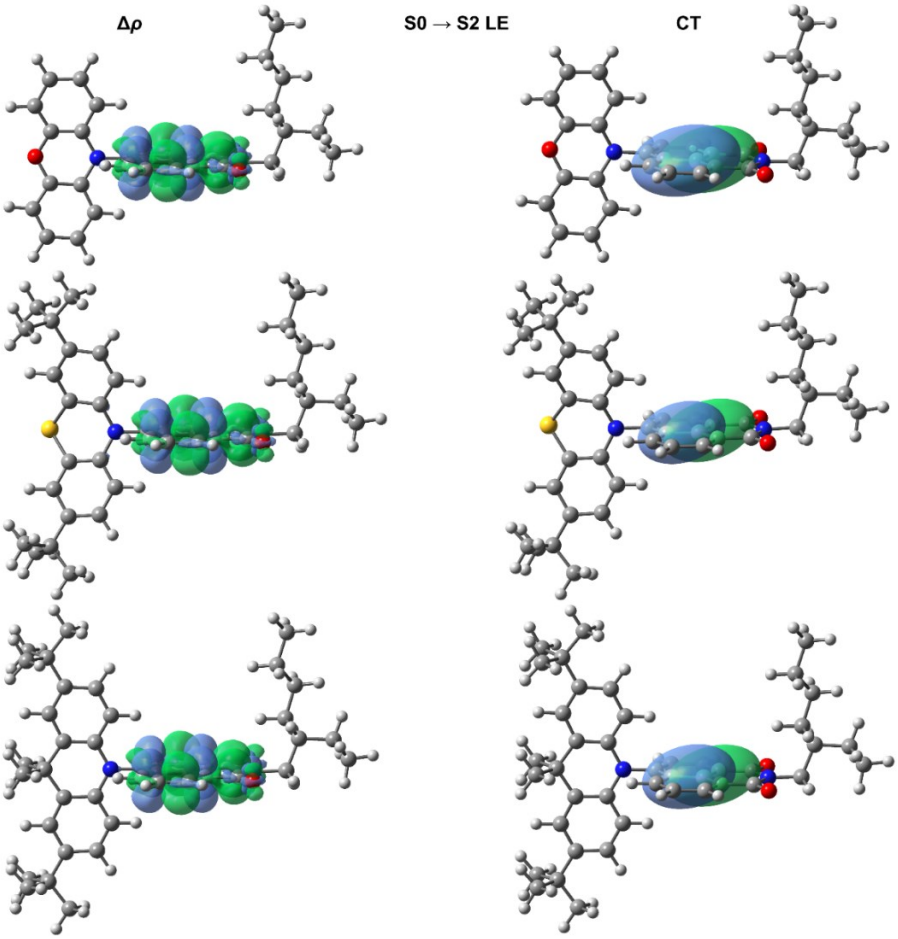

Fig. 17. wB97XD/6-31+G(d) calculated for compounds **C1–C3** in toluene plots of $\Delta\rho$ $S_2 \rightarrow S_0$ and $S_0 \rightarrow S_2$ CT. Green (blue) regions indicate an increase (decrease) in ρ upon electronic transition

The second maxima in absorption spectra ($S_0 \rightarrow S_2$ transitions) of compounds **C1**–**C3** can be attributed to the π-π* local excitation (LE) of 1,8-naphthalimide moiety (see Fig. 17 and 18). In contrast to the previously considered $S_0 \rightarrow S_1$ excitation, the $S_0 \rightarrow S_2$ transition is not accompanied by a significant change in the dipole moment and it corresponds to a large negative value of the τ-index for all compounds (see Table 9). The calculated values of $S_{+,-}$-indexes are close to 1, meaning the C_+ and C_- functions are strongly overlapped. Therefore, $S_0 \rightarrow S_1$ excitation is characterized by large values of the oscillator strength (Table 9). The largest coefficients in the CI expansion for $S_0 \rightarrow S_2$ excitation correspond to HOMO-2→LUMO (compounds **C1** and **C2**) or HOMO-1→LUMO (compound **C3**) transitions (Fig. 3). That is, S_2 state mainly results from π-π* local excitation of 1,8-naphthalimide moiety. The slight difference in absorption of compounds **C2** and **C3**, in comparison with compound **C1**,

is caused by more contribution in their HOMO-2 or HOMO-1 of the corresponding donors (Fig. 18).

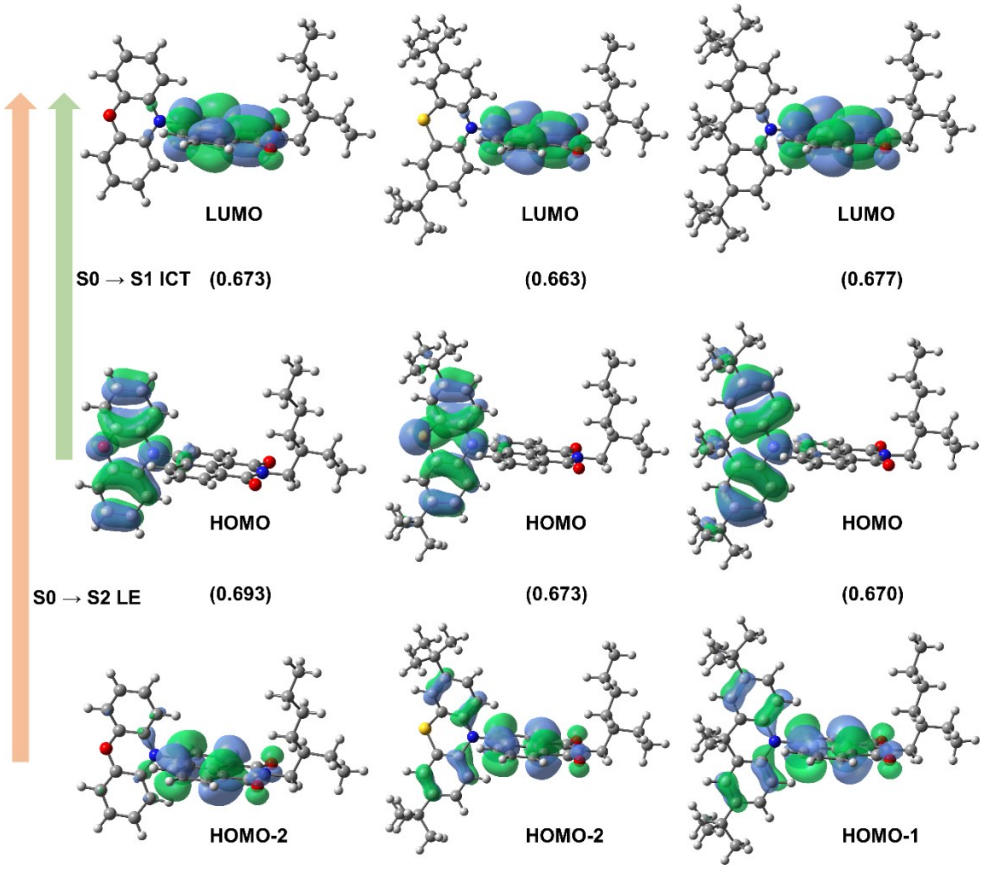

Fig. 18. wB97XD/6-31+G(d) calculated for compounds **C1–C3** in toluene plots of MOs and values of largest coefficients in the CI expansion (in brackets) for $S_0 \rightarrow S_1$ and $S_0 \rightarrow S_2$ excitation

Considering that the wB97WD functional significantly underestimates the wavelengths of absorption and emission maxima, the calculated values of λ_{PL}^{ICT} for compounds **C1–C3** in toluene (Table 10) are in reasonable agreement with the experimental ones (Table 10). That is, the largest value of λ_{PL}^{ICT} both in the experimental and in the calculated emission spectra corresponds to compound **C2** and the lowest one corresponds to compound **C3**. The hypsochromic shiftobserved in the PL spectra for compounds **C1** and **C2** with increasing polarity of solvent (see Table 10) is also in agreement with the results of the calculations (Table 9). According to the experimental data, PL spectrum of compound **C3** is almost unshifted with a change in the polarity of the solvent (Table 10). This result is in agreement with the calculated values of λ_{PL}^{ICT} in toluene and THF for compound **C3**, as well as with the lowest value of τ-index of compound **C3** among all considered compounds. The values calculated

for compounds **C1–C3** of singlet-triplet energy splitting (ΔE_{ST}) are very small (Table 10) which is also in agreement with the experimental data (see Table 10).

4.3.3. Thermal properties

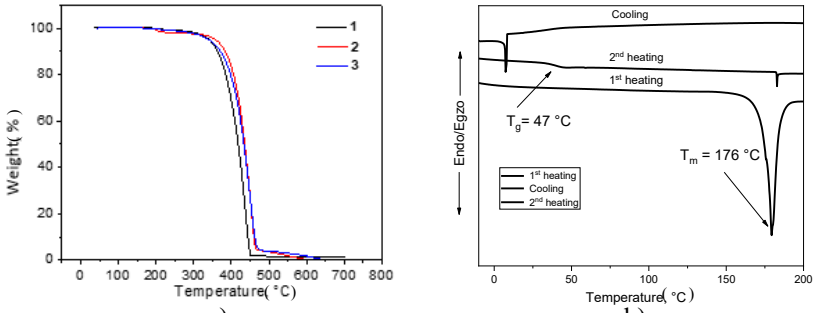

Fig. 19. TGA curves of **C1–C3** (a) and DSC thermograms of **C2** (b)

Thermal properties of compounds **C1–C3** were studied by thermogravimetric analysis (TGA) and differential scanning calorimetry (DSC) under a nitrogen atmosphere. From TGA curves, 5% weight loss temperatures ($T_{ID\text{-}5\%}$) higher than 370°C were obtained showing that compounds can be used for device fabrications by thermal processes (Fig. 19a, Table 10). Because of the similar molecular weights of compounds **C1–C3**, they demonstrated similar TGA trends with practically the same $T_{ID\text{-}5\%}$ temperatures. TGA curves of compounds **C1–C3** show a sublimation pattern. The compounds were obtained as crystalline substances after the synthesis and purification. The solid sample of **C2** melted at 176°C during the first DSC heating scan (Fig. 19b, Table 10). Derivatives **C1** and **C3** were characterized by similar melting point T_m values (Table 10). During the second scan, glass transition was detected for compound **C2** at 47°C. Compounds **C1** and **C3** exhibited considerably higher glass transition temperatures (T_g) of 76°C and 83°C, respectively.

4.3.4 Photophysical properties

Table 10. Thermal and photophysical parameters of compounds **C1–C3**

Compound	Media	**C1**	**C2**	**C3**
T_m[a], °C	Powder	179	176	181
T_g[b], °C		76	47	83
T_d^{onset} [c], °C		395	380	370
λ_{ABS}^{ICT}, nm	Toluene/THF	491/482	476/467	483/478
λ_{ABS}^{LE}, nm		344/341	347/344	348/346
λ_{PL}^{ICT}, nm		686/634	751/653	650/652
PLQY, %		2/1	2/1	3/1
PLQY, %	Non-doped film	23	8	26
ΔE_{ST}, eV		0.04	0.05	0.03
PLQY, %	Doped film	53	18	77
τ_{PF}, ns (ratio, %)		14.7 (16%)	14.9 (17%)	15.1 (16%)
τ_{DF}, μs (%)		3.87 (84%)	4.23 (83%)	3.57 (84%)
η_{PF}, %		8	3	12
η_{DF}, %		45	15	65
k_{PF}, s^{-1} ($\times 10^6$)		5.8	2.1	8.16
k_{ISC}, s^{-1} ($\times 10^6$)		0.92	0.35	1.31
k_{DF}, s^{-1} ($\times 10^6$)		0.12	0.04	0.18
k_{RISC}, s^{-1} ($\times 10^6$)		3.77	1.01	5.95

[a] T_m - melting temperature in the second heating (10°C/min, nitrogen atmosphere). [b] T_g - glass-transition temperature (2nd heating scan). [c] T_d^{onset} is the temperature of onset of thermal degradation (20°C/min, nitrogen atmosphere). $k_{PF} = \frac{\eta_{PF}}{\tau_{PF}}$, $k_{ISC} = \frac{\eta_{DF}}{\eta_{PF}+\eta_{DF}} k_{PF}$, $k_{DF} = \frac{\eta_{DF}}{\tau_{DF}}$, $k_{RISC} = \frac{\eta_{DF}}{\eta_{PF}} \cdot \frac{k_{PF}.k_{DF}}{k_{ISC}}$

Absorption bands in two spectral regions, high-energy (at wavelengths up to ca. 370 nm) and low-energy (at wavelengths from ca. 370 to 600 nm) ones, were observed in the absorption spectra of toluene and THF solutions of compounds **C1–C3** (Fig. 20a). Similar absorption properties were observed for the solid films of **C1–C3** (Fig. 20b). The absorption in the high-energy region is caused by p–p* transitions of the local excited (LE) state formed mainly by the 1,8-naphthalimide moiety[112]. The slight differences in absorption of compounds **C1–C3** are caused by the contribution to the LE states of the corresponding donors. The absorption in the low-energy region can be attributed to the ICT states formed between the electron-donating moieties and the electron-accepting 1,8-naphthalimide. Typically, ICT manifests as a single broad absorption band in the low-energy region[113,114]. The ICT bands of the compounds were located at ca. 500 nm, which can be attributed to the strong HOMO–LUMO separation required for TADF[115]. The absorption bands of the compounds exhibit negative solvatochromism (Fig. 20a) as the polarity of the solvents affects the energy levels of the excited states S_1 and S_2. A bigger blue shift of ca. 10 nm was observed for the low-energy band than for the short-wavelength band of absorption. This is additional evidence of the distinctive ICT nature of the S_1 band in contrast to the LE state of S_2.

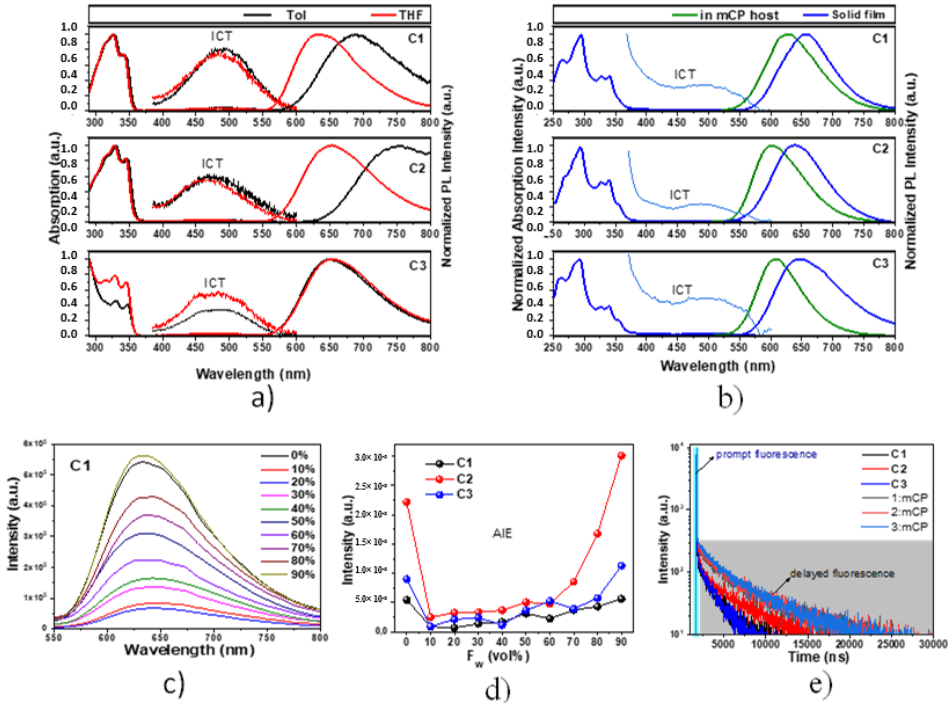

Fig. 20. Absorption and PL spectra of the solutions of compounds **C1–C3** in toluene/THF (a) and of the films of non-doped/doped (10 wt% in mCP) compounds (b) (the absorbance of the low-energy band is enhanced by 20 times for comparison). PL spectra (c) of the dispersions of compound C1 in THF/water mixtures with different water fractions (F_w) and dependencies (d) of the PL intensities versus volume fractions F_W for compounds **C1–C3** dispersed in THF/water mixtures. PL decay curves (e) of the non-doped/doped films of **C1–C3**. Excitation wavelengths are 350 nm for the PL spectra and 374 nm for the PL decay curves

The PL spectra of **C1–C3** in low-polarity toluene were characterized by broad bands peaking at 686, 751, and 650 nm, respectively (Fig. 20a). The red emission resulted from radiative recombination of optically excited ICT excitons of **C1–C3**. The bathochromic shift of emission spectrum of **C2** is apparently determined by the stronger donor attached[116]. PL spectra of the solid samples of **C1–C3** had maxima at 658, 638, and 646 nm, respectively. Hypsochromically shifted PL spectra relative to those of the films of the net compounds were recorded for 10 wt% solid solutions of **C1–C3** in 1,3-bis(N-carbazolyl)benzene (mCP) (Fig. 20b). These experimental data manifest the sensitivity of the ICT states to the media polarity similar to the blue-shift of the emission of the solution caused by the polarity of THF (Fig. 5a) as discussed above. The photoluminescence quantum yields (PLQYs) of toluene/ THF solutions of **C1–C3** were found to be lower than 3% (Table 10). It should be considered that these values were obtained in air and the PL intensity was considerably quenched by oxygen. Considerably higher PLQY values were observed for the solid samples of **C1–C3** especially for the films of the compounds doped in a host (up to 77%). The increase of efficiency of emission in the solid state can be attributed to AIEE[117]. To

study this effect in more detail, PL spectra of compounds **C1–C3** dispersed in THF/water mixtures with different water fractions were recorded (Fig. 20c). When water was added to the THF solution, the PL intensity of **C1–C3** decreased due to the high polarity of water, which induced nonradiative deactivation of ICT states of the compounds[118]. At high enough water fractions for the formation of aggregates, the PL intensities increased, which is the evidence of AIEE[117]. **C2** exhibits the most pronounced AIEE property of the series. As it was shown before, the phenothiazine-based compound can be characterized by a blue-shift of the emission spectra in the solid state when compared to solutions due to the effects of aggregation, arguably caused by phenothiazine-driven aggregation-caused suppression of ICT states in neat and doped films[116,119]. Since the films of compounds **C1–C3** demonstrated high PLQYs, their emission nature in the solid-state was further investigated. PL decay curves of films of **C1–C3** were recorded in a vacuum of $<10^4$ Barr (Fig. 20e). The PL decay curves of the films of the compounds were characterized by the fast and slow components related to prompt and delayed fluorescence. The absence of differences in the shapes of the PL spectra before and after deoxygenation proves that the long-lived emission of compounds **C1–C3** is delayed fluorescence. The enhanced intensities of delay fluorescence of the films of **C1–C3** doped in mCP are in good agreement with the enhanced PLQY values of the films of the compounds doped in mCP relative to those of the films of the pure compounds (Table 10). To check whether the delayed fluorescence is sensitive to temperature, PL decay curves of the films of compounds **C1–C3** were recorded at different temperatures in an inert atmosphere (Fig. 21a). The intensity of delayed fluorescence increased with the increase of temperature from 77 to 300 K. This observation can be attributed to the TADF nature of the emission of compounds **C1–C3**. This is in very good agreement with the small singlet–triplet splittings of 0.03–0.05 eV, which are typical for TADF emitters (Fig. 21b). In addition, the slopes of unity of the plots of delayed emission intensity versus excitation power allow the triplet–triplet annihilation emission nature of the long-lived fluorescence of compounds **C1–C3** to be excluded (Fig. 21c).[121, 122]

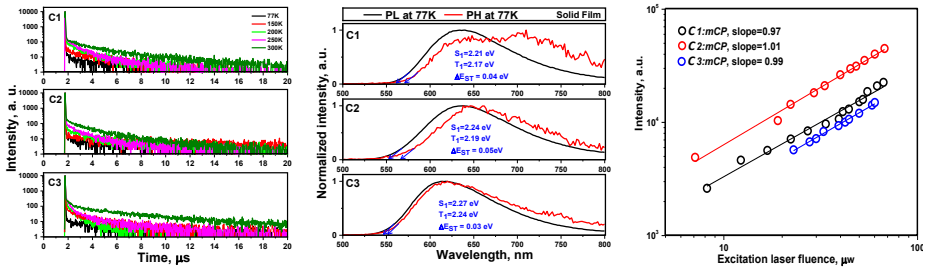

a) b) c)

Fig. 21. PL decay curves (a) recorded at different temperatures and PL/phosphorescence spectra (b) recorded at 77 K of the films of compounds **C1–C3**. Phosphorescence spectra were recorded using a delay of 0.1 ms after excitation. Insets show the energies of the first singlet (S_1) and first triplet (T_1) states and their splittings (DE_{ST}) estimated from the onsets of the high-energy edges of the fluorescence and phosphorescence spectra (shown by arrows). Plots of delayed emission intensity versus excitation power for compounds **C1–C3** (c)

To get more information on the TADF properties of differently substituted napthalimides (**C1–C3**), PL decay curves of the films of 10 wt% solid solutions in mCP were recorded and fitted by the exponential law in nanosecond and microsecond ranges to get the life-times of prompt (t_{PF}) and delayed (t_{DF}) fluorescence, respectively. The results of fitting of the PL decay curves are summarized in Table 10. Using the fitting results, the radiation transition rates (i.e. rate constants of prompt (k_{PF}) and delayed (k_{DF}) components as well as rate constants of intersystem crossing (k_{ISC}) and RISC (k_{RISC}) were estimated (Table 2). The yields of prompt (Z_{PF}) fluorescence and delayed fluorescence (Z_{DF}) were extracted from the total PLQY by comparison of the integrated intensities of the prompt and delayed components. The TADF efficiencies of compounds **C1–C3** can be represented by their rate constants k_{RISC}, the highest value of which (1.13×10^6 s^1) was obtained for compound **C3** (Table 10). The lowest k_{RISC} of 2.08×10^5 s^1 is for **C2** confirming the suggestion made previously[116,119] of phenothiazine causing ICT suppression in the solid mixture of **C2** and a host. This k_{RISC} value of **C3** is, however, among the best for state-of-the-art TADF emitters, displaying the potential of the synthesized compounds (especially of compound **C3**) for practical applications.[123,124]

4.3.5. Electrochemical and photoelectrical properties

Energy levels of compounds **C1–C3** were estimated by cyclic voltammetry (CV) and photoelectron emission (PE) spectrometry. The compounds showed quasi-reversible oxidation in cyclic voltammograms in the range of 0.42–0.60 V (Fig. 22a) that can be attributed to the oxidation of electron-donating moieties, i.e., phenoxazinyl, di-*tert*-butyl-phenothiazinyl or di-*tert*-butyl-9,9-dimethyl-9,10-dihydroacridinyl. Ionization potentials (IP_{CV}) of 5.23, 4.99, and 5.52 eV were obtained for compounds **C1**, **C2**, and **C3**, respectively, from the onset potentials versus the Fc/Fc^+ of their oxidation curves (Table 11). IP_{CV} value of compound **C2** was found to be lower than those of compounds **C1** and **C3**, indicating the stronger electron-donating ability of di-*tert*-butyl-phenothiazinyl moiety. Electron affinity (EA_{CV}) values were determined using equation $EA_{CV} = -(|IP_{CV}| - E_g^{opt})$. The optical band gap energies (E_g^{opt}) were taken from absorption spectra of toluene solutions (Fig. 20a). The EA_{CV} values of **C1–C3** were found to be in the range of 2.87–3.47 eV.

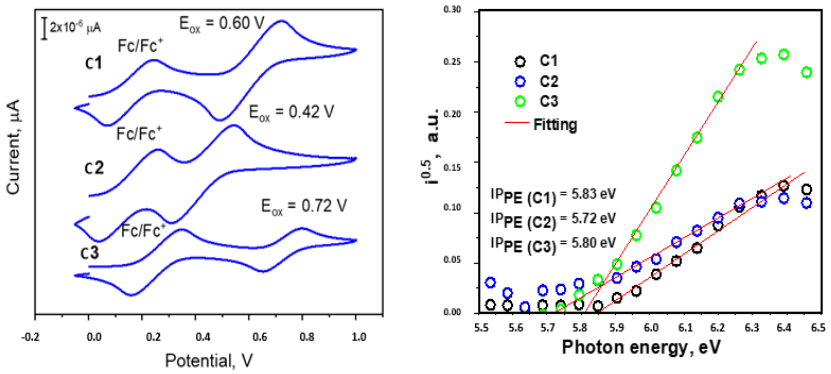

a) b)

Fig. 22. (a) Cyclic voltammograms of the solutions of compounds **C1–C3** in dichloromethane (sweep rate 100 mV/s). (b) Photoelectron emission spectra of vacuum-deposited films of compounds **C1–C3**

Ultraviolet photoelectron and inverse photoemission spectroscopies are required to estimate the ionization potentials (IP_{PE}) and electron affinities (EA_{PE}), respectively, of new organic semiconductors in solid-state for the design of optoelectronic devices based on them[110]. PE spectra of vacuum-deposited films of **C1–C3** on glass substrate with fluorine-doped *tin oxide* electrode were recorded in air (Fig. 22b). Higher IP_{PE} values (5.72–5.83 eV) were obtained for the films of **C1–C3** in comparison to the corresponding IP_{CV} values (4.99–5.52 eV) observed for the solutions (Table 11). The differences between IP_{PE} and IP_{CV} are typically expected. They are caused by the different polarization energy in a solid sample and solvation energy in solution observed for the same compound[110]. Since the inverse photoemission spectroscopy measurements were not possible at our laboratories, EA_{PE} values of the films were calculated by applying formula $EA_{PE} = IP_{PE} - 1.37 \times E_g^{opt}$ according to the procedure described elsewhere[110] (Table 11). The obtained EA_{PE} values are appropriate for efficient electron injection from a typical LiF/Al OLED cathode[111].

Table 11. Electrochemical characteristics, hole and electron mobilities of compounds **C1–C3**

Comp.	E^{ox}_{onset} *vs* Fc	P_{CV}[a]	EA_{CV}[b]	P_{PE}[c]	E_g^{opt} [d/e]	EA_{PE}[c]	μ_h[f]	μ_e[f]	β_h	β_e
	V	eV					$\times 10^{-3}$ cm^2/V×s		$\times 10^{-3}$ (cm/V)$^{0.5}$	
C1	0.45	5.23	3.12	5.83	2.11/2.13	2.91	0.65	4.5	6	4.3
C2	0.28	4.99	2.87	5.72	2.12/2.14	2.79	0.076	2.1	6.25	4.35
C3	0.47	5.52	3.47	5.8	2.09/2.15	2.85	0.7	4.5	6.1	3.85

[a] $IP_{CV} = |-(1.4 \times 1e^{-}E^{ox}_{onset}\ vs\ Fc/V) - 4.6|\ eV$ [47]; [b] $EA_{CV} = -(|IP_{CV}| - E_g^{opt})$ E^{ox}_{onset} is onset oxidation potential vs the Fc/Fc^+; $E_g^{opt} = 1240/\lambda_{edge}$, λ_{edge} is the onset wavelength of low-energy edge of absorption spectra of the dilute toluene solutions. [c]Obtained by photoelectron emission spectrometry for the films ($EA_{PE} = IP_{PE} - 1.37 \times E_g^{opt}$)[110]. [d/e] E_g^{opt} taken from absorption spectra of toluene solution/film. [f]Taken at the same electric field of 4.6×10^5 V/cm.

4.3.6. Charge transporting properties

To investigate charge-transporting properties of **C1–C3** in sandwich-like structures ITO/thermo-vacuum deposited layer/Al, the time-of-flight (TOF) method was exploited over a large range of electric fields (ca. 4×10^{-4}-4×10^{-5} V/cm) as it is shown in Fig. 23a. Under the negative voltage (V) of -80V applied to the ITO electrode through which the layer of **C1** with the thicknesses (d) of 2.6 μm was excited by laser beam (355 nm), TOF current transients were recorded. Transit times (t_{tr}) for electrons were well observed in the linear plots (Fig. 23b). Such shapes of TOF current transients can be attributed to the low-dispersity of electron transport in the layer of **C1**. When polarity of the applied voltage was switched to 80V at ITO, TOF current transient for holes was recorded. It showed a more dispersive character of hole-transport in comparison to that of electrons observed at the same electric field (Fig. 23c). From the TOF current transient plotted in linear scales, the t_{tr} value for holes at 80V was practically not possible to obtain. To calculate electron (μ_e) and hole (μ_h) mobilities at different electric fields using formula $\mu_{(h,e)}=d^2/t\times V$, the t_{tr} values were taken from TOF current transients plotted on a double logarithmic scales. Comparison of t_{tr} values observed for electrons and holes of 0.26 and 2.8 μs, respectively, clearly shows that at the voltage of 80V electrons can drift much faster across the 2.6 μm layer of **C1**. As a result, much higher μ_e of 3.2×10^{-3} $cm^2/V\times s$ than μ_h of 3×10^{-4} $cm^2/V\times s$ was obtained for compound **C1** at the external voltage of ±80 V (electric field of 3.1×10^5 V/cm) (Fig. 22a). For compounds **C2** and **C3**, similar trends in TOF current transients as well as in electron and hole mobility values were observed (Fig. 23). Thus, compounds **C1–C3** demonstrated high electron mobilities reaching of 10^{-3} $cm^2/V\times s$ at high electric fields and by one order of magnitude lower hole mobilities reaching of 10^{-4} $cm^2/V\times s$ at the same electric fields.

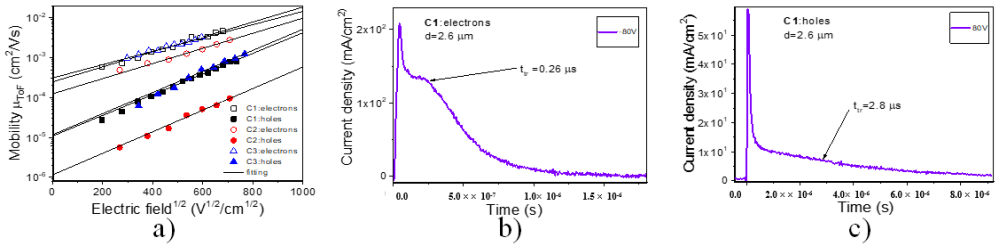

Fig. 23. Poole−Frenkel-type electric field dependences of hole and electron mobilities (a) in C**1**-**C3**-based sandwich structures obtained by TOF method and examples TOF transients for electrons (b) and holes (c) observed for the film of compound C**1** at different applied voltages/electric fields

To identify the effect of the nature of donor substituents attached to 1,8-naphthalimide moiety on charge-transporting properties of compounds **C1–C3**, their hole and electron mobilities were compared by plotting Poole−Frenkel dependences at different electric fields (E) described by the formula $\mu_{(h,e)}=\mu_{0(h,e)}\times\exp(\beta_{(h,e)}\times E^{0.5})$ (1) (Fig. 23a). In formula (1), $\mu_{0(h,e)}$ is zero-field mobility and $\beta_{(h,e)}$ is the electric field dependence parameters for holes or electrons. Electron

mobilities μ_e observed for compounds **C1–C3** were in the narrow range of ca. 2.1×10^{-3}–4.5×10^{-3} $cm^2/V\times s$ at the same electric field of 4.6×10^5 V/cm due to the same electron-accepting 1,8-naphthalimide moiety present in the molecular structures of **C1–C3** (Table 11). When extrapolations of fitting curves of experimental mobilities by formula (1) crossed the axis Y at zero electric fields, zero-field mobilities μ_{0e} in the range of 1.3×10^{-4}–3.1×10^{-4} $cm^2/V\times s$ were obtained for compounds **C1–C3**. Small differences between μ_e and μ_{0e} values of **C1–C3** can be attributed to the peculiarities of molecular packing in vacuum deposited films **C1–C3**. In addition, the similar β_e values of 3.85×10^{-3}–4.35×10^{-3} $(cm/V)^{0.5}$ were obtained for compounds **C1–C3** from the slopes of fitting plots. These values of β_e were smaller than the corresponding values for holes of β_h of 6×10^{-3}–6.25×10^{-3} $(cm/V)^{0.5}$ due to the lower dispersity of electron-transport in comparison to that of holes. In contrast to many previously published bipolar organic semiconductors[125,126], the phenoxazine, phenothiazine, or acridan substituted 1,8-naphthalimides demonstrated lower hole mobilities than electron mobilities (Fig 23a). Hole mobilities ranged from 7.55×10^{-5} to 7×10^{-4} $cm^2/V\times s$ at electric field of 4.6×10^5 V/cm. Such charge-transporting properties of bipolar OLED functional materials were shown to be useful for getting low roll-off efficiencies of blue phosphorescent OLEDs[127]. It should be mentioned that both hole and electron mobilities of compound **C2** were lower than those of **C1** and **C3** because of the relatively bulky sulfur atom of phenothiazine leading to bigger intramolecular distances and less HOMO-HOMO and LUMO-LUMO overlapping between neighboring molecules.

4.3.7. Electroluminescent characteristics

Electroluminescent properties of compounds **C1–C3** were studied using the non-optimized device structure ITO/MoO_3(0.5 nm)/NPB (40 nm)/light-emitting layer (20 nm)/TSPO1 (6 nm)/TPBi (34 nm)/LiF (1 nm)/Al (80 nm). Compounds **C1–C3** (10 wt%) doped in *m*CP were used as light-emitting materials. Molybdenum trioxide (MoO_3) was used for hole-injection layer, N,N′-di(1-naphthyl)-N,N′-diphenyl-(1,1′-biphenyl)-4,4′-diamine (NPB) for hole-transporting layer, diphenyl-4-triphenylsilyl-phenylphosphineoxide (TSPO1) was employed as hole-blocking material, 2,2',2''-(1,3,5-benzinetriyl)-tris(1-phenyl-1-H-benzimi-dazole) (TPBi) as electron-transporting material, a layer of lithium fluoride (LiF) was used as electron-injecting layer. According to the equilibrium energy diagram of devices (Fig. 23a), holes and electrons can be transported from electrodes to light-emitting layers without high energy barriers leading to relatively low turn-on voltages (V_{on}). The devices showed V_{on} values in the range of 4.86–4.98 V (Fig. 23b). Because of the high energy barriers of 1.0 and 0.4 eV on the interface **C1–C3**:*m*CP/TSPO1 for holes and on the interface NPB/**C1-C3**:*m*CP for electrons, respectively, the exciton formation and recombination zones were located within the light-emitting layers. As a result, orange-red electroluminescence with the CIE coordinates of (0.56, 0.36), (0.48, 0.49), and (0.59,0.39) were observed for devices I–III, respectively (Fig. 23c, Table 12). Those EL colors were the same under different applied voltages due to the stable EL spectra (Fig. 24d). The EL spectra of devices I–III were similar to the

corresponding PL spectra of systems **C1–C3**:*m*CP additionally proving that electroluminescence originated from compounds **C1–C3** (Fig. 24d).

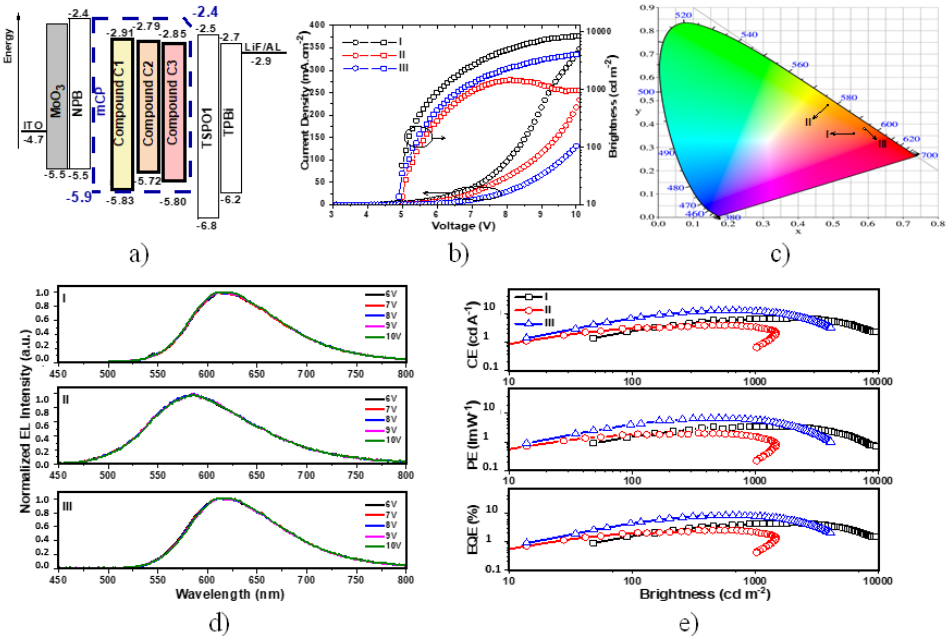

Fig. 24. Equilibrium energy diagram (a), voltage–current density and voltage–brightness dependencies (b), 1931 CIE coordinates (c), EL spectra recorded at the different voltages (d), current, power and external quantum efficiencies vs. brightness dependencies (e) of devices I–III

Current (CE), power (PE), and external quantum (EQE) efficiencies obtained for the devices were in the order device III>device I>device II. Thus, the OLED containing compound **C3** containing acridan donor moiety was the most efficient (**Fig. 24e,** Table11). Device III demonstrated maximum CE, PE, and EQE of 13.21 cd/A^{-1}, 6.75 lm/W^{-1} and 8.19%, respectively. It should be noted that the maximum efficiencies were reached at high brightness (L) which is favorable for practical use (Fig. 24e). These results can be attributed to the usage of host-guest systems **C1–C3**:mCP. mCP host is preferably hole-transporting material[128] while TADF guests (**C1–C3**) are preferably electron-transporting compounds (Fig. 24a). As a result, charge-transport balance was achieved under broad electric field values causing low efficiency roll-offs (high efficiencies at practical brightness of 700–2,200 cd/m^{-2}). The theoretical maximum EQE can be estimated using the following equation:[129]

$$EQE = PLQY.\ \eta_{charge\ capture}.\ \eta_{S\text{-}T}.\ \eta_{out} \qquad (3)$$

EQE is directly linked to the PLQY of the respective emitting layer. In the equation, $\eta_{charge\ capture}$ stands for efficiency of exciton formation, $\eta_{S\text{-}T}$ is a measure of singlet and triplet exciton utilization, and η_{out} is an out-coupling factor of EL from the emissive surface of the OLED. Usually, the usage of isotropic emitters and non-advanced substrates results in η_{out} of ca. 20%[63] manifesting the maximum EQE of 20% for delayed fluorescent materials and 5% for prompt fluorescent emitters. For the films of compounds **C1**–**C3** doped in the host, the maximum expected values of EQE of the corresponding OLEDs are 10.6, 3.6, and 15.4%, respectively. Although the obtained experimental values of EQE confirm the trend of PLQY observed for the investigated emitters, they are lower than the theoretical values. Similar observations were reported for other 1,8-naphthalimide derivatives. The reason for the efficiency drop may be attributed to the absence of the electron-blocking layer affecting the charge balance and decreasing $\eta_{charge\ capture}$. A minor consequence of that is the relatively high V_{on} of ca. 5 V observed for all OLEDs fabricated in this work.

Although the fabricated devices were not optimized, their characteristics are comparable with those of the previously reported OLEDs based on derivatives of 1,8-naphthalimide. It is also expected that bipolar compounds **C1–C3** with high electron mobilities can be promising hosts for infrared OLEDs.

Table 12. Characteristics of OLEDs

Device	V_{on}, (V)	L_{max}, (cd/m^2)	CE_{max}, (cd/A)	PE_{max}, (lm/W)	EQE_{max}, (%)	λ_{EL}, (nm)	CIE coordinates (x, y)
I	4.98	13,240	7.25	3.51	4.5	617	(0.56, 0.36)
II	4.90	1,480	4.04	2.06	2.5	585	(0.48, 0.49)
III	4.86	4,100	13.21	6.75	8.2	617	(0.59, 0.39)

4.4. Derivatives of 1,8-naphthalimide and triphenylamine

Over several years, various orange/red emitters, exhibiting fluorescence, phosphorescence, and thermally activated delayed fluorescence (TADF) have been contributing to the development of OLEDs[187,188,189]. Among emitters of the three generations of OLEDs, TADF materials have an advantage over traditional fluorescent and phosphorescent emitters. They do not contain noble metals and enable to reach 100% internal quantum efficiency of OLEDs[30,190]. The progress in the development of orange/red TADF emitters is considerably slower when compared to that of blue and green TADF emitters[31,191]. The considerable number of blue and green emitting OLEDs achieved EQE more than 30%[30]. However, in the case of orange/red emitting OLEDs only very few of the achieved EQE near 30% EQE[30,32]. The reasons for the slower development of orange/red emitters are related to the peculiarities of their molecular design and increased non-radiative transition affected by energy-gap law[32]. In this work, we designed, synthesized, and identified three derivatives of 1,8-naphthalimide and triphenylamine with different numbers of triphenylamino groups and different linkages between donor and acceptor moieties. The target compounds were characterized by different theoretical and experimental techniques. The strong

acceptor 1,8-naphthalimide moiety has high electron affinity due to the electron deficient centre[45]. Derivatives of 1,8-naphthalimide exhibit good electron-transporting or hole-blocking capabilities[192]. In this work, two bulky moieties i.e., triphenylamine and vinyl triphenylamine were employed as donor fragments[33]. The strong acceptor 1,8-naphthalimide fragment can be readily functionalized by introducing donor fragments at C-4 and C-5 positions. This can lead to the formation D-A compounds exhibiting orange/red emission[192]. Aiming to improve the efficiencies of OLEDs and to investigate the effect of hosting on the performance of devices, two different matrices were selected as hosts of newly synthesized compounds in emissive layers. We used time-resolved electroluminescence (TREL) technique which is suitable to investigate the charge mobilities and electroluminescence characteristics of devices[193,194,195]. A comparison of TREL decay curves of TADF host-based devices and well-known mCBP-based devices demonstrates the effect of TADF host on decay curves of the fabricated devices.

4.4.1 Synthetic procedure

The synthetic pathways of compounds **D1–D5** are shown in Scheme 15. Target materials **D1–D5** were synthesized in three steps: bromination, imidization, and Suzuki cross-coupling or Heck coupling reactions. All target compounds were purified by using column chromatography. Compounds **D1–D5** were found to be soluble in common organic solvents, such as acetone, tetrahydrofuran, and chloroform. The yield of final compounds **D3–D5** ranged from 63% to 76%. All synthesized final materials were fully characterized by ^{1}H and ^{13}C NMR, mass spectrometry, and IR spectroscopy.

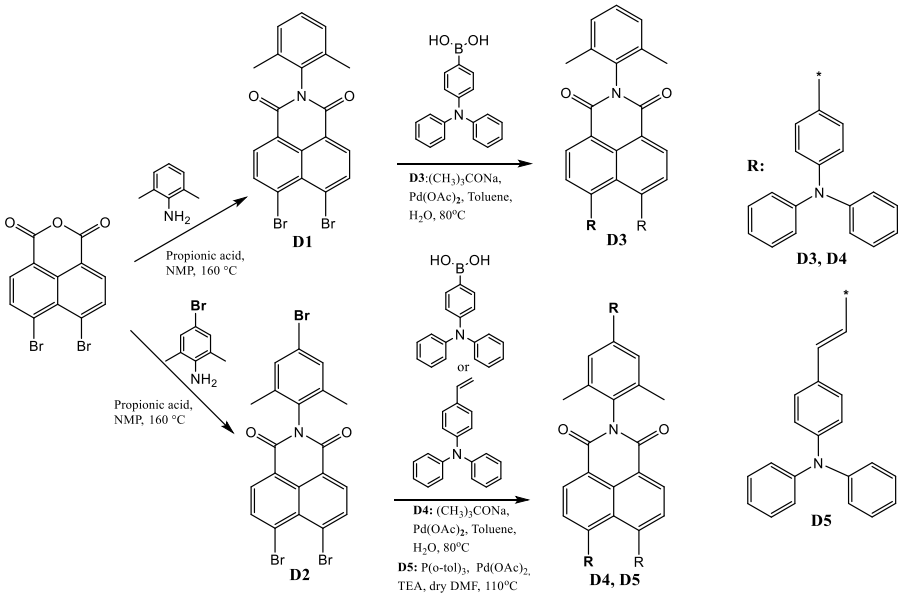

Scheme 15. Synthetic pathway of final compounds D3, D4, and D5

4.4.2 Experimental energy levels and thermal properties

The thermal transitions and thermal stability of compounds **D3–D5** were studied by thermogravimetric analysis (TGA) and differential scanning calorimetry (DSC) under a nitrogen atmosphere. The thermal characteristics of compounds **D3–D5** are outlined in Table 13.

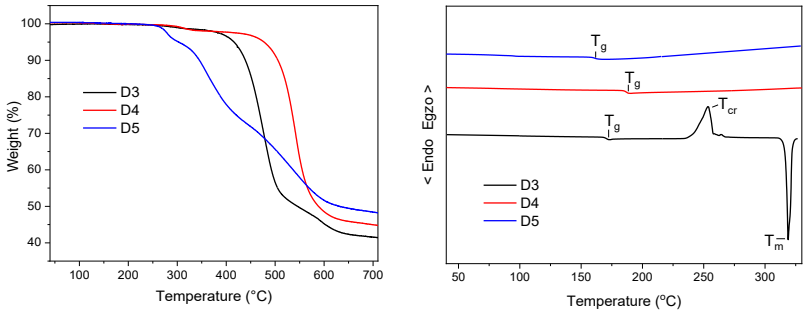

Fig. 25. (a) TGA curves (b) DSC thermograms of second heating scans of compounds **D3–D5**

The values of 5% weight loss temperatures (T_d) of 1,8-naphthalimide-based compounds **D3–D5** were determined to be in the range of 304–477°C as confirmed by TGA (Fig. 25a, Table 13). It is evident that the incorporation of the third triphenylamine group in the structure of the compound **D4** resulted in the increase of 5% weight-loss temperature by 63°C. Compounds **D3** and **D4** having triphenyl amino donor moieties show considerably higher thermal stability compared to compound **D5** having the donor moiety of vinylphenyldiphenylamino donor moieties. For compound **D5**, the complicated mechanism of thermal degradation with at least three stages was observed. Compounds **D3** and **D4** were isolated after the synthesis as crystalline compounds. The first DSC scans of compounds **D3** and **D4** revealed melting points (T_m) at 320°C and 346°C, respectively. After slow cooling, the second heating scans revealed for compound **D3** the signals of glass transition (T_g) at 172°C, crystallization (T_{cr}) at 264°C, and melting at 320°C (Fig. 25b). For compound **D4**, the second heating scan revealed only glass transition at 186°C, neither melting nor crystallization was observed (Fig. 25b). DSC measurements confirmed that compound **D5** was a fully amorphous material (Fig. 25b). Peaks due to crystallization or melting did not appear in cooling and heating cycles between 10°C and 250°C. The glass-transition temperatures obtained from the repeated heating scans of compound **D5** was 161°C (Table 13).

Table 13. Thermal characteristics of compound **D3–D5**

Compound	T_m[a], °C	T_g[a], °C	T_{cr}[a], °C	$T_{ID-5\%}$[b], °C
D3	320	172	264	414
D4	346	186	-	477
D5	-	161	-	304

[a] T_m - Melting point (T_m), glass transition temperature (T_g) and crystallization temperature (T_{cr}) determined by DSC, scan rate 10°C/min, nitrogen atmosphere. [b] 5% Weight loss temperature ($T_{ID-5\%}$) determined by TGA, heating rate 20°C/min, nitrogen atmosphere. - – Not observed.

The electrochemical properties of 1,8-naphthalimide derivatives **D3–D5** were studied by cyclic voltammetry (CV). Electrochemical data are collected in Table 14. Cyclic voltammograms of the solutions of the compounds in dichloromethane (DCM) were recorded using tetrabutylammonium hexafluorophosphate ($TBAHFP_6$) as the electrolyte (Fig. 26a). The oxidation peaks were observed in the region of 0.37–0.51 V while reduction peaks were detected in the range of -1.31 to -1.61 V. The values of ionization potential (IP_{CV}) and electron affinity (EA_{CV}) estimated from the onsets oxidation and reduction potentials are collected in Table 14. The values of EA_{CV} were found to be in the range 3.19–3.49 eV. The values of IP_{CV} were found to be in the range from 5.17–5.31 eV (Table 14).

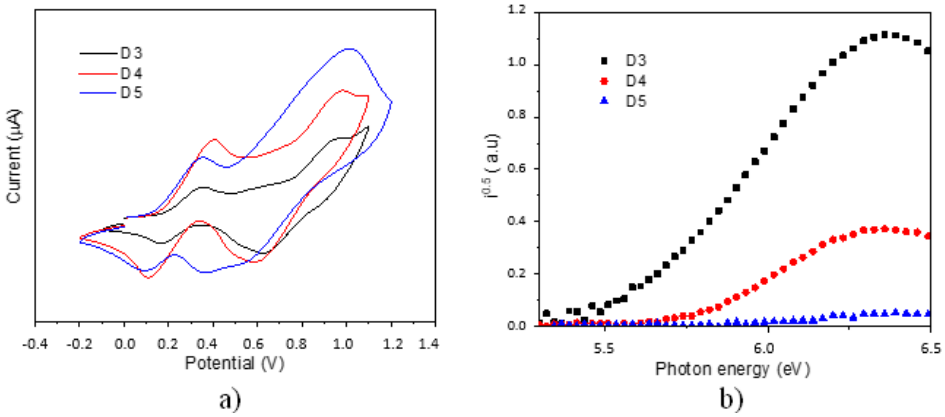

Fig. 26. Cyclic voltammograms (a), electron photoemission spectra (b) of compounds **D3–D5**

The ionization potentials (IP_{PE}) of investigated materials were also estimated using photoelectron emission (PE) method in air (Fig. 26b). The values are given in Table 14. The IP_{PE} values of compounds **D3–D5** were found to be 5.48 eV, 5.67 eV, and 5.76 eV, respectively. The values of EA_{PE} were obtained from the IP_{PE} values and the optical band gaps (E_g^{opt}), which were deduced from the edges of the absorption spectra of the vacuum deposited layers (Fig. 27a**)**.

Table 14. The data of cyclic voltammograms of the solutions of compounds **D3–D5** and their ionization potentials

Comp.	[a]E_{ox}, eV	[a]E_{red}, eV	[b]IP_{CV}, eV	[c]EA_{CV}, eV	[d]IP_{PE}, eV	[e]E_g^{opt}, eV	[f]EA_{PE}, eV
D3	0.50	-1.61	5.30	3.19	5.48	3.08	2.41
D4	0.51	-1.31	5.31	3.49	5.67	2.11	3.56
D5	0.37	-1.49	5.17	3.30	5.76	2.09	3.67

[a] E_{ox}, E_{red} – onsets of oxidation and redaction potentials respectively; [b] Ionization potential (IP_{CV}) measured by electrochemical studies, $IP_{CV} = E_{ox} + 4.8$; [c] Electron affinities (EA_{CV}) were determined by the equation $EA_{CV} = IP_{CV} - E_g^{opt}$; [d] Ionization potential (I_p^{ep}) was measured by using electron photoemission air method; [e] E_g^{opt} bandgap ($1239.84/\lambda_{abs}^{film}$); [f] Electron affinities (EA_{PE}) were determined with equation $EA_{PE} = IP_{PE} - E_g^{opt}$.

4.4.3 Photophysical properties

The photophysical properties of the derivatives of triphenylamine and 8-naphthalimide were investigated using tetrahydrofuran and toluene (concentration 1×10^{-5} mol/L) solutions as well as solid films deposited on quartz substrates by vapor deposition. The wavelengths of fluorescence maxima (λ^{PL}), fluorescence quantum yields (PLQY), and fluorescence life-times are summarized in Table 3. Absorption spectra of the solutions (Fig. 5a) have two prominent spectral bands in the range of 280–390 nm and 390–550 nm. The higher-energy band may be attributed to the delocalization of electronic photoexcitation on triphenylamino donor moieties[130,131]. The low-energy band of absorption is probably caused by amino substituents of the naphthalimide backbone of the accepting unit[132]. The differences in the absorption spectra of toluene and THF solutions are negligible for all three compounds of the series. The THF solutions of compounds **D3–D5** exhibited orange-red emission with the intensity maxima at 626, 626, and 682 nm with Stokes shifts of 195, 195, and 222 nm, respectively. The Stokes shifts of 152, 133, and 173 nm were found for the neat films of derivatives **D3–D5**, respectively. The small differences between the wavelengths of PL maxima of toluene and THF solutions of **D3-D5** confirm relatively weak intramolecular charge transfer between the donor and acceptor moieties[133]. As we can see in Fig. 5a and Table 3, PL decays of the toluene solutions of compounds **D3–D5** were in the nanosecond region, confirming that emissions were prompt fluorescence. PL decay curves of compounds **D3–D5** were adequately represented by single-exponential fitting. The emission lifetimes of toluene solutions were found to be of 5.9, 5.7, and 3.5 ns, respectively. The emission lifetimes slightly differed with the change of polarity of media. For THF solutions of **D3** and **D4**, the emission lifetimes of 7.4 and 7.3 ns were recorded while the life-time of THF solution of compound **D5** was the same as of toluene solution (3.5 ns).

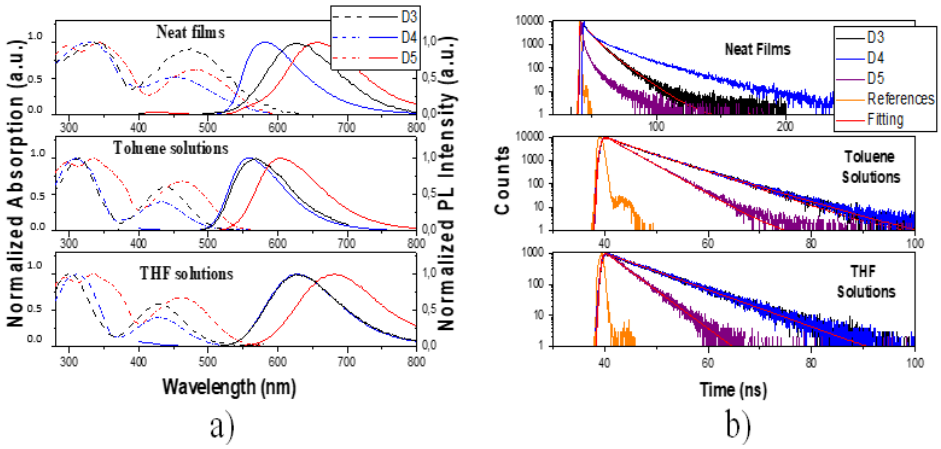

Fig. 27. UV-vis and photoluminescence spectra (a) and PL decay curves (b) of toluene or THF solutions and neat films of the studied compounds

Using an integrating sphere, photoluminescence quantum yield (PLQY) values of the toluene, THF solutions and solid samples of the compounds under ambient conditions were measured. The data are summarized in Table 15. The Solutions of compound D5 showed the highest PLQY among the studied compounds. The PLQY of 56.9 and 11% in toluene and THF solutions were recorded. The neat film of compound D1 showed PLQY of 20% which is the highest one among the investigated compounds.

Table 15. Photophysical parameters of compounds **D3–D5**

Parameter	Sample	**D3**	**D4**	**D5**
λ^{PL}, nm	Film	628	584	654
	Toluene	569	560	604
	THF	626	626	682
PLQY, %	Film	20	2	9.9
	Toluene	43	32.2	56.9
	THF	10.5	9.3	11.7
τ, ns	Toluene (THF)	5.9 (7.4)	5.7 (7.3)	3.5 (3.5)

4.4.4 Charge-transporting properties

To investigate charge-transporting properties of compounds **D3–D5**, time-of-flight (TOF) measurements were performed. Current transients for electrons (at negative voltage on the ITO electrode) and holes (at positive voltage on the ITO electrode) were recorded within the wide range of electric fields (*E*) (Fig. 28, a,b). In the case of compound **D5,** charges reached faster the second electrode at higher electric fields than at lower electric fields as it is well seen from normalized TOF current transients at two different electric-fields (Fig. 28, a,b). This observation means that transport of electrons and holes was detected for compound **D4**. Transit times (t_{tr})

were taken from TOF current transients plotted in log-log scales for electrons and holes from the interceptions of two lines drawn as it is shown in Fig. 28, a,b. Electron and hole mobility values were calculated at the different electric fields using equation[87]:

$$\mu_{TOF}=d/(t_{tr}\times E) \quad (4)$$

$$\mu = \mu_0 \exp \beta E^{1/2} \quad (5)$$

Electron and hole mobility dependences on electric-fields were plotted in Fig. 28 and fitted by the Poole–Frenkel question:

The zero-field mobilities (μ_0) of 5.95×10^{-7} and 3.35×10^{-7} $cm^2/V\cdot s$ for electrons and holes in the film of compound **D5** were estimated from the interception of the fitting lines with the axis Y at E=0 and the corresponding Poole–Frenkel electric field dependences (β) of 10.3×10^{-3} and 8.54×10^{-3} $(cm/V)^{0.5}$ were obtained from the slopes of the fitting lines. High β values can be related to very dispersive charge transport which is also evident from the shapes of TOF current transients (Fig. 28, a,b). At high electric field of 4×10^5 V/cm, electron and hole experimental mobility values reached 3.9×10^{-4} and 7.7×10^{-5} $cm^2/V\cdot s$, respectively (Fig. 28 c). These values are in very good agreement with those previously reported for other 1,8-naphthalimide derivatives[134]. Thus, compound **D5** can be used as a bipolar host of OLEDs with prevailing electron transport[135]. Transit times were not identified for TOF samples of compounds **D3** and **D4**.

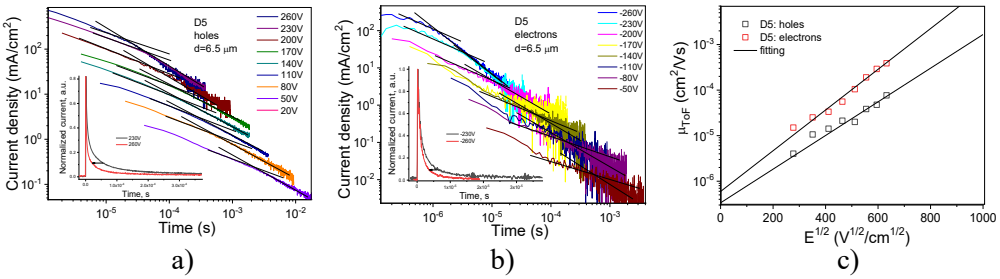

Fig. 28. TOF current transients for holes (a) and electrons (b) observed for vacuum-deposited film of compound **D5** at different external voltages. Poole–Frenkel plots and the corresponding fitting lines of electron and hole mobilities for compound **D5** (c). Insets show normalized TOF current transients at two different electric-fields

4.4.5. Fabrication and characterization of OLEDs

Electroluminescent (EL) properties of the compounds were investigated using different host matrices in the same device structures to study the influence of the host molecules on the electroluminescent (EL) properties of the synthesized compounds. Well-known 3,3′-di(9H-carbazol-9-yl)-1,1′-biphenyl (mCBP) and sky-blue TADF emitter Methyl-4'-cyano-2',3',5',6'-tetrakis(3,6-di-tert-butyl-9H-carbazol-9-yl)-2-methyl-[1,1'-biphenyl]-4-carboxylate (CNCOAM)[136] were used with the hosts concentration of 90% in the emissive layers. Considering high 5% weight loss temperatures and high glass-transition temperatures of the synthesized compounds,

vacuum thermal evaporation method was chosen for device fabrication. Using the films of mCBP-hosted emitters as the emitting layers (EML), multilayer OLEDs were fabricated with the structures of ITO / MoO3 (2 nm) / TAPC (40 nm) / mCBP (8 nm) / Light emitting layer (48 nm) / TSPO1 (8 nm) / TPBi (40 nm) / LiF (1 nm) / Al (Fig. 29a), where MoO_3, TAPC, mCBP, TSPO1, TPBi represent Molybdenum trioxide, 1,1-bis[(di-4-tolylamino)phenyl]cyclohexane, diphenyl-4-triphenylsilylphenyl-phosphine oxide and 2,2′,2′’-(1,3,5-benzine-triyl)-tris(1-phenyl-1-H-benzimidazole), respectively. MoO3 was used for the deposition of hole-injection layer, TAPC for hole-transporting layer, mCBP for exciton-blocking layer, TSPO1 for hole/exciton blocking layer, TPBi for electron-transporting layer, and lithium fluoride (LiF) for electron-injection layer. According to the equilibrium energy diagram of the devices, which is shown in Fig. 29a, holes and electrons can be transported from electrodes to light-emitting layers easily and without high energy barriers. This leads to relatively low turn-on voltages (V_{on}). The electroluminescence parameters are summarized in Table 16. OLEDs T1–T3 had the same structures as devices A1–A3, respectively, but in these devices, CNCOAM was used as a host instead of mCBP. The devices based on mCBP host showed V_{on} values in the range of 3.7–6.5 V (Fig. 30a). Host CNCOAM allowed to slightly decrease turn-on voltages of devices T1–T3 in comparison to turn-on voltages of the corresponding mCBP-doped devices A1–A3. Turn on voltages for these devices were in the range of 3.3 to 4 V (Fig. 30b). EL spectra of OLEDs based on compounds **D3** and **D5** were slightly blue-shifted with respect to their PL spectra. The slight differences between PL and EL spectra could be caused by the different excitation sources (optical and electrical ones). The fabricated devices showed EL spectra with similar shapes under different applied voltages proving that a recombination of electron-hole pairs occurred within the light-emitting layers. The exception was device T3 which was affected by incomplete energy transfer from host CNCOAM with a wide band gap to the red emitter (compound **D5**) (Fig. 29 b, c). In the EL spectra of device T3 (Fig. 29c) high energy peak (375 nm) originated from mCBP, blue emission peak (468 nm) stemmed from the TADF compound (CNCOAM) and red emission peak (613 nm) originated from the synthesized compound (D5).

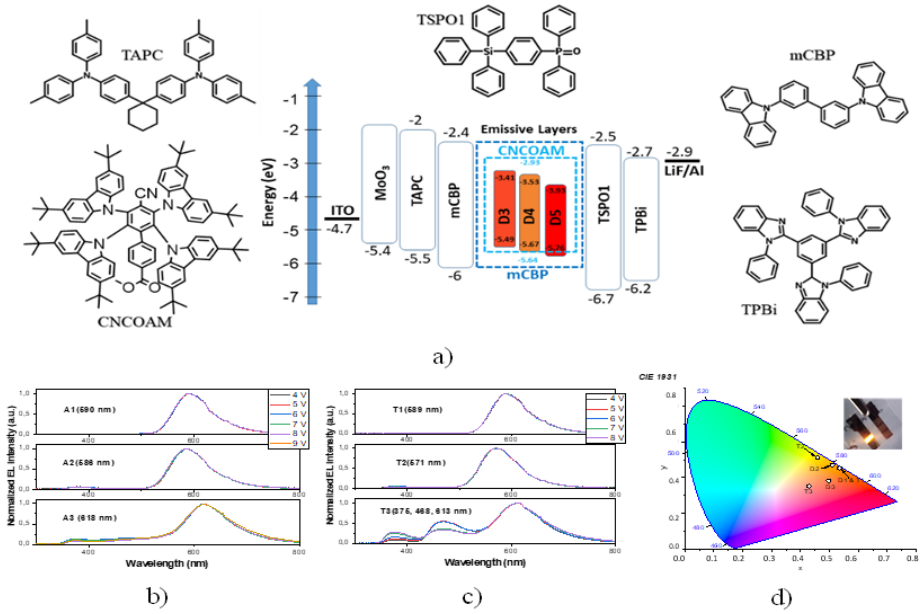

Fig. 29. Equilibrium energy diagram and the molecular structures of compounds used in the devices (a), normalized electroluminescence spectra recorded under different applied voltages (b,c), CIE1931 color coordinates (d) (inset shows a photo of fabricated device T2 at 6V)

As a result, orange-red EL with the *Commission Internationale de L'Eclairage* (CIE 1931) color +coordinates (x, y) of (0.53, 0.45), (0.51, 0.47) and (0.50, 0.38) was observed for devices A1–A3, and (0.53, 0.45), (0.46, 0.51) and (0.43, 0.35) for devices T1–T3, respectively (Fig. 29d and Table 16). The devices containing **CNCOAM** as a host exhibited higher efficiency. Maximum current, power, and external quantum efficiencies of 11.8 cd/A, 6.7 lm/W, and 4.7% were obtained for device T1 with compound **D3** containing two triphenylamino donor moieties as a fluorescent emitter (Fig. 30d and Table 16). Among mCBP-based devices, the highest maximum current, power, and external quantum efficiencies of 6.9 cd/A, 4.4 lm/W, and 2.5% were obtained for device A1 (Table 16). OLED T2 with the values of brightness up to 7765 cd/m^2 and maximum EQE of 1.8% surpassed the corresponding parameters of device A2 with the values of brightness up to 1470 cd/m^2 and maximum EQE of 0.5%. Maximum EQE of CNCOAM-based device T3 of 3.2% was higher than that (1.7%) of OLED A3 with mCP as a host.

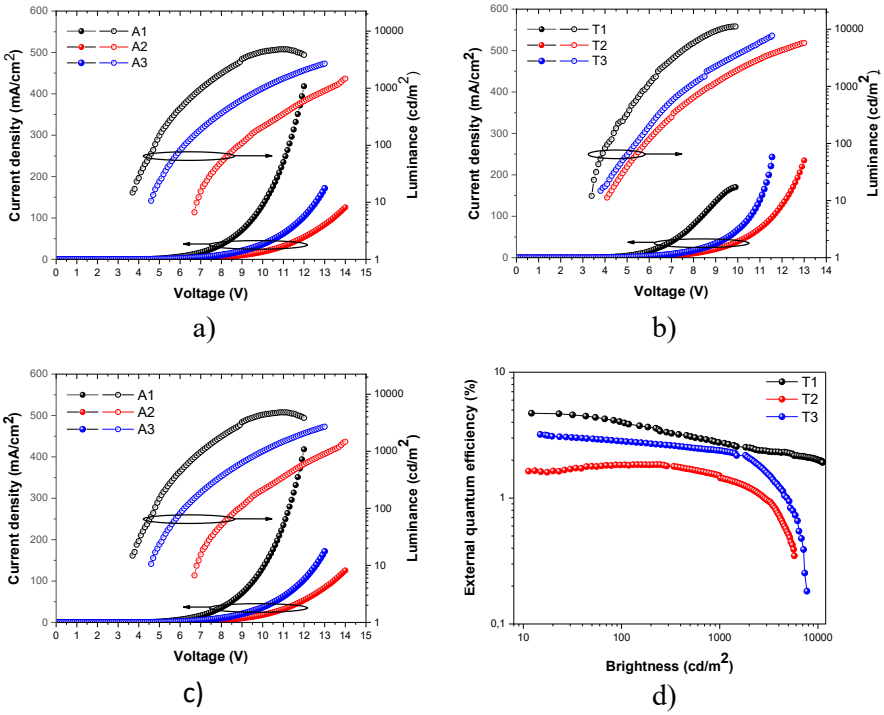

Fig. 30. Current density and luminance as the function of applied voltages (a, b), external quantum efficiency (EQE) versus luminance curves of the fabricated OLEDs (c, d)

Table 16. Parameters of OLED devices **A1–A3** and **T1–T3** of materials **D3–D5**

Devi-ce	EML	V_{on},[a] V	L_{max},[b] cd/m^2	$PE_{1000}/CE_{1000}/EQE_{1000}$ (lmW^{-1}/cdA^{-1}/%) [c]	$PE_{max}/CE_{max}/EQE_{max}$ (lmW^{-1}/cdA^{-1}/%) [d]	λ,[e] nm	CIE[f]
Doped OLEDs: ITO/MoO3/TAPC/mCBP/ Light-emitting layer/TSPO1/TPBi/LiF:Al							
A1	D3(10 wt%): mCBP	3.7	4796	2.1/5.1/1.8	4.4/6.9/2.5	590	(0.53, 0.45)
A2	D4(10 wt%): mCBP	6.6	1470	1/0.2/0.4	1.2/0.4/0.5	586	(0.51, 0.47)
A3	D5(10 wt%): mCBP	4.5	2698	0.4/1.4/0.7	2.2/3.4/1.7	618	(0.50, 0.38)
T1	D3(10 wt%): CNCOAM	3.3	11187	3.6/7.8/2.7	6.7/11.8/4.7	589	(0.53, 0.45)
T2	D4(10 wt%): CNCOAM	4	5765	1.1/4.4/1.5	2.8/5.3/1.8	571	(0.46, 0.51)
T3	D5(10 wt%): CNCOAM	3.7	7731	2/4.9/2.4	3.1/6.2/3.2	375, 468, 613	(0.43, 0.35)

[a] Turn-on voltage at a luminance of 10 cd m^{-1}, [b] Maximum brightness, [c] Power efficiency, current efficiency and external quantum efficiency at 1,000 cd m^{-2}, [d] Maximum power efficiency, Maximum current efficiency and maximum external quantum efficiency, [e] Maxima of EL (λ_{max}) Spectra at 6 V, [f] CIE 1931 Color Coordinate.

4.4.6 Time-resolved Electroluminescence (TRES)

The electroluminescence characteristics of OLEDs were investigated using the time-resolved electroluminescence (TREL) technique. This technique is a non-invasive method. It is particularly suited to measure the mobility and dynamics of charge carriers in optoelectronic devices[137,138,139]. Kang et al. used the TREL technique to investigate the effect of charge trapping on the electroluminescence characteristic of pristine and degraded OLEDs[140]. They found that degradation of materials caused dominant changes in the temporal profile of TREL curves[140]. Using the TREL method, we compared the charge carrier dynamics of devices with CNCOAM and mCBP as hosts. Fig. 31 shows the TREL decay curves of the fabricated devices. Unlike the time-resolved photoluminescence experiment in which we use a rectangular laser pulse to form excitons, in TREL measurements square voltage pulse is applied to inject charge carriers that ultimately generate excitons. It is important to highlight that excitons are directly generated by light in time resolved PL measurements. Meanwhile in TREL measurements, injected charge carriers subsequently form excitons and every TREL decay curve can be characterized by three steps: onset time, rise time, and decay time. Devices T1–T3 based on CNCOAM as a host showed considerably longer TREL decay curves in comparison with those of OLEDs A1–A3 devices. They are compatible with longer TREL decay curves of OLEDs based on TADF compounds[141].

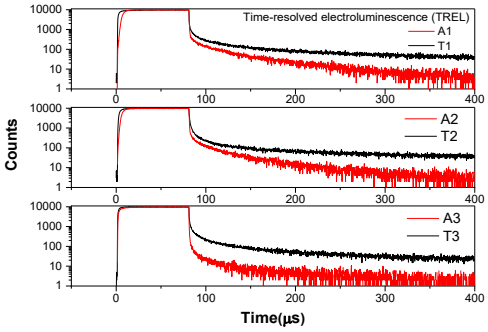

Fig. 31. Time-resolved electroluminescence curves of fabricated devices

5. CONCLUSIONS

1. Four derivatives of acridan with different substituents were synthesized as electroactive materials and their properties were investigated. It was determined that:
   - 1.1 The compounds exhibited relatively high thermal stability with 5% weight loss temperatures ranging from 271°C to 395°C and had the ability to form molecular glasses with glass transition temperatures in the range of 79°C–97°C.
   - 1.2 The of ionization potentials of the solid films of the compounds were found in the range of 5.39 to 5.62 eV, the highest ionization potential of 5.62 eV was obtained for 10-ethyl-2,7-bis(4-fluorophenyl)-9,9-dimethyl-9,10-dihydroacridine, which contains electron-accepting fluorine atoms.
   - 1.3 The compounds are capable of hole-transporting; the highest hole mobility was observed for 10-ethyl-9,9-dimethyl-2,7-di(naphthalen1-yl)-9,10-dihydroacridine, it exceeded 10^{-3} $cm^2/V.s$ at electric fields higher than 2.5×10^5 V/cm. These values revealed that the compounds can be employed as hosts in OLED device.
   - 1.4 The compounds exhibited blue or sky-blue emission with PLQY values of neat films in the range of 3–32%. The highest PLQY of 32% was observed for 10-ethyl-9,9-dimethyl-2,7-di(naphthalen1-yl)-9,10-dihydroacridine.
   - 1.5 Similar host performances were observed for electroluminescent devices with low turn-on voltages in the range of 3.2–3.6 V and maximum external quantum efficiencies in the range of 3.0–3.2%.
2. Carbazolyl-disubstituted tetraphenyl-substituted diphenyl sulfone was synthesized, and its properties were studied. It was established that:
   - 2.1 The thermal properties of synthesized compounds indicated that they exhibit high thermal stability with 5% weight loss temperature of 467°C, and showed the ability of forming molecular glass with the glass transition temperature of 153°C.
   - 2.2 The investigated ionization potential of the solid film of the synthesized compound exhibited value of 5.9 eV, which is in good agreement with the ionization potential of 5.88 eV obtained from cyclic voltammetry.
   - 2.3 PLQY values of dilute deoxygenated toluene, THF solutions and of neat film revealed that their values were found to be of 0.42, 0.42, and 0.31, respectively.
   - 2.4 The best device characteristics were observed when 9,9'-(Sulfonylbis([1,1':3′,1″-terphenyl]-5′,2′-diyl))bis(9H-carbazole) was employed as a host and 4CzIPN as an emitter in a highly efficient OLED based on TADF; it exhibited maximum current efficiency of 67.7 cd/A, maximum power efficiency of 60.9 lm/W and maximum external

quantum efficiency of 23.3% with low efficiency roll-off, which only a decrease by 4% (EQE = 22.3%) at 1,000 cd/m^2.

3. The series of new 1,8-naphthalimide-substituted derivatives were synthesized, and their properties were studied.
   3.1 The compounds exhibited ionization potentials of 5.72–5.83 eV and electron affinities of 2.79–2.91 eV.
   3.2 The compounds exhibited bipolar charge-transport properties with hole mobilities of 10^{-4} cm^2 V^{-1} s^{-1} and electron mobilities of 10^{-3} cm^2 V^{-1} s^{-1}.
   3.3 Aggregation-induced emission enhancement was detected for the compounds causing efficient TADF in the solid-state. The PLQY values of the solid films of compounds doped in host showed PLQY values to 77%.
   3.4 The investigation of electroluminescent properties of the compounds revealed that a device based on these compounds showed maximum current efficiency of 13.21 cd A^{-1}, power efficiency of 6.75 lm W^{-1}, and external quantum efficiency of 8.2%.
4. Three di- or tri-substituted 1,8-naphthalimide-containing derivatives were synthesized, and their properties were investigated.
   4.1 The compounds showed high thermal stability with 5% weight loss temperatures ranging from 304°C to 477°C, and they were capable of glass formation with extremely high glass transition temperatures ranging from 161°C to 186°C.
   4.2 The fluorescence quantum yields of the dilute solutions of compounds in toluene were in the range from 32% to 57%, while those of the neat films were in the range from 2% to 20%.
   4.3 The investigation of electroluminescence properties was done by employing the synthesized compounds as red fluorescent emitters in two different matrices; one of the best fabricated devices demonstrated maximum EQE, maximum current efficiency and maximum power efficiency of 4.7%, 11.8 cdA^{-1}, and 6.7 ImW^{-1}, respectively, along with low turn-on voltage of 3.3 V and high brightness of 11,187 cd/m^2 (at 9.9 V).

6. SANTRAUKA

6.1 ĮVADAS

Šviesa nuo pirmykščių laikų buvo vienas pagrindinių gyvų būtybių šaltinių ir poreikių. Žmonijos evoliucija pirmiausia siejama su šviesos egzistavimu, kuri tiesiogiai ar netiesiogiai suteikė gyvybę mikroorganizmams, augalams, gyvūnams ir žmonėms [1–4]. Vienintelis žinomas šviesos šaltinis žemėje buvo saulė, paskui žmonės įvaldė ugnį. Vėliau žmonija įdėjo milžiniškas pastangas, kad ištirtų su šviesa susijusias paslaptis. Izaokas Niutonas atrado tokį svarbų reiškinį, kaip spektrinis spalvų skilimas – naudodamas lęšį išmoko laužyti baltą šviesą į kitas spalvas [7]. Niutono dėka optikos žinios buvo susistemintos. Vėliau Albertas Einšteinas iki galo išplėtojo šią fotonų sampratą savo reliatyvumo teorijoje [10].

Tolesnė žmonių pažanga link šiuolaikinės gyvenimo eros labai susijusi su dirbtiniais šviesos šaltiniais, kurie priklauso nuo elektros energijos [5]. Mokslininkai iš viso pasaulio deda milžiniškas pastangas, norėdami sukurti įvairius šviesos šaltinius. OLED-ų technologija tyrėjų dėmesį patraukė dėl mažesnio energijos suvartojimo. Jie buvo sukurti devintojo dešimtmečio pabaigoje [16]. OLED-ų evoliuciją galima suskirstyti į tris kartas, pagrįstas fluorescencija, fosforescencija ir termiškai aktyvinama uždelstąja fluorescencija (TADF) [17]. Pirmosios kartos fluorescenciniuose OLED-uose tik 25% eksitonų galėjo būti panaudojami elektroliuminescencijai dėl sukinių statistikos, ir tai smarkiai ribojo OLED-ų efektyvumą [17–18]. Antrosios kartos OLED-ai, kurie paremti fosforescencija, nėra iki galo organiniai prietaisai, jų veikimas priklauso nuo neorganinio emiterio komplekso, kuriame yra sunkiųjų metalų, tokių kaip iridis ar platina [19]. Sunkiųjų metalų komplekso pagrindu pagamintų OLED-ų pranašumai yra tai, kad dėl metalo jonų buvimo singletinių ir tripletinių eksitonų būsenos susimaišo ir dėl stiprios elektronų ir orbitinės sąveikos tripletinė būsena tampa iš dalies leistina. Singuletinis ligando eksitonas sparčiai relaksuoja į metalo ligando CT būseną, iš kurios ir vyksta fluorescencija. OLED-ų IQE galima pasiekti iki 100%. Tačiau šie sunkiųjų metalų kompleksai yra reti, toksiški, brangūs, nestabilūs. Jie padidina išlaidas nuo OLED-ų gamybos iki perdirbimo [19]. Trečiosios kartos OLED-ų esmė yra sumažinti energijos tarpą tarp singletinių bei tripletinių eksitonų būsenų. Molekulėse, išsiskiriančiose krūvio pernašos būsenomis, elektronų tankis HOMO ir LUMO yra lokalizuotas skirtingose molekulės dalyse, tai lemia mažą jų persidengimą. Kuo persidengimas mažesnis, tuo ΔEST yra mažesnis. Taigi, CT molekulėse yra pasiekiama, kad tripletinės būsenos būtų termiškai sužadinamos ir įgytų energiją, pakankamą įveikti energetiniam barjerui (ΔEST) tarp tripetinių ir singletinių būsenų – tripletai gali būti termiškai aktyvuojami ir virsti singletiniais. Šie „atverstieji“ eksitonai rekombinuoja sąlygodami uždelstosios fluorescencijos atsiradimą. 100 % OLED-ų IQE galima pasiekti dėl šios uždelstos fluorescencijos emisijos, nenaudojant jokių sunkiųjų metalų [21]. Tačiau šie OLED-ai taip pat vis dar turi trūkumų, tokių kaip trumpas naudojimo laikas ir mažas mėlynų prietaisų stabilumas, palyginti didelė kaina,

neatsparumas vandens poveikiui [22]. Siekiama sukurti OLED-us, kurie išvengtų minėtų trūkumų.

Norint padidinti OLED-ų stabilumą ir efektyvumą, vykdomas kruopštus organinių junginių projektavimas ir tikslingas modifikavimas, apimantis OLED-ų donorinius (D) ir akceptorinius (A) fragmentus [20–23]. Modifikuojant organinių junginių struktūras, pavyzdžiui, jungiant donorinius (D) ir akceptorinius (A) fragmentus tiesiogiai arba per π-tiltelį, galima keisti jų fotofizikines, elektrines savybes, HOMO bei LUMO [23, 24]. D ir A fragmentus sujungus per π-tiltelį galimi D–π–A, D–A–π–A arba D–D–π–A struktūrų junginiai, o keičiant donorinių arba akceptorinių fragmentų stiprumą bei π-tiltelį galima koreguoti junginių savybes. Kad elektroliuminescenciniai (EL) junginiai būtų tinkami formuojant OLED-us, jie turi pasižymėti šiomis savybėmis: 1) turėti tinkamą jonizacijos potencialą ir gimiringumo elektronui energiją, kad būdų suderinami energetiniai lygmenys ir vyktų efektyvi krūvininkų injekcija, 2) sudaryti lygius sluoksnius, 3) sudaryti morfologiškai stabilius sluoksnius, 4) būti termiškai ir elektrochemiškai stabilūs, 5) turi pasižymėti efektyvia liuminescencija ir bipolinėmis krūvininkų pernašos savybėmis [27]. Todėl, siekiant pagerinti OLED-ų efektyvumą, buvo sukurti ir susintetinti nauji „donoras-akceptorius“ tipo junginiai.

Pastaruoju metu buvo kuriami įvairūs fluorescenciniai, fosforescenciniai bei TADF oranžinės / raudonos šviesos emiteriai ir naudojami formuojant OLED-us[28]. TADF emiteriai yra pranašesni už kitus emiterius, nes gali pasiekti 100% vidinį kvantinį OLED-ų efektyvumą [29]. Oranžinės / raudonos šviesos TADF emiteriai kol kas neprilygsta mėlyniems ir žaliems TADF emiteriams [30]. Mėlynos ir žalios šviesos TADF junginių pagrindu pagaminti OLED-ai pasižymi dideliu išoriniu kvantiniu efektyvumu (EQE). Aprašyti beveik 37 % EQE žydros ir daugiau kaip 30 % EQE žalios šviesos TADF OLED-ai. Tačiau tik nedaugelis oranžinės / raudonos šviesos OLED-ų pasiekė maždaug 30 % EQE [31]. Priežastis, dėl kurios oranžinės / raudonos šviesos TADF emiteriai vystosi lėčiau, gali būti siejama su sudėtingu jų molekulių dizainu ir sunkumais siekiant gauti mažesnį energijos tarpą (ΔE_{ST}), kad būtų sukurta efektyvi TADF emisija [32]. Atlikus emiterių struktūros modifikavimą galima pasiekti didesnio efektyvumo oranžinės / raudonos šviesos TADF OLED-uose [31–32]. Efektyvesnių oranžinės / raudonos šviesos TADF OLED-ų paklausa ir plėtra labai reikalinga ekranų gamybos pramonei, tyrimų ir plėtros sektoriui. Efektyvūs oranžinės / raudonos šviesos emiteriai reikalauja didelio molekulių standumo ir efektyvios krūvio perdavos (CT) „donoras-akceptorius“ tipo junginiuose [33]. Dėl stiprių elektronakceptorinių savybių ir aukštų *EA* verčių 1,8-naftalimido dariniai gali užpildyti oranžinės / raudonos šviesos TADF emiterių su tinkamomis savybėmis spragą.

Šio **darbo tikslas** yra naujų perspektyvių „donoras-akceptorius“ struktūros darinių, skirtų trečios kartos OLED-ams, turinčių akridano, difenilsulfono, 1,8-naftalimido fragmentus, sintezė ir savybių tyrimas.

Siekiant įvykdyti tikslą buvo iškelti šie uždaviniai:

- Sukurti ir susintetinti naujus arilpakeisto akridano darinius, skirtus TADF OLED-ams, ištirti jų termines, fotofizikines ir fotoelektrines savybes.
- Sukurti, susintetinti „donoras-akceptorius-donoras“ struktūros karbazolo fragmentus turintį difenilsulfondarinį, skirtą efektyviems OLED-ams su mažu išorinio kvantinio efektyvumo nuosmukiu, ištirti jo savybes.
- Sukurti, susintetinti naujus „donoras-akceptorius“ struktūros junginius su 1,8-naftalimido elektronakceptoriniu ir fenoksazino, fenthiazino arba akridano elektrondonoriniais fragmentais, kaip aukštu elektronų judriu ir raudonos spalvos emisija bei agregacijos sukeltu emisijos sustiprėjimu pasižyminčius TADF, skirtus OLED-ams; ištirti jų termines, fotofizikines, fotoelektrines ir elektroliuminescencines savybes.
- Sukurti ir susintetinti naujus „donoras-akceptorius“ bei „donoras-akceptorius-donoras“ tipo 1,8-naftalimido, difenilamino fenil- ir vinildifenilamino fenilfragmentus, turinčius junginius kaip raudonos spalvos TADF OLED-ų emiterius, ištirti jų termines, fotofizikines, fotoelektrines ir elektroliuminescencines savybes.

Darbo naujumas

- Susintetinta serija naujų aril-pakeisto akridano darinių, kurie buvo panaudoti kaip matricos TADF OLED-uose, pasižyminčiuose 3,0–3,2 % išoriniu kvantiniu našumu.
- Susintetintas naujas karbazolo pakaitus turinčio difenilsulfono darinys, kuris panaudotas kaip TADF matrica efektyviuose OLED-uose su mažu išorinio kvantinio efektyvumo nuosmukiu, 23,3 % išoriniu kvantiniu efektyvumu bei mažu nuosmukiu, esant 1000 cd/m^2.
- Susintetinti nauji fenoksazino, fenthiazino, akridano fragmentus turintys 1,8-naftalimido dariniai, pasižymintys TADF reiškiniu, dideliu elektronų dreifiniu judriu ir agregacijos sustiprinta emisija, pademonstruotas jų pritaikomumas raudonos šviesos OLED-uose, kurių išorinis kvantinis efektyvumas siekė 8,2 %, didžiausias srovės efektyvumas 13,21 cd A^{-1}, didžiausias galios efektyvumas 6,75 lm W^{-1}.
- Susintetinti nauji 1,8-naftalimido dariniai su donoriniais difenilaminofenil- arba vinildifenilamino fenilfragmentais ir pademonstruotas jų pritaikomumas OLED-uose. Jie panaudoti kaip raudonai šviečiantys emiteriai dviejose skirtingose matricose. Geriausiomis savybėmis pasižyminčio prietaiso didžiausias išorinis kvantinis efektyvumas, didžiausias srovės efektyvumas ir didžiausias galios efektyvumas siekė atitinkamai 4,7 %, 11,8 cdA^{-1} ir 6,7 ImW.

Autoriaus indėlis

Autorius sumodeliavo, susintetino, išgrynino ir apibūdino keturias naujas junginių serijas. Autorius išanalizavo termogravimetrinės analizės, diferencinės skenuojamosios kalorimetrijos, monokristalų rentgeno spindulių difrakcijos (XRD), fotofizikinių matavimų, krūvininkų pernašos rezultatus. Termogravimetrinės analizės ir diferencinės skenuojamosios kalorimetrijos matavimai atlikti padedant dr. Eigirdui Skuodžiui, monokristalų XRD matavimus atlikti padėjo dr. Audrius Bučinskas (Kauno technologijos universitetas). Sluoksnių jonizacijos potencialų ir krūvininkų pernašos matavimus atliko dr. DymytroVolyniuk (Kauno technologijos universitetas). Fotofizikinius matavimus atliko ir OLED-us suformavo dr. Oleksandr Bezvikonnyi (Kauno technologijos universitetas) ir Malek Mahmoudi (Kauno technologijos universitetas). Taip pat autorius atliko ir išanalizavo ciklinės voltamperometrijos rezultatus.

6.2. REZULTATAI IR JŲ APTARIMAS

6.2.1. Akridano fragmentą turintys junginiai

6.2.1.1. Sintezė

Akridano darinių sintezė ir struktūros pateiktos 6.2.1 schemoje. Tiksliniai akridano fragmentus turintys junginiai **A2-A5** gauti junginiui **A1** reaguojant su įvairiomis fenilboronrūgštimis Suzuki kryžminio jungimo reakcijų, katalizuojamų paladžio katalizatoriais, metu. Išeigos siekia nuo 27 % iki 50 %. Junginių **A2-A5** struktūra patvirtinta ^{1}H ir ^{13}C BMR spektroskopijos, masių spektrometrijos ir elementinės analizės metodais.

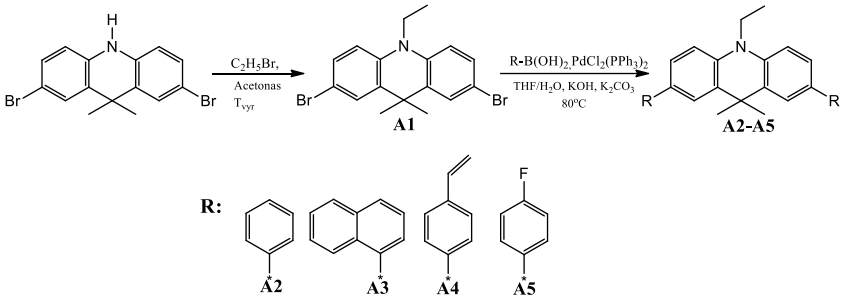

6.2.1 schema. Akridano darinių **A2-A5** sintezės schema

6.2.1.2. Teoriniai tyrimai

Geometrinės struktūros optimizuotos pagrindinėje elektroninėje būsenoje, naudojant tankio funkcinę teoriją (toliau – DFT), B3LYP/6-31G(d,p) (vakuume) teorinį lygmenį (6.2.1 pav.).

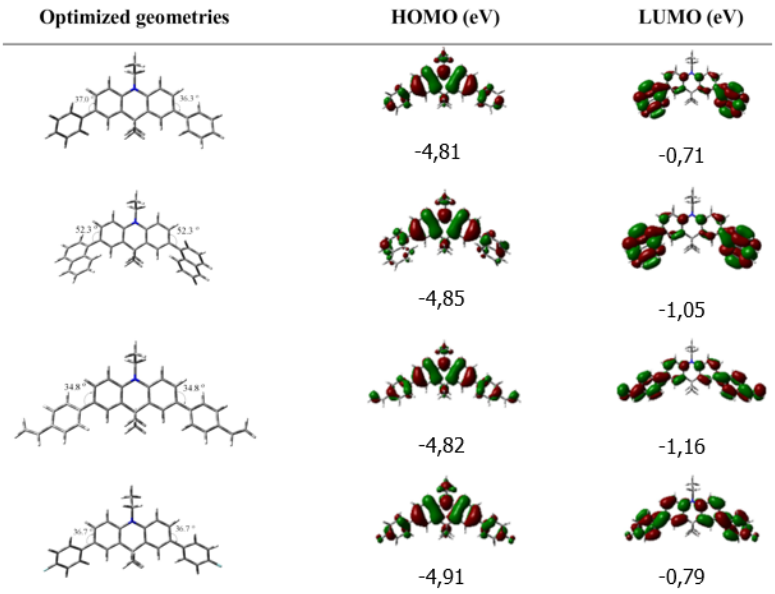

6.2.1 pav. Junginių **A2-A5** HOMO ir LUMO energetiniai lygmenys ir optimizuotos geometrinės struktūros (DFT B3LYP/6-31G(d, p))

Lygindami junginio **A2** dvisienius kampus tarp akridanil- ir fenilfragmentų (37.0 ir 36.3°) su junginių **A4**, **A5** dvisieniais kampais tarp akridanilfragmento ir vinilfenil- ar 4-fluorofenilfragmentų (atitinkamai 34,8 ir 36,7°), matome, kad jie yra panašūs. Taigi, *p*-pakaitai fenilo žiede neturi reikšmingos įtakos dvisienio kampo dydžiui. Naftilfragmentas su akridanilfragmentu junginyje **A3** sudaro didesnius dvisienius kampus (52,3°) (6.2.1 pav.). Junginiuose **A2–A5** tiek aukščiausios užimtos molekulinės orbitalės (toliau – HOMO), tiek žemiausios laisvos molekulinės orbitalės (toliau – LUMO) pasiskirsčiusios visoje molekulėje.

6.2.1.3. Terminės savybės

Susintetintų tikslinių junginių **A2-A5** terminė analizė atlikta diferencinės skenuojamosios kalorimetrijos (toliau – DSK) ir termogravimetrinės analizės (toliau – TGA) metodais, terminės charakteristikos pateiktos 6.2.1 lentelėje. Akridano dariniai 5 % savo masės praranda esant 271–395°C (6.2.1 lentelė). Galima daryti prielaidą, kad junginiai **A2** ir **A5** galimai sublimuoja, nes masės nuostoliai pasiekia maksimalią vertę. Nors visi junginiai išskirti kaip kristalinės medžiagos, junginiai **A2-A4** geba sudaryti molekulinius stiklus, stiklėjimo temperatūra (toliau – T_s) yra nuo 79 °C iki 97 °C. Aukštesnės T_s vertės gali būti paaiškinamos didesne molekuline mase, kuri sukelia stipresnę tarpmolekulinę sąveiką.

6.2.1 lentelė. Junginių **A2-A5** terminės charakteristikos

Junginys	[b]T_{lyd}, °C	[c]T_s, °C	[d]T_{kr}, °C	[e]$T_{ID-5\%}$, °C
A2	174, 174[a]	79[a]	102[a]	285
A3	201, 201[a]	86[a]	183[a]	344
A4	180	97[a]	242	395
A5	186, 186[a]	–	118	271

[a] – 2-as kaitinimas, [b]T_{lyd} – lydymosi temperatūra, [c]T_s – stiklėjimo temperatūra, [d]T_{kr} – kristalizacijos temperatūra, [e]$T_{ID-5\%}$ – temperatūra, kuriai esant medžiaga parranda 5 % masės.

6.2.1.4. Elektrocheminės ir fotoelektrinės savybės

Akridano darinių **A2-A5** elektrocheminės savybės ištirtos ciklinės voltametrijos (CV) metodu. Junginių **A2-A5** CV kreivės pavaizduotos 6.2.2 paveiksle. Visi junginiai pasižymi grįžtamąja oksidacija esant 0,3–0,4 V įtampai. Junginių **A2-A5** jonizacijos potencialo (IPcv) vertės yra artimos ir išsidėsto nuo 5,11 eV iki 5,18 eV. Apskaičiuotos giminingumo elektronui (EA_{cv}) vertės yra panašios ir svyruoja nuo 1,77 iki 1,91 eV. Elektronų fotoemisijos metodu išmatuoti junginių **A2-A5** sluoksnių jonizacijos potencialai (6.2.2 pav., b). Aukščiausia *IP* verte (5,62 eV) pasižymi **A5** junginys, turintis elektronakceptorinį fragmentą. Junginių **A2–A4** *IP* vertės yra artimos ir yra 5,39–5,46 eV.

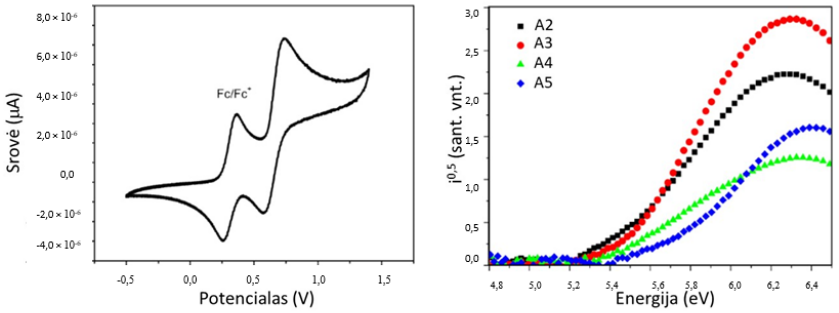

6.2.2 pav. Junginio **A2** ciklinė voltamperograma (a) ir junginių **A2-A5** elektronų fotoemisijos spektrai (b)

Elektronų fotoemisijos metodu išmatuotos junginių **A2-A5** *IP* vertės yra aukštesnės nei apskaičiuotos iš CV matavimų galimai dėl stipresnės tarpmolekulinės sąveikos kietoje būsenoje nei tirpale.

6.2.1.5. Fotofizikinės savybės

Junginių **A2-A5** sluoksnių ir praskiestų THF, tolueno tirpalų absorbcijos ir fotoliuminescencijos (PL) spektrai pateikti 6.2.3 paveiksle. Junginių **A2**, **A3** ir **A5** atveju intensyvios žemiausios energijos juostos yra ≈340 nm srityje. Junginio **A4** praskiestų tirpalų ir sluoksnių žemiausios energijos juostos sumažėjo apie 0,23 eV, palyginti su junginių **A2**, **A3** ir **A5,** dėl π-elektronų persidengimo tarp akridanil- ir

vinilfenilfragmentų. Tirpiklio poliškumas absorbcijos spektrams įtakos neturėjo. Junginių **A2-A5** tirpalų ir sluoksnių PL spektrai yra vibroniniai, taigi emisija vyksta dėl lokalaus elektronų sužadinimo (6.2.3 pav., a). Šių junginių THF tirpalų ir sluoksnių PL spektro kreivės yra šiek tiek pasislinkusios į raudoną pusę nei tolueno tirpalų dėl poliškumo bei agregatų susidarymo. Nepaisant to, junginių **A2-A5** emisiją daugiausia galime priskirti π–π* vietiniam sužadinimui. Tačiau galima pastebėti ir nagrinėjamų junginių emisijos CT pobūdį (6.2.3 pav., a). Toks spektro pobūdis yra būdingas intramolekulinei CT[35]. Nepaisant to, kad visų tiriamų junginių HOMO ir LUMO yra pasiskirsčiusios visoje molekulėje, dėl stiprių akridano fragmento elektrondonorinių savybių pastebimas dalinis orbitalių atskyrimas. Kaip matyti iš 6.2.1 pav., LUMO yra daugiau lokalizuota ant fenil-, naftalenil-, vinilfenil- ir fluorfenilfragmentų. Šie fragmentai pritraukia elektronus, sukeliančius dipolio momento pasikeitimą sužadintose būsenose. Todėl atskirus radiacinius procesus gali lydėti internolekulinė CT.

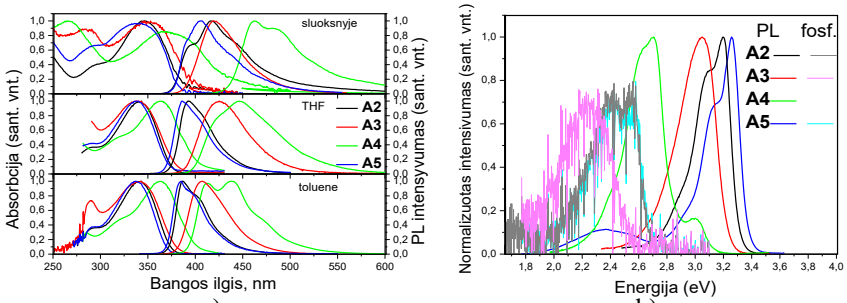

6.2.3 pav. Junginių **A2-A5** sluoksnių, praskiestų THF, tolueno tirpalų absorbcijos ir PL spektrai ($\lambda_{žad}$ = 330 nm) (a) ir praskiestų THF tirpalų PL ir fosforescencijos spektrai 77 K temperatūroje (b)

Lyginant junginio **A3** tolueno ir THF tirpalų emisijos spektrus, pastebimas batochrominis PL smailės poslinkis atitinkamai nuo 407 nm iki 425 nm. Taigi junginiui **A3** būdinga intermolekulinė CT emisija. Junginių **A2, A4, A5** PL juostų, priskiriamų π–π* sužadinimams, batochrominis poslinkis pakeitus tirpiklį buvo nedidelis. Junginio **A3** išskirtinumas gali būti paaiškinamas didesniu dvisieniu kampu tarp akridano ir naftilfragmentų ir dėl to sumažėjusios π-konjugacijos. Junginių **A2-A5** praskiestų THF tirpalų PL ir fosforescencijos spektrai užrašyti 77 K temperatūroje (6.2.3 pav., b). PL spektrai, užrašyti tiek 77 K, tiek kambario temperatūroje, yra labai panašūs. Junginių **A2-A5** singletinės (E_{S1}) ir tripletinės (E_{T1}) sužadintos būsenos energijos vertės yra atitinkamai 3,31, 3,24, 3,12 ir 3,37 eV. Junginių A2, A3 ir A5 E_{T1} vertės yra atitinkamai 2,67 eV, 2,54 eV ir 2,67 eV. Darinio A4 tripletinė energija nenustatyta, nes 77 K temperatūroje fosforescencijos nepavyko užfiksuoti.

6.2.2. Karbazolo pakaitus turintis difenilsulfondarinys

6.2.2.1. Sintezė

Junginio **B1** sintezė pavaizduota 6.2.2 schemoje. Pirma stadija – pradinio junginimo brominimas naudojant NBS sieros rūgštyje, tolesnė stadija – Suzuki kryžminio jungimo reakcija. Paskutinė stadija – nukleofilinės substitucijos reakcija, kurios metu fluoro atomai pakeisti karbazolilfragmentais ir gautas tikslinis junginys **B1**. Susintetintų junginių struktūra patvirtinta ^{1}H ir ^{13}C BMR spektroskopijos, IR, masių spektrometrijos ir elementinės analizės metodais. Junginys **B1** yra gerai tirpus įprastuose organiniuose tirpikliuose.

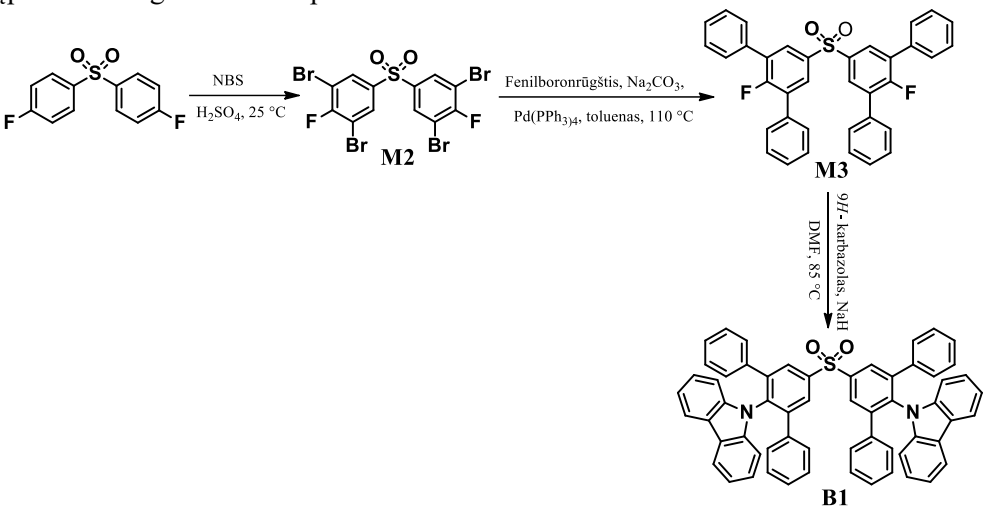

6.2.2 schema. Junginio **B1** sintezės schema

6.2.2.2 Teoriniai tyrimai

Junginio **B1** geometrinė struktūra optimizuota pagrindinėje elektroninėje būsenoje, naudojant DFT B3LYP/6-31G(d,p) (vakuume) teorinį lygmenį. Gauti duomenys pateikti 6.2.4 paveiksle. Nustatytos teorinės HOMO ir LUMO vertės yra atitinkamai 5,41 eV ir 1,81 eV. Kaip matyti iš 6.2.4 pav., junginys **B1** pasižymi gana dideliu susisukimo kampu, todėl matomas mažas HOMO ir LUMO persidengimas. HOMO yra delokalizuota ant karbazolilgrupių ir ant gretimų benzeno žiedų, LUMO – ant difenilsulfofragmento. Junginio **B1** apskaičiuotos energijų vertės S_1 yra 3,13 eV, T_1 yra 2,93 eV, ir a ΔE_{ST} yra 0,2 eV.

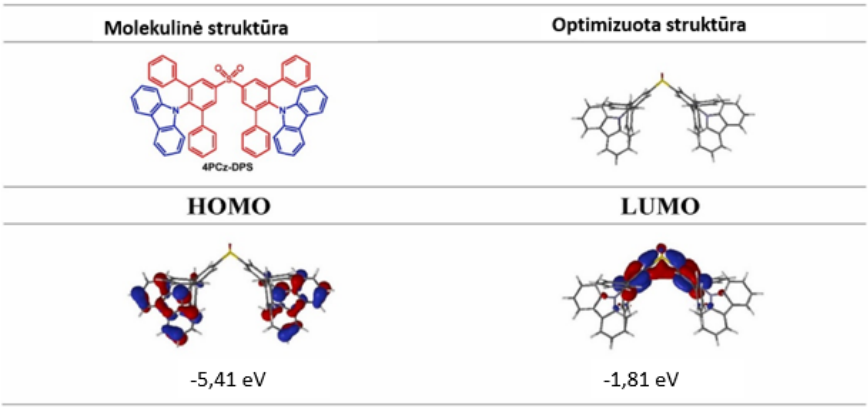

6.2.4 pav. Junginio **B1** molekulinė, optimizuota geometrinė struktūros ir HOMO / LUMO molekulinės orbitalės (DFT B3LYP/6-31G (d, p))

6.2.2.3 Terminės ir elektrocheminės savybės

DSK eksperimentas patvirtino, kad junginys **B1** po sintezės išskirtas kaip amorfinis junginys. Pirmojo DSK kaitinimo metu nefiksuojamos nei lydymosi, nei kristalizacijos smailės. Antrojo kaitinimo metu fiksuojama tik stiklėjimo temperatūra esant 153°C (6.2.5 pav., a). TGA eksperimento metu **B1** junginys sublimavosi, 5 % masės prarado 467 °C temperatūroje (6.2.5 pav., a).

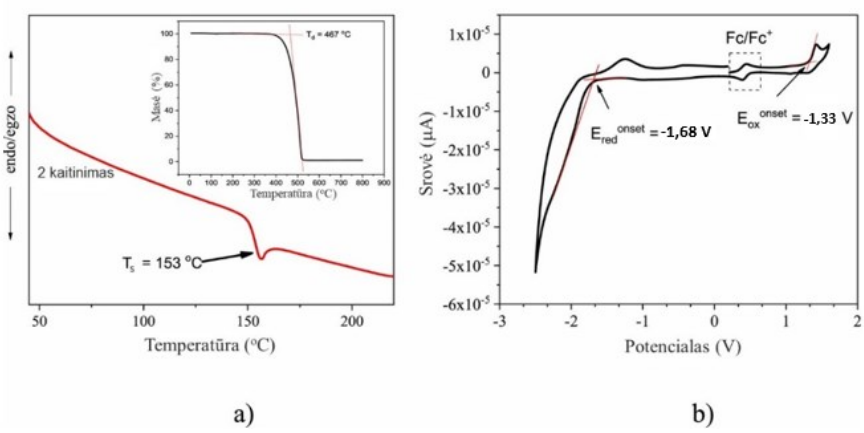

6.2.5 pav. Junginio **B1** DSK termograma ir TGA kreivė(a); junginio **B1** dichlormetano tirpalo CV kreivės (100 mV/s) (b)

6.2.5 pav. pateiktos junginio **B1** dichlormetano tirpalo CV kreivės. Susintetinto junginio oksidacijos (E^{ox}) vertė yra 1,33 V. Nustatyta, kad susintetintas junginys sudaro stabilius katijonradikalus ir gali grįžtamai oksiduotis. Junginio **B1** IP_{CV} reikšmė apskaičiuota pagal formulę |-(1,4 × 1e$^-$. E^{ox} *vs Fc/V*) – 4,6| eV[36] ir yra 5,88

eV. EA_{CV} vertė yra 2,78 eV, ji nustatyta iš IP_{cv} ir optinio draustinės juostos pločio (E_g=3,1 eV).

6.2.2.4. Fotofizikinės savybės

Pagrindinės fotofizikinės junginio **B1** charakteristikos pateiktos 6.2.6 paveiksle. Nustatyta, kad sluoksnio ir tirpalų sugerties spektrai yra panašūs. Smailės ties maždaug 289, 323 ir 334 nm gali būti priskirtos karbazolo fragmento π-π* sužadinimams [37]. Peties formos smailė ties 350 nm gali būti priskirta ICT tarp donorinio ir akceptorinio fragmentų. Didėjant tirpiklio poliškumui, matomas nedidelis mažiausios energijos absorbcijos juostų poslinkis į mėlyną pusę ir absorbcijos intensyvumo sumažėjimas (6.2.6 pav., a). Junginio **B1** sluoksnio absorbcijos kraštas yra batochromiškai pasislinkęs dėl didesnės tarpmolekulinės sąveikos kietoje būsenoje.

Junginio **B1** tirpalų PL spektrams būdinga viena siaura emisijos juosta, ir, didėjant tirpiklio poliškumui, emisijos spektrai pasislenka į raudonų bangų pusę. Tokie batochrominiai poslinkiai būdingi ICT emisijai [38]. Kaip ir tikėtasi, difenilsulfono darinio su donoriniais karbazolo fragmentais emisija išsidėsto violetinės spalvos regimojo spektro diapazone [39]. Nustatyta, kad praskiestų bedeguonių tolueno, THF tirpalų ir sluoksnio fotoliuminescencijos kvantinė išeiga (*PLQY*) yra atitinkamai 0,42, 0,42 ir 0,31. Junginys **B1** pasižymėjo PL intensyvumo sustiprėjimu 1,4 karto pašalinus orą (6.2.6 pav., b). **B1** THF praskiesto tirpalo fosforescencijos spektras, užrašytas 77 K temperatūroje, atitinka karbazolo emisiją [40]. E_{S1} ir E_{T1} vertės, apskaičiuotos junginio praskiesto THF tirpalo PL ir fosforescencijos spektrų, užrašytų skysto azoto temperatūroje, yra atitinkamai 3,36 ir 2,98 eV (6.2.6 pav., c). Gauti rezultatai patvirtina, kad junginys **B1** gali būti naudojamas kaip matrica emiteriui.

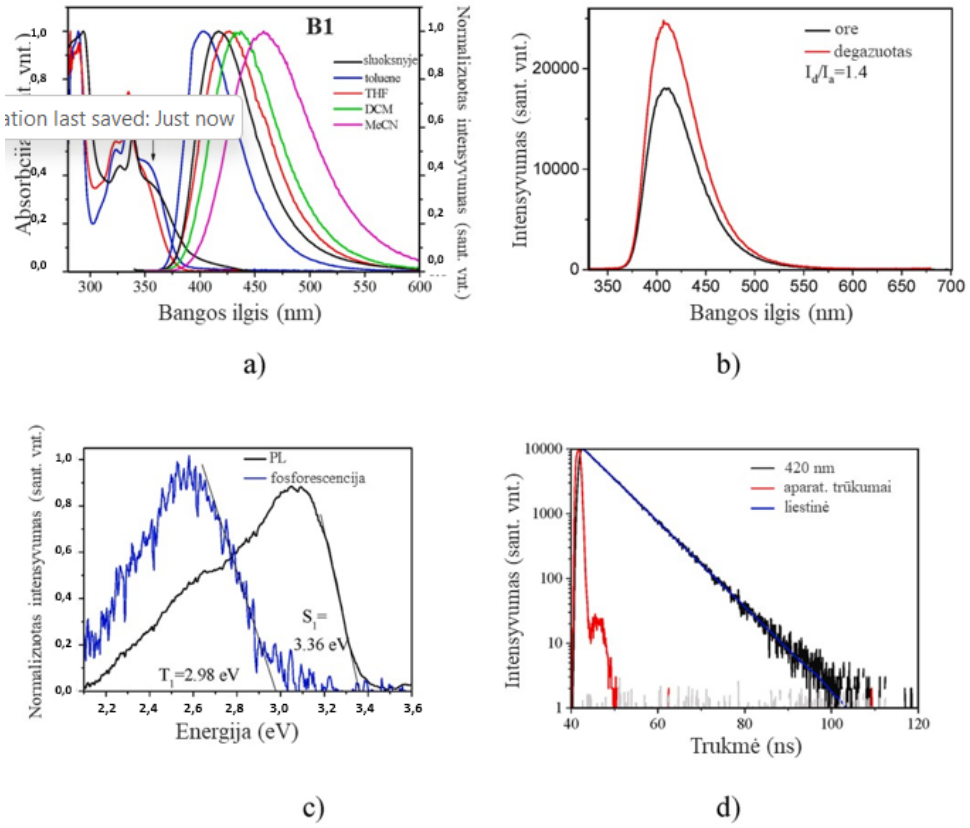

6.2.6 pav. Junginio **B1** bedeguonių praskiestų tolueno, THF tirpalų ir sluoksnio absorbcijos ir PL spektrai (a); praskiestų tolueno tirpalų PL spektrai oro atmosferoje ir pašalinus deguonį (b); praskiestų THF tirpalų PL ir fosforescencijos spektrai (c) ir PL gyvavimo trukmės kreivės (d)

Junginio **B1** praskiesto tolueno tirpalo PL gesimo kreivė parodė tik nuostoviąją fluorescenciją (PF) (6.2.6 pav., d). Emisijos gyvavimo trukmės vertės nustatytos iš diekponentinės funkcijos ir yra 1,69 ir 6,6 ns.

6.2.3. 1,8-naftalimido fragmentus turintys junginiai

6.2.3.1 Sintezė

Junginiai **C1**–**C3** susintetinti paladžio katalizuojamu Buchwaldo ir Hartwigo kryžmino jungimo metodu 4-brom-*N*-(2-etilhksil)-1,8-naftalimidui reaguojant atitinkamai su 10*H*-fenoksazinu, 3,7-di-tert-butil-10*H*-fentiazinu ar 2,7-di-tert-butil-9,9-dimetil-9,10-dihidroakridinu (6.2.3 schema). Susintetintų junginių struktūra patvirtinta ^{1}H ir ^{13}C BMR spektroskopijos, IR, masių spektrometrijos ir elementinės analizės metodais.

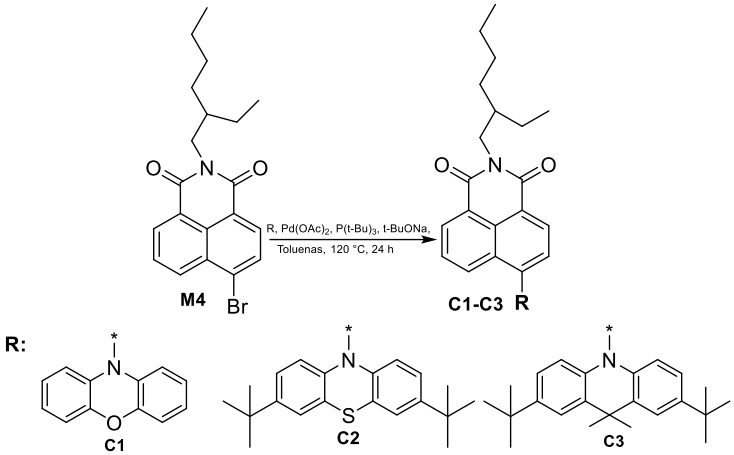

6.2.3 schema. Junginių **C1–C3** sintezės schema

6.2.3.2. Terminės savybės

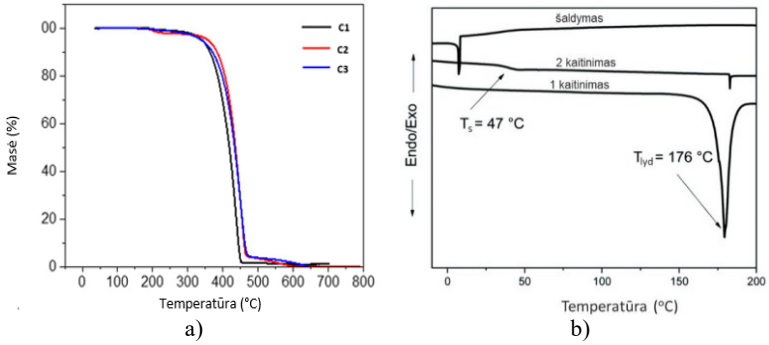

6.2.7 pav. Junginių **C1–C3** TGA kreivės (a) ir junginio **C2** DSK termogramos (b)

Junginių **C1–C3** terminės savybės ištirtos TGA ir DSK metodais azoto atmosferoje. Jų masės 5 % nuostolio temperatūra viršija 370 °C (6.2.7 pav., a, 6.2.2 lentelė). Labai maži karbonizuotų likučių kiekiai rodo, kad sublimacija galėtų būti pagrindinė masės nuostolių priežastis. Junginiai **C1–C3** išskirti kaip kristalinės medžiagos. Junginio **C2** pirmojo DSK kaitinimo metu matoma endoterminė lydymosi smailė 176 °C temperatūroje (6.2.7 pav., a, 6.2.2 lentelė). Junginiai **C1** ir **C3** pasižymi panašiomis T_{lyd} reikšmėmis (6.2.2 lentelė). Antrojo kaitinimo metu nustatytos junginių **C1**–**C3** stiklėjimo temperatūros yra atitinkamai 76, 47 ir 83 °C.

6.2.3.3 Fotofizikinės savybės

6.2.2 lentelė. Junginių **C1–C3** terminės ir fotofizikinės charakteristikos

Junginys	Bandinys	**C1**	**C2**	**C3**
T_{lyd}[a], °C	Milteliai	179	176	181
T_s[b], °C		76	47	83
$T_{ID\text{-}5\%}$[c], °C		395	380	370
λ_{ABS}^{ICT}, nm	Toluenas/THF	491/482	476/467	483/478
λ_{ABS}^{LE}, nm		344/341	347/344	348/346
λ_{PL}^{ICT}, nm		686/634	751/653	650/652
PLQY, %		2/1	2/1	3/1
PLQY, %	Nelegiruotas sluoksnis	23	8	26
ΔE_{ST}, eV		0,04	0,05	0,03
PLQY, %	Legiruotas sluoksnis	53	18	77
τ_{PF}, ns (santykis, %)		14,7 (16 %)	14,9 (17 %)	15,1 (16 %)
τ_{DF}, μs (%)		3,87 (84 %)	4,23 (83 %)	3,57 (84 %)
η_{PF}, %		8	3	12
η_{DF}, %		45	15	65
k_{PF}, s^{-1} ($\times 10^6$)		5,8	2,1	8,16
k_{ISC}, s^{-1} ($\times 10^6$)		0,92	0,35	1,31
k_{DF}, s^{-1} ($\times 10^6$)		0,12	0,04	0,18
k_{RISC}, s^{-1} ($\times 10^6$)		3,77	1,01	5,95

[a] T_{lyd} – lydymosi temperatūra, nustatyta 2-ojo kaitinimo metu (10 °C/min, N_2 atmosfera). [b] T_s – stiklėjimo temperatūra (2-as kaitinimas). [c] $T_{ID\text{-}5\%}$ – temperatūra, kuriai esant medžiaga praranda 5 % masės. $k_{PF} = \frac{\eta_{PF}}{\tau_{PF}}$, $k_{ISC} = \frac{\eta_{DF}}{\eta_{PF}+\eta_{DF}} k_{PF}$, $k_{DF} = \frac{\eta_{DF}}{\tau_{DF}}$, $k_{RISC} = \frac{\eta_{DF}}{\eta_{PF}} \cdot \frac{k_{PF} \cdot k_{DF}}{k_{ISC}}$

Junginių **C1**–**C3** praskiestų tolueno ir THF tirpalų absorbcijos spektruose buvo matomos absorbcijos juostos dviejose spektro srityse – didelės energijos (esant bangos ilgiui iki maždaug 370 nm) ir mažos energijos (esant bangos ilgiams nuo 370 iki 600 nm) (6.2.8 pav., a). Toks pats spektrų pobūdis pastebėtas ir junginių **C1**–**C3** sluoksnių (6.2.8 pav., b). Darinių **C1**–**C3** didelės energijos sugerties juostos susidaro dėl π–π* lokalaus elektronų sužadinimo 1,8-naftalimido fragmentuose [112]. Nedidelius junginių **C1**–**C3** absorbcijos skirtumus lemia atitinkamų donorų įtaka. Mažos energijos sugerties juostas galima priskirti ITC tarp elektrondonorinių ir elektronakceptorinio 1,8-naftalimido fragmentų. Paprastai ITC būdinga viena plati mažos energijos juosta [43, 44]. Junginių ITC juostos yra maždaug ties 500 nm, o tai gali būti siejama su stipriu HOMO ir LUMO atskyrimu, reikalingu TADF [45]. Junginių absorbcijos juostoms būdingas neigiamas solvatochromizmas (6.2.8 pav., a).

Užfiksuotas didesnis (apie 10 nm) mažos energijos juostų poslinkis į mėlyną pusę nei didelės energijos sugerties juostų poslinkis.

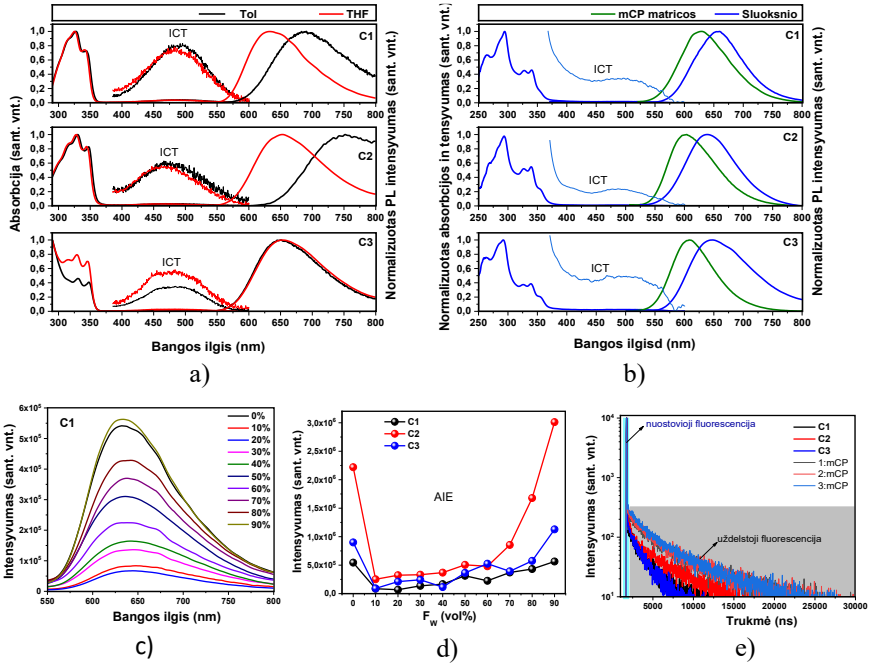

6.2.8 pav. Junginių **C1**–**C3** praskiestų tolueno / THF tirpalų absorbcijos ir PL spektrai (a) ir nelegiruotų bei legiruotų (10 wt% mCP) sluoksnių (b); junginio **C1** dispersijų THF / vanduo PL spektrai; (c) junginių **C1–C3** dispersijų THF/vanduo PL intensyvumo ir tūrio frakcijų F_W priklausomybė (d); junginių **C1–C3** PL gyvavimo trukmių kreivės (e)

Junginių **C1**–**C3** tolueno tirpalų PL spektrams būdingos plačios juostos su viršūnėmis atitinkamai 686, 751 ir 650 nm (6.2.8 pav., a). Junginio **C2** emisijos batochrominį poslinkį, matyt, lemia stipresnis donoras [46]. Junginių **C1–C3** kietųjų bandinių PL spektrų bangos ilgio maksimumai yra atitinkamai 658, 638 ir 646 nm. Pastebimas junginių **C1–C3** kietųjų tirpalų 1,3-bis(N-karbazolil)benzene (10 masės %) hipsochrominis PL spektrų poslinkis, palyginti su šių junginių sluoksnių PL spektrais (6.2.8 pav., b). Eksperimentiniai duomenys parodo, kad terpės poliškumas turi įtakos ITC, panašiai kaip tirpiklio poliškumas PL poslinkiui (6.2.8 pav., a). Junginių **C1–C3** tolueno / THF tirpalų fotoliuminescencijos kvantinis našumas (*PLQY*) mažesnis nei 3 % (6.2.2 lentelė). Reikėtų atsižvelgti į tai, kad šios vertės nustatytos oro aplinkoje, o PL intensyvumas buvo gerokai užgesintas deguonies. Daug didesnės *PLQY* vertės buvo nustatytos junginių **C1**–**C3** sluoksnių, ypač junginių legiruotų matricoje sluoksnių (iki 77 %).

Pastebėtas junginių **C1**–**C3** emisijos sustiprėjimas kietoje būsenoje gali būti siejamas su AIEE [47]. Norint išsamiau ištirti šį reiškinį, užrašyti junginių **C1**–**C3** disperguotų THF / vandens mišinių su skirtingomis vandens frakcijomis PL spektrai (6.2.8 pav., c). Didinant vandens kiekį nuo 0 % iki 20 %, junginių **C1–C3** PL intensyvumas sumažėja dėl vandens poliškumo, ir tai sukelia ICT deaktyvavimą [48]. Tačiau tolesnis vandens frakcijos kiekio didinimas junginių dispersijose iki 90 %

lemia PL intensyvumo padidėjimą, tai rodo, kad yra AIEE reiškinys [47]. Junginys **C2** pasižymi labiausiai išreikšta AIEE (6.2.8 pav., d). Užrašytos junginių **C1–C3** sluoksnių PL gyvavimo trukmės kreivės $<10^4$ Bar vakuume (6.2.8 pav., e). Grynų medžiagų sluoksnių PL gesimo kreivių daugiaeksponentinė aproksimacija atskleidė PF ir uždelstąją fluorescenciją (DF).

Norint patvirtinti TADF reiškinį, junginių **C1–C3** sluoksnių PL gyvavimo trukmės kreivės užrašytos esant temperatūrai nuo 77 iki 300 K (6.2.9 pav., a). Uždelstos fluorescencijos intensyvumas didėjo temperatūrai keičiantis nuo 77 iki 300 K, tai gali būti paaiškinama junginių **C1–C3** TADF emisija. Mažas singletinės ir tripletinės energijų skirtumas 0,03–0,05 eV būdingas TADF emiteriams (6.2.9 pav., b). Taip pat DF mechanizmą patvirtina ir leidžia atmesti tripletų anihiliaciją (TTA) DF intensyvumo priklausomybė nuo sužadinimo galios (6.2.9 pav., c) [50, 51].

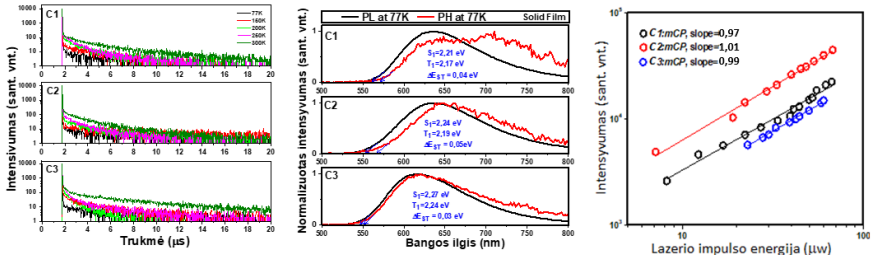

6.2.9 pav. Junginių sluoksnių **C1–C3** fotoliuminescencijos gyvavimo trukmės kreivės (a) ir PL / fosforescencijos spektrai 77 K temperatūroje (b); uždelstosios fluorescencijos intensyvumo priklausomybė nuo sužadinimo galios (c)

Užrašytos naftalimido darinių C1–C3 10 % kietųjų tirpalų mCP matricų gyvavimo trukmės kreivės, nustatytos nuostoviosios ir uždelstosios fluorescencijos gyvavimo trukmės (atitinkamai (t_{PF}) ir (t_{DF})). Rezultatai pateikti 6.2.2 lentelėje. Junginių **C1–C3** TADF efektyvumą galima įvertinti greičio konstantomis k_{RISC}, kurių didžiausia vertė (1,13 10^6 s^1) nustatyta junginio **C3** (6.2.2 lentelė).

6.2.3.4. Elektrocheminės ir fotoelektrinės savybės

Junginių **C1–C3** energetiniai lygmenys nustatyti CV ir elektronų fotoemisijos metodais, gauti duomenys pateikti 6.2.3 lentelėje. Trys 1,8-nafthalimido dariniai **C1–C3** demonstruoja quasi-grįžtamuosius oksidacijos procesus nuo 0,42 V iki 0,60 V pirmojo CV skenavimo metu (6.2.10 pav., a). Junginių **C1–C3** IP_{CV} vertės yra atitinkamai 5,23, 4,99 ir 5,52 eV (6.2.3 lentelė). Junginio **C2** mažesnė IP_{CV} vertė, palyginti su junginių **C1** ir **C3,** galimai dėl stipresnių elektrondonorinių di-*tert*-butil-fentiazinilfragmento savybių. EA_{CV} apskaičiuota pagal formulę $EA_{CV} = -(|IP_{CV}| - E_g^{opt})$. Junginių **C1–C3** EA_{CV} reikšmės išsidėsto nuo 2,87 eV iki 3,47 eV (6.2.3 lentelė).

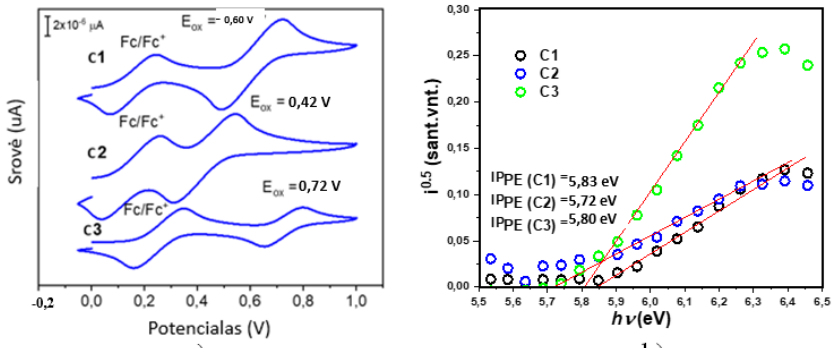

6.2.10 pav. Junginių **C1–C3** dichlormetano tirpalų ciklinės voltamperogramos (a) ir elektronų fotoemisijos spektrai (b)

Junginių **C1–C3** jonizacijos potencialai matuoti elektronų fotoemisijos ore metodu, spektrai pateikti 6.2.10 pav., b. Junginiai buvo vakuuminiu būdu užgarinti ant stiklo plokštelės, padengto fluoru legiruoto alavo oksido (FTO) sluoksniu. Junginių **C1–C3** sluoksnių IP_{PE} vertės (5,72-5,83 eV) yra didesnės, palyginti su tirpalų IP_{CV} vertėmis (4,99–5,52 eV) (6.2.3 lentelė). Skirtumai tarp IP_{PE} ir IP_{CV} yra dėl skirtingos junginių poliarizacijos energijos kietoje būsenoje ir solvatacijos energijos tirpale [41]. Sluoksnių EA_{PE} vertės apskaičiuotos pagal formulę $EA_{PE}= IP_{PE}-1.37\times E_g^{opt}$ [41] (6.2.3 lentelė). Gautos EA_{PE} vertės yra tinkamos efektyviam elektronų perėjimui iš įprastinio LiF/Al OLED katodo [42]. Visi susintetinti junginiai **C1–C3** pasižymi efektyvia krūvininkų pernaša, jų sluoksnių elektronų judris siekia 10^{-3} cm^2 V^{-1} s^{-1} , o skylių dreifinis judris – 10^{-4} cm^2 V^{-1} s^{-1}, esant aukštam elektros lauko stipriui (6.2.3 lentelė).

6.2.3 lentelė. Junginių **C1–C3** elektrocheminės, optinės ir krūvininkų transporto savybės

Jung.	E^{ox}_{onset} *vs Fc*	IP_{CV}[a]	EA_{CV}[b]	IP_{PE}[c]	E_g^{opt} [d/e]	EA_{PE}[c]	μ_h[f]	μ_e[f]	β_h	β_e
	V	eV					×10^{-3} cm^2/V×s		×10^{-3} (cm/V)$^{0.5}$	
C1	0,45	5,23	3,12	5,83	2,11/2,13	2,91	0,65	4,5	6	4,3
C2	0,28	4,99	2,87	5,72	2,12/2,14	2,79	0,6	2,1	6,25	4,35
C3	0,47	5,52	3,47	5,8	2,09/2,15	2,85	0,7	4,5	6,1	3,85

[a] $IP_{CV} = |-(1.4 \times 1e^{-}E^{ox}_{onset}\ vs\ Fc/V) - 4.6|\ eV$ [47]; [b] $EA_{CV} = -(|IP_{CV}| - E_g^{opt})$. E^{ox}_{onset} yra oksidacijos pradžios potencialas įvertinus Fc/Fc^+; $E_g^{opt} = 1240/\lambda_{edge}$, [c] nustatyta elektronų fotoemisijos ore metodu ($EA_{PE}= IP_{PE}-1,37\times E_g^{opt}$)[110]. [d/e] E_g^{opt} nustatytas iš tolueno tirpalų / sluoksnių absorbcijos spektrų. [f] elektros lauko stipris 4,6×10^5 V/cm.

6.2.4. 1,8-naftalimido ir trifenilamino darinių sintezė

6.2.4.1 Sintezė

Tiksliniai junginiai **D3–D5** gauti atlikus trijų stadijų sintezę. Pirma stadija – brominimas, antra stadija – imidizacija ir paskutinė stadija – Suzuki kryžminio jungimo arba Hecko jungimo reakcija. Junginių **D3–D5** sintezės kelias pavaizduotas 6.2.4 schemoje. Junginiai **D3–D5** gryninti kolonėlinės chromatografijos būdu. Tikslinių junginių išeiga siekia 63–76 %. Susintetinti 1,8-naftalimido ir trifenilamino dariniai gerai tirpsta įprastuose organiniuose tirpikliuose, tokiuose kaip acetonas, tetrahidrofuranas, chloroformas. Susintetintų junginių struktūra patvirtinta ^{1}H ir ^{13}C BMR spektroskopijos, IR, masių spektrometrijos ir elementinės analizės metodais.

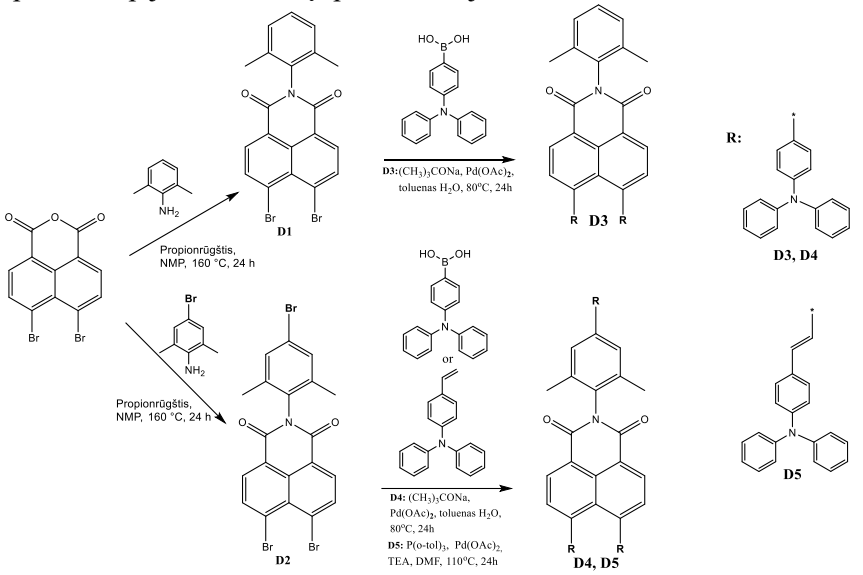

6.2.4 schema. Junginių **D3**-**D5** sintezės schema

6.2.4.2 Terminės, elektrocheminės ir fotoelektrinės savybės

Junginių **D3**-**D5** terminės charakteristikos pateiktos 6.2.4 lentelėje. 1,8-naftalimido darinių 5 % masės nuostolių temperatūra išsidėsto nuo 304 °C iki 477 °C (6.2.11 pav., 6.2.4 lentelė). Lygindami **D3** ir **D4** matome, kad trečios trifenilamino grupės prijungimas T_d padidina 63 °C. Junginiai **D3** ir **D4**, turintys trifenilamino fragmentus, pasižymi daug didesniu terminiu stabilumu nei junginys **D5**, turintis vinildifenilamino fenilfragmentus. 6.2.11 pav. pateiktoje TGA kreivėje matome, kad **D5** junginio terminis skilimas vyksta mažiausiai trimis stadijomis.

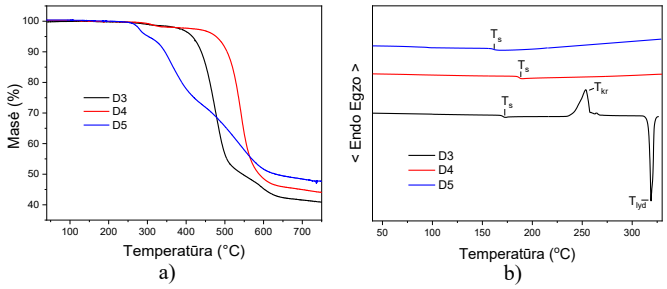

6.2.11 pav. Junginių **D3-D5** TGA kreivės (a) ir DSC antrojo kaitinimo termogramos (b)

Po sintezės junginiai **D3** ir **D4** išskirti kaip kristalinės medžiagos, bet jie gali būti transformuojami į kietą amorfinę būseną. Pirmojo kaitinimo metu atitinkamai 320 ir 346 °C temperatūroje užfiksuotos endoterminės lydymosi smailės. Antrojo kaitinimo metu **D3** termogramoje matome stiklėjimo (172 °C), kristalizacijos (264 °C) ir lydymosi (320 °C) temperatūras (6.2.11 pav., b). Junginio **D4** antrojo kaitinimo termogramoje užfiksuotas tik virsmas iš kietos amorfinės būsenos į skystą amorfinę būseną 186 °C temperatūroje. Junginys **D5** yra visiškai amorfinė medžiaga, DSK termogramose fiksuojama tik stiklėjimo temperatūra esant 161 °C (6.2.4 lentelė).

6.2.4 lentelė. Junginių **D3–D5** terminės charakteristikos

Junginys	T_{lyd}[a], °C	T_s[a], °C	T_{kr}[a], °C	$T_{ID\text{-}5\%}$[b], °C
D3	320	172	264	414
D4	346	186	-	477
D5	-	161	-	304

[a]T_{lyd} – lydymosi temperatūra, [b]T_s – stiklėjimo temperatūra, [c]T_{kr} – kristalizacijos temperatūra, [d] $T_{ID\text{-}5\%}$ – temperatūra, kuriai esant medžiaga parranda 5 % masės.

Užfiksuotos 1,8-naftalimido darinių dichlormetano tirpalų, turinčių 0,1 M palaikančiojo elektrolito tetrabutilamonio heksafluorfosfato ($TBAHFP_6$), ciklinės voltamperogramos. Oksidacijos vertės (E_{ox}) yra 0,37–0,51 V, o redukcijos vertės (E_{red}) nuo -1,31 iki -1,61 V. Junginių **D3**–**D5** IP_{CV} vertės yra 5,17–5,31 eV, o EA_{CV} vertės yra nuo 3,19 eV iki 3,49 eV (6.2.5 lentelė).

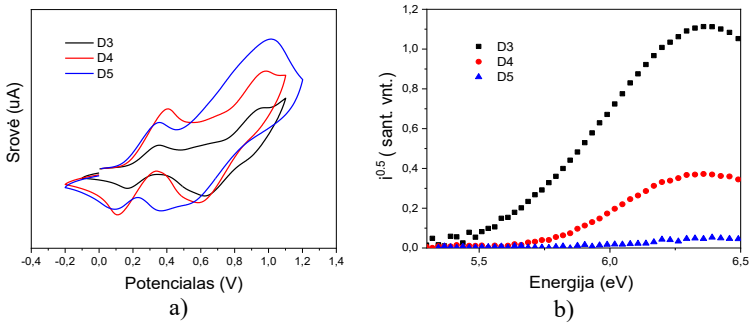

6.2.12 pav. Junginių **D3–D5** ciklinės voltamperogramos (a) ir elektronų fotoemisijos spektrai (b)

Taip pat buvo nustatyti junginių **D3–D5** sluoksnių IP_{PE} elektronų fotoemisijos ore metodu, spektrai pateikti 6.2.12 pav., b. 1,8-naftalimido darinių **D3–D5** IP_{PE} vertės yra atitinkamai 5,48 eV, 5,67 eV ir 5,76 eV. EA_{PE} nustatytos iš IP_{PE} ir E_g^{opt} ir yra nuo 2,41 eV iki 3,67 eV (6.2.5 lentelė).

6.2.5 lentelė. Junginių **D3–D5** elektrocheminės ir optinės savybės

Jung.	[a]E_{ox}, eV	[a]E_{red}, eV	[b]IP_{CV}, eV	[c]EA_{CV}, eV	[d]IP_{PE}, eV	[e]E_g^{opt}, eV	[f]EA_{PE}, eV
D3	0,50	-1,61	5,30	3,19	5,48	3,08	2,41
D4	0,51	-1,31	5,31	3,49	5,67	2,11	3,56
D5	0,37	-1,49	5,17	3,30	5,76	2,09	3,67

[a] E_{ox}, E_{red} – oksidacijos ir redukcijos pradžios potencialai; [b] – jonizacijos potencialas (IP_{CV}), nustatytas CV metodu, $IP_{CV} = E_{ox} + 4,8$; [c] – elektronų gimiringumo energija (EA_{CV}) $EA_{CV} = IP_{CV} - E_g^{opt}$; [d] – jonizacijos potencialas (I_p^{ep}) elektronų fotoemisijos ore metodu; [e] – E_g^{opt} ($1239,84/\lambda_{abs}^{film}$); [f] – $EA_{PE} = IP_{PE} - E_g^{opt}$.

6.2.4.3 Fotofizikinės savybės

Ištirtos trifenilamino ir 8-naftalimido darinių tetrahidrofurano ir toluene tirpalų (koncentracija 1×10^{-5} mol/l) bei sluoksnių ant kvarcinio stikliuko fotofizinės savybės. Fluorescencijos maksimumų bangos ilgiai (λ_{PL}), fluorescencijos kvantinės išeigos (*PLQY*) ir fluorescencijos gyvavimo trukmės yra pateikti 6.2.6 lentelėje. Tirpalų absorbcijos spektrai (6.2.13 pav., a) turi dvi juostas ties 280–390 nm ir 390– 550 nm, kurios priskiriamos atitinkamai trifenilamino donoriniams ir naftalimido akceptoriniams fragmentams [54,55,56]. Junginių **D3–D5** THF tirpalams būdinga oranžinė / raudona emisija su emisijos maksimumais ties 626, 626 and 682 nm, o Stokso poslinkis atitinkamai 195, 195 ir 222 nm. Junginių **D3–D5** sluoksnių Stokso poslinkis buvo atitinkamai 152, 133 ir 173 nm. Tiriamų junginių tolueno ir THF tirpalų PL maksimumų bangų ilgiai labai artimi, tai patvirtina silpną ICT tarp donorinių ir akceptorinių fragmentų [57]. Kaip matyti iš 6.2.13 pav., a, junginių **D3–D5** tolueno tirpalai pasižymi PF. Emisijos gyvavimo trukmės vertės, nustatytos iš monoeksponentinės funkcijos, yra atitinkamai of 5,9, 5,7 ir 3,5 ns. PL gyvavimo trukmei įtakos turėjo terpės poliškumas. Junginių **D3** ir **D4** THF tirpalų PL gyvavimo trukmė buvo atitinkamai 7,4 ir 7,3 ns, o junginio D5 THF tirpalo tokia pati, kaip ir tolueno tirpalo (3,5 ns) (6.2.6 lentelė).

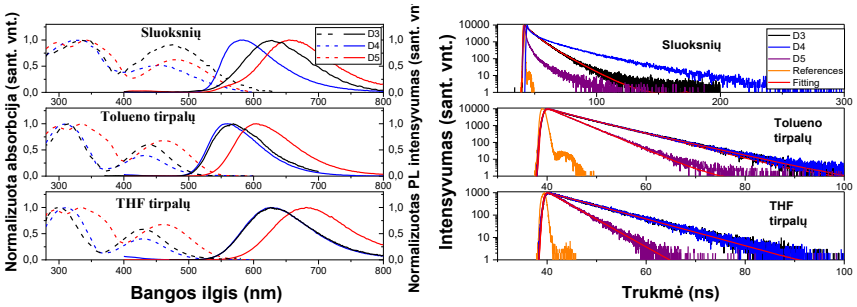

6.2.13 pav. Junginių toluено ar THF tirpalų bei sluoksnių UV-vis ir fotoliuminescencijos spektrai (a) it PL gyvavimo trukmės kreivės (b)

Nustatytos junginių **D3–D5** toluено, THf tirpalų ir sluoksnių *PLQY*, rezultatai pateikti 6.2.6 lentelėje.

6.2.6 lentelė. Junginių **D3–D5** fotofizikinės charakteristikos

Parametras	Bandinys	**D3**	**D4**	**D5**
λ^{PL}, nm	Sluoksnis	628	584	654
	Toluenas	569	560	604
	THF	626	626	682
PLQY, %	Sluoksnis	20	2	9,9
	Toluenas	43	32,2	56,9
	THF	10,5	9,3	11,7
τ, ns	Toluenas (THF)	5,9 (7,4)	5,7 (7,3)	3,5 (3,5)

Didžiausia *PLQY* pasižymi junginio **D5** tirpalai – 56,9 % ir 11 % atitinkamai toluено ir THF tirpalų. Aukščiausia sluoksnio *PLQY* yra D3 junginio – 20 %.

6.3. IŠVADOS

1. Susintetinti keturi nauji elektroaktyvūs skirtingus pakaitus turinčio akridano dariniai ir ištirtos jų savybės.
   1.1 Junginiams būdingas santykinai didelis terminis stabilumas, jų 5 % masės nuostolių temperatūra yra 271–395 °C. Šie junginiai geba sudaryti molekulinius stiklus, jų stiklėjimo temperatūra yra 79–97 °C.
   1.2 Šių junginių jonizacijos potencialai yra 5,39–5,62 eV. Didžiausia jonizacijos potencialo vertė 5,62 eV yra 10-etil-2,7-bis(4-fluorfenil)-9,9-dimetil-9,10-dihidroakridino, turinčio elektronakceptorinius fluoro atomus.
   1.3 Susintetinti junginiai geba pernešti skyles; geriausiomis krūvininkų pernašos savybėmis pasižymi 10-etil-9,9-dimetil-2,7-di(naftalen1-il)-9,10-dihidroakridinas. Esant elektros lauko stipriui aukštesniam nei $2,5 \times 10^5$ V/cm, skylių dreifinis judris siekia 10^{-3} $cm^2/V.s$. Šie rezultatai patvirtina, kad šie junginiai tinkami naudoti kaip OLED-ų matricos.
   1.4 Susintetintiems junginiams būdinga mėlyna ar žydra emisija, jų sluoksnių fotoliuminescencijos kvantinės išeigos yra 3–32 %. Didžiausia fotoliuminescencijos kvantine išeiga (32 %) pasižymi 10-etil-9,9-dimetil-2,7-di(naftalen-il)-9,10-dihidroakridinas.
   1.5 Junginiai išbandyti kaip matricos elektroliuminescenciniuose prietaisuose, kurių įsijungimo įtampa yra 3,2–3,6 V, išorinis kvantinis efektyvumas siekia 3,0–3,2 %.
2. Susintetintas karbazolo pakaitus turintis difenilsulfonio darinys ir ištirtos jo savybės. Nustatyta, kad:
   2.1 Susintetintam junginiui būdingas didelis terminis stabilumas, jo 5 % masės nuostolių temperatūra siekia 467 °C, šis junginys gali sudaryti molekulinį stiklą, kurio stiklėjimo temperatūra yra 153 °C.
   2.2 Elektronų fotoemisijos bei ciklinės voltamperometrijos metodais nustatytos jonizacijos potencialo vertės yra panašios ir yra atitinkamai 5,9 eV ir 5,88 eV.
   2.3 Bedeguonių tolueno, THF tirpalų ir sluoksnio fotoliuminescencijos kvantinės išeigos yra atitinkamai 0,42, 0,42 ir 0,31.
   2.4 Geriausiomis charakteristikomis pasižymintis TADF OLED-as gautas, kai 9,9'-(sulfonilbis([1,1':3′,1″-terfenil]-5′,2′-diil))bis(9*H*-karbazolas) panaudotas kaip matrica ir 4CzIPN – kaip emiteris; didžiausias srovės efektyvumas siekia 67,7 cd/A, didžiausias energinis efektyvumas – 60,9 lm/W. Išorinis kvantinis efektyvumas siekia 23,3 % ir pasižymi mažu nuosmukiu, esant 1000 cd/m^2, išorinis kvantinis efektyvumas sumažėja 4 %.
3. Susintetinta serija naujų 1,8-naftalimido fragmentus turinčių junginių, ištirtos jų savybės.

3.1 Nustatyta, kad šie junginiai pasižymi efektyvia skylių ir elektronų pernaša, jonizacijos potencialų vertės yra 5,72–5,83 eV, elektroninio giminingumo vertės yra 2,79–2,91 eV.

3.2 Kietos būsenos bandiniams, pasižymintiems termiškai aktyvinama uždelstąja fluorescencija, būdingas agregacijos sukeltas emisijos sustiprėjimas. Junginių legiruotų sluoksnių fotoliuminescencijos kvantinė išeiga viršija 77 %.

3.3 Junginių pagrindu suformuotų elektroliuminescencinių prietaisų išorinis kvantinis efektyvumas siekia 8,2 %, didžiausias srovės efektyvumas 13,21 cd A^{-1}, didžiausias galios efektyvumas 6,75 lm W^{-1}.

4. Susintetinti nauji di- arba tripakeisto 1,8-naftalimido dariniai, ištirtos jų savybės:

4.1 Susintetintiems junginiams būdingas didelis terminis stabilumas, jų 5 % masės nuostolių temperatūra yra nuo 304 iki 477 °C; šie junginiai sudaro stiklus, kurių stiklėjimo temperatūra yra 161–186 °C.

4.2 Junginių praskiestų tolueno tirpalų fluorescencijos kvantinės išeigos yra 32 %–57 %, o sluoksnių – 2 %–20 %.

4.3 Elektroliuminescencinio prietaiso su susintetintu spinduoliu didžiausias išorinis kvantinis efektyvumas, didžiausias srovės efektyvumas ir didžiausias galios efektyvumas siekia atitinkamai 4,7 %, 11,8 cdA^{-1} ir 6,7 ImW^{-1}; kai įsijungimo įtampa 3,3 V, skaisčio vertė 11187 cd/m^2, esant 9,9 V įtampai.

7. REFERENCES

1. Raftopoulos, A., Kalyfommatou, N., & Constantinou, C. P. (2005). The properties and the nature of light: The study of newton's work and the teaching of Optics. *Science & Education*, *14*(7-8), 649–673. Retrieved from doi.org/10.1007/s11191-004-5609-6.
2. Forbes, M. D. (2015). What we talk about when we talk about light. *ACS Central Science, 1*(7), 354-363. doi:10.1021/acscentsci.5b00261.
3. Weisbuch, C. (2018). Historical perspective on the physics of artificial lighting. *Comptes rendus physique*, *19* (3), 89–112. Retrieved from doi:10.1016/j.crhy.2018.03.001.
4. Bloembergen, N. (1997). A brief history of light breakdown. *Journal of Nonlinear Optical Physics & Materials, 06*(04), 377-385. doi:10.1142/s0218863597000289.
5. Giavi, S., Blösch, S., Schuster, G. & Knop, E. (2020). Artificial light at night can modify ecosystem functioning beyond the lit area. *Scientific reports*, *10* (1), 11870. Retrieved from doi:10.1038/s41598-020-68667-y.
6. V. Rumyantsev, V. (2015). Towards a History of Concepts of Light-Matter Coupling. *Journal of photonic materials and technology*, *1* (1), 545. Retrieved from doi:10.11648/j.jmpt.20150101.11.
7. Fara, P. (2015). Newton shows the light: a commentary on Newton (1672) 'A letter … containing his new theory about light and colours…'. *Philosophical transactions of the royal society A: mathematical, physical and engineering sciences*, *373* (2039), 20140213. Retrieved from doi:10.1098/rsta.2014.0213.
8. TEICH, N. (1944). Influence of Newton's work on scientific thought*. *Nature, 153*(3871), 42-45. Retrieved from doi:10.1038/153042a0.
9. Henry, J. (2017). Enlarging the bounds of moral philosophy: Why did Isaac Newton conclude the Opticks the way he did?. *Notes and records: the royal society journal of the history of science*, *71* (1), s. 21–39. Retrieved from doi:10.1098/rsnr.2016.0011.
10. Robertson, H. P. (1949). PostulateversusObservation in the Special Theory of Relativity. *Reviews of modern physics*, *21* (3), s. 378–382. Retrieved from doi:10.1103/revmodphys.21.378.
11. Iagăr, A., Popa, G. N., & Diniş, C. M. (2017). Study of electromagnetic radiation produced by household equipment. *IOP Conference Series: Materials Science and Engineering, 200*, 012014. Retrieved from doi:10.1088/1757-899x/200/1/012014.
12. Williams, F. E. (1949). Review of the interpretations of luminescence phenomena*. *Journal of the Optical Society of America, 39*(8), 648. Retrieved from doi:10.1364/josa.39.000648.
13. Nichols, E. L. (1926). Links connecting fluorescence and the luminescence of incandescent solids. *Journal of the Optical Society of America, 13*(6), 661. Retrieved from doi:10.1364/josa.13.000661.

14. Owusu, P. A. & Asumadu-Sarkodie, S. (2016). A review of renewable energy sources, sustainability issues and climate change mitigation. *Cogent engineering*, *3* (1), s. 1167990. Retrieved from doi:10.1080/23311916.2016.1167990.
15. Corzo, D., Tostado-Blázquez, G., & Baran, D. (2020). Flexible electronics: Status, challenges and opportunities. *Frontiers in Electronics, 1*, 594003. Retrieved from doi:10.3389/felec.2020.594003.
16. Hong, G., Gan, X., Leonhardt, C., Zhang, Z., Seibert, J., Busch, J. M., & Bräse, S. (2021). A brief history of oleds—emitter development and Industry Milestones. *Advanced Materials, 33*(9), 2005630. Retrieved from doi:10.1002/adma.202005630.
17. Ha, J. M., Hur, S. H., Pathak, A., Jeong, J.-E. & Woo, H. Y. (2021). Recent advances in organic luminescent materials with narrowband emission. *NPG asia materials*, *13* (1), 1-36. Retrieved from doi:10.1038/s41427-021-00318-8.
18. Fröbel, M., Fries, F., Schwab, T., Lenk, S., Leo, K., Gather, M. C., & Reineke, S. (2018). Three-terminal RGB full-color OLED pixels for ultrahigh density displays. *Scientific Reports, 8*(1), 9684. Retrieved from doi:10.1038/s41598-018-27976-z.
19. Bizzarri, C., Spuling, E., Knoll, D. M., Volz, D., & Bräse, S. (2018). Sustainable Metal Complexes for organic light-emitting diodes (oleds). *Coordination Chemistry Reviews, 373*, 49-82. Retrieved from doi:10.1016/j.ccr.2017.09.011.
20. Yin, X., He, Y., Wang, X., Wu, Z., Pang, E., Xu, J., & Wang, J.-an. (2020). Recent advances in thermally activated delayed fluorescent polymer—molecular designing strategies. *Frontiers in Chemistry*, *8*, 725. Retrieved from https://doi.org/10.3389/fchem.2020.00725.
21. Zhang, L. & Cheah, K. W. (2018). Thermally Activated Delayed Fluorescence Host for High Performance Organic Light-Emitting Diodes. *Scientific reports*, *8* (1), 8832. Retrieved from doi:10.1038/s41598-018-27238-y.
22. Wang, J., Zhang, F., Zhang, J., Tang, W., Tang, A., Peng, H., Wang, Y. (2013). Key issues and recent progress of high efficient organic light-emitting diodes. *Journal of Photochemistry and Photobiology C: Photochemistry Reviews, 17*, 69-104. Retrieved from doi:10.1016/j.jphotochemrev.
23. Li, Y., Liu, J.-Y., Zhao, Y.-D. & Cao, Y.-C. (2017). Recent advancements of high efficient donor–acceptor type blue small molecule applied for OLEDs. *Materials today*, *20* (5), s. 258–266. Retrieved from doi:10.1016/j.mattod.
24. Wang, G., Miao, S., Zhang, Q., Liu, H., Li, H., Li, N., Wang, L. (2013). Effect of a π-spacer between a donor and an acceptor on small molecule-based data-storage device performance. *Chemical Communications, 49*(82), 9470. Retrieved from doi:10.1039/c3cc44704a.
25. Panja, S. K., Dwivedi, N., & Saha, S. (2016). Tuning the intramolecular charge transfer (ICT) process in push–pull systems: Effect of Nitro Groups.

RSC Advances, 6(107), 105786-105794. Retrieved from doi:10.1039/c6ra17521j.
26. Sakr, M. E., Abou Kana, M. T., Elwahy, A. H., Kandel, H. M., Abdelwahed, M. S., El-Daly, S. A., & Ebeid, E. M. (2020). Optical, photo physical parameters and photo stability of 6-substituted-1, 2, 4-triazine mono glucosyl derivative to act as a laser dye in various solvents. *Spectrochimica Acta Part A: Molecular and Biomolecular Spectroscopy, 232*, 118145. Retrieved from doi: 10.1016/j.saa.2020.118145.
27. Shirota, Y. (2000). Organic materials for electronic and optoelectronic devices. *Journal of Materials Chemistry, 10*(1), 1-25. Retrieved from doi:10.1039/a908130e.
28. Wang, Y., Wang, W., Huang, Z., Wang, H., Zhao, J., Yu, J., & Ma, D. (2018). High-efficiency red organic light-emitting diodes based on a double-emissive layer with an external quantum efficiency over 30%. *Journal Of Materials Chemistry C*, *6*(26), 7042-7045. Retrieved from doi: 10.1039/c8tc01639a.
29. Chen, X., Tan, S., Qin, C., Wang, Y., Lee, H. L., Lee, K. H., Qin, K., Ma, H., Zhu, W., & Lee, J. Y. (2022). Molecular design strategy for orange-red thermally activated delayed fluorescence emitters via intramolecular energy transfer and their application in solution processable organic light-emitting diodes. *Chemical Engineering Journal*, *428*, 131691. Retrieved from https://doi.org/10.1016/j.cej.2021.131691.
30. Liang, J., Li, C., Cui, Y., Li, Z., Wang, J., & Wang, Y. (2020). Rational design of efficient orange-red to red thermally activated delayed fluorescence emitters for oleds with external quantum efficiency of up to 26.0% and reduced efficiency roll-off. *Journal of Materials Chemistry C*, *8*(5), 1614–1622. Retrieved from https://doi.org/10.1039/c9tc05892c.
31. Zhou, C., Cao, C., Yang, D., Cao, X., Liu, H., Ma, D., Lee, C.-S., & Yang, C. (2021). Highly efficient red thermally activated delayed fluorescence emitters by manipulating the molecular horizontal orientation. *Materials Chemistry Frontiers*, *5*(7), 3209–3215. Retrieved from https://doi.org/10.1039/d1qm00155h.
32. Xie, F. M., Wu, P., Zou, S. J., Li, Y. Q., Cheng, T., Xie, M., Tang, J. X., & Zhao, X. (2019). Efficient Orange–red delayed fluorescence organic light-emitting diodes with external quantum efficiency over 26%. *Advanced Electronic Materials*, *6*(1), 1900843. Retrieved from https://doi.org/10.1002/aelm.201900843.
33. Zhang, Y. L., Ran, Q., Wang, Q., Liu, Y., Hänisch, C., Reineke, S., Fan, J., & Liao, L. S. (2019). High-Efficiency red organic light-emitting diodes with external quantum efficiency close to 30% based on a novel thermally activated delayed fluorescence emitter. *Advanced Materials*, *31*(42), 1902368. Retrieved from https://doi.org/10.1002/adma.201902368.
34. Thejokalyani, N., & Dhoble, S. J. (2014). Novel approaches for energy efficient solid state lighting by RGB organic light emitting diodes – A

Review. *Renewable and Sustainable Energy Reviews*, *32*, 448–467. Retrieved from https://doi.org/10.1016/j.rser.2014.01.013.

35. Sasabe, H., & Kido, J. (2010). Multifunctional materials in high-performance oleds: Challenges for solid-state lighting. *Chemistry of Materials*, *23*(3), 621–630. Retrieved from https://doi.org/10.1021/cm1024052.

36. Wang, S., Zhang, H., Zhang, B., Xie, Z., & Wong, W.-Y. (2020). Towards high-power-efficiency solution-processed oleds: Material and device perspectives. *Materials Science and Engineering: R: Reports*, *140*, 100547. Retrieved from https://doi.org/10.1016/j.mser.2020.100547.
37. Hong, G., Gan, X., Leonhardt, C., Zhang, Z., Seibert, J., Busch, J. M., & Bräse, S. (2021). A brief history of oleds—emitter development and Industry Milestones. *Advanced Materials*, *33*(9), 2005630. Retrieved from https://doi.org/10.1002/adma.202005630.

38. Adachi, C., Lee, S., Nakagawa, T., Shizu, K., Goushi, K., Yasuda, T., & Potscavage, W. J. (2015). Organic light-emitting diodes (oleds): Materials, Photophysics, and device physics. *Organic Electronics Materials and Devices*, 43–73. Retrieved from https://doi.org/10.1007/978-4-431-55654-1_2.
39. Olivier, Y., Moral, M., Muccioli, L., & Sancho-García, J.-C. (2017). Dynamic nature of excited states of donor–acceptor TADF materials for oleds: How theory can reveal structure–property relationships. *Journal of Materials Chemistry C*, *5*(23), 5718–5729. Retrieved from https://doi.org/10.1039/c6tc05075a.
40. Jou, J.-H., Sahoo, S., Dubey, D. K., Yadav, R. A., Swayamprabha, S. S., & Chavhan, S. D. (2018). Molecule-based monochromatic and polychromatic oleds with wet-process feasibility. *Journal of Materials Chemistry C*, *6*(43), 11492–11518. Retrieved from https://doi.org/10.1039/c8tc04203a.
41. Sudheendran Swayamprabha, S., Dubey, D. K., Shahnawaz, Yadav, R. A., Nagar, M. R., Sharma, A., Tung, F. C., & Jou, J. H. (2020). Approaches for long lifetime organic light emitting diodes. *Advanced Science*, *8*(1), 2002254. Retrieved from https://doi.org/10.1002/advs.202002254.
42. Haremsa, S. (2000). Naphthalimide dyes and pigments. *Ullmann's Encyclopedia of Industrial Chemistry*, *23,* 727-731. Retrieved from https://doi.org/10.1002/14356007.a17_059.
43. Dodangeh, M., Grabchev, I., Staneva, D., & Gharanjig, K. (2021). 1,8-naphthalimide derivatives as dyes for textile and polymeric materials: A Review. *Fibers and Polymers*, *22*(9), 2368–2379. Retrieved from https://doi.org/10.1007/s12221-021-0979-9.
44. Kagatikar, S., & Sunil, D. (2022). A systematic review on 1,8-naphthalimide derivatives as emissive materials in organic light-emitting diodes. *Journal of Materials Science*, *57*(1), 105–139. Retrieved from https://doi.org/10.1007/s10853-021-06602-w.
45. Roy, S., Saha, S., Majumdar, R., Dighe, R. R., & Chakravarty, A. R. (2009). Photocytotoxic 3D-metal scorpionates with a 1,8-naphthalimide

chromophore showing photoinduced DNA and protein cleavage activity. *Inorganic Chemistry*, *48*(19), 9501– 9509. Retrieved from https://doi.org/10.1021/ic9015355.

46. Banerjee, S., Veale, E. B., Phelan, C. M., Murphy, S. A., Tocci, G. M., Gillespie, L. J., Frimannsson, D. O., Kelly, J. M., & Gunnlaugsson, T. (2013). Recent advances in the development of 1,8-naphthalimide based DNA targeting binders, anticancer and fluorescent cellular imaging agents. *Chemical Society Reviews*, *42*(4), 1601. Retrieved from https://doi.org/10.1039/c2cs35467e.
47. Poddar, M., Sivakumar, G., & Misra, R. (2019). Donor–acceptor substituted 1,8-naphthalimides: Design, synthesis, and structure–property relationship. *Journal of Materials Chemistry C*, *7*(47), 14798–14815. Retrieved from https://doi.org/10.1039/c9tc02634g.
48. Panchenko, P. A., Fedorova, O. A., & Fedorov, Y. V. (2014). Fluorescent and colorimetric chemosensors for cations based on 1,8-naphthalimide derivatives: Design principles and optical signalling mechanisms. *Russian Chemical Reviews*, *83*(2), 155–182. Retrieved from https://doi.org/10.1070/rc2014v083n02abeh004380.
49. Gudeika, D. (2020). A review of investigation on 4-substituted 1,8-naphthalimide derivatives. *Synthetic Metals*, *262*, 116328. Retrieved from https://doi.org/10.1016/j.synthmet.2020.116328.
50. Oelgemöller, M., & Kramer, W. H. (2010). Synthetic photochemistry of naphthalimides and related compounds. *Journal of Photochemistry and Photobiology C: Photochemistry Reviews*, *11*(4), 210–244. Retrieved from https://doi.org/10.1016/j.jphotochemrev.2011.02.002.
51. Xiao, H., Chen, M., Shi, G., Wang, L., Yin, H., & Mei, C. (2010). A novel fluorescent molecule based on 1,8-naphthalimide: Synthesis, spectral properties, and application in cell imaging. *Research on Chemical Intermediates*, *36*(9), 1021–1026. Retrieved from https://doi.org/10.1007/s11164-010-0214-6.
52. Duke, R. M., Veale, E. B., Pfeffer, F. M., Kruger, P. E., & Gunnlaugsson, T. (2010). Colorimetric and fluorescent anion sensors: An overview of recent developments in the use of 1,8-naphthalimide-based chemosensors. *Chemical Society Reviews*, *39*(10), 3936. Retrieved from https://doi.org/10.1039/b910560n.
53. Zhu, H., Liu, C., Su, M., Rong, X., Zhang, Y., Wang, X., Wang, K., Li, X., Yu, Y., Zhang, X., & Zhu, B. (2021). Recent advances in 4-hydroxy-1,8-naphthalimide-based small-molecule fluorescent probes. *Coordination Chemistry Reviews*, *448*, 214153. Retrieved from https://doi.org/10.1016/j.ccr.2021.214153.
54. Gopala, L., Cha, Y., & Lee, M. H. (2022). Versatile naphthalimides: Their optical and biological behavior and applications from sensing to therapeutic purposes. *Dyes and Pigments*, *201*, 110195. Retrieved from https://doi.org/10.1016/j.dyepig.2022.110195.

55. Wang, B., Zheng, Y., Wang, T., Ma, D., & Wang, Q. (2021). 1,8-naphthalimide-based hybrids for efficient red thermally activated delayed fluorescence organic light-emitting diodes. *Organic Electronics*, *88*, 106012. Retrieved from https://doi.org/10.1016/j.orgel.2020.106012.
56. Qi, S., Kim, S., Nguyen, V.-N., Kim, Y., Niu, G., Kim, G., Kim, S.-J., Park, S., & Yoon, J. (2020). Highly efficient aggregation-induced red-emissive organic thermally activated delayed fluorescence materials with prolonged fluorescence lifetime for time-resolved luminescence Bioimaging. *ACS Applied Materials & Interfaces*, *12*(46), 51293–51301. Retrieved from https://doi.org/10.1021/acsami.0c15936.
57. Jena, S., Dhanalakshmi, P., Bano, G., & Thilagar, P. (2020). Delayed fluorescence, room temperature phosphorescence, and mechanofluorochromic naphthalimides: Differential Imaging of normoxia and hypoxia live cancer cells. *The Journal of Physical Chemistry B*, *124*(26), 5393–5406. Retrieved from https://doi.org/10.1021/acs.jpcb.0c04115.
58. Lin, C., Wu, Z., Liu, J., Deng, W.-T., Zhuang, Y., Xuan, T., Xue, J., Zhang, L., Wei, G., & Xie, R.-J. (2022). Extremely low efficiency roll-off in vacuum- and solution-processed deep-red/near-infrared oleds based on 1,8-naphthalimide TADF emitters. *Journal of Luminescence*, *243*, 118683. Retrieved from https://doi.org/10.1016/j.jlumin.2021.118683.
59. Wu, Y., Chen, X., Mu, Y., Yang, Z., Mao, Z., Zhao, J., Yang, Z., Zhang, Y., & Chi, Z. (2019). Two thermally stable and aie active 1,8-naphthalimide derivatives with red efficient thermally activated delayed fluorescence. *Dyes and Pigments*, *169*, 81–88. Retrieved from https://doi.org/10.1016/j.dyepig.2019.04.071.
60. Cho, D. W., Fujitsuka, M., Chan Yoon, U., & Majima, T. (2008). Intermolecular photoinduced electron-transfer of 1,8-naphthalimides in protic polar solvents. *Physical Chemistry Chemical Physics*, *10*(30), 4393. Retrieved from https://doi.org/10.1039/b802074d.
61. Poddar, M., Rout, Y., & Misra, R. (2021). Donor-acceptor based 1,8-naphthalimide substituted phenothiazines: Tuning of homo-lumo gap. *Asian Journal of Organic Chemistry*, *11*(1), e2021006. Retrieved from https://doi.org/10.1002/ajoc.202100628.
62. Zeng, W., Lai, H.-Y., Lee, W.-K., Jiao, M., Shiu, Y.-J., Zhong, C., Gong, S., Zhou, T., Xie, G., Sarma, M., Wong, K.-T., Wu, C.-C., & Yang, C. (2017). Achieving nearly 30% external quantum efficiency for orange-red organic light emitting diodes by employing thermally activated delayed fluorescence emitters composed of 1,8-naphthalimide-acridine hybrids. *Advanced Materials*, *30*(5), 1704961. Retrieved from https://doi.org/10.1002/adma.201704961.
63. Zeng, W., Zhou, T., Ning, W., Zhong, C., He, J., Gong, S., Xie, G., & Yang, C. (2019). Realizing 22.5% external quantum efficiency for solution-processed thermally activated delayed-fluorescence oleds with red emission at 622 nm via a synergistic strategy of Molecular Engineering and host

selection. *Advanced Materials*, *31*(33), 1901404. Retrieved from https://doi.org/10.1002/adma.201901404.

64. Zeng, X., Huang, Y.-H., Gong, S., Yin, X., Lee, W.-K., Xiao, X., Zhang, Y., Zeng, W., Lu, C.-H., Lee, C.-C., Dong, X.-Q., Zhong, C., Wu, C.-C., & Yang, C. (2020). Rational design of perfectly oriented thermally activated delayed fluorescence emitter for efficient red electroluminescence. *Science China Materials*, *64*(4), 920–930. https://doi.org/10.1007/s40843-020-1501-1.
65. Gudeika, D., Grazulevicius, J. V., Sini, G., Bucinskas, A., Jankauskas, V., Miasojedovas, A., & Jursenas, S. (2014). New derivatives of triphenylamine and naphthalimide as Ambipolar Organic Semiconductors: Experimental and theoretical approach. *Dyes and Pigments*, *106*, 58–70. Retrieved from https://doi.org/10.1016/j.dyepig.2014.02.023.
66. Arunchai, R., Sudyoadsuk, T., Prachumrak, N., Namuangruk, S., Promarak, V., Sukwattanasinitt, M., & Rashatasakhon, P. (2015). Synthesis and characterization of new triphenylamino-1,8-naphthalimides for organic light-emitting diode applications. *New Journal of Chemistry*, *39*(4), 2807–2814. Retrieved from https://doi.org/10.1039/c4nj01785d.
67. Gudeika, D., Sini, G., Jankauskas, V., Sych, G., & Grazulevicius, J. V. (2016). Synthesis and properties of the derivatives of triphenylamine and 1,8-naphthalimide with the olefinic linkages between chromophores. *RSC Advances*, *6*(3), 2191–2201. Retrieved from https://doi.org/10.1039/c5ra24820e
68. Li, X., Shan, D., Oh, W., & Son, Y.-A. (2016). A bright yellow emissive dye configured by attaching triarylamine to naphthalimide with –NHN= bridge. *Molecular Crystals and Liquid Crystals*, *635*(1), 172–180. Retrieved from https://doi.org/10.1080/15421406.2016.1200928.
69. Jin, R.-fa, Tang, S.-shan, & Sun, W.-dong. (2014). Rational design of donor–π–acceptor n-butyl-1,8-naphthalimide-cored branched molecules as charge transport and luminescent materials for organic light-emitting diodes. *Tetrahedron*, *70*(1), 47–53. Retrieved from https://doi.org/10.1016/j.tet.2013.11.042.
70. Gudeika, D., Michaleviciute, A., Grazulevicius, J. V., Lygaitis, R., Grigalevicius, S., Jankauskas, V., Miasojedovas, A., Jursenas, S., & Sini, G. (2012). Structure properties relationship of donor–acceptor derivatives of triphenylamine and 1,8-naphthalimide. *The Journal of Physical Chemistry C*, *116*(28), 14811–14819. Retrieved from https://doi.org/10.1021/jp303172b.
71. Li, J., Meng, F., Tian, H., Mi, J., & Ji, W. (2005). Highly fluorescent naphthalimide derivatives for two-photon absorption materials. *Chemistry Letters*, *34*(7), 922–923. Retrieved from https://doi.org/10.1246/cl.2005.922.
72. Gudeika, D., Grazulevicius, J. V., Volyniuk, D., Juska, G., Jankauskas, V., & Sini, G. (2015). Effect of ethynyl linkages on the properties of the derivatives of triphenylamine and 1,8-naphthalimide. *The Journal of Physical Chemistry C*, *119*(51), 28335–28346. Retrieved from https://doi.org/10.1021/acs.jpcc.5b10163.

73. Zhu, W., Xu, Y., Zhang, Y., Shen, J., & Tian, H. (2005). Singlet energy transfer and photoinduced electron transfer in star-shaped naphthalimide derivatives based on triphenylamine. *Bulletin of the Chemical Society of Japan*, *78*(7), 1362–1367. Retrieved from https://doi.org/10.1246/bcsj.78.1362.
74. Rout, Y., & Misra, R. (2021). Design and synthesis of 1,8-naphthalimide functionalized benzothiadiazoles. *New Journal of Chemistry*, *45*(22), 9838–9845. Retrieved from https://doi.org/10.1039/d1nj00919b.
75. Kukhta, N. A., Volyniuk, D., Peciulyte, L., Ostrauskaite, J., Juska, G., & Grazulevicius, J. V. (2015). Structure–property relationships of star-shaped blue-emitting charge-transporting 1,3,5-triphenylbenzene derivatives. *Dyes and Pigments*, *117*, 122–132. Retrieved from https://doi.org/10.1016/j.dyepig.2015.02.013
76. Obolda, A., Zhang, M., & Li, F. (2016). Evolution of emission manners of organic light-emitting diodes: From emission of singlet exciton to emission of doublet exciton. *Chinese Chemical Letters*, *27*(8), 1345–1349. Retrieved from https://doi.org/10.1016/j.cclet.2016.06.030.
77. Pålsson, L.-O., Wang, C., Batsanov, A. S., King, S. M., Beeby, A., Monkman, A. P., & Bryce, M. R. (2010). Efficient intramolecular charge transfer in oligoyne-linked donor-π-acceptor molecules. *Chemistry - A European Journal*, *16*(5), 1470–1479. Retrieved from https://doi.org/10.1002/chem.200902099.
78. Brocke, C., Pflumm, C., Parham, A., & Fortte, R (2012). Compounds for Electronic Devices. U.S. Pat. Appl. US2012/0319052 A1. Retrieved from https://patents.google.com/patent/WO2012143079A1/en.
79. Li, N., Shin, D. W., Hwang, D. S., Lee, Y. M., & Guiver, M. D. (2010). Polymer electrolyte membranes derived from new sulfone monomers with pendent sulfonic acid groups. *Macromolecules*, *43*(23), 9810–9820. Retrieved fromhttps://doi.org/10.1021/ma102107a
80. Gudeika, D., Sini, G., Jankauskas, V., Sych, G., & Grazulevicius, J. V. (2016). Synthesis and properties of the derivatives of triphenylamine and 1,8-naphthalimide with the olefinic linkages between chromophores. *RSC Advances*, *6*(3), 2191–2201. Retrieved from https://doi.org/10.1039/c5ra24820e
81. Kormos, C. M., & Leadbeater, N. E. (2006). Direct conversion of aryl halides to phenols using high-temperature or near-critical water and microwave heating. *Tetrahedron*, *62*(19), 4728–4732. Retrieved from https://doi.org/10.1016/j.tet.2006.01.103
82. Yofu, K., Nomura, K., Fukuzaki, E., Hirai, Y., Hamano, M., & Mitsui, T. (2016) Photoelectric conversion material, film containing the material, photoelectric conversion device, method for preparing photoelectric conversion device, method for using photoelectric conversion device, photosensor and imaging device. United States Patent US9349965. Retrieved from https://patents.google.com/patent/CN102020573A/en.

83. Xue, J. Y., Nakanishi, W., Tanimoto, D., Hara, D., Nakamura, Y., & Isobe, H. (2013). Convergent synthesis of hexameric naphthylene macrocycles with dicarboxylic imide appendages. *Tetrahedron Letters*, *54*(36), 4963–4965. Retrieved from https://doi.org/10.1016/j.tetlet.2013.07.025.
84. Fang, Y.-K., Lee, W.-Y., Tuan, C.-S., Lu, L.-H., Teng, W.-J., & Chen, W.-C. (2010). New poly(4,4′-dicyano-4″-vinyl-triphenylamine) host material for single-layer IR complex phosphorescent light-emitting devices. *Polymer Journal*, *42*(4), 327–335. Retrieved from https://doi.org/10.1038/pj.2010.1.
85. FRISCH, M. J., et al. (2016). Gaussian 09, Revision E.01, Gaussian, Inc., Wallingford CT. Retrieved from: http://gaussian.com/g09citation/.
86. Kim, S.-Y., Cho, Y.-J., Lee, A.-R., Son, H.-jin, Han, W.-S., Cho, D. W., & Kang, S. O. (2017). Influence of π-conjugation structural changes on intramolecular charge transfer and photoinduced electron transfer in donor–π–Acceptor Dyads. *Physical Chemistry Chemical Physics*, *19*(1), 426–435. Retrieved from https://doi.org/10.1039/c6cp06566j
87. Tse, S., Cheung, C., & So, S. (2009). Charge transport and injection in amorphous organic semiconductors. *Organic Electronics*, 61–109. Retrieved from https://doi.org/10.1201/9781420072914-c3
88. Juška, G., Arlauskas, K., Viliūnas, M., & Kočka, J. (2000). Extraction current transients: New method of study of charge transport in Microcrystalline Silicon. *Physical Review Letters*, *84*(21), 4946–4949. Retrieved from https://doi.org/10.1103/physrevlett.84.4946
89. Kaji, H., Suzuki, H., Fukushima, T., Shizu, K., Suzuki, K., Kubo, S., Komino, T., Oiwa, H., Suzuki, F., Wakamiya, A., Murata, Y., & Adachi, C. (2015). Purely organic electroluminescent material realizing 100% conversion from electricity to light. *Nature Communications*, *6*(1). Retrieved from https://doi.org/10.1038/ncomms9476
90. Dandrade, B., Datta, S., Forrest, S., Djurovich, P., Polikarpov, E., & Thompson, M. (2005). Relationship between the ionization and oxidation potentials of molecular organic semiconductors. *Organic Electronics*, *6*(1), 11–20. Retrieved from https://doi.org/10.1016/j.orgel.2005.01.002
91. Siraj, N., Das, S., Hasan, F., Lu, C., Kiruri, L. W., Steege Gall, K. E., & Warner, I. M. (2015). Enhanced S2 emission in carbazole-based ionic liquids. *RSC Advances*, *5*(13), 9939–9945. Retrieved from https://doi.org/10.1039/c4ra12362j
92. Li, H., Li, J., Liu, D., & Mei, Y. (2020). Mechanism evolution from normal fluorescence to thermally activated delayed fluorescence and color tuning over visible light range: Effect of intramolecular charge transfer strength. *Dyes and Pigments*, *183*, 108732. Retrieved from https://doi.org/10.1016/j.dyepig.2020.108732
93. Huang, B., Yin, Z., Ban, X., Ma, Z., Jiang, W., Tian, W., Yang, M., Ye, S., Lin, B., & Sun, Y. (2016). Nondoped Deep Blue Oleds based on bis-(4-benzenesulfonyl-phenyl)-9-phenyl-9 h -carbazoles. *Journal of Luminescence*, *172*, 7–13. Retrieved from https://doi.org/10.1016/j.jlumin.2015.11.012

94. Bonesi, S. M., Mesaros, M., Cabrerizo, F. M., Ponce, M. A., Bilmes, G. M., & Erra-Balsells, R. (2007). The photophysics of nitrocarbazoles used as UV-MALDI matrices: Comparative spectroscopic and optoacoustic studies of mononitro- and dinitrocarbazoles. *Chemical Physics Letters*, *446*(1-3), 49–55. Retrieved from https://doi.org/10.1016/j.cplett.2007.08.015.
95. Mayr, C., Lee, S. Y., Schmidt, T. D., Yasuda, T., Adachi, C., & Brütting, W. (2014). Efficiency enhancement of organic light-emitting diodes incorporating a highly oriented thermally activated delayed fluorescence emitter. *Advanced Functional Materials*, *24*(33), 5232–5239. Retrieved from https://doi.org/10.1002/adfm.201400495.
96. Lee, Y.-T., Tseng, P.-C., Komino, T., Mamada, M., Ortiz, R. J., Leung, M.-kit, Chiu, T.-L., Lin, C.-F., Lee, J.-H., Adachi, C., Chen, C.-T., & Chen, C.-T. (2018). Simple molecular-engineering approach for enhancing orientation and outcoupling efficiency of thermally activated delayed fluorescent emitters without red-shifting emission. *ACS Applied Materials & Interfaces*, *10*(50), 43842–43849. Retrieved from https://doi.org/10.1021/acsami.8b16199.
97. Giebink, N. C., D'Andrade, B. W., Weaver, M. S., Mackenzie, P. B., Brown, J. J., Thompson, M. E., & Forrest, S. R. (2008). Intrinsic luminance loss in phosphorescent small-molecule organic light emitting devices due to bimolecular annihilation reactions. *Journal of Applied Physics*, *103*(4), 044509. Retrieved from https://doi.org/10.1063/1.2884530.
98. Uoyama, H., Goushi, K., Shizu, K., Nomura, H., & Adachi, C. (2012). Highly efficient organic light-emitting diodes from delayed fluorescence. *Nature*, *492*(7428), 234–238. Retrieved from https://doi.org/10.1038/nature11687.
99. Xiang, C., Peng, C., Chen, Y., & So, F. (2015). Origin of sub-bandgap electroluminescence in organic light-emitting diodes. *Small*, *11*(40), 5439–5443. Retrieved from https://doi.org/10.1002/smll.201501355.
100. Xu, B., Mu, Y., Mao, Z., Xie, Z., Wu, H., Zhang, Y., Jin, C., Chi, Z., Liu, S., Xu, J., Wu, Y.-C., Lu, P.-Y., Lien, A., & Bryce, M. R. (2016). Achieving remarkable mechanochromism and white-light emission with thermally activated delayed fluorescence through the molecular heredity principle. *Chemical Science*, *7*(3), 2201–2206. Retrieved from https://doi.org/10.1039/c5sc04155d.
101. Etherington, M. K., Gibson, J., Higginbotham, H. F., Penfold, T. J., & Monkman, A. P. (2016). Revealing the spin–vibronic coupling mechanism of thermally activated delayed fluorescence. *Nature Communications*, *7*(1). Retrieved from https://doi.org/10.1038/ncomms13680.
102. Chai, J.D., & Head-Gordon, M. (2008). Systematic optimization of long-range corrected hybrid density functionals. *The Journal of Chemical Physics*, *128*(8), 084106. Retrieved from https://doi.org/10.1063/1.2834918.
103. Marenich, A. V., Cramer, C. J., & Truhlar, D. G. (2009). Universal solvation model based on solute electron density and on a continuum model of the solvent defined by the bulk dielectric constant and atomic surface tensions.

The Journal of Physical Chemistry B, *113*(18), 6378–6396. Retrieved from https://doi.org/10.1021/jp810292n.
104. Cammi, R., & Mennucci, B. (1999). Linear response theory for the polarizable continuum model. *The Journal of Chemical Physics*, *110*(20), 9877–9886. Retrieved from https://doi.org/10.1063/1.478861.
105. Matulis, V. E., Ragoyja, E. G., & Ivashkevich, O. A. (2020). Accurate theoretical prediction of optical properties of Bodipy dyes. *International Journal of Quantum Chemistry*, *120*(9). Retrieved from https://doi.org/10.1002/qua.26159.
106. FRISCH, M. J., et al. (2016). Gaussian 16, Revision E.01, Gaussian, Inc., Wallingford CT. Retrieved from: http://gaussian.com/g16citation/.
107. Lu, T., & Chen, F. (2011). Multiwfn: A multifunctional wavefunction analyzer. *Journal of Computational Chemistry*, *33*(5), 580–592. Retrieved from https://doi.org/10.1002/jcc.22885.
108. Zara, Z., Iqbal, J., Ayub, K., Irfan, M., Mahmood, A., Khera, R. A., & Eliasson, B. (2017). A comparative study of DFT calculated and experimental UV/visible spectra for thirty carboline and carbazole based compounds. *Journal of Molecular Structure*, *1149*, 282–298. Retrieved from https://doi.org/10.1016/j.molstruc.2017.07.093.
109. Isegawa, M., Peverati, R., & Truhlar, D. G. (2012). Performance of recent and high-performance approximate density functionals for time-dependent density functional theory calculations of valence and Rydberg electronic transition energies. *The Journal of Chemical Physics*, *137*(24), 244104. Retrieved from https://doi.org/10.1063/1.4769078.
110. Sworakowski, J. (2018). How accurate are energies of HOMO and LUMO levels in small-molecule organic semiconductors determined from cyclic voltammetry or optical spectroscopy? *Synthetic Metals*, *235*, 125–130. Retrieved from https://doi.org/10.1016/j.synthmet.2017.11.013.
111. Shaheen, S. E., Jabbour, G. E., Morrell, M. M., Kawabe, Y., Kippelen, B., Peyghambarian, N., Nabor, M.-F., Schlaf, R., Mash, E. A., & Armstrong, N. R. (1998). Bright blue organic light-emitting diode with improved color purity using a LIF/Al Cathode. *Journal of Applied Physics*, *84*(4), 2324–2327. Retrieved from https://doi.org/10.1063/1.368299.
112. Demeter, A., Bérces, T., Biczók, L., Wintgens, V., Valat, P., & Kossanyi, J. (1996). Comprehensive model of the photophysics of *n*-phenylnaphthalimides: the role of solvent and rotational relaxation. *The Journal of Physical Chemistry*, *100*(6), 2001–2011. Retrieved from https://doi.org/10.1021/jp951133n.
113. Chen, S., Pei, J., Pang, Z., Wu, W., Yu, X., & Zhang, C. (2020). Axial-symmetric conjugated group promoting intramolecular charge transfer performances of triphenylamine sensitizers for dye-sensitized solar cells. *Dyes and Pigments*, *174*, 108029. Retrieved from https://doi.org/10.1016/j.dyepig.2019.108029.

114. Kulszewicz-Bajer, I., Zagorska, M., Banasiewicz, M., Guńka, P. A., Toman, P., Kozankiewicz, B., Wiosna-Salyga, G., & Pron, A. (2020). Effect of the substituent position on the electrochemical, optical and structural properties of donor–acceptor type acridone derivatives. *Physical Chemistry Chemical Physics*, *22*(16), 8522–8534. Retrieved from https://doi.org/10.1039/d0cp00521e.
115. Wu, Q., Wang, M., Cao, X., Zhang, D., Sun, N., Wan, S., & Tao, Y. (2018). Carbazole/α-carboline hybrid bipolar compounds as electron acceptors in exciplex or non-exciplex mixed cohosts and Exciplex-TADF emitters for high-efficiency oleds. *Journal of Materials Chemistry C*, *6*(32), 8784–8792. Retrieved from https://doi.org/10.1039/c8tc02353k.
116. Gudeika, D., Bezvikonnyi, O., Volyniuk, D., & Grazulevicius, J. V. (2020). Differently substituted benzonitriles for non-doped oleds. *Dyes and Pigments*, *172*, 107789. https://doi.org/10.1016/j.dyepig.2019.107789.
117. Mei, J., Leung, N. L., Kwok, R. T., Lam, J. W., & Tang, B. Z. (2015). Aggregation-induced emission: Together we shine, united we soar! *Chemical Reviews*, *115*(21), 11718–11940. Retrieved from https://doi.org/10.1021/acs.chemrev.5b00263.
118. Lakowicz, J. R. (2006). Principles of fluorescence spectroscopy. Retrieved from https://doi.org/10.1007/978-0-387-46312-4
119. Yang, X., Lu, R., Zhou, H., Xue, P., Wang, F., Chen, P., & Zhao, Y. (2009). Aggregation-induced blue shift of fluorescence emission due to suppression of TICT in a phenothiazine-based organogel. *Journal of Colloid and Interface Science*, *339*(2), 527–532. Retrieved from https://doi.org/10.1016/j.jcis.2009.07.033.
120. Han, C., Zhang, Z., Ding, D., & Xu, H. (2018). Dipole-dipole interaction management for efficient blue thermally activated delayed fluorescence diodes. *Chem*, *4*(9), 2154–2167. Retrieved from https://doi.org/10.1016/j.chempr.2018.06.005.
121. Ren, Z., Nobuyasu, R. S., Dias, F. B., Monkman, A. P., Yan, S., & Bryce, M. R. (2016). Pendant homopolymer and copolymers as solution-processable thermally activated delayed fluorescence materials for organic light-emitting diodes. *Macromolecules*, *49*(15), 5452–5460. Retrieved from https://doi.org/10.1021/acs.macromol.6b01216.
122. Ward, J. S., Nobuyasu, R. S., Batsanov, A. S., Data, P., Monkman, A. P., Dias, F. B., & Bryce, M. R. (2016). The interplay of thermally activated delayed fluorescence (TADF) and room temperature organic phosphorescence in sterically-constrained donor–acceptor charge-transfer molecules. *Chemical Communications*, *52*(12), 2612–2615. Retrieved from https://doi.org/10.1039/c5cc09645f.
123. Zhang, D., Song, X., Gillett, A. J., Drummond, B. H., Jones, S. T., Li, G., He, H., Cai, M., Credgington, D., & Duan, L. (2020). Efficient and stable deep-blue fluorescent organic light-emitting diodes employing a sensitizer with fast triplet upconversion. *Advanced Materials*, *32*(19), 1908355. Retrieved from https://doi.org/10.1002/adma.201908355

124. Wada, Y., Nakagawa, H., Matsumoto, S., Wakisaka, Y., & Kaji, H. (2020). Organic light emitters exhibiting very fast reverse intersystem crossing. *Nature Photonics*, *14*(10), 643–649. Retrieved from https://doi.org/10.1038/s41566-020-0667-0.
125. Xu, J., Liu, H., Li, J., Zhao, Z., & Tang, B. Z. (2021). Multifunctional Bipolar Materials Serving as Emitters for Efficient Deep-Blue Fluorescent OLEDs and as Hosts for Phosphorescent and White OLEDs. *Advanced Optical Materials*, *9*(6), 2001840. Retrieved from https://doi.org/10.1002/adom.202001840.
126. Bao, L., Zhu, J., Song, W., Zhou, H., Huang, J., Mu, H., & Su, J. (2020). New carbazole-based bipolar hosts for efficient green phosphorescent organic light-emitting diodes. *Organic Electronics*, *83*, 105672. Retrieved from https://doi.org/10.1016/j.orgel.2020.105672.
127. Lee, J.-H., Chen, C.-H., Lin, B.-Y., Lan, Y.-H., Huang, Y.-M., Chen, N.-J., Huang, J.-J., Volyniuk, D., Keruckiene, R., Grazulevicius, J. V., Wu, Y.-R., Leung, M.-kit, & Chiu, T.-L. (2020). Bistriazoles with a biphenyl core derivative as an electron-favorable bipolar host of efficient blue phosphorescent organic light-emitting diodes. *ACS Applied Materials & Interfaces*, *12*(44), 49895–49904. Retrieved from https://doi.org/10.1021/acsami.0c13705.
128. Wu, M.-F., Yeh, S.-J., Chen, C.-T., Murayama, H., Tsuboi, T., Li, W.-S., Chao, I., Liu, S.-W., & Wang, J.-K. (2007). The quest for high-performance host materials for electrophosphorescent Blue Dopants. *Advanced Functional Materials*, *17*(12), 1887–1895. Retrieved fromhttps://doi.org/10.1002/adfm.200600800.
129. Maasoumi, F., Jansen-van Vuuren, R. D., Shaw, P. E., Puttock, E. V., Nagiri, R. C., McEwan, J. A., Bown, M., O'Connell, J. L., Dunn, C. J., Burn, P. L., & Namdas, E. B. (2018). An external quantum efficiency of >20% from solution-processed poly(dendrimer) organic light-emitting diodes. *Npj Flexible Electronics*, *2*(1). Retrieved from https://doi.org/10.1038/s41528-018-0038-9.
130. Pelczarski, D., Grygiel, P., Falkowski, K., Klein, M., & Stampor, W. (2015). Electromodulation and magnetomodulation of exciton dissociation in electron donor (starburst amine) : Electron Acceptor (bathocuproine) system. *Organic Electronics*, *25*, 362–376. Retrieved from https://doi.org/10.1016/j.orgel.2015.06.050.
131. Ranasinghe, M. I., Varnavski, O. P., Pawlas, J., Hauck, S. I., Louie, J., Hartwig, J. F., & Goodson, T. (2002). Femtosecond excitation energy transport in triarylamine Dendrimers. *Journal of the American Chemical Society*, *124*(23), 6520–6521. Retrieved from https://doi.org/10.1021/ja025505z.
132. Xiao, P., Dumur, F., Zhang, J., Graff, B., Gigmes, D., Fouassier, J. P., & Lalevée, J. (2015). Amino and Nitro substituted 2-amino-1h-benzo[de]isoquinoline-1,3(2h)-diones: As versatile photoinitiators of

polymerization from violet-blue led absorption to a panchromatic behavior. *Polymer Chemistry*, *6*(7), 1171–1179. Retrieved from https://doi.org/10.1039/c4py01409j.
133. Gudeika, D., Michaleviciute, A., Grazulevicius, J. V., Lygaitis, R., Grigalevicius, S., Jankauskas, V., Miasojedovas, A., Jursenas, S., & Sini, G. (2012). Structure properties relationship of donor–acceptor derivatives of triphenylamine and 1,8-naphthalimide. *The Journal of Physical Chemistry C*, *116*(28), 14811–14819. Retrieved from https://doi.org/10.1021/jp303172b.
134. Masimukku, N., Gudeika, D., Volyniuk, D., Bezvikonnyi, O., Simokaitiene, J., Matulis, V., Lyakhov, D., Azovskyi, V., & Gražulevičius, J. V. (2022). Bipolar 1,8-naphthalimides showing high electron mobility and red aie-active TADF for OLED applications. *Physical Chemistry Chemical Physics*, *24*(8), 5070–5082. Retrieved from https://doi.org/10.1039/d1cp05942d.
135. Lee, J.-H., Chen, C.-H., Lin, B.-Y., Lan, Y.-H., Huang, Y.-M., Chen, N.-J., Huang, J.-J., Volyniuk, D., Keruckiene, R., Grazulevicius, J. V., Wu, Y.-R., Leung, M.-kit, & Chiu, T.-L. (2020). Bistriazoles with a biphenyl core derivative as an electron-favorable bipolar host of efficient blue phosphorescent organic light-emitting diodes. *ACS Applied Materials & Interfaces*, *12*(44), 49895–49904. Retrieved from https://doi.org/10.1021/acsami.0c13705.
136. Mahmoudi, M., Gudeika, D., Volyniuk, D., Leitonas, K., Butkute, R., Danyliv, I., & Grazulevicius, J. V. (2021). Tuning of spin-flip efficiency of blue emitting multicarbazolyl-substituted benzonitriles by exploitation of the different additional electron accepting moieties. *Chemical Engineering Journal*, *423*, 130236. Retrieved from https://doi.org/10.1016/j.cej.2021.130236.
137. Hosokawa, C., Tokailin, H., Higashi, H., & Kusumoto, T. (1992). Transient behavior of organic thin film electroluminescence. *Applied Physics Letters*, *60*(10), 1220–1222. Retrieved from https://doi.org/10.1063/1.107411.
138. Han, T.-H., Song, W., & Lee, T.-W. (2015). Elucidating the crucial role of hole injection layer in degradation of organic light-emitting diodes. *ACS Applied Materials & Interfaces*, *7*(5), 3117–3125. Retrieved fromhttps://doi.org/10.1021/am5072628.
139. Lee, J.-H., Lee, S., Yoo, S.-J., Kim, K.-H., & Kim, J.-J. (2014). Langevin and trap-assisted recombination in Phosphorescent Organic Light Emitting Diodes. *Advanced Functional Materials*, *24*(29), 4681–4688. Retrieved fromhttps://doi.org/10.1002/adfm.201303453.
140. Kang, J., Son, J. B., Kim, G. W., Bae, S., Min, K. S., Sul, S., Jeon, W. S., Jang, J., Park, G.-S., Shin, J. K., Kwon, J. H., & Kim, S. K. (2020). Time-resolved electroluminescence study for the effect of charge traps on the Luminescence Properties of Organic light-emitting diodes. *Physica Status Solidi (a)*, *217*(17), 2000081. Retrieved from https://doi.org/10.1002/pssa.202000081.
141. Dias, F. B., Penfold, T. J., & Monkman, A. P. (2017). Photophysics of thermally activated delayed fluorescence molecules. *Methods and*

Applications in Fluorescence, *5*(1), 012001. Retrieved from https://doi.org/10.1088/2050-6120/aa537e.
142. Liu, Y., Li, C., Ren, Z., Yan, S., & Bryce, M. R. (2018). All-organic thermally activated delayed fluorescence materials for organic light-emitting diodes. *Nature Reviews Materials*, *3*(4). Retrieved from https://doi.org/10.1038/natrevmats.2018.20.
143. Goushi, K., Yoshida, K., Sato, K., & Adachi, C. (2012). Organic light-emitting diodes employing efficient reverse intersystem crossing for triplet-to-singlet state conversion. *Nature Photonics*, *6*(4), 253–258. Retrieved from https://doi.org/10.1038/nphoton.2012.31.
144. Lee, J.-H., Chen, C.-H., Lee, P.-H., Lin, H.-Y., Leung, M.-kit, Chiu, T.-L., & Lin, C.-F. (2019). Blue Organic Light-emitting diodes: Current status, Challenges, and future outlook. *Journal of Materials Chemistry C*, *7*(20), 5874–5888. Retrieved from https://doi.org/10.1039/c9tc00204a.
145. Yang, Z., Mao, Z., Xie, Z., Zhang, Y., Liu, S., Zhao, J., Xu, J., Chi, Z., & Aldred, M. P. (2017). Recent advances in organic thermally activated delayed fluorescence materials. *Chemical Society Reviews*, *46*(3), 915–1016. Retrieved from https://doi.org/10.1039/c6cs00368k.
146. Wong, M. Y., & Zysman-Colman, E. (2017). Purely organic thermally activated delayed fluorescence materials for organic light-emitting diodes. *Advanced Materials*, *29*(22), 1605444. Retrieved from https://doi.org/10.1002/adma.201605444.
147. Cho, Y. J., Yook, K. S., & Lee, J. Y. (2014). A universal host material for high external quantum efficiency close to 25% and long lifetime in green fluorescent and phosphorescent oleds. *Advanced Materials*, *26*(24), 4050–4055. Retrieved from https://doi.org/10.1002/adma.201400347
148. Cheng, S.-H., Hung, W.-Y., Cheng, M.-H., Chen, H.-F., Chaskar, A., Lee, G.-H., Chou, S.-H., & Wong, K.-T. (2014). Highly twisted biphenyl-linked carbazole–benzimidazole hybrid bipolar host materials for efficient pholeds. *J. Mater. Chem. C*, *2*(40), 8554–8563. Retrieved from https://doi.org/10.1039/c4tc01463d.
149. Mondal, E., Hung, W.-Y., Dai, H.-C., & Wong, K.-T. (2013). Fluorene-based asymmetric bipolar universal hosts for White Organic Light Emitting Devices. *Advanced Functional Materials*, *23*(24), 3096–3105. Retrieved from https://doi.org/10.1002/adfm.201202889.
150. Gao, Y., Pivrikas, A., Xu, B., Liu, Y., Xu, W., van Loosdrecht, P. H. M., & Tian, W. (2015). Measuring electron and hole mobilities in organic systems: Charge selective celiv. *Synthetic Metals*, *203*, 187–191. Retrieved from https://doi.org/10.1016/j.synthmet.2015.02.036.
151. Bezvikonnyi, O., Gudeika, D., Volyniuk, D., Rutkis, M., & Grazulevicius, J. V. (2020). Diphenylsulfone-based hosts for electroluminescent devices: Effect of donor substituents. *Dyes and Pigments*, *175*, 108104. Retrieved from https://doi.org/10.1016/j.dyepig.2019.108104.

152. Wang, S., Zhang, Y., Chen, W., Wei, J., Liu, Y., & Wang, Y. (2015). Achieving high power efficiency and low roll-off oleds based on energy transfer from thermally activated delayed excitons to fluorescent dopants. *Chemical Communications*, *51*(60), 11972–11975. Retrieved from https://doi.org/10.1039/c5cc04469c.
153. Kim, M., Jeon, S. K., Hwang, S.-H., & Lee, J. Y. (2015). Stable blue thermally activated delayed fluorescent organic light-emitting diodes with three times longer lifetime than phosphorescent organic light-emitting diodes. *Advanced Materials*, *27*(15), 2515–2520. Retrieved from https://doi.org/10.1002/adma.201500267.
154. Cui, L. S., Kim, J. U., Nomura, H., Nakanotani, H., & Adachi, C. (2016). Benzimidazobenzothiazole-based bipolar hosts to harvest nearly all of the excitons from blue delayed fluorescence and phosphorescent organic light-emitting diodes. *Angewandte Chemie International Edition*, *55*(24), 6864–6868. Retrieved from https://doi.org/10.1002/anie.201601136.
155. Furukawa, T., Nakanotani, H., Inoue, M., & Adachi, C. (2015). Dual enhancement of electroluminescence efficiency and operational stability by rapid upconversion of triplet excitons in oleds. *Scientific Reports*, *5*(1). Retrieved from https://doi.org/10.1038/srep08429.
156. Rajamalli, P., Senthilkumar, N., Huang, P.-Y., Ren-Wu, C.-C., Lin, H.-W., & Cheng, C.-H. (2017). New molecular design concurrently providing superior pure blue, thermally activated delayed fluorescence and optical out-coupling efficiencies. *Journal of the American Chemical Society*, *139*(32), 10948–10951. Retrieved from https://doi.org/10.1021/jacs.7b03848.
157. Zhang, D., Cai, M., Bin, Z., Zhang, Y., Zhang, D., & Duan, L. (2016). Highly efficient blue thermally activated delayed fluorescent oleds with record-low driving voltages utilizing high triplet energy hosts with small singlet–triplet splittings. *Chemical Science*, *7*(5), 3355–3363. Retrieved from https://doi.org/10.1039/c5sc04755b.
158. Han, C., Zhang, Z., Ding, D., & Xu, H. (2018). Dipole-dipole interaction management for efficient blue thermally activated delayed fluorescence diodes. *Chem*, *4*(9), 2154–2167. Retrieved from https://doi.org/10.1016/j.chempr.2018.06.005.
159. Chatterjee, T., & Wong, K.-T. (2018). Perspective on host materials for thermally activated delayed fluorescence organic light emitting diodes. *Advanced Optical Materials*, *7*(1), 1800565. Retrieved from https://doi.org/10.1002/adom.201800565.
160. Schrögel, P., Langer, N., Schildknecht, C., Wagenblast, G., Lennartz, C., & Strohriegl, P. (2011). Meta-linked CBP-derivatives as host materials for a blue iridium carbene complex. *Organic Electronics*, *12*(12), 2047–2055. Retrieved from https://doi.org/10.1016/j.orgel.2011.08.012.
161. Bucinskas, A., Bezvikonnyi, O., Gudeika, D., Volyniuk, D., & Grazulevicius, J. V. (2020). Methoxycarbazolyl-disubstituted dibenzofuranes as holes- and electrons-transporting hosts for phosphorescent and TADF-

based oleds. *Dyes and Pigments*, *172*, 107781. Retrieved from https://doi.org/10.1016/j.dyepig.2019.107781.
162. Yang, H., Liang, Q., Han, C., Zhang, J., & Xu, H. (2017). A phosphanthrene oxide host with close sphere packing for ultralow-voltage-driven efficient blue thermally activated delayed fluorescence diodes. *Advanced Materials*, *29*(38), 1700553. Retrieved from https://doi.org/10.1002/adma.201700553.
163. Jou, J.-H., Kumar, S., Agrawal, A., Li, T.-H., & Sahoo, S. (2015). Approaches for fabricating high efficiency organic light emitting diodes. *Journal of Materials Chemistry C*, *3*(13), 2974–3002. Retrieved from https://doi.org/10.1039/c4tc02495h.
164. Xu, Z., Tang, B. Z., Wang, Y., & Ma, D. (2020). Recent advances in high performance blue organic light-emitting diodes based on fluorescence emitters. *Journal of Materials Chemistry C*, *8*(8), 2614–2642. Retrieved from https://doi.org/10.1039/c9tc06441a.
165. Song, X., Zhang, D., Lu, Y., Yin, C., & Duan, L. (2019). Understanding and manipulating the interplay of wide-energy-gap host and TADF sensitizer in high-performance fluorescence oleds. *Advanced Materials*, *31*(35), 1901923. Retrieved from https://doi.org/10.1002/adma.201901923.
166. Gao, M., Lee, T., Burn, P. L., Mark, A. E., Pivrikas, A., & Shaw, P. E. (2019). Revealing the interplay between charge transport, luminescence efficiency, and morphology in organic light-emitting diode blends. *Advanced Functional Materials*, *30*(9), 1907942. Retrieved from https://doi.org/10.1002/adfm.201907942.
167. Nishimoto, T., Yasuda, T., Lee, S. Y., Kondo, R., & Adachi, C. (2014). A six-carbazole-decorated cyclophosphazene as a host with high triplet energy to realize efficient delayed-fluorescence oleds. *Mater. Horiz.*, *1*(2), 264–269. Retrieved from https://doi.org/10.1039/c3mh00079f.
168. Nakanotani, H., Higuchi, T., Furukawa, T., Masui, K., Morimoto, K., Numata, M., Tanaka, H., Sagara, Y., Yasuda, T., & Adachi, C. (2014). High-efficiency organic light-emitting diodes with fluorescent emitters. *Nature Communications*, *5*(1). Retrieved from https://doi.org/10.1038/ncomms5016.
169. Wang, S., Zhang, Y., Chen, W., Wei, J., Liu, Y., & Wang, Y. (2015). Achieving high power efficiency and low roll-off oleds based on energy transfer from thermally activated delayed excitons to fluorescent dopants. *Chemical Communications*, *51*(60), 11972–11975. Retrieved from https://doi.org/10.1039/c5cc04469c.
170. Zhang, D., Duan, L., Zhang, D., & Qiu, Y. (2014). Towards ideal electrophosphorescent devices with low dopant concentrations: The key role of triplet up-conversion. *J. Mater. Chem. C*, *2*(42), 8983–8989. https://doi.org/10.1039/c4tc01757a.
171. Che, W., Xie, Y., & Li, Z. (2020). Structural design of blue-to-red thermally-activated delayed fluorescence molecules by adjusting the strength between donor and acceptor. *Asian Journal of Organic Chemistry*, *9*(9), 1262–1276. Retrieved from https://doi.org/10.1002/ajoc.202000128.

172. Zhang, Q., Li, B., Huang, S., Nomura, H., Tanaka, H., & Adachi, C. (2014). Efficient blue organic light-emitting diodes employing thermally activated delayed fluorescence. *Nature Photonics*, *8*(4), 326–332. Retrieved from https://doi.org/10.1038/nphoton.2014.12.
173. Gibson, J., Monkman, A. P., & Penfold, T. J. (2016). The importance of vibronic coupling for efficient reverse intersystem crossing in thermally activated delayed fluorescence molecules. *ChemPhysChem*, *17*(19), 2956–2961. Retrieved from https://doi.org/10.1002/cphc.201600662.
174. Chen, X.-K., Zhang, S.-F., Fan, J.-X., & Ren, A.-M. (2015). Nature of highly efficient thermally activated delayed fluorescence in organic light-emitting diode emitters: Nonadiabatic effect between excited states. *The Journal of Physical Chemistry C*, *119*(18), 9728–9733. Retrieved from https://doi.org/10.1021/acs.jpcc.5b00276.
175. Xu, S., Liu, T., Mu, Y., Wang, Y.-F., Chi, Z., Lo, C.-C., Liu, S., Zhang, Y., Lien, A., & Xu, J. (2014). An organic molecule with asymmetric structure exhibiting aggregation-induced emission, delayed fluorescence, and Mechanoluminescence. *Angewandte Chemie International Edition*, *54*(3), 874–878. Retrieved from https://doi.org/10.1002/anie.201409767.
176. Zhang, Q., Li, J., Shizu, K., Huang, S., Hirata, S., Miyazaki, H., & Adachi, C. (2012). Design of efficient thermally activated delayed fluorescence materials for pure Blue Organic Light Emitting Diodes. *Journal of the American Chemical Society*, *134*(36), 14706–14709. Retrieved from https://doi.org/10.1021/ja306538w.
177. Etherington, M. K. (2020). Thermally activated delayed fluorescence: Beyond the single molecule. *Frontiers in Chemistry*, *8*. Retrieved from https://doi.org/10.3389/fchem.2020.00716.
178. Andruleviciene, V., Leitonas, K., Volyniuk, D., Sini, G., Grazulevicius, J. V., & Getautis, V. (2021). TADF versus TTA emission mechanisms in acridan and carbazole-substituted dibenzo[a,c]phenazines: Towards triplet harvesting emitters and hosts. *Chemical Engineering Journal*, *417*, 127902. Retrieved from https://doi.org/10.1016/j.cej.2020.127902.
179. Dhali, R., Phan Huu, D. K., Bertocchi, F., Sissa, C., Terenziani, F., & Painelli, A. (2021). Understanding TADF: A joint experimental and theoretical study of DMAC-Trz. *Physical Chemistry Chemical Physics*, *23*(1), 378–387. Retrieved from https://doi.org/10.1039/d0cp05982.j
180. Li, N., Shin, D. W., Hwang, D. S., Lee, Y. M., & Guiver, M. D. (2010). Polymer electrolyte membranes derived from new sulfone monomers with pendent sulfonic acid groups. *Macromolecules*, *43*(23), 9810–9820. Retrieved from https://doi.org/10.1021/ma102107a.
181. Lin, T.-A., Chatterjee, T., Tsai, W.-L., Lee, W.-K., Wu, M.-J., Jiao, M., Pan, K.-C., Yi, C.-L., Chung, C.-L., Wong, K.-T., & Wu, C.-C. (2016). Sky-Blue Organic Light emitting diode with 37% external quantum efficiency using thermally activated delayed fluorescence from spiroacridine-triazine hybrid. *Advanced Materials*, *28*(32), 6976–6983. Retrieved from https://doi.org/10.1002/adma.201601675.

182. Wong, M. Y., & Zysman-Colman, E. (2017). Purely organic thermally activated delayed fluorescence materials for organic light-emitting diodes. *Advanced Materials*, *29*(22), 1605444. Retrieved from https://doi.org/10.1002/adma.201605444.
183. Lee, D. R., Kim, B. S., Lee, C. W., Im, Y., Yook, K. S., Hwang, S.-H., & Lee, J. Y. (2015). Above 30% external quantum efficiency in green delayed fluorescent organic light-emitting diodes. *ACS Applied Materials & Interfaces*, *7*(18), 9625–9629. Retrieved from https://doi.org/10.1021/acsami.5b01220
184. Tsujimoto, H., Ha, D.-G., Markopoulos, G., Chae, H. S., Baldo, M. A., & Swager, T. M. (2017). Thermally activated delayed fluorescence and aggregation induced emission with through-space charge transfer. *Journal of the American Chemical Society*, *139*(13), 4894–4900. Retrieved from https://doi.org/10.1021/jacs.7b00873.
185. Cui, L.-S., Gillett, A. J., Zhang, S.-F., Ye, H., Liu, Y., Chen, X.-K., Lin, Z.-S., Evans, E. W., Myers, W. K., Ronson, T. K., Nakanotani, H., Reineke, S., Bredas, J.-L., Adachi, C., & Friend, R. H. (2020). Fast spin-flip enables efficient and stable organic electroluminescence from charge-transfer states. *Nature Photonics*, *14*(10), 636–642. Retrieved from https://doi.org/10.1038/s41566-020-0668-z.
186. Keruckiene, R., Volyniuk, D., Ostrauskaite, J., Peciulyte, L., Grazulevicius, J. V., Kostjuk, S. V., & Lazauskas, A. (2017). Derivatives of 2-phenylindole and carbazole as host materials for Phosphorescent Organic Light Emitting Diodes. *Dyes and Pigments*, *137*, 58–68. Retrieved from https://doi.org/10.1016/j.dyepig.2016.09.038.
187. Rayappa Naveen, K., Prabhu CP, K., Braveenth, R., & Hyuk Kwon, J. (2022). Molecular design strategy for orange red thermally activated delayed fluorescence emitters in organic light-emitting diodes (oleds). *Chemistry – A European Journal*, *28*(12). Retrieved from https://doi.org/10.1002/chem.202103532.
188. Ikai, M., Takeuchi, H., Fujikawa, H., & Taga, Y. Red Phosphorescent Organic Light-emitting Diodes. *R&D Rev Toyota CRDL, 41*(2), 63-69. Retrieved from https://www.tytlabs.co.jp/en/english/review/rev412e.html.
189. Forget, S., Chenais, S., Tondelier, D., Geffroy, B., Gozhyk, I., Lebental, M., & Ishow, E. (2010). Red-emitting fluorescent organic light emitting diodes with low sensitivity to self-quenching. *Journal of Applied Physics*, *108*(6), 064509. Retrieved from https://doi.org/10.1063/1.3481460.
190. He, J. -L., Kong, F.-C., Sun, B., Wang, X.-J., Tian, Q.-S., Fan, J., & Liao, L.-S. (2021). Highly efficient deep-red TADF organic light-emitting diodes via increasing the acceptor strength of fused polycyclic aromatics. *Chemical Engineering Journal*, *424*, 130470. Retrieved from https://doi.org/10.1016/j.cej.2021.130470.
191. Chen, J.-X., Tao, W.-W., Xiao, Y.-F., Wang, K., Zhang, M., Fan, X.-C., Chen, W.-C., Yu, J., Li, S., Geng, F.-X., Zhang, X.-H., & Lee, C.-S. (2019).

Efficient Orange-red thermally activated delayed fluorescence emitters feasible for both thermal evaporation and solution process. *ACS Applied Materials & Interfaces*, *11*(32), 29086–29093. Retrieved from https://doi.org/10.1021/acsami.9b08729.

192. Gudeika, D., Grazulevicius, J. V., Volyniuk, D., Butkute, R., Juska, G., Miasojedovas, A., Gruodis, A., & Jursenas, S. (2015). Structure-properties relationship of the derivatives of carbazole and 1,8-naphthalimide: Effects of the substitution and the linking topology. *Dyes and Pigments*, *114*, 239–252. Retrieved from https://doi.org/10.1016/j.dyepig.2014.11.013.
193. Beaudoin, N., Essiambre, S., & Gauvin, S. (2006). Simple hybrid current-voltage source for the characterization of organic light-emitting devices. *Review of Scientific Instruments*, *77*(2), 026102. Retrieved from https://doi.org/10.1063/1.2169502.
194. Hosokawa, C., Tokailin, H., Higashi, H., & Kusumoto, T. (1992). Transient behavior of organic thin film electroluminescence. *Applied Physics Letters*, *60*(10), 1220–1222. Retrieved from https://doi.org/10.1063/1.107411.
195. Han, T.-H., Song, W., & Lee, T.-W. (2015). Elucidating the crucial role of hole injection layer in degradation of organic light-emitting diodes. *ACS Applied Materials & Interfaces*, *7*(5), 3117–3125. Retrieved from https://doi.org/10.1021/am5072628.
196. OLED DISPLAYS. (n.d.). Https://Cynora.Com/. Retrieved June 28, 2022. Retrieved from from https://cynora.com/technology-and-products/oled-displays/.
197. Gudeika, D., Grazulevicius, J. V., Volyniuk, D., Butkute, R., Juska, G., Miasojedovas, A., Gruodis, A., & Jursenas, S. (2015). Structure-properties relationship of the derivatives of carbazole and 1,8-naphthalimide: Effects of the substitution and the linking topology. *Dyes and Pigments*, *114*, 239–252. Retrieved from https://doi.org/10.1016/j.dyepig.2014.11.013.
198. Jiang, W., Tang, J., Qi, Q., Wu, W., Sun, Y., & Fu, D. (2009). The synthesis, crystal structure and photophysical properties of three novel naphthalimide dyes. *Dyes and Pigments*, *80*(1), 11–16. Retrieved from https://doi.org/10.1016/j.dyepig.2008.04.005.
199. Li, H., Jin, Z., Li, N., Xu, Q., Gu, H., Lu, J., Xia, X., & Wang, L. (2011). A small-molecule-based device for data storage and electro-optical switch applications. *Journal of Materials Chemistry*, *21*(16), 5860. Retrieved from https://doi.org/10.1039/c1jm00065a.
200. Gudeika, D., Ivanauskaite, A., Lygaitis, R., Kosach, V., Volyniuk, D., Butkute, R., Naumenko, A. P., Yashchuk, V., & Grazulevicius, J. V. (2016). Retrieved fromCharge-transporting blue emitters having donor and acceptor moieties. *Journal of Photochemistry and Photobiology A: Chemistry*, *315*, 121–128. Retrieved from https://doi.org/10.1016/j.jphotochem.2015.10.002.

8. CURRICULUM VITAE

Name, Surname: Naveen Masimukku

Organisation: Department of Polymer Chemistry, K. Barsausko g. 59, LT-51423, Kaunas, Lithuania.

Email: masimukkunaveen@gmail.com

Education:

2010–2015

Bachelor's Degree in Applied Chemistry, Kakathiya University and Osmania University, India.

2016–2018

Master's Degree in Chemical Engineering, Kaunas University of Technology, Kaunas, Lithuania.

2018–2022

PhD in Material Engineering, Kaunas University of Technology, Kaunas, Lithuania.

9. LIST OF ARTICLES AND PRESENTATIONS AT SCIETIFIC CONFERENCES

List of publications on the dissertation topic:

1. Masimukku, Naveen; Gudeika, Dalius; Bezvikonnyi, Oleksandr; Syvorotka, Ihor; Keruckiene, Rasa; Volyniuk, Dmytro; Grazulevicius, Juozas Vidas. Aryl-substituted acridanes as hosts for TADF-based OLEDs // Beilstein Journal of Organic Chemistry. 2020, Vol. 16, p. 989-1000.
2. Gudeika, Dalius; Bezvikonnyi, Oleksandr; Masimukku, Naveen; Volyniuk, Dmytro; Chen, ChiaHsun; Ding, Wen-Cheng; Lee, Jiun-Haw; Chiu, Tien-Lung; Grazulevicius, Juozas Vidas. Tetraphenyl ornamented carbazolyl disubstituted diphenyl sulfone as bipolar TADF host for highly efficient OLEDs with low efficiency roll-offs // Dyes and Pigments. 2021, vol. 194, p. 1-8.
3. Masimukku, Naveen; Gudeika, Dalius; Volyniuk, Dmytro; Bezvikonnyi, Oleksandr; Simokaitiene, Jurate; Matulis, Vitaly; Lyakhov, Dmitry; Azovskyi, Volodymyr; Gražulevičius, Juozas Vidas. Bipolar 1,8- naphthalimides showing high electron mobility and red AIE-active TADF for OLED applications // Physical Chemistry Chemical Physics. 2022, vol. 24, p. 5070-5082.

List of presentations at the international conferences:

1. Masimukku, Naveen; Gudeika, Dalius; Volyniuk, Dmytro; Grazulevicius, Juozas Vidas. Synthesis and investigation of ambipolar 1,8- naphthalimide-based derivatives // Open readings: 62nd international conference for students of physics and natural sciences / 19th-22nd Match, 2019, Vilnius, Lithuania.
2. Masimukku, Naveen; Gudeika, Dalius; Volyniuk, Dmytro; Grazulevicius, Juozas Vidas. Synthesis and properties of 1,8-naphthalimide-based compounds // 24th international Krutyń summer school / 01st-07th September, 2019, Krutyń, Poland.
3. Masimukku, Naveen; Gudeika, Dalius; Volyniuk, Dmytro; Grazulevicius, Juozas Vidas. Design, preparation and studies of naphthalimide materials // Open readings: 63rd international conference for students of physics and natural sciences / 17th-20th March, 2020, Vilnius, Lithuania.
4. Masimukku, Naveen; Gudeika, Dalius; Volyniuk, Dmytro; Grazulevicius, Juozas Vidas. Design, synthesis and investigation of 1,8-naphthalimide based compounds // ICEPOM -12: Electronic processes in organic and inorganic materials / 1st-5th June, 2020, Kamianets-Podilskyi, Ukraine.
5. Masimukku, Naveen; Gudeika, Dalius; Bezvikonnyi, Oleksandr; Volyniuk, Dmytro; Grazulevicius, Juozas Vidas. 1,8-Naphthalimide-based derivatives exhibiting orange-red thermally activated delayed fluorescence and their application in OLED // The vital nature sign: 14th international scientific conference / 15th-16th October, 2020, Kaunas, Lithuania.

6. Masimukku, Naveen; Gudeika, Dalius; Bezvikonnyi, Oleksandr; Volyniuk, Dmytro; Grazulevicius, Juozas Vidas. 1,8-naphthalimide derivatives exhibiting thermally activated delayed fluorescence // Open readings: 64th international conference for students of physics and natural sciences / 16th-19th March, 2021, Vilnius, Lithuania.
7. Masimukku, Naveen; Gudeika, Dalius; Ghasemi, Melika; Mahmoudi Sharabiani, Malek; Volyniuk, Dmytro; Grazulevicius, Juozas Vidas. Synthesis and properties of derivatives of 3,6-disubstituted naphthlimide // The vital nature sign: 15th international scientific conference / 20th-21st May, 2021, Kaunas, Lithuania.
8. Masimukku, Naveen; Gudeika, Dalius; Bezvikonnyi, Oleksandr; Volyniuk, Dmytro; Grazulevicius, Juozas Vidas. Naphthalimide derivatives as emitters for organic light emitting diodes // IMRC: 19th international materials research congress / 15th-20th August, 2021, Cancun, Mexico.
9. Masimukku, Naveen; Gudeika, Dalius; Dabuliene, Asta; Mahmoudi, Malek; Volyniuk, Dmytro; Grazulevicius, Juozas Vidas. Synthesis and properties of star-shaped 1,8-naphthalimide based derivatives // Advanced materials and technologies: book of abstracts of 23rd international conference-school / 23rd-27th August, 2021, Palanga, Lithuania.
10. Masimukku, Naveen; Gudeika, Dalius; Dabuliene, Asta; Ghasemi, Melika; Mahmoudi, Malek; Volyniuk, Dmytro; Grazulevicius, Juozas Vidas. Bromine containing naphthalimides exhbiting room-tempareture phosporescence // Chemistry and chemical technology: 16th international conference of Lithuanian Chemical Society / 24th September, 2021, Vilnius, Lithuania.

10. ACKNOWLEDGEMENTS

I would like to express my deepest gratitude from the bottom of my heart to my scientific advisor, Prof. Habil. dr. Juozas Vidas Gražulevičius (Department of Polymer Chemistry and Technology, Kaunas University of Technology) for the outstanding moral and kind support, new ideas, inspiration and for providing opportunities to work in the group.

I would like to express my greatest gratitude to my supervisors dr. Asta Dabuliene and dr. Dalius Gudeika for their expert supervision and valuable advice.

I would like to extend my deepest gratitude to my family for their encouragement, love, and relentless support.

Also, I would also like to express my deepest gratitude to our entire group of organic chemists, physicists, my labmates, colleagues and co-workers for valuable suggestions, practical advice and for providing a great friendly atmosphere during my study years.

UDK 547.7+621.383.52](043.3)

SL344. 2022-*-*, * leidyb. apsk. l. Tiražas 14 egz. Užsakymas * .
Išleido Kauno technologijos universitetas, K. Donelaičio g. 73, 44249 Kaunas
Spausdino leidyklos „Technologija“ spaustuvė, Studentų g. 54, 51424 Kaunas